In vitro reconstitution of the hemolysin A T1SS from uropathogenic *Escherichia coli*

Inaugural-Dissertation

zur Erlangung des Doktorgrades
der Mathematisch-Naturwissenschaftlichen Fakultät
der Heinrich-Heine-Universität Düsseldorf

vorgelegt von
Florestan Leander Bilsing
aus Duisburg

Düsseldorf, Februar 2024

aus dem Institut für Biochemie
der Heinrich-Heine-Universität Düsseldorf

Gedruckt mit der Genehmigung der
Mathematisch-Naturwissenschaftlichen Fakultät der
Heinrich-Heine-Universität Düsseldorf

Berichterstatter:

1. Prof. Dr. rer. nat. Lutz Schmitt

2. Prof. Dr. rer. nat. Johannes Hegemann

Tag der mündlichen Prüfung: 13.03.2024

“There is nothing like looking, if you want to find something. You certainly usually find something, if you look, but it is not always quite the something you were after.”

J. R. R. Tolkien, The Hobbit

Abstract

Gram-negative bacteria have evolved a variety of transport and secretion systems to enable transport across one, two or three biological membranes. The secretion systems are classified into different groups numbered from type 1 onwards. The type 1 secretion system (T1SS) is a rather simple system with a translocation channel built by only three different proteins: an ATP-binding cassette (ABC) transporter, a membrane fusion protein (MFP) and an outer membrane protein (OMP). The secretion process is powered by ATP hydrolysis and allows secretion of the unfolded substrate from the cytosol to the extracellular space in one single step.

One of the best studied T1SSs is the hemolysin A (HlyA) T1SS from uropathogenic *E. coli*, which transports the pore forming toxin HlyA. The ABC transporter is hemolysin B (HlyB), the MFP is hemolysin D (HlyD) and the OMP is TolC. HlyB and HlyD form a so-called inner membrane complex (IMC) in the inner membrane, while TolC is located in the outer membrane. Although the HlyA T1SS is known for more than 70 years, there are still many open questions regarding its molecular organisation and mode of action.

In this thesis, the establishment of the *in vitro* reconstitution of the HlyA T1SS is shown. Additionally, I present an *in vitro* transport assay which was successfully performed to serve as a first proof of principle. This *in vitro* set up provides a powerful tool for the future to investigate the system in further detail. The purification and reconstitution of the ABC transporter HlyB and the IMC were studied here intensively. The protocol for HlyB purification was optimized for structural studies and the reconstitution into MSP-based nanodiscs established. A protocol for reconstitution of IMC in MSP-based nanodiscs was established as well. TolC reconstituted in liposomes was used to complete the assembly *in vitro*.

Furthermore, the ABC transporter RtxB, part of the homologous RtxA T1SS from the emerging pathogen *Kingella kingae*, was characterized biochemically and structurally. A purification protocol for RtxB was established that allowed initial structural analysis using cryo-EM including the construction of a 3D volume map. RtxB showed a higher basal ATPase activity in detergent than its homolog HlyB. Reconstitution into MSP-based nanodiscs increased the ATPase activity of RtxB and further stabilized the ABC transporter *in vitro*.

Zusammenfassung

Gram-negative Bakterien haben im Laufe der Zeit eine Vielzahl an Transport- und Sekretionssystemen entwickelt, welche den Transport über eine, zwei oder drei biologische Membranen ermöglichen. Die Sekretionssysteme werden in verschiedene Gruppen eingeteilt und durchnummeriert, beginnend mit Typ 1. Das Typ 1 Sekretionssystem (T1SS) hat einen vergleichsweise einfachen Aufbau mit einem Transportkanal, der aus nur drei verschiedenen Proteinen besteht: ein *ATP-binding cassette* (ABC) Transporter, ein Membranfusionsprotein (MFP) und ein Membranprotein der äußeren Membran (OMP). Die Sekretion wird durch Hydrolyse von ATP angetrieben und das Substrat wird im ungefalteten Zustand in einem Schritt vom Zytosol in den extrazellulären Raum sekretiert.

Eines der am besten untersuchten T1SS ist das Hämolysin A (HlyA) T1SS aus uropathogenen *E. coli* Stämmen. Es transportiert das porenbildende Toxin HlyA. Der ABC Transporter in diesem System ist Hämolysin B (HlyB), das MFP ist Hämolysin D (HlyD) und das OMP ist TolC. HlyB und HlyD formen einen Komplex (IMC) in der inneren Membran, während sich TolC in der äußeren Membran befindet. Obwohl das HlyA T1SS seit über 70 Jahren bekannt ist, gibt es immer noch viele offene Fragen hinsichtlich seiner molekularen Organisation und dem detaillierten Ablauf des Sekretionsprozesses.

In dieser Arbeit wird die Etablierung der *in vitro* Rekonstitution des HlyA T1SS gezeigt. Außerdem präsentiere ich einen ersten erfolgreichen *in vitro* Transporttest, der als Machbarkeitsnachweis dient. Das hier beschriebenen *in vitro* System ermöglicht in Zukunft eine noch detailliertere Untersuchung des HlyA T1SS. Die Reinigung und Rekonstitution des ABC Transporters HlyB und des IMC wurden in dieser Arbeit ausführlich untersucht. Das Reinigungsprotokoll für HlyB wurde für strukturelle Analysen optimiert und die Rekonstitution in Lipid-Nanopartikel, basierend auf dem Membrangerüst bildenden Protein (MSP), wurde etabliert. Zusätzlich wurde ein Protokoll zur Rekonstitution des IMC in MSP basierte Lipid-Nanopartikel entwickelt. Dazu wurde TolC in Liposomen rekonstituiert, um die *in vitro* Assemblierung zu ermöglichen.

Des Weiteren wurde der ABC Transporter RtxB biochemisch und strukturell untersucht. RtxB ist Teil das homologen RtxA T1SS aus dem neu aufkommenden Erreger *Kingella kingae*. Ein Reinigungsprotokoll für RtxB wurde etabliert, das erste

strukturelle Analysen mittels Kryo-EM bis hin zur Erstellung einer 3D Klasse ermöglichte. RtxB zeigte in Detergenz eine basale ATPase Aktivität, welche höher als die seines Homologs HlyB war. Darüber hinaus erhöhte die Rekonstitution von RtxB in MSP basierte Lipid-Nanopartikel die ATPase Aktivität und führte zu einer zusätzlichen Stabilisierung von RtxB *in vitro*.

Abbreviations

ABC	ATP-binding cassette
ACP	acyl carrier protein
BAM	barrel assembly module
BN	Blue Native
CLD	C39 peptidase-like domain
csg	curli specific genes
CU	chaperone-usher
CV	column volumes
DDM	n-dodecyl-β-D-maltopyranoside
DIBMA	diisobutylene maleic acid copolymers
DOPC	1,2-dioleoyl-sn-glyero-3-phosphocholine
DOPE	1,2-dioleoyl-sn-glyero-3-phosphoethanolamine
DOPG	1,2-dioleoyl-sn-glyero-3-phospho-(1'-rac-glycerol)
DSF	differential scanning fluorimetry
DTT	dithiotreitol
E. coli	Escherichia coli
FC-14	Fos-Choline-14
FSC	fourier shell correlation
GDN	glyco-diosgenin
GG repeats	glycine-rich nonapeptide sequences
GUV	giant unilamellar vesicle
His	histidine-tag
HlyA	hemolysin A
HlyA1	hemolysin A1
HlyB	hemolysin B
HlyD	hemolysin D
IM	inner membrane
IMAC	immobilized metal ion affinity chromatography
IMC	inner membrane complex
IPTG	isopropyl-β-D-thiogalacto-pyranoside
K. kingae	Kingella kingae
khalf	ATP concentration producing half-maximal turnover rates
LMNG	lauryl maltose neopentyl glycol

LPC	lysophosphatidylcholin
LPG	lysophosphatidylglycerol
MFP	membrane fusion protein
MFS	major facilitator superfamily
MSP	membrane scaffold protein
NBD	nucleotide binding domain
NBS	nucleotide binding site
NSP	nanodisc scaffold protein
NSPr	nanodisc scaffold protein in reversed order of the amino acids
OM	outer membrane
OMP	outer membrane protein
PDB	protein data base
PG	peptidoglycan
PMF	proton motif force
pro-HlyA	pro-hemolysin A
RND	resistance-noduclation-division
RTX	repeats in toxin
RtxA	RTX toxin from Kingella kingae
RtxB	ABC transporter from *K. kingae* RtxA T1SS
RtxD	membrane fusion protein from *K. kingae* RtxA T1SS
salipro	saposin A lipid protein
SapA	saposin A
SEC	size exclusion chromatography
SMA	styrene maleic acid copolymers
SPR	surface plasmon resonance
SRP	single recognition particle
Strep	Strep-tag
T4P	type 4 pilus
TAM	translocation and assembly module
Tat	twin-arginine translocation
TLC	thin layer chromatography
TMD	transmembrane domain
TMH	transmembrane helix
TMHs	transmembrane helices

TS	TwinStrep-tag
TXSS	type X secretion system
TXSSs	type X secretion systems
vmax	maximum turnover rate

List of figures

Table of contents

1. Introduction

Bacteria are unicellular organisms shielded from their environment by a lipid membrane. Whereas Gram-positive bacteria have one cellular membrane and a thick peptidoglycan layer on the outside [1], Gram-negative bacteria have an inner membrane (IM), an outer membrane (OM) and a comparatively thin peptidoglycan layer in between the two membranes [2]. The cell membrane of Gram-positive bacteria contains mostly anionic phospholipids like phosphatidylglycerol and cardiolipin and glycolipids. This makes it a potent barrier for charged and hydrophilic compounds [1-3]. The IM in Gram-negative bacteria adopts a similar function in repelling charged and hydrophilic compounds and contains mainly zwitterionic phosphatidylethanolamine besides phosphatidylglycerol and cardiolipin. [2, 4]. The OM of Gram-negative bacteria is an asymmetric bilayer with mainly lipopolysaccharides (LPS) in the outer leaflet [2]. The densely packed LPS functions as a barrier against hydrophobic molecules [5]. On the one hand, this repellent property of bacterial membranes protect the cell from all types of molecules, on the other hand, it requires specific transport systems to overcome the membrane barriers for uptake and secretion. In case of invasive secretion systems such as the type 3, type 4, or type 6 secretion systems, a third membrane belonging to the target cell, must be crossed in order for secretion to take place.

Bacteria have evolved numerous systems to secrete molecules across one, two or even three biological membranes [6]. This enables for instance transport from inside the cell to the extracellular space and beyond. Today, several different specialised secretion systems of bacteria are known, most of which have been described for Gram-negative bacteria. One of them and focus of this work is the type 1 secretion system (T1SS) [7, 8]. The other specialised secretion systems type 2 – 9 will be only shortly described here in their general operating principle. For detailed reviews see Costa *et al.* [9] and Christie *et al.* [6]. More commonly distributed among prokaryotes and present in many plant chloroplasts is the twin-arginine translocation (Tat) pathway. Present in all domains of life and of highest biological importance is the general secretory (Sec) pathway. The Sec and Tat systems will be described in the following.

1.1. General Membrane Transport Systems

1.1.1. The Sec System

The Sec pathway is conserved among all domains of life with slight changes in terms of the proteins involved and their nomenclature. For simplicity all described proteins and protein names will refer to the Sec pathway of *Escherichia coli* (*E. coli*).

The Sec pathway enables transport of unfolded proteins from the cytosol to the periplasm. The main component of the Sec pathway is the SecYEG translocon located in the IM of *E. coli*. It is a heterotrimeric channel forming complex build by the proteins SecY, SecE and SecG [10]. The channel is narrowed in the centre, comparable to the shape of an hourglass [11]. In the centre of this hourglass-shape a ring of six isoleucines acts as a hydrophobic channel gate [12]. Furthermore, a short helix of SecY acts as a plug from the periplasmic side [13, 14]. Proteins intended for transport via the Sec pathway contain an N-terminal hydrophobic signal sequence [15]. Depending on the final destination of the protein two different pathways within the Sec system are differentiated. Both pathways use the SecYEG channel for translocation, but differ in the way how the pre-protein is targeted to the SecYEG complex (Figure 1).

On the one hand, pre-proteins can be targeted to SecYEG via the SecB dependant pathway. Substrates for the SecB dependent pathway are usually soluble proteins destined for the periplasm or the extracellular space and membrane proteins destined for the OM. The unfolded protein is fully synthesized by the ribosome and afterwards bound and stabilized by the chaperon SecB [16]. SecB recognizes unfolded proteins and keeps them in an unfolded state acting as a holdase [17]. Next SecB delivers its cargo to SecA which directs it to SecYEG and enables transport via its ATPase activity [18]. This pathway is referred to as post-translational secretion (Figure 1, left).

On the other hand, pre-proteins can be targeted to SecYEG via the signal recognition particle (SRP) dependant pathway. Substrates for the SRP dependant pathway are in general transmembrane proteins of the IM [19]. The hydrophobic signal sequence is recognised and bound by the SRP and translation stops [20]. SRP together with the ribosome are targeted to SecYEG via the membrane bound receptor FtsY [21]. Translation continues and the pre-protein is secreted with the help of SecA through the SecYEG channel. Membrane helices leave the SecYEG channel via a lateral gate

directly into the lipid bilayer of the membrane [22, 23]. This pathway is referred to as co-translational secretion (Figure 1, right).

The translocation process through SecYEG is powered by hydrolysis of ATP by SecA as well as by the proton motif force (PMF) [24, 25]. After secretion of the pre-protein the N-terminal signal peptide is cleaved by a membrane bound periplasmic signal peptidase and the mature protein is released [26].

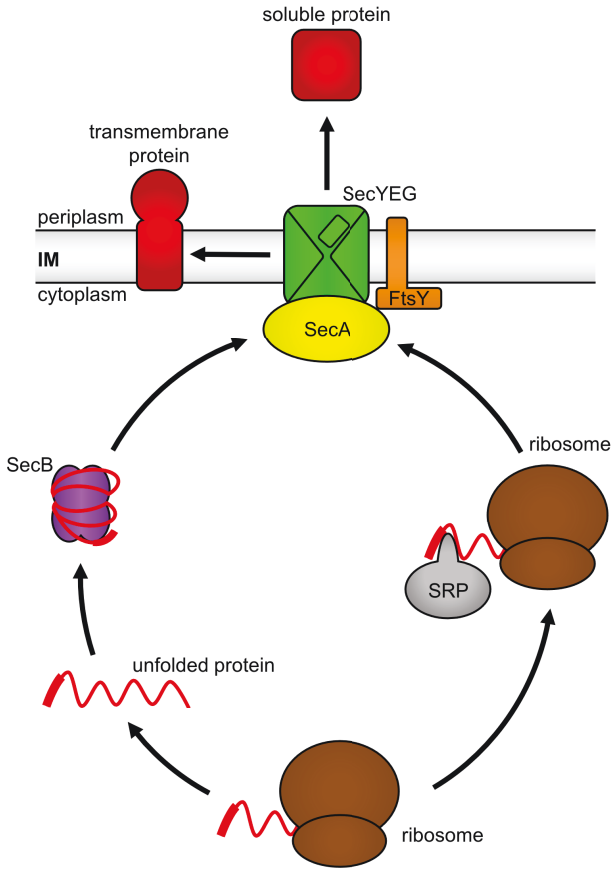

Figure 1: Schematic representation of the Sec pathway in E. coli. *IM: inner membrane.* ***Post-translational pathway (left):*** *Translation occurs at the ribosome (brown) and targeting of the unfolded protein (red line) to the SecYEG translocon (green) occurs via SecB (purple) and SecA (yellow).* ***Co-translational pathway (right):*** *During translation the substrates signal peptide (bold part of the red line) is recognized by the signal recognition particle (SRP, grey) and translation is stopped. Via the membrane bound FtsY (orange) the SRP stalled ribosome is targeted to the SecYEG translocon (green). Independent of the targeting mechanisms SecA (yellow) together with SecYEG (green) transport the unfolded substrate across the IM and the protein either folds in the periplasm (soluble protein, red square) or leaves SecEG via the lateral gate into the IM (transmembrane protein, red). This figure makes no claim to the accuracy of the stoichiometry or scale.*

1.1.2. The Tat system

In contrast to the Sec system, the twin-arginine translocation (Tat) pathway transports folded proteins across the membrane [27]. The Tat system was detected in 77 % of all bacterial genomes and in archaea as well as in plant chloroplasts [28]. For the sake of

simplicity all described proteins and protein names will refer to the Tat pathway of *E. coli*. Here the Tat pathway enables transport of folded protein across the IM to the periplasm.

The basis of the Tat pathway in its simplest form is built by two structural protein families: TatA and TatC [29]. In *E. coli* additional members of the TatA family are present which differ in functionality from TatA and of which TatB is the most abundant one [30]. TatA as well as TatB have a single trans membrane helix (TMH), an amphipathic helix and a highly charged unstructured C-terminal end [31-33]. TatC possesses six trans membrane helices (TMHs) that form a baseball glove-like structure with an opening towards the membrane [34]. TatB and TatC form a multisubunit complex in the IM with a stoichiometry of 1:1 [35]. Upon substrate recognition TatA is recruited to the TatBC complex and its oligomeric assembly enables transport across the IM [36, 37] (Figure 1B). The substrate is recognized via its N-terminal signal peptide [19]. This Tat signal peptide is composed of at least 30 amino acids with a consensus sequence of seven amino acids (Ser-Arg-Arg-X-Phe-Leu-Lys, X being a polar residue or glycine) containing the name giving twin-arginine residues [38]. After transport, the signal peptide is cleaved on the periplasmic side and the TatABC complex disassembles again into TatBC and TatA [39, 40]. Transport via the Tat pathway relies on the PMF although the details are not known to date [29, 41].

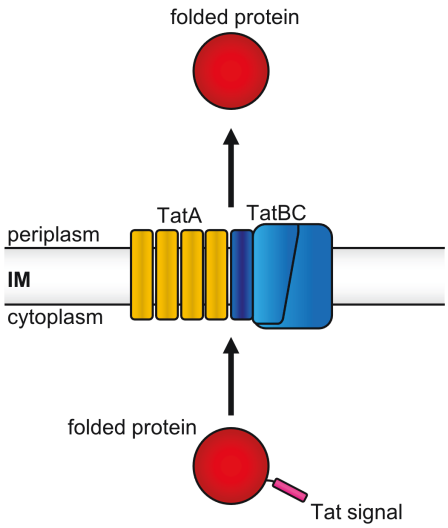

Figure 2: Schematic representation of the Tat pathway in E. coli. *IM: inner membrane. Protein transport via the Tat pathway in E. coli. The folded protein (red circle) is recognized by TatBC (colours of blue) via its signal peptide (pink). TatA (yellow) and TatBC assemble into TatABC transport complex and transport the folded protein across the membrane. After transport the signal peptide is cleaved and the folded protein is released into the periplasm. This figure makes no claim to the accuracy of the stoichiometry or scale.*

1.2. Specialised transport across one membrane

1.2.1. OM secretion systems

More specific secretion systems for the transport across the OM in Gram-negative bacteria are the type 5 secretion system (T5SS), type 8 secretion system (T8SS) and Chaperone-Usher secretion pathway (Figure 3A). Those systems span the OM and rely on the transport of their substrates to the periplasm via the Sec pathway [42, 43]. Furthermore the type 7 secretion system (T7SS) enables transport across the cell envelope in mycobacteria [44] (Figure 3B).

Type 5 secretion systems (T5SSs) are also referred to as 'autotransporters' and summarise a variety of transport systems that harbour a so-called translocator and a passenger domain [45]. Those domains are usually part of the same polypeptide chain, with the passenger domain being the substrate and the translocator domain being the translocation channel [43]. Most of the substrates are important for biofilm formation, cell-cell-attachment or virulence [46]. T5SSs were thought to be independent of other factors and perform transport across the OM only by their translocator domain [6]. However, over the past years it was shown that T5SSs rely on interaction with other systems like the periplasmic chaperone network, the barrel assembly machinery (BAM) or the translocation and assembly module (TAM) [47-49]. T5SSs are grouped in 6 different sub-families (a – f) varying in the number, organisation or structural details of the different domains [45].

Another OM spanning secretion system is the T8SS or nucleation-precipitation machinery [50]. Type 8 secretion systems (T8SSs) were first described about 35 years ago as a secretion machinery for *E. coli* surface structures called curli [51]. Those surface structures are built by repetitive assembly of the curli protein CsgA into an amyloid like fibre and are important for biofilm formation [52-54]. The curli biosynthesis pathway was found in different *Enterobacteriaceae* such as *E. coli* [55-57]. The *E. coli* T8SS is organised in two different operons harbouring curli-specific genes (csg) [56]. The first operon contains *csgBAC*, relevant for the formation of the fibre and the second operon contains *csgDEFG*, relevant for transcription activation and secretion of the fibre components [58-60].

Last but not least the chaperone-usher (CU) system represents another OM spanning system which relies on the Sec pathway for transport of its components across the IM [61]. The CU pathway consists of a chaperone in the periplasm for substrate targeting

and an usher in the OM for substrate transport and polymerisation [62, 63]. This interplay enables the assembly of so-called CU fimbriae that are important virulence factors and contribute to surface adhesion and biofilm formation [62]. A variety of CU fimbriae have been discovered in Gram-negative bacteria, of which the type 1 fimbriae of *E. coli* are among the best characterised [64-66]. The periplasmic chaperone in case of type 1 fimbriae is FimC [67] and the usher is the beta-barrel forming FimD [68]. Although much is known about these OM transport systems a lot of open questions remain. As no ATP or any other source of energy such as ion gradients is present in the periplasm it is for instance still an open question what energizes the transport across the OM. Energy might come from the proper folding of the substrate in the extracellular space or from entropy gradients [69-73].

1.2.2. Mycobacterial type 7 secretion systems

Additional single membrane spanning systems are the type 7 secretion systems (T7SSs) from mycobacteria [74]. Five different T7SSs were reported that share the same structural organisation with five membrane and two cytosolic components [44]. The five membrane components are sufficient to assemble the secretion apparatus consisting of a pore surrounded by a collar-like assembly [75, 76]. Substrate secretion relies on an exceptional ATPase containing three nucleotide binding domains [77].

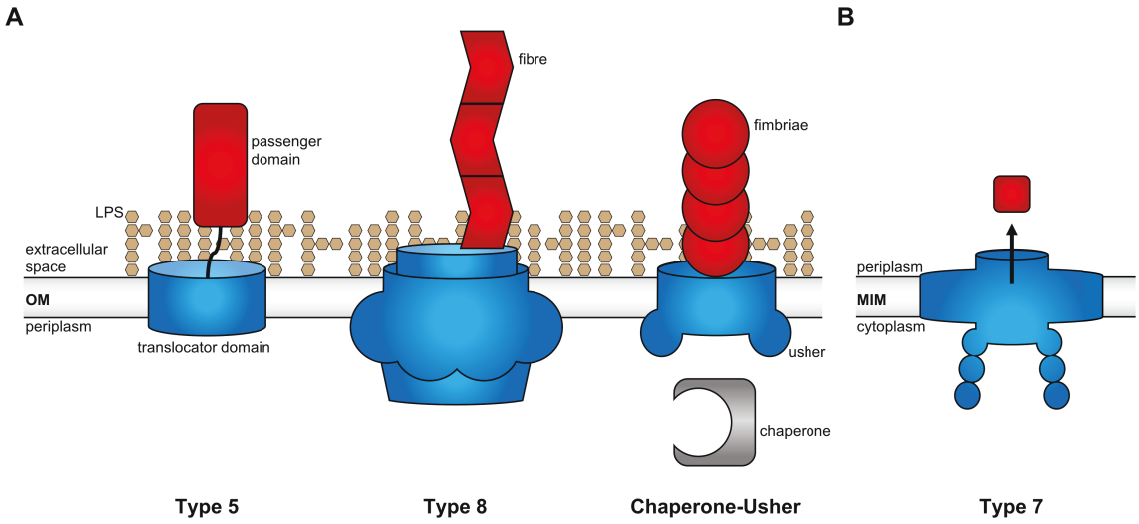

Figure 3: Schematic of single membrane secretion systems. A: Outer membrane secretion systems type 5 (left), 8 (middle) and chaperone-usher (right). *OM: outer membrane. LPS: lipopolysaccharides.* ***Left:*** *Type 5 secretion system consisting of the translocator domain (blue) located in the OM and passenger domain (red) in the extracellular space connected via a linker domain (black line).* ***Middle:*** *Type 8 secretion system consisting of the secretion pore (blue) in the OM and the multimeric fibre (red) attached in the extracellular space.* ***Right:*** *Chaperone-Usher system consisting of the chaperone in the periplasm (grey) and the usher (blue) in the OM. The multimeric fimbriae (red) assembles in the extracellular space. The peptidoglycan has been omitted for reasons of clarity.* ***B: Mycobacterial type 7 secretion system.*** *MIM: Mycobacterial inner membrane. Type 7 secretion system consisting*

of the collar-like pore assembly (blue) in the membrane and cytoplasmic nucleotide binding domains (blue circles). The substrate (red square) is secreted to the periplasm through the central pore. The mycobacterial outer membrane has been omitted for reasons of clarity. This figure makes no claim to the accuracy of the stoichiometry or scale.

1.2.3. OM secretion systems with an IM part

Further OM transport systems are the type 2 secretion system (T2SS), type 4 pilus (T4P) and type 9 secretion system (T9SS) (Figure 4). They are present in Gram-negative bacteria and are also dependent on the Sec or Tat pathway [78] for substrate translocation across the IM. They transport folded substrates from the periplasm to the extracellular space, but in contrast to the T5SSs, T8SSs and CU system they have an inner membrane part as well as an outer membrane part. This allows these systems to use cytosolic or IM related energy sources such as ATP or PMF [79-81].

The type 2 secretion systems (T2SSs) transport a brought variety of folded substrates like toxins, lipases and other proteins important for biofilm formation [82]. The T2SS consists of an OM pore complex, an IM platform, a periplasmic pseudopilus and a cytoplasmic ATPase [83]. The OM pore complex and the IM platform connect via their periplasmic domains [84]. The pseudopilus does not cross the OM and expands only within the periplasm, pushing substrates through the OM pore complex in an either piston-like or Archimedes' screw mechanism [85-87]. ATPase activity is responsible for substrate translocation across the OM and probably also involved in pseudopilus assembly [80, 88]. The T4P has a similar architecture to the T2SS [89], but type 4 pili systems contain a pilus instead of a pseudoplius, that elongates beyond the OM and enables cell-cell contacts for biofilm formation, twitching motility or DNA uptake [90]. In addition, T4P usually have a retraction ATPase for pilus retraction [91].

The type 9 secretion systems (T9SSs) were only discovered about 20 years ago as responsible gene cluster for gliding motility and transport of gingipains and adhesins [92, 93]. Nowadays it is known that T9SSs are present mostly in *Bacteroidetes* and that transport of a variety of substrates occurs in parallel to gliding motility [94, 95]. T9SSs substrates possess a C-terminal signal peptide for OM transport besides the signal peptide for the Sec pathway [96]. The T9SS is built by an PMF driven IM motor and an OM pore complex that transports folded substrates and cleaves the C-terminal signal peptide [97, 98]. However, the exact interplay between inner and outer membrane components of the T9SSs are still unknown [99].

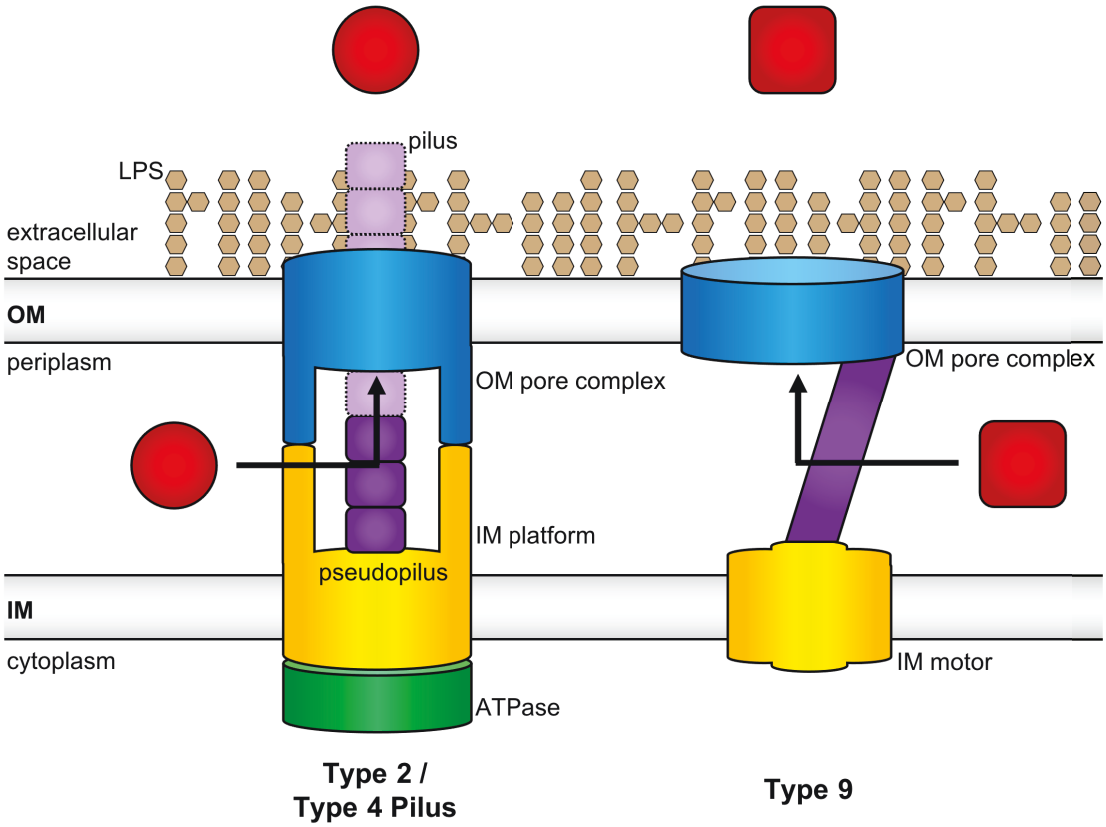

Figure 4: Schematic of outer membrane secretion systems with an inner membrane part. *OM: outer membrane. IM: inner membrane. LPS: lipopolysaccharides.* ***Left:*** *Type 2 secretion system (T2SS) consisting of an OM pore complex (blue) and an IM platform (yellow) connected via their periplasmic domains. A pseudopilus (purple) in the periplasm translocates the substrate (red circle) from the periplasm to the extracellular space. The ATPase (green) in the cytoplasm delivers the energy for the transport. The type 4 pilus (T4P) shares a similar structural organization with the T2SS. Instead of a pseudopilus the T4P has a pilus (light purple with dotted lines) that expands into the extracellular space.* ***Right:*** *Type 9 secretion system (T9SS) consisting of an OM pore complex (blue) and an IM motor (yellow) connected via a periplasmic part (purple). The IM motor uses the PMF to transport substrates (red squares) across the OM. The peptidoglycan has been omitted for reasons of clarity. This figure makes no claim to the accuracy of the stoichiometry or scale.*

1.3. Specialised transport across three membranes

Besides these previously described Sec pathway dependent OM transport systems, Gram-negative bacteria also developed specialised secretion systems that span the inner and outer membrane and can even transport substrates across a third membrane. Those systems are the type 3 secretion system (T3SS), type 4 secretion system (T4SS) and type 6 secretion system (T6SS) (Figure 5).

The type 3 secretion systems (T3SSs) are present in mostly pathogenic Gram-negative bacteria and allow transport of effector proteins from the cytoplasm into host cells [100-104]. These systems are built by four distinct parts: the sorting platform on the cytosolic side of the IM; the basal body, built by different rings in the inner and outer

membrane, spanning the whole cellular envelope; the needle, reaching from the basal body to the target cell and the pore forming translocon complex in the target cell which is connected to the needle [105]. In the bacterial cytosol T3SS chaperones target substrates to the sorting platform [106]. The substrates of the T3SS have an N-terminal secretion signal and secretion follows a strictly controlled hierarchy [107]. The dimensions of the needle only allow the passage of unfolded substrates [108]. It is assumed that ATPase activity is responsible for substrate unfolding and initial steps of the secretion process while the PMF powers the secretion [109]. T3SSs are related to the flagellum and hypotheses assume a common origin [110].

The type 4 secretion systems (T4SSs) are present in Gram-negative as well as Gram-positive bacteria and play an important role in effector protein secretion into eukaryotic target cells as well as transfer of DNA between procaryotes [111]. Besides direct cell-to-cell transfer, T4SSs can also be used to secrete DNA into or take it up from the extracellular space [112, 113]. T4SSs can be classified in three different subfamilies: conjugation machines for DNA transfer, effector translocators for cell-to-cell transport and an import/export subfamily for release into and uptake from the extracellular space [114]. The T4SSs are diverse in structural details and substrates but share the common modular architecture of an outer membrane core complex and an inner membrane complex, connected via a so-called stalk in the periplasm [115]. In addition, many systems assemble an extracellular pilus [116]. Transport via T4SSs is powered by three different ATPases that are all essential for the secretion process [117].

The type 6 secretion systems (T6SSs) were first described approximately 20 years ago as a cytotoxic cell contact dependant protein secretion machinery in *Vibrio cholerae* and many other pathogenic Gram-negative bacteria [118]. Those systems secrete a brought variety of effectors into prokaryotic or eukaryotic target cells by penetrating the cellular membrane of the target cell [119-121]. Especially in competition with other bacteria, the T6SS plays a vital role in occupying a biological niche [122]. The system is built by a channel-forming multiprotein membrane complex spanning inner and outer membrane and a so called baseplate at the cytosolic side of the IM [123]. Furthermore, a tube in a contractile sheath with a spike complex at the tip assembles in the cytosol connected to the baseplate [124]. Upon an extracellular trigger event the sheath contracts and the spike complex with the tube advances through the membrane channel into the host cell [125, 126]. Substrates are either attached to the outside of

the spike complex or to the tube inside the sheath [127]. Energy from an ATPase disassembles the sheath after contraction for a new assembly round [128].

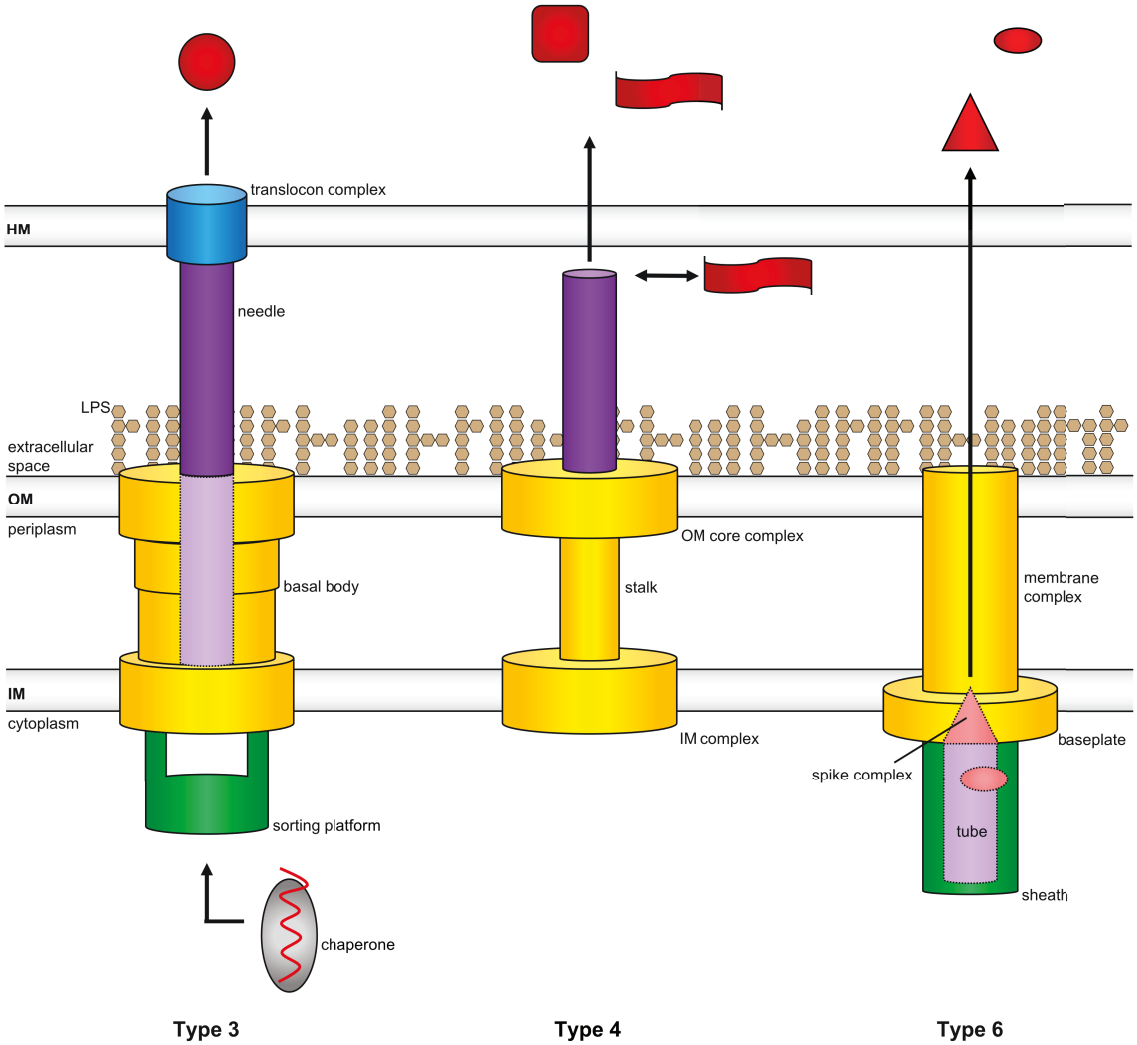

Figure 5: Schematic of secretion systems across three membranes. *IM: inner membrane. OM: outer membrane. HM: host membrane. LPS: lipopolysaccharides.* ***Left:*** *Type 3 secretion system (T3SS) consisting of a cytosolic sorting platform (green), a basal body (yellow) spanning inner and outer membrane, a needle (purple) and a translocon complex (blue) in the HM. A T3SS specific chaperone (grey) in the cytosol targets the unfolded substrate (red line) to the sorting platform. After injection, the substrate (red circle) operates in the target host cell. Hidden parts are shown in light colours and dotted lines.* ***Middle:*** *Type 4 secretion system (T4SS) consisting of an IM complex and an OM core complex connected via a stalk (yellow) and an extracellular pilus (purple). Substrates (red band, red square) are either transported into the host cell or secreted to or received from the extracellular space.* ***Right:*** *Type 6 secretion system (T6SS) consisting of a baseplate (yellow), a membrane complex (yellow), a sheath (green) with a tube inside (light purple) that is capped by a spike complex (light red triangle). Upon sheath contraction the spike complex (red triangle) and substrates (red oval) in the sheath penetrate the HM and enter the target cell. Hidden parts are shown in light colours and dotted lines. The peptidoglycan has been omitted for reasons of clarity. This figure makes no claim to the accuracy of the stoichiometry or scale.*

1.4. Specialised transport across two membranes – The T1SS

In Gram-negative bacteria the T1SS enables transport across IM and OM to the extracellular space [129]. Type 1 secretion systems (T1SSs) are rather straightforward systems with a secretion channel built in its simplest version by only three structural elements [130]. These tripartite assemblies contain an ATP-binding cassette (ABC) transporter, a membrane fusion protein (MFP) and an outer membrane protein (OMP) [8] (Figure 6). In the IM the ABC transporter and MFP form the so-called inner membrane complex (IMC). In the OM the OMP forms a beta-barrel pore with a large periplasmic part. The IMC and the OMP connect in the periplasm and form the secretion channel [131]. The substrates of T1SSs are very diverse, but in general specific for its cognate T1SS and are secreted in the unfolded state [7]. The energy for the secretion is derived from ATP hydrolysis by the ABC transporter [132].

For T1SSs, it has long been a dogma that transport occurs in an unfolded state from the cytoplasm to the extracellular space in one single step and without a periplasmic intermediate [133]. However, recent findings on a retention module at the N-terminus of a T1SS substrate in *Pseudomonas fluorescens*, which retains a part of the protein in the periplasm, show that there might be exceptions [134]. Furthermore, discoveries, like the Aat system of *E. coli*, which shares T1SS elements and accepts substrates from the periplasm, may revise our understanding of a T1SS in the future [135]. T1SSs show similarities to other tripartite systems for instance the major facilitator superfamily (MFS) efflux systems, like EmrAB-TolC [136], resistance-nodulation-division-type (RND-type) efflux pumps, like AcrAB-TolC [137], or other non-T1SS tripartite efflux systems, like MacAB-TolC [138]. All share the tripartite assembly of an IM transporter, a MFP and an OMP, but differ in functionality of the transporter. While the MacAB-TolC system also possesses an ABC transporter, it binds substrates in the periplasm instead of the cytosol and transports multiple small molecules to the extracellular space (for details see chapter 1) [139]. The MFS tripartite efflux systems transport substrates from the cytosol to the extracellular space but contain a secondary active transporter and use the PMF instead of ATP to power the secretion [140]. The RND-type tripartite efflux systems use the PMF via a secondary active transporter as well and secrete various small molecules from the periplasm to the extracellular space [141].

The hemolysin A (HlyA) T1SS was the first described T1SS. It was discovered in uropathogenic *E. coli* in 1951, however the first steps to determine its molecular

architecture were published in 1985 [142, 143]. Since then several different T1SSs in Gram-negative bacteria have been described [144-147]. Different approaches were used to classify T1SSs into subgroups according to the identity of the ABC transporter or the transported substrate and its transport mechanism [8, 148]. The classification according to the ABC transporter is based on its N-terminus. Three different groups were defined by presence of either a C39 peptidase domain, a C39 peptidase-like domain (CLD) or no N-terminal appendix [148]. The classification according to the substrate and its transport mechanism defines five groups (a – e): repeats in toxin (RTX) proteins (a), non-RTX Ca^{2+}-binding proteins (b), non-RTX proteins (c), class II microcins (d) and lipoproteins (e) [8]. Until today the HlyA T1SS from uropathogenic *E. coli* is one of the best studied T1SSs [149-154]. It is classified as group 2 T1SS, containing an ABC transporter with a CLD or as group a, secreting an RTX protein [8, 148]. The components of the HlyA T1SS are the ABC transporter HlyB, the MFP HlyD, the OMP TolC and the substrate HlyA.

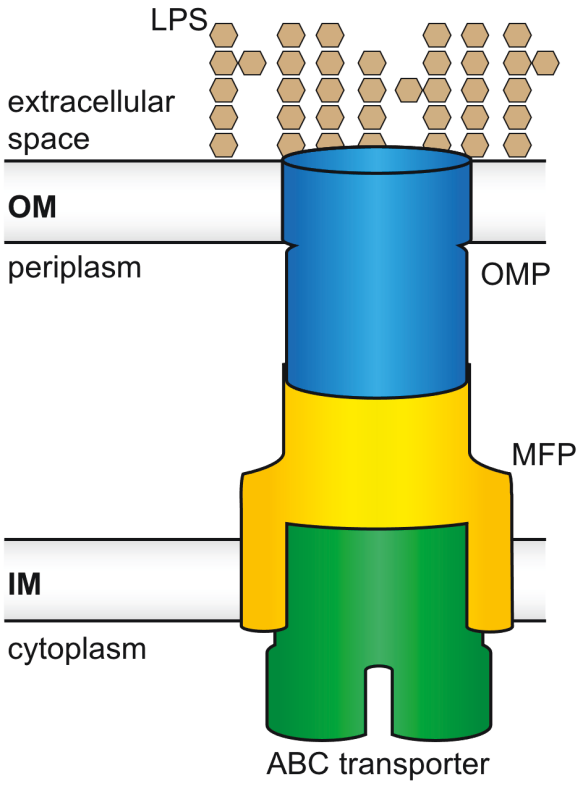

***Figure 6: Schematic of type 1 secretion systems**. IM: inner membrane. OM: outer membrane. LPS: lipopolysaccharides. The ABC transporter (green) in the inner membrane (IM) powers secretion of the substrate from the cytoplasm through the membrane fusion protein (MFP) (yellow) and outer membrane protein (OMP) (blue) to the extracellular space in one step. The peptidoglycan has been omitted for reasons of clarity. This figure makes no claim to the accuracy of the stoichiometry or scale.*

1.5. The HlyA T1SS

1.5.1. The substrate – Hemolysin A

The substrate HlyA belongs to the repeats in toxin (RTX) protein family and contains glycine-rich nonapeptide sequences (GG repeats) with a consensus sequence of GGxGxDxUx, where U is a large hydrophobic amino acid and x is any amino acid [155]. Those GG repeats are capable of binding calcium ions with a µM affinity and promote folding of the toxin in the extracellular space [156, 157]. HlyA contains at least six of those GG repeats which are located close to the C-terminus and build the RTX domain [158]. Tightly controlled calcium ion levels in the nM range in the cytosol prevent calcium ion binding prior to secretion [159]. Overall HlyA consists of 1024 amino acids with a size of 110 kDa (Figure 7) [142, 160]. Besides the RTX domain, it contains a large N-terminal hydrophobic domain that interacts with the target cell membrane after secretion [161]. Acylation of the two lysin residues K564 and K690 strongly influences hemolytic activity of HlyA [162]. It was shown that acylation is only required for lysis, but not for membrane binding and insertion [163, 164]. Acylation is performed by the cytosolic acyltransferase HlyC and the acyl carrier protein (ACP) [165]. Interestingly non-acylated HlyA, also referred to as pro-HlyA, is secreted just as efficient as HlyA [166]. Within the very last 50 - 60 amino acids, HlyA contains a C-terminal secretion signal that is most likely recognized due to the formation of an amphipathic helix rather than a consensus sequence [133, 152, 167, 168]. In addition, a truncated version of HlyA (HlyA1) was identified, that contains a C-terminal fragment with a size of 23 kDa, which is sufficient for secretion [169, 170]. The secretion signal is not cleaved during secretion and secretion occurs in an unfolded state with the C-terminus first [171]. Recently it was postulated that efficient secretion of HlyA via its T1SS is effected by the distance between secretion signal and the most C-terminal GG repeat enabling simultaneous binding to the IMC [153].

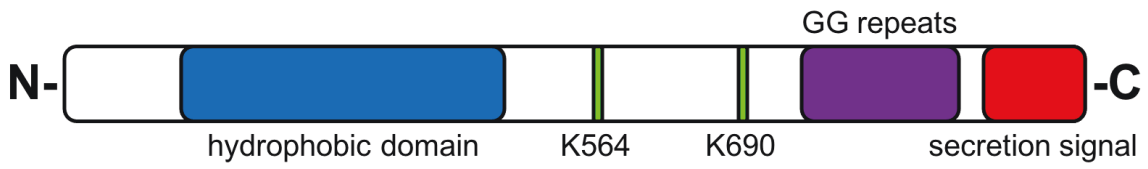

Figure 7: Schematic view of HlyA primary structure. *The hydrophobic domain whichis proposed to interact with the target membrane is shown in blue. The lysines, K564 and K690, that are acylated by HlyC are highlighted in green. The area of the GG repeats (RTX domain) is coloured in purple. The C-terminal secretion signal is coloured in red. N- and C-terminus are indicated.*

1.5.2. The inner membrane complex – Hemolysin B and Hemolysin D

The IMC of the HlyA T1SS is formed by the ABC transporter HlyB and the MFP HlyD. It was shown already in 1998 that HlyB and HlyD form a complex in the IM even in the absence of the substrate HlyA [172]. Recently, the single particle cryo-EM structure of the IMC provided important and unexpected insights into the stoichiometry and organisation of the complex [154]. HlyB adapts a trimer of dimers within the IMC and each dimer is flanked by two copies of HlyD. This results in an assembly of six copies of each protein with a molar ratio of HlyB to HlyD of 1: 1. Unfortunately the large periplasmic part of HlyD is not well resolved due to its intrinsic flexibility [154] (Figure 8).

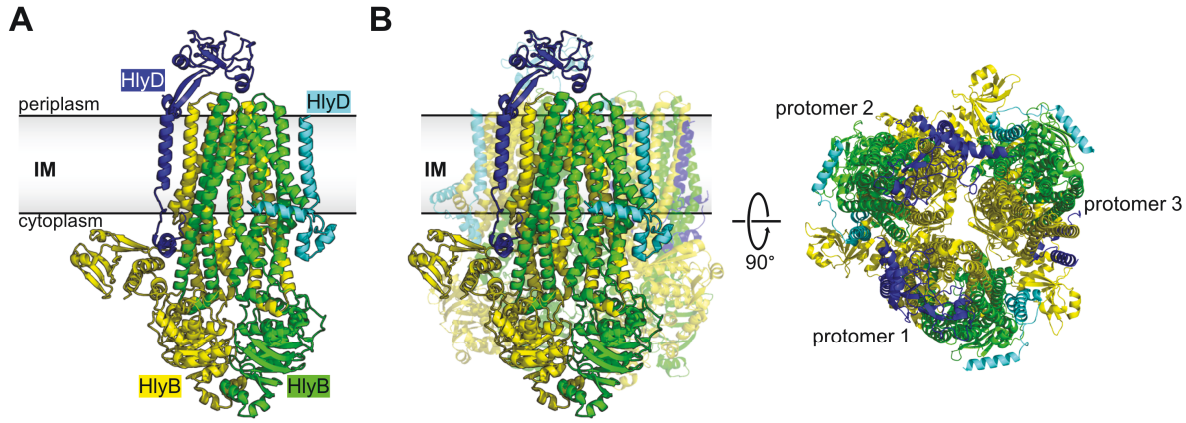

Figure 8: Structure of the inner membrane complex (IMC) of the HlyA T1SS. *PDB: 7SGR. IM: inner membrane* ***A:*** *Structure of one protomer of the IMC. Two copies of HlyB (yellow and green) and two copies of HlyD (blue and cyan) are shown. The other two protomers are omitted for reasons of clarity. The CLD of only one HlyB monomer (yellow) was resolved. The periplasmic parts of HlyD were not resolved, except for one beta-barrel domain of (blue).* ***B:*** *Structure of the IMC with all three protomers. HlyB is shown in yellow and green. HlyD is shown in blue and cyan. The CLD of only one HlyB monomer (yellow) was resolved. The periplasmic parts of HlyD were not resolved, except for one beta-barrel domain of (blue).* ***Left:*** *Side view of the IMC. The protomer in the front is highlighted, the two in the back are slightly transparent.* ***Right:*** *Top view of the IMC. The three different protomers are indicated.*

One component of the IMC is the ABC transporter HlyB, which consists of 707 amino acids with a molecular weight of 79 kDa [160]. HlyB is a member of the ABC half-size transporter family and therefore active as a dimer [173]. It contains three domains: a C39 peptidase-like domain (CLD), followed by a transmembrane domain (TMD) and a nucleotide binding domain (NBD) [174-177]. The CLD was shown to lack peptidase activity but interacted with the unfolded substrate HlyA [177]. Furthermore, it was shown that the CLD has a regulatory effect on the basal ATPase activity of HlyB demonstrated by increase of basal ATPase activity of a HlyBΔCLD variant [150]. The

TMD of HlyB comprises six transmembrane helices (TMH) that sum up to 12 TMH in the dimer. Based on the TMD fold HlyB is classified as a type IV ABC transporter [178]. This class has a domain-swapping arrangement in the TMD and two short coupling helices per TMD connecting to the NBDs [178, 179]. The NBDs of HlyB provide the energy for the transport via ATP binding and hydrolysis [176, 180-182]. They contain the conserved motifs: Walker A (GxxGxGKS, x being any amino acid), Walker B (hhhhDE, h being a hydrophobic amino acid), Pro-loop, A-loop, D-loop, Q-loop, H-loop and C-loop with the ABC signature motif (LSGGQ) [176, 183]. The NBDs dimerize upon ATP binding in a way that Walker A, Q-loop and Walker B from one NBD together with the C-loop of the other NBD form the so-called nucleotide binding site (NBS). A histidine residue at position 662 was identified to be the 'linchpin' in this complex interaction network [183].

The other component of the IMC is the MFP HlyD, which consists of 478 amino acids and has a size of 55 kDa [160]. It contains an N-terminal cytosolic domain, one TMH, and a large periplasmic domain, which can be subdivided into a beta-barrel domain, a lipoyl domain and an alpha-helical domain [154, 174, 184]. In contrast to MFPs involved in drug efflux systems, HlyD and other MFPs operating in T1SSs lack a membrane proximal domain [8, 131]. The N-terminal cytosolic domain of HlyD forms an amphipathic helix and contains a small cluster of charged amino acids. These two features are important for substrate binding and subsequent TolC recruitment [172, 185]. Interestingly the structure of the IMC revealed that the charged cluster at the N-terminus of HlyD interacts with the CLD of HlyB, forming an essential electrostatic interaction network. In addition, HlyD interacts via its TMH with the HlyB TMD via nonpolar interactions [154]. The exact role of the beta-barrel and lipoyl domain still remain elusive, although structural information is available. However, truncation of the last 10 C-terminal amino acids, relating to the beta-barrel domain, completely abolishes secretion of HlyA [184]. The structure of the alpha-helical domain was derived from the crystal structure of a soluble periplasmic part of HlyD, containing the alpha-helical domain and the lipoyl domain [186]. A pulldown assay with the crystalized construct supports a tip-to-tip interaction between the alpha helical tip of HlyD and the OMP TolC [186].

1.5.3. The outer membrane protein – TolC

The OMP of the HlyA T1SS is TolC [187]. It is a protein of 493 amino acids and has a size of 54 kDa. It forms a homotrimer in the outer membrane and possesses a large periplasmic part [188]. In 2000 the structure of TolC revealed a so far unique architecture [189]. TolC builds a single beta-barrel pore in the outer membrane and a long alpha-helical barrel in the periplasm (Figure 9A). With a length of 140 Å TolC protrudes far into the periplasm. While the beta-barrel is a solvent accessible cavity, the alpha-helical barrel seals the tunnel at the far periplasmic tip [189]. Mutational analysis of the periplasmic tip indicated an iris-like opening of TolC, that might be triggered by interaction with other components of a tripartite assembly [190]. A complete open conformation of the periplasmic tip was visualized in the structures of tripartite assemblies of TolC with MacAB or AcrAB [138, 191] (Figure 9B). TolC is not only part of the HlyA T1SS but also part of other tripartite efflux systems, like the MacAB-TolC multidrug efflux system, the AcrAB-TolC RND-type efflux system or the EmrAB-TolC efflux complex [136, 138, 192]. However, the amount of TolC in the bacterial cell is limited which strengthens the assumptions that the tripartite assemblies are transient [193]. For the HlyA T1SS it was shown that recruitment of TolC occurs only upon substrate recognition [172]. Also *in situ* studies on AcrAB-TolC revealed a large number of subcomplexes that were lacking TolC [194]. Furthermore, it was shown that the affinity of TolC to MFP differs between the systems and is influenced by the oligomerisation kinetic of the MFP and the pH [195].

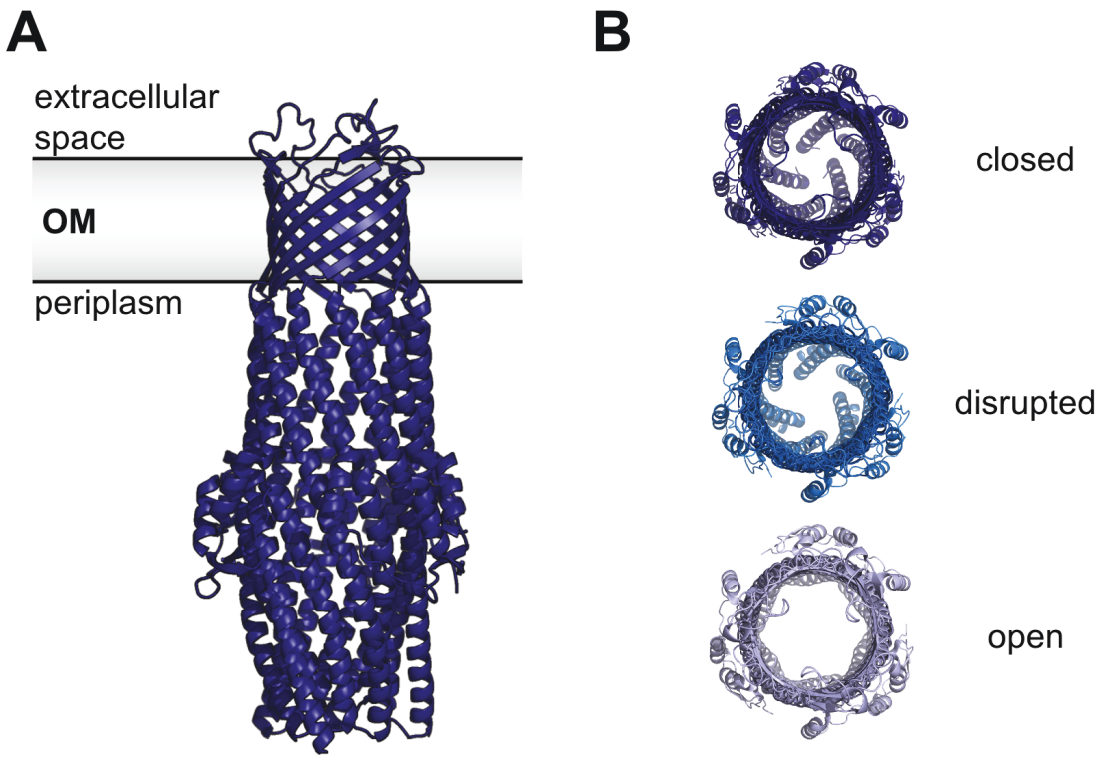

Figure 9: Structure of the outer membrane protein (OMP) TolC. *OM: outer membrane.* ***A:*** *Side view of TolC (dark blue) in its closed state (PDB: 1EK9).* ***B:*** *Top view through TolC from beta-barrel down to the periplasmic alpha-helical barrel. TolC is shown in a closed (dark blue), mutationally disrupted (blue) and open (light blue) state. PDB: 1EK9 (closed), 2XMN (disrupted), 5NIL (open).*

1.5.4. The secretion process of HlyA

The HlyA T1SS from *E. coli* is genetically organised as an operon containing four genes: *hlyCABD* [160, 196]. While *hlyA* codes for the substrate HlyA, *hlyB* codes for the ABC transporter HlyB and *hlyD* codes for the MFP HlyD. The fourth gene, *hlyC*, codes for an acyltransferase called HlyC. Interestingly, the OMP TolC is part of the HlyA T1SS but not encoded in the *hly* operon [187]. Transcription regulation of the *hly* operon is not yet fully understood. A stem-loop transcription terminator-like structure between *hlyA* and *hlyB* was identified and in line with this finding different transcripts containing either *hlyCA* or *hlyCABD* were isolated *in vivo* [142, 196]. Furthermore, it was shown that RfaH can enhance transcript elongation of *hlyCABD* [197]. In addition, specific motifs upstream of the operon were identified to regulate hly gene expression in cooperation with RfaH [198, 199]. Ones HlyC and HlyA are produced, HlyC acylates HlyA in the cytosol prior to secretion in an acyl carrier protein dependant manner [165]. The acylation of HlyA is relevant for its efficient lytic activity, but not for the secretion process across inner and outer membrane [162, 166]. HlyA that is missing this

acylation is referred to as pro-Hemolysin A (pro-HlyA) [165]. So far no chaperone was identified to stabilize unfolded HlyA in the cytosol [129]. Nevertheless, it was shown that secretion efficiency relies on a slow folding rate of the substrate [200]. The IMC of HlyB and HlyD forms independent of HlyA or TolC and increases stability of the proteins involved [172, 201]. Binding of HlyA to the HlyD recruits TolC to the IMC [172]. The amount of TolC in the outer membrane is constant and does not change with overexpression of the HlyA T1SS components [193]. Furthermore, the HlyA T1SS does not show polarized localisation but random cluster distribution [193]. This is in contrast to T3SSs and T4SSs which showed such a polarized localisation [202-204]. HlyA can simultaneously bind via its amphipathic helix and the GG repeats to the different domains of HlyB, which is supposed to be necessary for sufficient secretion [153]. HlyA is secreted with a speed of approximately 16 amino acids per second per transporter and independent of extracellular calcium levels with the C-terminus first in an unfolded state [149, 171]. Recent structural and biochemical data propose a secretion mechanism, where all three HlyB dimers hydrolyse ATP to generate energy for the transport, but only one dimer secretes the substrate through its dimer interface [154]. In the extracellular space HlyA folds upon calcium binding to its hemolytic active form [156]. It is assumed that IMC and TolC disassemble after successful secretion of the substrate (Figure 10).

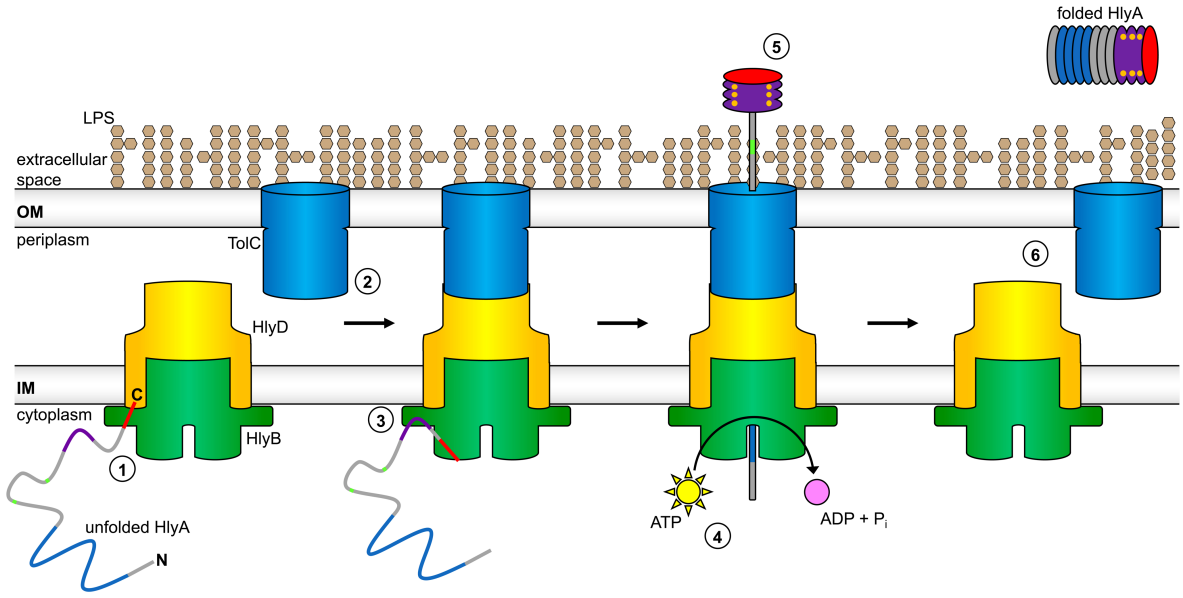

Figure 10: Schematic of the secretion of HlyA via its T1SS. *IM: inner membrane. OM: outer membrane. LPS: lipopolysaccharides. HlyD (yellow) recognizes the C-terminus of unfolded HlyA (grey line)* ***(1)*** *and recruits TolC (blue) to the inner membrane complex (IMC)* ***(2).*** *HlyB (green) binds simultaneously secretion signal (red) and RTX domain (purple) of HlyA. Upon hydrolysis of ATP (yellow sun) to ADP + P_i (pink circle) by HlyB* ***(4)****, HlyA is secreted in one step with the C-terminus first from the cytosol to the extracellular space. In the extracellular space the RTX domain binds calcium (orange dots) and promotes folding of HlyA* ***(5)****. After successful secretion the T1SS disassembles again into IMC and TolC* ***(6)****. The peptidoglycan has been omitted for reasons of clarity. This figure makes no claim to the accuracy of the stoichiometry or scale.*

2. Aims

The HlyA T1SS was first discovered in 1951 in uropathogenic *E. coli* strains and is one of the best studied T1SSs today [143]. Although only three proteins are involved in building the secretion system and naturally only one specific substrate is translocated, the exact interplay between all components of the T1SS is not fully understood yet [7, 142]. The ABC transporter HlyB and the MFP HlyD form the IMC in the inner membrane and the OMP TolC forms the conduit in the OM. The systems substrate is the pore forming RTX protein HlyA. The IMC is assembled even in the absence of the substrate HlyA and only upon recognition of the substrate by HlyD, the OMP TolC is recruited to the IMC [172]. HlyA is recognized by HlyB via its secretion signal and the RTX domain. This dual recognition is necessary for successful and efficient secretion [153]. When the projects of this thesis were started, structures were available only for the NBD and the CLD of HlyB and for a periplasmic part of HlyD [176, 177, 186]. The structure of the IMC was only recently published, shortly before the projects described in this thesis were finalised [154].

The main aim of this thesis was to set up an *in vitro* reconstitution of the HlyA T1SS, in order to investigate its assembly and function in a controlled environment. This approach would allow to investigate for example the number of hydrolysed ATP molecules per transported substrate or the influences of different conditions on transport efficiency, like lipids, ion concentration gradients or pH. To set up such an *in vitro* transport assay it is essential to purify and reconstitute the different components of the T1SS in an active state. For this reason, both the ABC transporter HlyB as well as the IMC were topics of this thesis. The purification and reconstitution of the OMP TolC was already established previously, as well as the purification of the truncated substrate HlyA1 [205].

For the ABC transporter HlyB, the aim was to solve the structure on the one hand and investigate influences of the lipid bilayer on the other hand. Therefore, purification as well as reconstitution of the protein was necessary. The idea was to optimize a previously published protocol [151] and improve sample quality for structural studies via cryo-EM.

For the IMC, the aim was not only to establish functional reconstitution for an *in vitro* transport assay, but also to purify the IMC to enable structural investigations. The IMC should be purified from membranes or assembled from its individual components after these have been purified separately.

Besides HlyA, numerous RTX toxins are known and transported via a T1SS, such as the homologous RtxA T1SS from the Gram-negative pathogen *Kingella kingae* [206]. The investigation of such homologous systems can be very useful as they can provide insights into conserved structural and functional motifs or molecular differences specific to the investigated system. Furthermore, homologs can exhibit a higher stability which is beneficial for structural analysis. Therefore an additional aim of this thesis was the biochemical characterization and structural investigation of the ABC transporter RtxB from the RtxA T1SS from *Kingella kingae*. For this purpose RtxB should be expressed, purified and reconstituted.

3. Publications

3.1. Chapter 1: ABC Transporters in Bacterial Nanomachineries

Title: ABC Transporters in Bacterial Nanomachineries

Authors: **Florestan L. Bilsing**, Manuel T. Anlauf, Eymen Hachani, Sakshi Khosa, Lutz Schmitt

Published in: International Journal of Molecular Sciences (2023)
Impact Factor: 5.6 (2023)

Own contribution: Writing of the manuscript

International Journal of
Molecular Sciences

MDPI

Review

ABC Transporters in Bacterial Nanomachineries

Florestan L. Bilsing, Manuel T. Anlauf, Eymen Hachani, Sakshi Khosa and Lutz Schmitt *

Institute of Biochemistry, Heinrich Heine University, Universitätsstr. 1, 40225 Düsseldorf, Germany
* Correspondence: lutz.schmitt@hhu.de; Tel.: +49-211-81-10773; Fax: +49-211-81-15310

Abstract: Members of the superfamily of ABC transporters are found in all domains of life. Most of these primary active transporters act as isolated entities and export or import their substrates in an ATP-dependent manner across biological membranes. However, some ABC transporters are also part of larger protein complexes, so-called nanomachineries that catalyze the vectorial transport of their substrates. Here, we will focus on four bacterial examples of such nanomachineries: the Mac system providing drug resistance, the Lpt system catalyzing vectorial LPS transport, the Mla system responsible for phospholipid transport, and the Lol system, which is required for lipoprotein transport to the outer membrane of Gram-negative bacteria. For all four systems, we tried to summarize the existing data and provide a structure-function analysis highlighting the mechanistical aspect of the coupling of ATP hydrolysis to substrate translocation.

Keywords: ABC transporter; nanomachineries; Mac system; Lpt system; Mla system; Lol system

check for updates

Citation: Bilsing, F.L.; Anlauf, M.T.; Hachani, E.; Khosa, S.; Schmitt, L. ABC Transporters in Bacterial Nanomachineries. *Int. J. Mol. Sci.* **2023**, *24*, 6227. https://doi.org/10.3390/ijms24076227

Academic Editor: Anthony M George

Received: 24 February 2023
Revised: 18 March 2023
Accepted: 23 March 2023
Published: 25 March 2023

1. The Classical View of an ABC Exporter

ATP-Binding Cassette (ABC) transporters are present in all domains of life, from prokaryotes to eukaryotes [1]. ABC exporters consist of two nucleotide-binding domains (NDBs) and two transmembrane domains (TMDs) [2,3]. The NBDs are responsible for binding and hydrolyzing ATP, and the TMDs allow substrate translocation across the membrane [4]. The conformational changes of the NBDs, due to ATP binding and hydrolysis, are translated via coupling helices to the TMDs [5,6]. While the NBDs are highly conserved among all ABC transporters, the TMDs show a huge variety that goes in line with the huge variety of ABC transporter substrates [7]. Within this review, we will focus on prokaryotic ABC exporters functioning in nanomachineries. Some of the prokaryotic ABC exporters are "half-size" transporters with one NBD and one TMD fused together on a single polypeptide chain, while most harbor NBDs and TMDs as separate polypeptide chains allowing heterooligomeric assemblies (see Figure 1) [3].

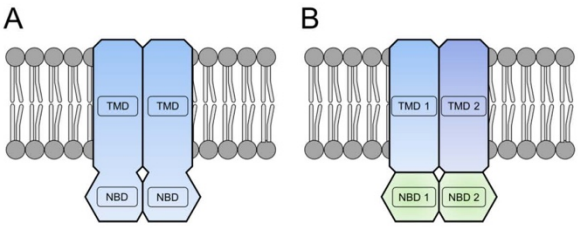

Figure 1. Domain organization of prokaryotic ABC exporters. (**A**)**:** Half-size homodimer. (**B**)**:** Single domain heterodimer. TMD = transmembrane domain. NBD = nucleotide-binding domain. The TMD and NBD are either fused on one polypeptide chain (**A**) or exist as separate polypeptides (**B**).

Without any structural information, Jardetzky et al. proposed already in 1966 two configurations for a membrane transporter enabling a 'two-sided access' to a central cavity

within the transporter [8]. Today we know from multiple protein structures that most of the ABC exporters change during substrate translocation from an inward-facing (IF) state to an outward-facing (OF) state [9–13]. This model of a translocation cycle (see Figure 2) was extended by the outward-occluded state observed for the peptide transporter McjD [14] and for other exporters as well [15]. New findings revealed even more transition states within one translocation cycle [16]. Besides this classical understanding of changing between IF and OF states, there are further models expanding the mechanisms for substrate translocation. On the one hand, there is the alternate access model, where a substrate is not entering from the cytoplasm but from a lateral opening in the TMDs (PCAT1 [17]). On the other hand, there is the outward-only model, where the substrate cavity is open and closing without an inward-facing state (PglK [18]). Similar to this outward-only model, simulations suggested a Constant Contact Model of the NBDs without a wide open IF state [19].

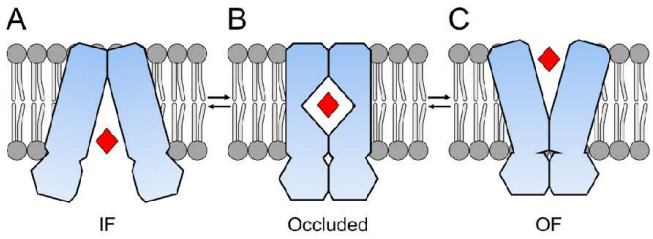

Figure 2. Schematic of a transport cycle of a type IV ABC exporter. (**A**)**:** In the inward-facing (IF) conformation, the transporter binds the substrate. (**B**)**:** During substrate translocation across the membrane, the occluded state is formed with the substrate pocket closed to the inside and outside. (**C**)**:** The transporter adopts the outward-facing (OF) conformation, and the substrate leaves the transporter to the outside.

The power stroke for transmission from IF to OF state, and along with this, the substrate translocation, is supposed to be the binding of ATP. ATP hydrolysis, therefore, only resets the system back into the IF state [20,21]. Moreover, it is conceivable that there is a difference in the power stroke for heterodimeric ABC exporters that contain an intrinsically impaired nucleotide binding site, as it is proposed for BmrCD. Here, turnover from IF to OF state is exclusively attributed to ATP hydrolysis [22]. In addition, novel findings on the homodimeric ABC exporter MacB award at least a part of the power stroke for substrate translocation to the ATP hydrolysis step [23].

Based on the variety of TMDs, a new nomenclature was introduced to categorize ABC transporters on the basis of the different TMD folds into seven different types [24]. Type I–III cover classical ABC importers, and type IV to VII mostly cover ABC exporters. A large number of structures and functional information are known for the type IV ABC transporters that are defined by the architecture of Sav1866. Type V also includes a few ABC transporters with importer functions. Type VI ABC transporters are defined by the fold of $LptB_2FG$ and Type VII by the fold of MacB [24]. These classes of Type VI and VII are of special interest for this review and are complemented by the MlaFEDB system (recently assigned as founding member of type VIII [25]) and the LolCDE system (type VII). Although the classical understanding of the transport cycle from an IF state to an OF state with an occluded state trapping the substrate in a binding pocket is feasible for small substrates such as ions, amino acids, or even smaller peptides, this model cannot apply to large substrates such as lipopolysaccharide (LPS) or lipoproteins. In the following sections, we will summarize the recent findings with respect to the structure and function of these selected ABC transporter systems of MacB, $LptB_2FGC$, MlaFEDB, and LolCDE (Figure 3) as a wide range of information is available for these nanomachineries.

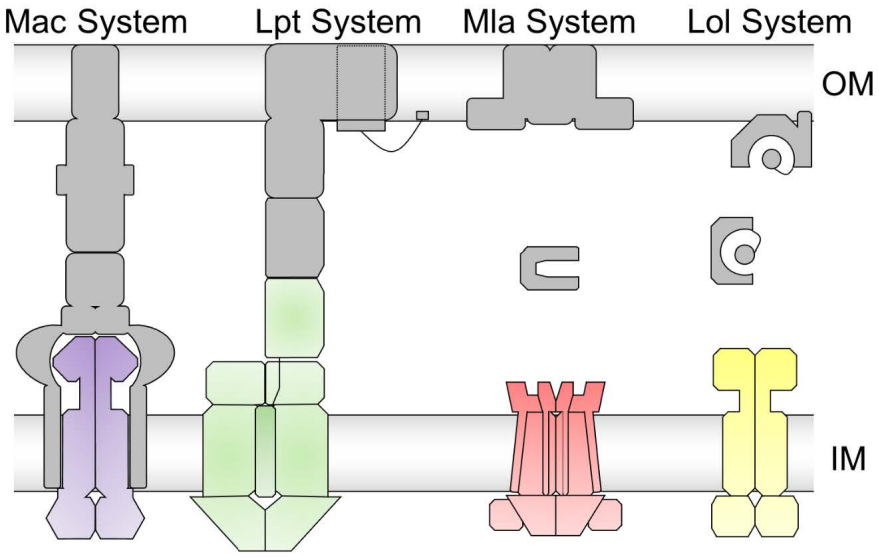

Figure 3. Schematic representation of the Mac, Lpt, Mla, and Lol system. For the Mac system, the ABC transporter MacB is shown in purple. The membrane fusion protein MacA and the outer membrane protein TolC are shown in grey. For the Lpt system, the ABC transporter $LptB_2FGC$ is shown in green. The periplasmic protein LptA and the translocon in the outer membrane LptDE are shown in grey. For the Mla system, the ABC transporter MlaFEDB is shown in red. The periplasmic protein MlaC and the outer membrane protein MlaA, together with OmpF, are shown in grey. For the Lol system, the ABC transporter LolCDE is shown in yellow. The periplasmic protein LolA and the outer membrane protein LolB are shown in grey. Inner membrane (IM) and outer membrane (OM) are depicted as grey bars. The peptidoglycan layer is omitted for reasons of clarity.

2. The MacAB-TolC System

The first experimental evidence of an ABC antibiotic efflux transporter in Gram-negative organisms was published in 2001 by Kobayashi et al. [26]. They investigated a system that gave resistance to erythromycin and other macrolide-type antibiotics and was therefore termed macrolide-specific ABC-type efflux carrier, short "MacAB". Furthermore, they showed that TolC is necessary for MacAB efflux activity [26]. Today it is known that the MacAB-TolC system also exports the extracellular peptide toxin STII [27], the heme precursor protoporphyrin IX [28], cyclic peptides like bacitracin and colistin [29], and penicillin-type antibiotics as well as arsenite [30]. Furthermore, overexpression of MacAB in *Klebsiella pneumoniae* increased resistance against the synthetic tetracycline-class antibiotic eravacycline [31]. All substrates of the MacAB-TolC system are transported from the periplasm across the outer membrane to the extracellular space [27,29]. Interestingly *macB* homologs can be found in Gram-positive bacteria as well, although they lack a periplasm and a second membrane (reviewed in Greene et al. [32]). The expression of *macA* and *macB* is controlled by the PhoP/PhoQ system [33] and therefore downregulated in case of low Mg^{2+} levels, which was shown using real-time quantitative polymerase chain reaction (rt-qPCR) [34].

The structure of the outer membrane protein TolC was determined in 2000 by Koronakis et al. [35]. Due to DNA sequence analysis, it was already proposed in 2001 without having a high-resolution structure that MacB is a transmembrane protein with four transmembrane helices (TMH) and that MacA is a peripheral membrane protein belonging to the membrane fusion protein (MFP) family [26]. Biochemical and biophysical data by

Lin et al. revealed in 2009 that MacA stabilizes the tripartite assembly of the MacAB-TolC efflux system through specific interactions with MacB as well as TolC. In addition, it was shown that the N-terminal transmembrane helix of MacA, anchoring it into the inner membrane, is not essential for the functional assembly of the system [36]. In contrast, Tikhonova et al. could show that a MacA mutant lacking the N-terminal transmembrane helix was not able to confer an increase in erythromycin resistance in vivo, although in vitro studies showed that this mutant can still interact with MacB [37]. Furthermore, MacA increases MacB's affinity for ATP and the substrate erythromycin. Mass spectrometry (MS) and atomic force microscopy (AFM) revealed a dimeric organization of MacB [36]. Bound lipids such as phosphatidylethanolamine (PE) and cardiolipin could only be observed for the dimeric protein using detailed MS analysis [38]. In 2009, the first crystal structure of the periplasmic domain of MacB [39], as well as the crystal structure of a hexameric arrangement of the periplasmic part of MacA from *Actinobacillus actinomycetemcomitans* [40], became available. Further analysis of the interface between MacA and TolC supported a strongly conserved tip-to-tip interaction between those two proteins [41–43]. In 2017, the single-particle cryo-EM structure of the fully assembled MacAB-TolC efflux system (see Figure 4) from *Escherichia coli* (*E. coli*) was published in a nucleotide- and substrate-free conformation by Fitzpatrick et al. [44]. This structural information on the MacAB-TolC system was complemented by an ADP-bound crystal structure of MacB from *Acinetobacter baumannii* published by Okada et al. [45] and an ATP-bound crystal structure of MacB from *Aggregatibacter actinomycetemcomitans* published by Crow et al. [29] in the same year (see Figure 5). Moreover, the crystal structure of a Gram-positive MacAB-like efflux pump from *Streptococcus pneumoniae* was published by Yang et al. in 2018 [46].

The structure of the full MacAB-TolC efflux system was derived by Fitzpatrick et al. [44] from a hybrid electron density map combining density maps from two different stabilizing approaches of the tripartite assembly. The first approach was a fusion of the C-terminus of MacB to the N-terminus of MacA as they were expected to be in close proximity. Interestingly, the fusion construct resolved only two copies of MacB, which were forming the dimer in the inner membrane. The other four copies of MacB, each fused to one MacA, were not resolved in the electron density map but produced diffuse density in the two-dimensional classifications. The second approach was a stabilization using disulfide bonds between MacA and MacB introduced via cysteine mutations. Only two of the MacA protomers formed a disulfide bond with MacB. Both approaches stabilized MacAB-TolC sufficiently for the acquisition of high-resolution structural data without loss of functionality in vivo [44]. This confirmed the overall organization of the MacAB-TolC system comprising a dimer of MacB in the inner membrane linked to a hexamer of MacA in the periplasm, which in turn is connected to a trimer of TolC in the outer membrane. This tripartite assembly with approximately 320 Å spans the inner and outer membrane in vivo [44].

Within the fully assembled complex, MacA adopts a hexameric structure, as seen for MacA alone [40], with four domains: a cylindrical α-helical hairpin domain, a ring-forming lipoyl domain, a ring-forming β-barrel domain, and a membrane-proximal domain. A density for the N-terminal transmembrane helix was missing, just as for the already existing crystal structure [40]. The already proposed tip-to-tip interaction between the trimeric TolC and MacA [41,42] was located between the α-helical hairpin region of MacA and the intra- and inter-protomer grooves of TolC [44]. A loop in the lipoyl domain of MacA allows highly conserved glutamine residues [40] to form an inter-protomer hydrogen-bond network that acts like a gating ring. Molecular dynamics simulations suggested that this gating ring acts as a one-way valve for the outward-directed transfer of the substrate [44]. The β-barrel domain and the membrane-proximal domain from three MacA protomers interact with the periplasmic domain of one MacB protomer [44].

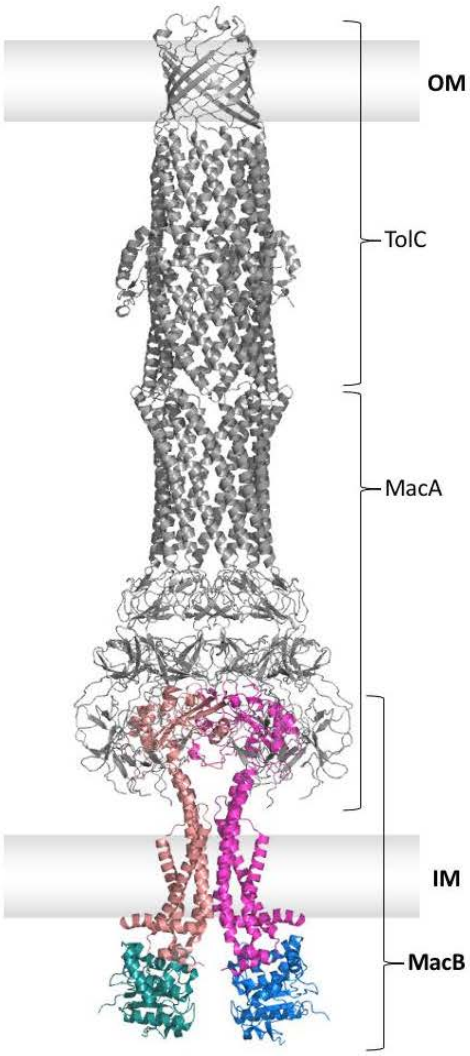

Figure 4. Single particle cryo-EM structure of the assembled MacAB-TolC efflux system (PDB entry 5NIL). Trimeric TolC and hexameric MacA are shown in grey and dimeric MacB in color. The nucleotide-binding domains of MacB are shown in deep teal and marine, and the transmembrane domains, plus the periplasmic part, are shown in salmon and light magenta. The outer membrane (OM) and inner membrane (IM) are displayed as grey boxes. The peptidoglycan layer is omitted for reasons of clarity.

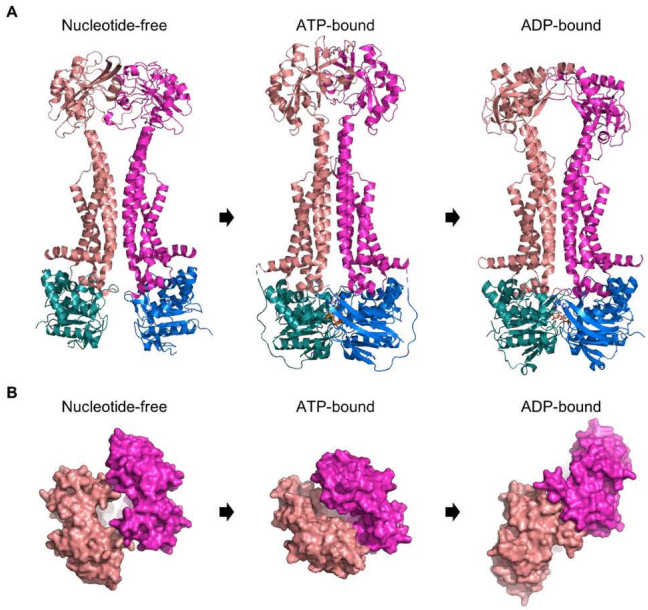

Figure 5. Structures of MacB in a nucleotide-free (PDB entry 5NIL), ATP-bound (PDB entry 5LIL), and ADP-bound (PDB entry 5WS4) state. NBDs are shown in deep teal and marine, and the TMDs with the periplasmic part are shown in salmon and light magenta. (**A**)**:** Side view of MacB in the different nucleotide-free/-bound states. (**B**)**:** Top view of the periplasmic part of MacB in the different nucleotide-free/-bound states.

MacB forms a homodimer in the tripartite assembly, with each protomer consisting of a NBD, a TMD, and a periplasmic domain (PD). The NBD is connected to the TMD via a long loop and an amphipathic helix. The TMD of MacB is unlike other ABC transporters, built up by only four TMH. TMH1 and TMH2 are elongated and reach above the membrane plane into the periplasm. In between these two helices, the PD is located. This PD contains a so-called porter domain that is a structural homolog to the AcrB "porter domain" and a sabre (small alpha beta-rich extracytoplasmic) domain. The porter domain is formed by two subunits that are located before and after the sabre domain. TMH3 and TMH4 are shorter than TMH1 and TMH2 and are connected via the so-called shoulder loop [29]. The major coupling helix is located in between TMH2 and TMH3; the minor coupling helix is located C-terminal of TMH4 [44]. The major and minor coupling helix interact with the NBD from the same protomer as there is no domain swapping [29]. The role of the minor coupling helix is not fully understood as, according to Crow et al. [29], the deletion of this helix did not influence MacB activity significantly, but for Okada et al. [45], deletion of the minor coupling helix resulted in the loss of drug export.

Although substrate-bound structures are lacking, the nucleotide-free MacAB-TolC cryo-EM structure [44], together with the ATP-bound crystal structure [29] and the ADP-bound crystal structure [45], allow prediction about the function of MacAB-TolC mediated efflux.

In the nucleotide-free state (see Figure 5A, left panel), the transmembrane dimer interface adopts a V-shape form having the periplasmic parts of TMH1 and TMH2 of one protomer far away from the other protomer and thereby forming a cavity on the periplasmic site margined by the periplasmic domains of MacB. This arrangement also brings the periplasmic domains into an open conformation forming a small gap towards

the periplasm (see Figure 5B, left panel). In the cryo-EM structure, an additional electron density was observed in this periplasmic cavity between the periplasmic elongations of the TMHs. The orientation of this additional density already indicates a lateral substrate entrance. Nevertheless, it was not possible to examine the identity of this molecule. The NBDs are also separated and far away from each other in the nucleotide-free structure [44]. In the ATP-bound state (see Figure 5A, middle panel), the NBDs are dimerized and form a tightly packed classical head-to-tail arrangement. TMH1 and TMH2 of each protomer align parallel to each other in a rigid dimer interface, omitting the V-shaped form but adopting a so-called "zipped stalk" conformation. The PD adopts a closed form without an opening towards the periplasmic side (see Figure 5B, middle panel). The NBDs dimerization is supposed to mediate the "zipping" of the stalk and closure of the PD via the major coupling helix and movement of TMH2, which changes the dimer interface favoring close proximity of TMH1 and TMH2 of each protomer. This transfer of structural movements from one side of the membrane to the other via the transmembrane helices is referred to as mechanotransmission. The mechanotransmission mechanism was investigated in vivo by using cysteine mutants that lock MacB TMH1 and TMH2 in the zipped conformation. Those mutants showed decreased resistance to erythromycin [29]. In the ADP-bound state (see Figure 5A, right panel), the NBDs are dimerized but not as tight as in the ATP-bound state. TMH1 and TMH2 adopt a V-shape-like open conformation as in the nucleotide-free state, but the PDs arrange differently, and the opening towards the periplasm is absent (see Figure 5B, right panel) [45].

Biochemical data of Tikhonova et al. showed that MacB exhibits basal ATPase activity in detergent, which is little to none affected by the addition of either substrates or MacA or TolC [37]. When reconstituted into proteoliposomes, the basal ATPase activity of MacB is reduced about 10-fold but is strongly stimulated in the presence of MacA. MacA mutants missing either an N- or C-terminal part of MacA could not stimulate MacB ATPase activity in proteoliposomes in vitro and were also not able to increase erythromycin resistance in vivo, although the N-terminal truncated mutant was capable of binding MacB in vitro [37]. Modali et al. revealed that MacA stabilizes the ATP-bound state of MacB, and a single mutation in the membrane-proximal domain of MacA abolishes the macrolide efflux function of MacAB-TolC [47]. Lu et al. discovered that the periplasmic domain of MacB is essential for MacA-dependent stimulation of MacB ATPase activity. Furthermore, ATP binding of MacB increases affinity towards MacA [48]. In 2021, Souabni et al. determined a transport rate of three molecules per hydrolyzed ATP molecule for the substrate roxithromycin [23]. Recently, Batista dos Santos et al. [49] showed that the presence of TolC increases MacB ATPase activity in detergent as well as in lipid nanodiscs. Furthermore, they could also show a substrate-induced increase in MacB ATPase activity for the fully assembled MacAB-TolC system in a lipid environment [49].

Based on the available structures, Crow et al. [29] postulated a mechanism for substrate efflux of the MacAB-TolC system in 2017 termed the "molecular bellows" mechanism. In the nucleotide-free state, the cavity between the periplasmic part of TMH1 and TMH2 of MacB and MacA is open to the membrane, and substrates can enter. Upon ATP binding, the dimerization of the NBDs on the cytosolic side causes closure of the TMDs of MacB and constrains the volume of the cavity. This generates pressure and pushes the substrate through MacA towards TolC. The gating ring inside MacA prevents backflow of the substrate once the pressure is balanced. After ATP hydrolysis, the system switches back to the nucleotide-free open state [29]. This mechanism was further expanded by Souabni et al. [23] in 2021, investigating the role of ATP hydrolysis using a quantum dots-based real-time analysis of substrate transport and ATP turnover. They suggested a "modified bellows mechanism" where ATP hydrolysis is additionally energizing the transport of the substrate across the MacA gating ring towards TolC. In this modified mechanism, MacA and its transmembrane helix act as a mediator for the additional energetic input. In their study, substrate translocation and ATP hydrolysis are shown to be synchronous events [23].

Although much is known due to biochemical and structural data, many open questions remain regarding the function of the MacAB-TolC system. Examples are: How is the substrate recognized? Is there a specific substrate binding site? Is there a feedback mechanism from the periplasm to the NBDs? How is lateral substrate leakage prevented? These questions require further research using intermediate or substrate-bound structures.

3. The Lpt System

The cell envelope of Gram-negative bacteria exhibits a complex architecture. It not only consists of an inner membrane (IM), made up of phospholipids in the inner and outer leaflet, and an additional outer membrane (OM) but also a periplasm in between with a cell wall formed by crosslinked peptidoglycan. The OM protects the cell from the environment and serves as a potent barrier for hydrophobic molecules. Its composition is highly asymmetrical, with glycerophospholipids in the inner leaflet and mainly LPS molecules in the outer leaflet [50,51]. The interested reader is referred to comprehensive reviews focusing on the structure and synthesis of LPS [52–54], as it will be only briefly described here. The LPS structure can vary among different bacteria; typically, it can be divided into three parts: LPS is anchored to the membrane via its Lipid A moiety, a β-1′-6-linked glucosamine disaccharide, every sugar being acylated with fatty acid chains. Additionally, in *E. coli*, the glucosamine is phosphorylated at positions 1 and 4′ and can be further modified, e.g., upon polymyxin exposure with ethanolamine or 4-amino-4-deoxy-L-arabinose to decrease the negative net charge [55,56]. The core oligosaccharide moiety is connected to Lipid A via 3-deoxy-D-manno-oct-2-ulosonic acid (Kdo), which itself is linked with several heptose and hexose molecules. On top of the core oligosaccharide is the O antigen, also called O-antigenic polysaccharide (O-PS); it represents the terminal part of LPS and, as the name suggests, is a polymer made up of different kinds of oligosaccharides. The composition of the O antigen varies greatly, not only between different but also within the same species. *E. coli*, as one example, displays over one hundred different serotypes [52]. LPS is found in most, but not all, Gram-negative bacteria, with exceptions like *Sphingomonas paucimobilis* and *Treponema pallidum* [57,58]. In *E. coli* and *Salmonella*, the presence of LPS is essential, although this is not the case for all LPS-containing bacteria. Certain strains of *Neisseria*, *Moraxella*, and *Acinetobacter* can live without genes necessary for the synthesis or transport of LPS to the OM [59].

The LPS homeostasis displays a delicate challenge. Even though it is exclusively present in the outer leaflet of the OM, the biogenesis starts on the complete opposite side of the cell envelope: The inner leaflet of the IM (and the cytoplasm). Therefore, it does not only need to be extracted from the IM—an energy-consuming process—but the amphipathic LPS molecule also needs to traverse the aqueous periplasm on its route to the OM. Ultimately, the LPS needs to be incorporated into the outer leaflet of the OM. This process must occur repetitively during the life cycle of the cell in a highly ordered manner, as processes in the periplasm and outer membrane cannot be energized directly through ATP hydrolysis.

This part of the review will deal with the LPS transport (Lpt) machinery (see Figure 6), which mediates the extraction of LPS from the IM, its transport across the periplasm, and insertion into the OM. A special focus lies on the ABC transporter, including a step-by-step examination of its functionality and recent discoveries.

Intensive research on the LPS transport over more than five decades, starting with genetic approaches along with biochemical and structural studies, gradually revealed the Lpt system to be a multiprotein assembly with an ABC transporter $LptB_2FGC$ in the inner membrane [60] and a translocon LptDE in the outer membrane [61] which are connected by a periplasmic bridge built up by (most likely) oligomeric LptA [62] (see Figure 6). In this complex, $LptB_2FGC$ provides the energy for the extraction and transport of LPS by ATP binding and hydrolysis. Although its TMD fold is reminiscent to type V ABC transporters, $LptB_2GFC$ is considered to be the first member of the new type VI ABC transporter family, as there are several aspects that led researchers to classify this transporter into its distinct group [24,63].

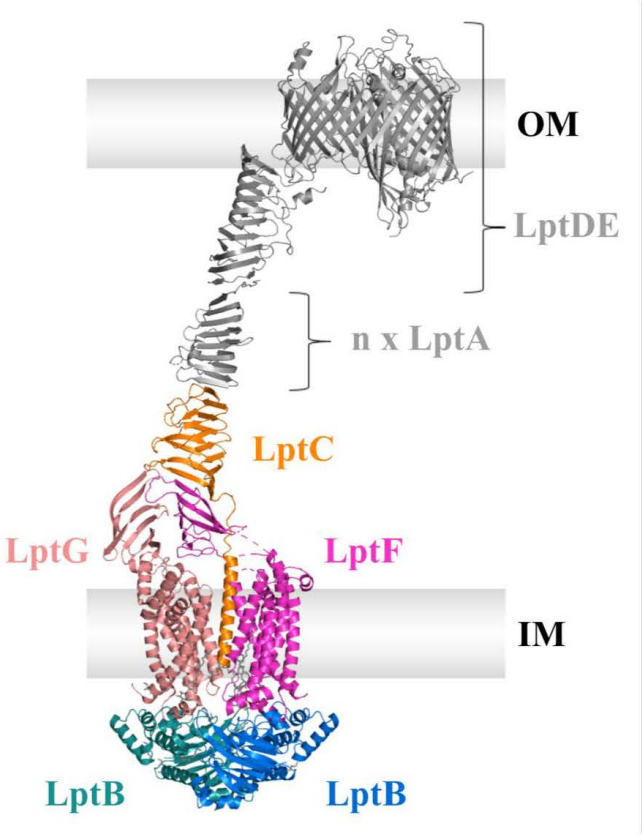

Figure 6. Overview of the Lpt machinery spanning both membranes and the periplasm. Note that the number of LptA oligomers forming the periplasmic bridge is unknown. The figure was created using PyMOL and the PDB entries of LptDE (5IV9, grey in the outer membrane), LptA (2R19, grey in the periplasm), and $LptB_2FGC$ (6MJP, orange, salmon, light magenta, deep teal and marine in the inner membrane). The outer membrane (OM) and inner membrane (IM) are displayed as grey boxes. The peptidoglycan layer is omitted for reasons of clarity.

In the domain organization of the LPS extractor, the two homologous proteins, LptF and LptG, form the TMD [64,65]. Both proteins have an additional periplasmic domain, the so-called β-jellyroll domain. This protein fold is a hallmark of the Lpt system, as it occurs in five of the seven Lpt proteins (LptA, LptC, LptD, LptF, and LptG; see Figure 6). The homo-dimeric LptB shows the fold of a canonical NBD and serves as the motor domain of the extractor. Its structure as an isolated protein was resolved by two independent groups in the same year, Sherman et al. and Wang et al. [66,67]. It is present as a dimer in the cytoplasm, where it binds and hydrolyzes ATP to energize the LPS translocation and forms the functional transporter with LptFG [60]. What makes the LPS transporter complex unique is the presence of a mysterious protein within the inner membrane complex: LptC. It is a small protein, only consisting of an N-terminal TMH and a periplasmic β-jellyroll domain [68]. Like all other Lpt proteins, it is essential for LPS transport, as deletion strains show phenotypes attributed to defective LPS transport, such as increased sensitivity to hydrophobic compounds [69].

LptD and LptE build the translocon in the outer membrane [61,70–73]. LptD is a large, 26-stranded β-barrel protein in which the lipoprotein LptE resides, forming a barrel-and-plug complex. The N-terminal part of LptD features a β-jellyroll domain as well and is connected to the jellyrolls of $LptB_2FGC$ via the periplasmic LptA, in which this protein fold was first discovered [74]. The N-terminal part of LptAs β-jellyroll domain interacts with LptC, while its C-terminal part showed crosslinks to the β-jellyroll domain of LptD. Studies also showed that LptA is capable of forming oligomeric structures in vivo and in vitro, although the exact number of LptA molecules necessary for establishing the periplasmic bridge between the complexes in the IM and OM remains unknown [74–76].

Early models based on initial structures of $LptB_2FG$ by Dong et al. and Luo et al., who only had the transporter in a single functional state available, proposed a sequence in which ATP binding would open the cavity, allowing LPS to enter and subsequent ATP hydrolysis and release of ADP would push LPS out of the transporter [65,77]. Today, additional structures of $LptB_2FG$ together with LptC, bound LPS, and/or bound nucleotide by the groups of Li, Luo, Tang, and Owens suggest the following model [78–81]: In the initial state of the transport cycle, the TMH of LptC ($LptC^{TM}$) resides between LptF and LptG (see Figure 7, state i). LPS enters the cavity first (see Figure 7, state ii) and triggers in a not completely understood manner the release of $LptC^{TM}$. Here, a strict NBD-TMD coupling is apparently involved (see Figure 7, state iii). By this, the cavity narrows, and its residues bind tightly to the LPS molecule and elevate it inside the cavity. The NBDs of $LptB_2$ bind tightly to each other, which results in a complete collapse of the cavity and expulsion of LPS (see Figure 7, state iv). ATP, which can bind before ejection of $LptC^{TM}$, as new data suggest, is hydrolyzed to ADP and released from the NBDs. This reopens the cavity, and $LptC^{TM}$ can bind again between TMH5 of LptF ($THM5_F$) and TMH1 of LptG ($TMH1_G$) to allow the next transport cycle (see Figure 7, state v) [82].

Together, LptF and LptG are adopting a V-shaped fold with an opening to the periplasm and only a few contacts between their interfaces, namely TMH1 and TMH5 (see Figure 7B and C). The limited interaction sites suggested early on that one, or both interfaces may open further to allow the lateral entry of LPS into the cavity [65,77]. The formed cavity is covered with residues of hydrophobic amino acids, which was confirmed by the structures of $LptB_2FG(C)$ with bound LPS. Additional charged residues stabilize bound LPS via salt bridges to the phosphate groups and glucosamine disaccharides of the lipid A moiety as well as the core oligosaccharide [78,79]. Even before the structure of $LptB_2FGC$ with LPS was revealed, Hamad et al. and Bertano et al. used mutational studies and bacterial strains, which constitutively modify lipid A phosphates to show that a cluster of charged residues in the TMH1 of LptG is important for LPS transport, most likely by binding LPS through establishing contact sites with the phosphate moieties of lipid A [83,84]. The first step in the LPS transport is the entry of the LPS molecule into this cavity for extraction, and this process already raises two questions: (i) From which side of the transporter does LPS enter? The structure of $LptB_2FGC$ allows LPS entry in principle from both LptFG interfaces, $TMH1_F$:$TMH5_G$ or $TMH5_F$:$TMH1_G$. (ii) How does the transporter differentiate between LPS and other phospholipids, which are also present in the outer leaflet of the inner membrane?

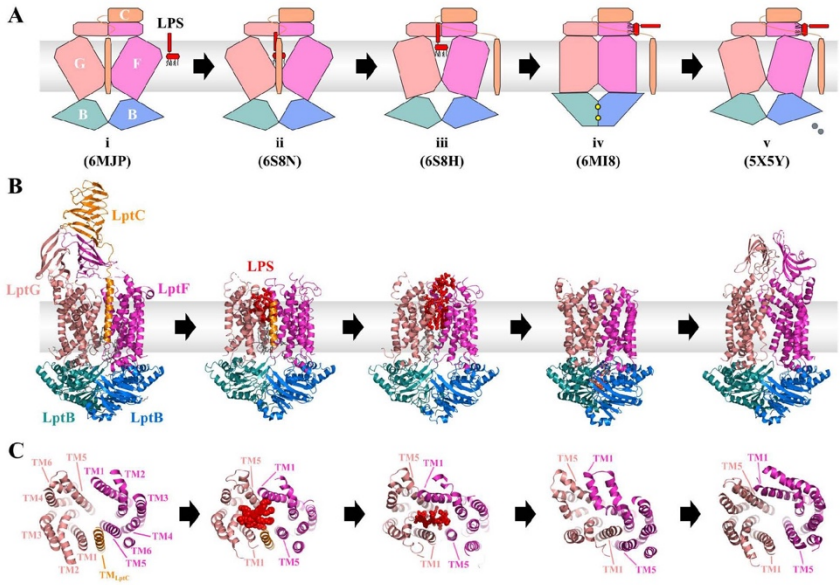

Figure 7. Model and structures of the Lpt systems transport cycle. LptC is shown in orange, while LptF and LptG are shown in light magenta and salmon, respectively. Both LptB protomers are shown in marine and deep teal. LPS is shown in red. Lipids and detergent molecules in the structure are shown as grey sticks,

while nucleotides are shown as spheres. (**A**)**:** Schematic model of LPS extraction by the extractor $LptB_2FGC$. The different states of the transporter are labeled i-v with the PDB entry for the respective structure. i,ii: LPS enters the $LptB_2FGC$ cavity from the reader's side. ii,iii: The LptC TMH leaves the LptFG interface, the cavity tightens and elevates LPS, forming tighter contacts. iii,iv: The $LptB_2$ dimer closes, causing the cavity to collapse and pushes LPS upwards to the β-jellyroll domain of LptF. iv,v: ATP (yellow dots) is hydrolyzed to ADP (grey circles) and P_i, thereby opening $LptB_2$ and the cavity for a new extraction cycle. (**B**)**:** Crystal structures and single particle cryo-EM structures according to the different states (**C**)**:** View on the cavity from the periplasmic side (β-jellyroll domains are omitted for clarity). Note that only structures of states ii and iii show LPS. Even though only the structure of state iv shows bound nucleotides, latest data suggest that ATP can bind already during earlier states. Structures of states ii–iv did not resolve the β-jellyroll domain of LptFG. The structure of state ii did not resolve the β-jellyroll domain of LptC, while the structures of states iii–v were lacking LptC completely.

The first question was answered by crosslinking studies using unnatural amino acids as photo-crosslinkers, together with structures of $LptB_2FGC$, in which the periplasmic domains of LptF and LptG were resolved. Owens et al. detected crosslinks of LPS to residues in TMH1 of LptG and TMH5 of LptF as well as LptC, but not with the possible cavity opening formed by TMH1 of LptF and TMH5 of LptG [81]. Moreover, structures of the LPS ABC transporter with LptC revealed that the $LptC^{TM}$ is positioned between the interface of $TMH5_F$:$TMH1_G$, which is in line with the aforementioned crosslinking studies. So far, no data supported the proposal that LPS might enter from the $TMH5_G$:$TMH1_F$ interface or LptC to reside in that position. Additionally, the structure of $LptB_2FGC$ showed that the β-jellyroll domains of the transporter are placed above the interface formed by $TMH1_F$ and $TMH5_G$, possibly blocking the entry of LPS from this side due to the bulky core oligosaccharide and O-antigen moieties [81].

The second question, why phospholipids are not transported by the Lpt system, is not easily answered. The aforementioned study by Owens et al. showed that even in the absence of ATP, LPS is able to enter the cavity of the transporter [81]. One possibility is that phospholipids can enter the cavity through the TMD interface as well but are not recognized by the transporter as a substrate due to the lack of interactions mentioned above. Since the simplest LPS structure, enabling cell viability, contains lipid A and Kdo, it is likely, that the presence of these key components is necessary for substrate recognition by the Lpt transporter [52,85].

We know now that the $TMH5_F$:$TMH1_G$ interface—in which $LptC^{TM}$, at least at some point of the transport cycle, resides—is the entry for LPS. However, how does LPS enter the cavity of LptFG with a TMH of another protein in its way? The $LptB_2FG(C)$ structures of Li et al. revealed that $LptC^{TM}$ pushes away TMH1-3 of LptG, preventing the interaction of bound LPS with the charged residues mentioned above (see Figure 7B and C). The tighter binding of LPS might therefore push $LptC^{TM}$ out of the cavity [79]. The constriction of the cavity ultimately results in its full collapse and the transfer of LPS from the cavity to the β-jellyroll domains. This movement, as well as the reopening of the cavity, is performed by the NBDs $LptB_2$, which bind and hydrolyze ATP. Closure and opening of the NBD interface are thought to be tied to the collapse and opening of the TMD cavity by a rigid body mechanism, as suggested for other transporters as well [5,86,87]. The LptB structure features a groove region in which the coupling helices of LptF and LptG are embedded [66]. These coupling helices are conserved in the TMD of ABC transporters and are crucial for the TMD-NBD interaction and can be found between TMH2 and TMH3 in LptFG [7,65,77]. They were identified using photo-crosslinking and mutational studies, in which defects induced by substituting a conserved glutamate in both LptF (E84) and LptG (E88) could be suppressed by altering an amino acid in the groove region of LptB (R91) [88]. Interestingly, the same study showed that LptF and LptG do not act symmetrically, as identical changes at equivalent positions led to different defects. Following the signature motif is the signature helix, in which Simpson et al. identified an arginine residue (R144) to be important for forming contacts with the Q-Loop and Walker B motif. Altering this residue led to reduced LPS extraction due to a lower ATP binding affinity, favoring the open conformation of the transporter. Strikingly, an alteration in the C-terminal domain (CTD) of LptB (F239), a domain unique to this transporter, is usually lethal but could complement the change in the signature helix. The data for this mutation showed a decreased ATP hydrolysis, indicating that this mutant is favoring the closed conformation, and the combination of these two defects complement each other, resulting in a functional transporter with decreased ATPase activity. Since full restoration of ATP hydrolysis in this double mutant is not necessary for LPS transport, the researchers proposed that the binding of ATP leads to the collapse of the LptFG cavity and hydrolysis to its reopening [89]. This correlation is supported by structures of the transporter in its closed form with bound β-γ-imidoadenosine 5′-triphosphate (AMP-PNP), a nonhydrolyzable ATP analog, and with bound ADP-vanadate [78,79]. ATP binding leads to the closure of the $LptB_2$ dimer interface

and the concomitant anti-clockwise rotation of the LptFG TMH1-5, ultimately closing its cavity [78].

Since this review focuses on the transporter of the Lpt system, subsequent transport steps will be only briefly described here. At the end of each transport cycle, a new LPS molecule is placed into the β-jellyroll domains of the transporter. The functionality of the transport system is often compared with a PEZ candy dispenser, where the $LptB_2FGC$ transporter acts like a spring, with each cycle loading a new LPS "candy" onto the bridge, pushing the former one further ahead on the LptA bridge towards LptDE and the OM [90]. Although both LptF and LptG feature β-jellyroll domains, structural, mutational, and crosslinking studies so far only showed that LPS travels from the cavity to the β-jellyroll domain of LptF, but not LptG, and further to the one of LptC [81]. The backflow into the cavity must be prevented if the entry of new LPS is not much faster since LPS does not diffuse away from the transporter. Owens et al. proposed on the basis of their $LptB_2FGC$ structure that the β-jellyroll domain of LptF can adopt a closed conformation, preventing a backward flow much like a valve [81]. Another possibility for the unidirectional flow might be different binding affinities of LPS for the different proteins, as this was at least shown for the transfer of LPS from LptC to LptA [68]. Even though LptA is known to form oligomers in vivo and in vitro, the exact number forming the bridge is unknown [62,74]. Sherman et al. succeeded with the in vitro reconstitution of the complete system, proving that LptA physically connects $LptB_2FGC$ with LptDE [91]. Once LPS reaches LptDE in the outer membrane, it is first placed into the β-jellyroll domain of LptD. The lipid A moiety of LPS is proposed to enter the membrane directly through a cavity between its β-jellyroll domain and the 26-strand β-barrel. The hydrophilic part of LPS would then first enter the β-barrel from the periplasmic side before exiting it through a lateral gate between helices 1 and 26, which showed to have only a few interacting residues [73,92,93]. LptE, the barrel's plug, is not only important for the biogenesis and proper folding of LptD but was also shown to bind LPS and extract it from aggregates, suggesting that its role is to accept LPS coming from the periplasm, weaken neighboring LPS-LPS interactions and assisting its insertion into the OM [61,93–97]. Once the hydrophilic part of LPS has passed the lateral gate, it becomes part of the already existing LPS network. Intriguingly, there is evidence that the activity of the LPS transporter $LptB_2FGC$ in the inner membrane is influenced by the translocon LptDE. For an in vitro setup, inhibition of LPS transport and ATPase activity of $LptB_2FGC$ in liposomes was observed when adding LPS-preloaded LptDE-containing liposomes [98]. Lately, $LptB_2FGC$ has been shown to exhibit an adenylate kinase activity in addition to the ATPase activity, as it was reported for other ABC transporters like MsbA and CFTR [99–101].

Due to recent advances in structural biology, many answers regarding LPS transport could be answered. However, still some key questions remain, especially regarding the enigmatic LptC: What role does LptC play in the transport process since no other ABC transporter features a protein alike? Even though LptC is found in structures with $LptB_2FG$, its TMH is neither required for LPS to enter the cavity nor for transport in general. Studies showed that LptC variants, in which the TMH was deleted, are still able to form a complex with the other Lpt proteins to transport LPS [102]. Experimental data suggest that the $LptC^{TM}$ plays a regulatory role in the ATPase activity of the transporter. In vitro, $LptB_2FG$ displays an increased ATP hydrolysis when no LptC or only variants without TM helix ($LptC^{\Delta TM}$) are present. Therefore, the helix might reduce futile ATP hydrolysis by coupling it efficiently to substrate extraction [78,79,81]. Lethal LptC deletions can be suppressed when the arginine residue R212 in the β-jellyroll domain of LptF is substituted with glycine, restoring wildtype LPS transport and ATPase activity of the transporter, even though affinity to LptA is reduced [103,104]. Interestingly, this point mutation is still able to form a complex with LptC when it is present. This indicates that the periplasmic β-jellyroll domain of LptC is responsible for the interaction with the other Lpt components and enhances the stability of the transporter to the periplasmic bridge. The availability of LPS-bound $LptB_2FG$ structures with and without LptC allows a comparison of the cavity

and interactions with the LPS molecule. With the $LptC^{TM}$ missing, the transporter cavity is significantly smaller (see Figure 7C). Simultaneously, the LPS structure in those structures is better resolved, indicating an improved binding of LPS once the $LptC^{TM}$ is removed from the transporter. When, how, and why the $LptC^{TM}$ is removed during the transport cycle is still not completely clear.

Recently, Wilson et al. approached these questions by combining $LptC^{\Delta TM}$ with mutations in other Lpt transporter components and searched for synergistic or suppressive effects on the phenotypes. They aimed to elucidate the exact role of $LptC^{TM}$ in the different steps of the extraction cycle, as deletion of the TM helix should strengthen or weaken the phenotype when a mutant is affected in the same step, while no change to the phenotype was expected when $LptC^{\Delta TM}$ was combined with mutants, in which the TM helix plays no role. Two observations were made: (i) The presence of the $LptC^{TM}$ increases the stability of the protein, possibly by benefiting from a complex formation with $LptB_2FG$, and ii) the phenotype of LptB and LptF/G mutants with defects in ATP binding and NBD-TMD coupling were affected, indicating that the $LptC^{TM}$ plays a role in these steps. This new data hints that i) binding of ATP to LptB can occur with the $LptC^{TM}$ associated with LptFG (although it is not obligatory) and (ii) the coupling helices in LptFG, as well as the corresponding groove region in LptB, take part in $LptC^{TM}$ displacement from the transporters cavity, meaning that the sole entry of LPS into the cavity is not sufficient for this process [82]. The proposal that ATP can bind to $LptB_2FG$ with $LptC^{TM}$ still present is contrary to former models, in which LPS binding and formation of tighter contacts to LptFG is displacing $LptC^{TM}$ with ATP binding afterwards, particularly as structures of $LptB_2FG$ with bound LPS and displaced $LptC^{TM}$ were lacking nucleotides so far [79]. It is surprising that the essential process of LPS extraction, which takes place countless times during the lifetime of a cell, features an apparently useless step. One possible explanation is that the intercalation of $LptC^{TM}$ slows down ATP hydrolysis [78,79,81,87,99] to synchronize the hydrolysis of ATP with the binding of LPS to the cavity of the extractor, preventing futile ATP hydrolysis. It also remains enigmatic if the placement of $LptC^{TM}$ is a step that is not performed during active LPS transport but rather to slow it down before turning it off.

4. The Mla System

As mentioned in the previous section, the OM is an asymmetric bilayer, and all the components for building the OM envelope are synthesized either in the cytoplasm or the IM before being transported across the periplasm to be inserted into the OM [105]. As mentioned in the previous section, LPS is trafficked across the cell envelope via the Lpt system. The *m*aintenance of *l*ipid *a*symmetry (Mla) pathway is involved in maintaining the asymmetry of the OM by trafficking phospholipids (PLs) between the IM and OM [106–108]. The Mla pathway is a multi-component system and uses a ferry-like mechanism to shuttle phospholipids across the periplasm. Its mutation leads to the accumulation of PLs in the outer leaflet of the OM, increased OM permeability, and increased susceptibility to antibiotics [106–109]. Although translocation of phospholipids between outer and inner membrane was initially discovered in *Salmonella typhimurium* as early as 1977, it was not until 2009 that the components of the phospholipid transport system in Gram-negative bacteria were discovered via homology of conserved transporters in Actinobacteria and chloroplasts [106,110–112]. The orthologous TGD pathway of plants transports phosphatidic acid from the OM to the IM of chloroplasts [110], while the Mce4 pathway in Actinobacteria is paralogous and imports exogenous cholesterol [111,112].

In *E. coli*, the genes representing the Mla system are located on the *mlaFEDCB* operon, which is conserved among Gram-negative bacteria. Although *mlaA* and *ompC/G* are part of the Mla system, these genes are located outside the *mla* locus [106].

The Mla system is a six-component system with components present in each compartment of the cell envelope. It includes an OM lipoprotein termed MlaA; the OM major porins OmpF/OmpC, which act as a scaffold for MlaA; a soluble periplasmic component known as MlaC, which acts as a carrier of PLs, shuttling them between the membranes; a

mammalian cell entry (MCE) domain protein called MlaD which is anchored in the plasma membrane; the transmembrane domain of the ABC transporter MlaE; a sulphate transporter and anti-sigma factor antagonist (STAS) domain protein called MlaB and the ATPase MlaF. These components create the following three main parts of the Mla system [113,114]: (a) the trimeric porin OmpC, which forms a complex with lipoprotein MlaA at the OM; (b) a soluble lipid-binding protein, MlaC, located in the periplasm; and (c) MlaFEDB, an ABC transporter localized in the plasma membrane (see Figure 8).

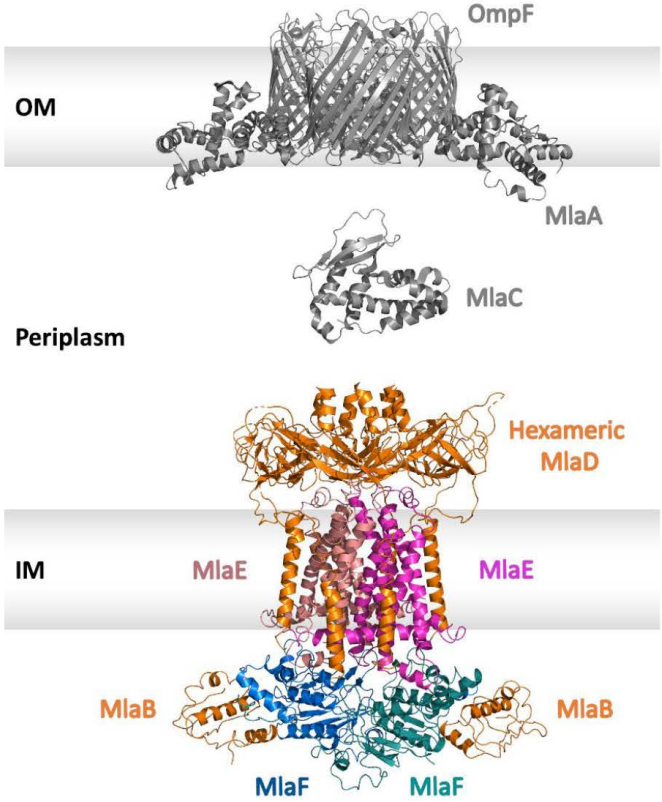

Figure 8. Structural components of the Mla system in a cartoon representation. The homo-trimeric complex of OmpF and MlaA (PDB: 5NUO) situated in the outer membrane is shown in grey color. MlaC (PDB: 6GKI) is shown in the periplasm in grey color. Note: the exact number of MlaC molecules in the periplasm is unknown. The inner membrane complex of MlaFEDB (PDB: 6ZY2) is shown in color: hexameric MlaD, and both MlaB molecules are shown in orange. The two MlaE molecules are shown in salmon and light magenta. The two molecules of MlaF are shown in marine and deep teal. Outer membrane (OM) and inner membrane (IM) are displayed as grey boxes. The peptidoglycan layer is omitted for reasons of clarity.

MlaA is a lipid transport protein and assembles into a ring-shaped α-helical structure that contains a central pore [115]. It forms a complex with both the OM porin proteins, OmpC and OmpF [115,116]. However, the complex of OmpC-MlaA is the active species, as MlaA copurifies with OmpC. MlaA binds in the groove between the two OmpF/C monomers, and the interaction between MlaA and OmpF/C is mainly mediated via van

der Waals forces [115]. Since MlaA might be unstable on its own in the lipid bilayer, the porins might function as a scaffold to ensure the proper functioning of MlaA [115].

MlaC is a periplasmic lipid-binding protein. The crystal structure of MlaC was resolved and comprised four ß-sheets and seven helices with a large hydrophobic pocket in the core of the protein. Since MlaC can bind to both IM and OM complexes, it probably exhibits a central role in the transport of PLs between the membranes [117]. MlaC has a high affinity towards phospholipids and can bind three different PLs: phosphatidylglycerol, phosphatidylethanolamine, and cardiolipin [118,119].

MlaD is anchored to the IM through a single N-terminal TMH with its MCE domain residing in the periplasm. The MCE domains have been involved in lipid uptake in Gram-negative bacteria and retrograde transport of PLs in chloroplasts [110,117,120]. MlaD forms a ring-shaped homo-hexamer with a central hydrophobic pore that allows movement of PLs [114,117–119].

MlaE represents the transmembrane domain of the ABC transporter, which forms a homodimer. In contrast to the previously described TMDs of MacB and LptF/G (Sections 3 and 4), MlaE has five TMHs. Recently, it has been assigned as a founding member of the type VIII group of ABC transporters [24,117]. Each subunit contains one elbow helix (EH), five transmembrane helices (TMH1–5), one coupling helix (CH), and one periplasmic helix (PH). TMH1, TMH2 and TMH5 of the two subunits of MlaE form a central hydrophobic cavity. EH runs parallel to the inner membrane plane while the CH connects TMH2 and TMH3 and is involved in interaction with MlaF. The PH is placed between TMH3 and TMH4 and interacts with MlaD [121].

MlaF represents the nucleotide-binding domain of the ABC transporter with a conserved structure representative of the ABC superfamily and is present as a dimer [121]. MlaB contains a STAS domain and represents the accessory protein, which is involved in cross-talk with the NBDs of ABC transporters. The two MlaB subunits are located on the opposite side of the MlaF dimer [122,123] and are involved in stabilizing the complex and ATP hydrolysis [109,124].

The inner membrane complex (IMC) of the Mla pathway is composed of MlaFEDB, which represents the ABC transporter. Overall, the complex comprises of four different proteins: MlaF, MlaE, MlaD, and MlaB in a stoichiometry of 2:2:6:2 [109,117,121,125]. The homodimers of MlaE and MlaF function as the TMDs and the NBDs, respectively. Associated with the homodimers are the unique auxiliary proteins: MlaB and MlaD. While there are two copies of MlaB, MlaD is present as a hexamer in the complex [109]. The two MlaB proteins in the cytoplasm do not contact each other, and each MlaB molecule interacts with one MlaF [121]. The MlaD hexamer rests on top of the periplasmic side of the MlaE dimer [117]. The six α-helices form a hollow hydrophobic channel to allow the transport of lipids. A total of six MlaD TMHs in the MlaFEDB complex are inserted into the membrane [121]. Each three MlaD subunits incorporate one MlaE where the interaction between the TMH of MlaD and the EH of MlaE is critical for the phospholipid transport function of MlaFEDB [121].

Recent cryo-EM structural work on the Mla system has provided further insights into this intriguing complex. The high-resolution structures from *E. coli* [114,121,126], *Pseudomonas aeruginosa* [127], and *Acinetobacter baumannii* [128,129] clearly indicate that the overall architecture of the whole complex is conserved throughout these species.

These structures show that in the absence of ATP, MlaE embraces a V-shaped open conformation to frame a cavity with the wider side confronting the hydrophobic channel of MlaD. In the case of *E. coli*, the lipid binding site has been shown to be the outward-open pocket of MlaE [114,126], while for *A. baumannii*, lipid binding is described to happen at the pore of MlaD and in between the pore loops of the MCE domain of the MlaD hexamer [128]. A few of the structures contain residual electron density in the cavity and in different locations and could represent PLs or bound detergent [114,121,126–129] (see Figure 9A). The direction of lipid transport by the Mla system is discussed as controversial. A retrograde transport mechanism was originally described for the Mla system, where it maintained

the lipid asymmetry by removing mislocated phospholipids from the outer leaflet of the OM and importing them back to the plasma membrane [106–109,113,115,116,130]. However, there is also data that supports the export of phospholipids (anterograde transport) from the IM to the OM [119,125,126,131] or even a bi-directional transport between both membranes [114].

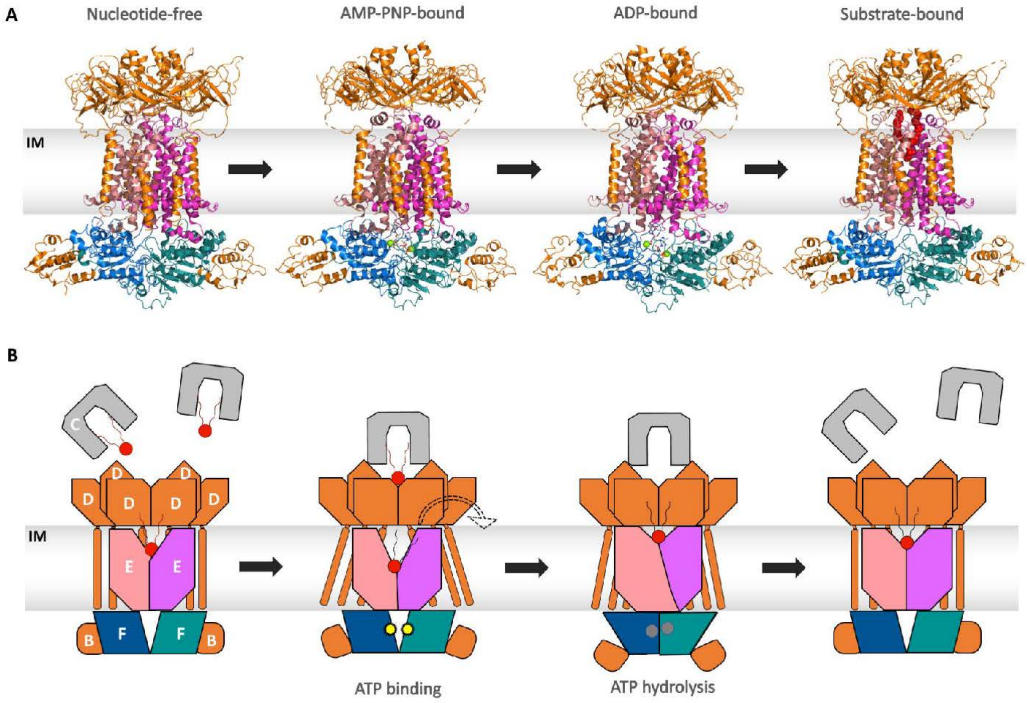

Figure 9. Structures and model representing the transport cycle of the Mla pathway. MlaC is shown in grey. The hexameric MlaD and both MlaB are shown in orange. MlaE is shown in salmon and light magenta. MlaF is shown in marine and deep teal. Lipid molecules are shown in red, and nucleotides are shown as spheres. The IM is displayed as a grey box. The peptidoglycan layer is omitted for reasons of clarity. (**A**)**:** Different states of the ABC transporter during the transport cycle: nucleotide-free (PDB: 6ZY2), AMP-PNP-bound (PDB: 6ZY9), ADP-bound(PDB: 6ZY4), and substrate-bound (PDB: 6ZY3). (**B**)**:** A schematic model of the retrograde transport of the lipid via MlaFEDB. Lipid-loaded MlaC binds to MlaD in the resting state of MlaFEDB. Binding of ATP (yellow dots) prompts the exit of the lipid molecule present in the cavity of MlaE from the last transport cycle. ATP hydrolysis to ADP (grey circles) and P_i prompts dimerization of MlaF and conformational changes in MlaE, which ultimately lead to the extraction of lipid from MlaD-MlaC into the cavity of MlaE. Upon release of hydrolyzed products, the conformation gets back to the resting state.

For simplicity, we only describe here the proposed retrograde transport mechanism in the context of phospholipid import (see Figure 9B). However, reversing the outlined steps could result in anterograde transport of phospholipids, as also described [119,125].

As part of the OmpF/C complex, MlaA is embedded inside the OM, and together they form a channel across the membrane [115]. Phospholipids are extracted from the outer leaflet of the OM into the channel via a lateral pathway. Interaction of MlaC to the MlaA-OmpC/OmpF complex results in phospholipid transfer to the hydrophobic pocket of MlaC [114,117,118]. Then, MlaC diffuses across the periplasm to deliver the lipids to

the MlaFEDB complex in the IM. A hexameric ring formed by MlaD subunits creates a central hydrophobic tunnel for the transport of lipids [117]. MlaC acts as a chaperone and directly binds to MlaD [117], transferring the lipid into a continuous channel from MlaD to an outward-facing MlaE [114,121,127–129]. ATP binding induces a conformational change in MlaE, resulting in the collapse of the lipid-binding pocket, thereby facilitating the incorporation of the lipids into the IM [121]. The auxiliary protein MlaB is known to regulate the transport [109,124].

Although the recent advances in research have added a plethora of information about the Mla system, a major unresolved question is still the directionality of lipid transport. MCEs are usually involved in the retrograde transport of misplaced phospholipids; however, there are still crucial details missing regarding the transfer of PLs from MlaC to MlaD.

Another open question is the reason behind the formation of stable complexes of MlaA with both OmpF and OmpC. Interestingly only one of these assemblies is functional, although functionality towards the transport of PLs lies within MlaA. These questions need to be addressed in the future to better understand the system.

5. The Lol System

Lipoproteins are crucial elements in bacteria. They are either located in the outer leaflet of the cytoplasmic membrane or in the leaflets of the OM. The latter case is most often true for Gram-negative bacteria, which is also the focus of this section. Lipoproteins are a compelling object of study for many reasons. One of them is their strong involvement in building and maintaining the OM of Gram-negative bacteria. As the OM is the first line of defense against xenobiotics, lipoproteins, their synthesis, and their transport pathway are attractive targets for novel antibiotics [132,133]. This section focuses specifically on the ABC transporter, which is involved in the transport of lipoproteins, and shows a transport mechanism differing from the classical ABC transporter mechanism. For a better overview regarding the synthesis, sorting, and function of lipoproteins, the interested reader is referred to other reviews [132,133], as these aspects will only be briefly mentioned here.

Lipoproteins are synthesized in the cytoplasm together with a cleavable signal peptide, which contains a consensus sequence that is highly conserved among lipoproteins, called the lipobox. The consensus sequence is L-A/S-G/A-C and was confirmed by various sequence analyses [134,135]. After translocation to the IM via the Sec [132,136] or, in some cases, via the Tat machinery [132,137], lipoproteins undergo further maturation steps in the outer leaflet of the IM. In the first step, the enzyme Lgt attaches a diacyl moiety to the cysteine in the aforementioned consensus sequence [138]. Subsequently, the enzyme Lsp [139,140] cleaves the signal sequence from the cysteine, and therefore this residue is named Cys^{+1} and becomes the new N-Terminus of the lipoprotein. In the last maturation step, another acyl group is attached to the free amino group of the cysteine by Lnt [141,142]. The sorting of lipoproteins either to the IM or the OM is determined in *E. coli* by the amino acid next to the N-terminal cysteine of mature lipoproteins (the +2 position). If this amino acid is aspartate, the lipoprotein is retained in the IM [143]. In the case of most other naturally occurring residues, the lipoprotein is localized to the OM [144].

The trafficking of lipoproteins to the OM of Gram-negative bacteria is mediated by the *l*ocalization *o*f *l*ipoproteins (Lol) system [133]. The discovery of the Lol system started with the discovery of the periplasmic chaperone LolA (called p20 at that time), which was found to form a soluble complex with a lipoprotein [145]. Soon, the interaction partner of LolA, namely LolB, was also discovered [146]. LolB was localized to the OM and was identified as an essential protein for *E. coli*, as depletion of LolB is lethal. It was further shown that the incubation of a lipoprotein-LolA complex with a soluble LolB derivative led to the transfer of the lipoprotein to the OM. Through these findings, an initial mechanism for lipoprotein localization was already emerging. Soon after that, the crystal structures of LolA and LolB were solved [147]. Remarkably, both proteins showed a similar overall structure, despite their different amino acid sequences. Both proteins show a beta-barrel structure with a hydrophobic inside and alpha-helical lid. The hydrophobic cavities were identified as the

possible binding sites for the acyl chains of the transported lipoproteins. This was further supported by finding polyethylene glycol 2000 monomethyl ether (PEGMME2000), which was used for the crystallization, in the hydrophobic cavity in one of the LolB structures [147].

It was later discovered that the detachment of lipoproteins from the membrane is ATP-dependent, and the corresponding protein is an ABC transporter [148]. Yakushi et al. solved the stoichiometry of this transporter termed LolCDE. It is a tetrameric and asymmetric ABC transporter composed of the proteins LolC and LolE, which make up the TMDs, and two copies of LolD, which form the NBDs. It was predicted that both proteins, LolC and LolE, each possess four transmembrane helices and a large periplasmic domain [148]. Due to the topology of LolCDE, the transporter can be assigned to the group of type VII ABC transporters [24]. Taking together all main findings, a general transport cycle, as shown in Figure 10, was derived.

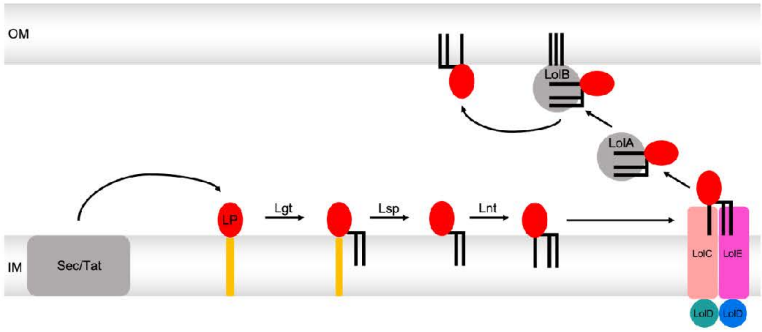

Figure 10. Overview of the Lol pathway. After insertion of lipoproteins (red, labeled one time with LP) via the Sec or the Tat pathway into the IM, they are diacylated (black) by Lgt in a first modification step. This is followed by cleavage of the N-terminal signal sequence (orange) by Lsp. Subsequently, Lnt acylates the newly N-terminally located cysteine, which makes the now mature lipoprotein ready for transport via the Lol machinery. This starts with the extraction of the lipoprotein from the cytoplasmic membrane via the ABC transporter LolCDE (salmon, light magenta, deep teal, and marine), which leads to the delivery of the lipoprotein to the periplasmic chaperone LolA (grey). LolA shuffles the lipoprotein to the last checkpoint LolB (grey), which finally inserts the lipoprotein into the outer membrane.

One major unknown factor was certainly the ABC transporter LolCDE. Its mechanism has to surely differ from the mechanism of classical ABC transporter, as the substrate is located in the outer leaflet of the inner membrane and not in the cytoplasm. However, for a relatively long time after the discovery of the Lol pathway, the ABC transporter LolCDE lacked structural analysis, and thus, a detailed understanding of its molecular mechanisms was missing. The first published structure related to LolCDE comprised a crystal structure of a soluble periplasmic domain of LolC solved by the Koronakis lab [29]. This structural analysis was done to confirm the structural similarity of the periplasmic domain of LolC to that of the homologous ABC transporter MacB, which is involved inter alia in the efflux of antibiotic macrolides (described in Section 2). The confirmation of the similarity of the two periplasmic domains of LolC and MacB led to the conclusion that LolC could also follow the mechanotransmission mechanism. This characteristic periplasmic domain is divided into two subdomains named sabre and porter. The superposition of the sabre domains of LolC and MacB showed a prominent loop in LolC which is not present in MacB. Accordingly, this loop was investigated further by the Koronakis lab, and they solved the crystal structure of the periplasmic domain of LolC in complex with the periplasmic chaperone LolA [149]. This structure sheds light on the molecular details of the interactions within the complex and highlights the importance of this loop, which was termed “hook”.

Furthermore, an additional important interacting domain was found in LolC, which was termed "pad". The hook and the pad were determined to be essential for the recruitment of LolA. These findings further underpin the assignment of LolCDE into the group of type VII ABC transporters, as MacB is the founding member of this group [24]. In a more recent study, the crystal structure of LolA bound to a ligand was also solved by the Koronakis lab [150]. The structure shows the precise interaction of the acyl chains of the lipoprotein with the hydrophobic cavity in LolA. In addition, an overlap between the acyl binding sites and the LolC binding sites of LolA were found by comparison with other LolC-LolA structures. This indicates that the substrate binding to LolA is inducing the detachment from LolC. These findings further complete our understanding of the Lol system.

Since 2021, major breakthroughs have been made regarding the structural characterization of LolCDE. Tang et al. started this by solving six structures of the transporter representing different states of the transport via cryo-EM [151]. The structures represent LolCDE solubilized in the detergent LMNG. In the apo state, the NBDs show a relaxed conformation, whereas the rest of the transporter shows a rather compact conformation. More precisely, the transmembrane (TM) segments of LolC twist around the TM segments of LolE, and the PD of LolC rotates to the front of the PD of LolE. In the substrate-bound conformation, the TMDs of LolCDE are outward-opened, leading to a V-shaped central channel. In addition, two lateral gates are observable, which are formed by TMH1 and TMH2 of each of the proteins, LolC and LolE. The triacyl chains and a small N-terminal segment of the lipoprotein were resolved in a vertical arrangement in the upper part of the V-shaped channel. This suggests that the lipoprotein was extracted laterally from the periplasmic side of the IM, as this is also the arrangement of the lipoprotein in the IM. Furthermore, two AMP-PNP-bound LolCDE structures were solved by Tang et al. [151]. Only one of these structures contains a bound lipoprotein. Since AMP-PNP is a non-hydrolyzable ATP analog, these structures represent LolCDE after ATP binding. In the lipoprotein-bound structure, the transporter maintains its V-shaped cavity, and the NBDs are open. In the structure without the lipoprotein, the NBDs are closed. The closure of the NBDs leads to conformational changes in the TMDs, which leads to the closure of the central channel. In particular, TMH1 and TMH2 of LolE are shifted towards LolC. Additionally, the TMH2 of LolE clashes with the triacylcysteine of the lipoprotein of the ligand-bound state, which leads to the extrusion of the lipoprotein.

Sharma and colleagues published cryo-EM structures of LolCDE in a nucleotide-free and a nucleotide-bound state reconstituted in nanodiscs, which represent a native-like lipid environment [152]. In summary, the two determined structures show a very high similarity to the structural counterparts determined by Tang et al. [151]. The nucleotide-bound state was determined using an ADP-vanadate complex trapped in the ATP binding site. In addition, in the vanadate-trapped structure, the two LolD proteins come into close contact, which leads to the uplifting of the TMH2. Thus, ATP-binding leads to the extrusion of the lipoproteins from the TMDs to LolA. Sharma et al. further points out that in this conformation, TMH2 closes the lateral opening between LolC and LolE [152]. This could serve as a further mechanism for preventing substrate entry before the completion of a full transport cycle. In comparison to the structures of Tang et al. [151], the nucleotide-free structure of Sharma et al. [152] shows a significant difference in the binding of the lipoproteins. In the structure of Sharma et al. [152], the N-terminally linked acyl chain of the lipoprotein adopts a rather horizontal conformation in the cavity of LolCDE compared to the rather vertical arrangement of this acyl chain in the structure of Tang et al. [151].

In a relatively recent study, Bei et al. presented cryo-EM structures of nanodisc-reconstituted LolCDE in the apo, lipoprotein-bound, and AMP-PNP-bound states [153]. In general, the structures are highly similar to the corresponding structures published by Tang et al. [151] and Sharma et al. [152]. However, Bei et al. [153] pointed out a remarkable difference in the distances of the periplasmatic domains of LolC and LolE in the apo state compared to the apo state determined by Tang et al. [151]. Nevertheless, the structures of Bei et al. [153] also suggested that the binding of ATP leads to the closure

of the central cavity and to the extrusion of the lipoprotein. The three structures determined by Bei et al. [153] are depicted exemplarily for the LolCDE transport mechanism in Figure 11. Panel B shows how the movement of TMH2 of LolE leads to the blockage of the central cavity and, thus, to the extrusion of the lipoprotein.

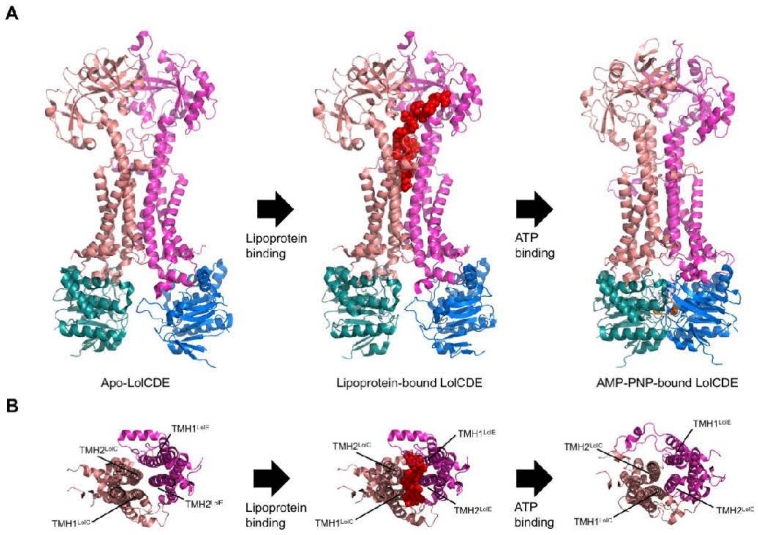

Figure 11. Structures of LolCDE in the Apo (PDB: 7V8M), lipoprotein-bound (PDB: 7V8L), and AMP-PNP-bound (PDB: 7V8I) form. LolC is shown in salmon, LolE is shown in light magenta, one LolD monomer is shown in deep teal, and the other LolD monomer is shown in marine. The lipoprotein is shown in red spheres. (**A**)**:** Side-view of LolCDE. In the Apo state, LolCDE exhibits a V-shaped cavity that the lipoprotein enters from the membrane. Upon ATP binding (AMP-PNP-bound state), the central cavity is closed, and the substrate is shuffled out of LolCDE to LolA. (**B**)**:** Cross-sectional view of the TMDs of LolCDE in the different substrate- or nucleotide-bound states. Movement of TMH2 of LolE upon ATP-binding into the central cavity extrudes the substrate out of the transporter.

Putting it all together, the published LolCDE structures in different transport states show a high similarity and correspond well with each other, especially regarding the connection of ATP-binding and release of the substrate to the periplasmic chaperone LolA [152,153]. All studies suggested a similar transport mechanism. In the apo state, the lipoprotein is extracted from the outer leaflet of the IM in an energy-independent manner into the V-shaped cavity inside LolCDE. Through ATP-binding, the NBDs dimerize, which leads to movements in the TMDs, resulting in the shuffling of the lipoprotein to LolA. After the dissociation of ADP and the lipoprotein-LolA complex, the central cavity opens again, and the transporter is primed for the next transport cycle. Despite the vast similarities, slight differences exist between specific structures. There are also differences between the ATPase activities of the different structures. For instance, LolCDE prepared in nanodiscs by Sharma and colleagues shows a several-fold higher activity than LolCDE purified in LMNG by Tang et al. [151,152]. The differences could be attributed to the different detergent and lipid environments in which the structures were solved. This further emphasizes the significance and involvement of lipids in the function of membrane transporters and membrane proteins in general. The ABC transporter LolCDE falls in line with a group of emerging ABC transporters, which show a non-classical transport mechanism. The initial suggestion that LolCDE also follows a mechanotransmission mechanism due to the resemblance to MacB [29] was confirmed by the various discussed LolCDE structures. The study of such ABC transporters with non-conventional transport mechanisms enhances

our understanding of living systems and could pave the way for novel drug targets and biotechnological applications.

6. Conclusions

Here, we have reviewed four ABC transporters that form the energizing component of four bacterial nanomachineries. We also tried to highlight how the use of ATP deviates from the classic "two-side access" [8] and how these machineries adapted to the particular needs of transporting quite different substrates. Although we have witnessed a tremendous increase in knowledge about the function and structure of the nanomachineries, we have also summarized the obvious questions.

Despite the availability of structural information on the whole MacAB-TolC nanomachinery, detailed insights about substrate binding and recognition are still lacking, including intermediate or substrate-bound structures. Especially the role of ATP hydrolysis in substrate translocation and possible feedback from the putative binding site to the NBDs require further investigations.

Similarly, there are still some intriguing features of the Lpt system, such as the role of LptC during the inactive state or the influence of LptC on the binding of $LptB_2FG$ to ATP and substrate, that need to be studied in detail towards an in-depth understanding of the Lpt system. Additionally, the oligomeric organization of LptA forming the periplasmic bridge is still unknown.

For the Mla system, the fundamental question regarding the directionality of the transport remains open. The influence of the cell wall on the movement of MlaC is also unknown. Furthermore, the role of a non-functional OMP-MlaA assembly remains elusive.

In terms of the Lol system, the variety of structures is impressive though a detailed functional understanding of the shuttling process between IM and OM remains unclear. This emphasizes the necessity of a combination of all kinds of structural, biochemical, and biophysical data to understand these complex systems in detail.

These questions need to be addressed in the future to fully understand and maybe even exploit the beautiful variety of these different nanomachineries in prokaryotes.

Author Contributions: All authors wrote, drafted, and revised the review and searched for literature. L.S. was responsible for the ideation. All authors have read and agreed to the published version of the manuscript.

Funding: Work on ABC transporters is funded by the DFG (CRC 1208 project A01 and Schm1279/17-1 to L.S.).

Institutional Review Board Statement: Not applicable.

Informed Consent Statement: Not applicable.

Data Availability Statement: No new data were created or analyzed in this study. Data sharing is not applicable to this article.

Acknowledgments: We thank all current and former members of the Institute of Biochemistry for their support and many stimulating discussions. Apologies to all our colleagues whose work was not referenced. We thank the Center for Structural Sciences (CSS) at Heinrich Heine University for excellent support and infrastructure, which enables structural studies of our ABC systems.

Conflicts of Interest: The authors declare no conflict of interest.

References

1. Higgins, C.F. ABC transporters: Physiology, structure and mechanism–an overview. *Res. Microbiol.* **2001**, *152*, 205–210. [CrossRef] [PubMed]
2. Davidson, A.L.; Dassa, E.; Orelle, C.; Chen, J. Structure, function, and evolution of bacterial ATP-binding cassette systems. *Microbiol. Mol. Biol. Rev.* **2008**, *72*, 317–364. [CrossRef] [PubMed]
3. Biemans-Oldehinkel, E.; Doeven, M.K.; Poolman, B. ABC transporter architecture and regulatory roles of accessory domains. *FEBS Lett.* **2006**, *580*, 1023–1035. [CrossRef] [PubMed]

4. Thomas, C.; Tampe, R. Structural and Mechanistic Principles of ABC Transporters. *Annu. Rev. Biochem.* **2020**, *89*, 605–636. [CrossRef] [PubMed]
5. Oldham, M.L.; Davidson, A.L.; Chen, J. Structural insights into ABC transporter mechanism. *Curr. Opin. Struct. Biol.* **2008**, *18*, 726–733. [CrossRef]
6. Higgins, C.F.; Linton, K.J. The ATP switch model for ABC transporters. *Nat. Struct. Mol. Biol.* **2004**, *11*, 918–926. [CrossRef]
7. Hollenstein, K.; Dawson, R.J.; Locher, K.P. Structure and mechanism of ABC transporter proteins. *Curr. Opin. Struct. Biol.* **2007**, *17*, 412–418. [CrossRef]
8. Jardetzky, O. Simple allosteric model for membrane pumps. *Nature* **1966**, *211*, 969–970. [CrossRef]
9. Dawson, R.J.; Locher, K.P. Structure of a bacterial multidrug ABC transporter. *Nature* **2006**, *443*, 180–185. [CrossRef]
10. Bonifer, C.; Glaubitz, C. MsbA: An ABC transporter paradigm. *Biochem. Soc. Trans.* **2021**, *49*, 2917–2927. [CrossRef]
11. Liu, F.; Zhang, Z.; Csanády, L.; Gadsby, D.C.; Chen, J. Molecular Structure of the Human CFTR Ion Channel. *Cell* **2017**, *169*, 85–95.e8. [CrossRef]
12. Chen, S.; Oldham, M.L.; Davidson, A.L.; Chen, J. Carbon catabolite repression of the maltose transporter revealed by X-ray crystallography. *Nature* **2013**, *499*, 364–368. [CrossRef]
13. Aller, S.G.; Yu, J.; Ward, A.; Weng, Y.; Chittaboina, S.; Zhuo, R.; Harrell, P.M.; Trinh, Y.T.; Zhang, Q.; Urbatsch, I.L.; et al. Structure of P-glycoprotein reveals a molecular basis for poly-specific drug binding. *Science* **2009**, *323*, 1718–1722. [CrossRef] [PubMed]
14. Choudhury, H.G.; Tong, Z.; Mathavan, I.; Li, Y.; Iwata, S.; Zirah, S.; Rebuffat, S.; Van Veen, H.W.; Beis, K. Structure of an antibacterial peptide ATP-binding cassette transporter in a novel outward occluded state. *Proc. Natl. Acad. Sci. USA* **2014**, *111*, 9145–9150. [CrossRef] [PubMed]
15. Kopcho, N.; Chang Gand Komives, E.A. Dynamics of ABC Transporter P-glycoprotein in Three Conformational States. *Sci. Rep.* **2019**, *9*, 15092. [CrossRef] [PubMed]
16. Hofmann, S.; Januliene, D.; Mehdipour, A.R.; Thomas, C.; Stefan, E.; Brüchert, S.; Kuhn, B.T.; Geertsma, E.R.; Hummer, G.; Tampé, R.; et al. Conformation space of a heterodimeric ABC exporter under turnover conditions. *Nature* **2019**, *571*, 580–583. [CrossRef]
17. Lin, D.Y.; Huang, S.; Chen, J. Crystal structures of a polypeptide processing and secretion transporter. *Nature* **2015**, *523*, 425–430. [CrossRef]
18. Perez, C.; Mehdipour, A.R.; Hummer, G.; Locher, K.P. Structure of Outward-Facing PglK and Molecular Dynamics of Lipid-Linked Oligosaccharide Recognition and Translocation. *Structure* **2019**, *27*, 669–678.e5. [CrossRef]
19. George, A.M.; Jones, P.M. An asymmetric post-hydrolysis state of the ABC transporter ATPase dimer. *PLoS ONE* **2013**, *8*, e59854. [CrossRef]
20. Prieß, M.; Göddeke, H.; Groenhof, G.; Schäfer, L.V. Molecular Mechanism of ATP Hydrolysis in an ABC Transporter. *ACS Cent. Sci.* **2018**, *4*, 1334–1343. [CrossRef]
21. Stefan, E.; Hofmann, S.; Tampé, R. A single power stroke by ATP binding drives substrate translocation in a heterodimeric ABC Transporter. *Elife* **2020**, *9*, e55943. [CrossRef] [PubMed]
22. Mishra, S.; Verhalen, B.; Stein, R.A.; Wen, P.C.; Tajkhorshid, E.; Mchaourab, H.S. Conformational dynamics of the nucleotide binding domains and the power stroke of a heterodimeric ABC transporter. *Elife* **2014**, *3*, e02740. [CrossRef] [PubMed]
23. Souabni, H.; Batista dos Santos, W.; Cece, Q.; Catoire, L.J.; Puvanendran, D.; Bavro, V.N.; Picard, M. Quantitative real-time analysis of the efflux by the MacAB-TolC tripartite efflux pump clarifies the role of ATP hydrolysis within mechanotransmission mechanism. *Commun. Biol.* **2021**, *4*, 493. [CrossRef] [PubMed]
24. Thomas, C.; Aller, S.G.; Beis, K.; Carpenter, E.P.; Chang, G.; Chen, L.; Dassa, E.; Dean, M.; Duong Van Hoa, F.; Ekiert, D.; et al. Structural and functional diversity calls for a new classification of ABC transporters. *FEBS Lett.* **2020**, *594*, 3767–3775. [CrossRef]
25. Ekiert, D.C.; Coudray, N.; Bhabha, G. Structure and mechanism of the bacterial lipid ABC transporter, MlaFEDB. *Curr. Opin. Struct. Biol.* **2022**, *76*, 102429. [CrossRef] [PubMed]
26. Kobayashi, N.; Nishino, K.; Yamaguchi, A. Novel macrolide-specific ABC-type efflux transporter in Escherichia coli. *J. Bacteriol.* **2001**, *183*, 5639–5644. [CrossRef]
27. Yamanaka, H.; Kobayashi, H.; Takahashi, E.; Okamoto, K. MacAB is involved in the secretion of Escherichia coli heat-stable enterotoxin II. *J. Bacteriol.* **2008**, *190*, 7693–7698. [CrossRef]
28. Turlin, E.; Heuck, G.; Simões Brandão, M.I.; Szili, N.; Mellin, J.R.; Lange, N.; Wandersman, C. Protoporphyrin (PPIX) efflux by the MacAB-TolC pump in Escherichia coli. *Microbiologyopen* **2014**, *3*, 849–859. [CrossRef]
29. Crow, A.; Greene, N.P.; Kaplan, E.; Koronakis, V. Structure and mechanotransmission mechanism of the MacB ABC transporter superfamily. *Proc. Natl. Acad. Sci. USA* **2017**, *114*, 12572–12577. [CrossRef]
30. Shi, K.; Cao, M.; Li, C.; Huang, J.; Zheng, S.; Wang, G. Efflux proteins MacAB confer resistance to arsenite and penicillin/macrolide-type antibiotics in Agrobacterium tumefaciens 5A. *World J. Microbiol. Biotechnol.* **2019**, *35*, 115. [CrossRef]
31. Zheng, J.X.; Lin, Z.W.; Sun, X.; Lin, W.H.; Chen, Z.; Wu, Y.; Qi, G.B.; Deng, Q.W.; Qu, D.; Yu, Z.J. Overexpression of OqxAB and MacAB efflux pumps contributes to eravacycline resistance and heteroresistance in clinical isolates of Klebsiella pneumoniae. *Emerg. Microbes. Infect.* **2018**, *7*, 139. [CrossRef]
32. Greene, N.P.; Kaplan, E.; Crow, A.; Koronakis, V. Antibiotic Resistance Mediated by the MacB ABC Transporter Family: A Structural and Functional Perspective. *Front. Microbiol.* **2018**, *9*, 950. [CrossRef] [PubMed]
33. Groisman, E.A. The pleiotropic two-component regulatory system PhoP-PhoQ. *J. Bacteriol.* **2001**, *183*, 1835–1842. [CrossRef] [PubMed]

34. Nishino, K.; Latifi, T.; Groisman, E.A. Virulence and drug resistance roles of multidrug efflux systems of Salmonella enterica serovar Typhimurium. *Mol. Microbiol.* **2006**, *59*, 126–141. [CrossRef] [PubMed]
35. Koronakis, V.; Sharff, A.; Koronakis, E.; Luisi, B.; Hughes, C. Crystal structure of the bacterial membrane protein TolC central to multidrug efflux and protein export. *Nature* **2000**, *405*, 914–919. [CrossRef]
36. Lin, H.T.; Bavro, V.N.; Barrera, N.P.; Frankish, H.M.; Velamakanni, S.; van Veen, H.W.; Robinson, C.V.; Borges-Walmsley, M.I.; Walmsley, A.R. MacB ABC transporter is a dimer whose ATPase activity and macrolide-binding capacity are regulated by the membrane fusion protein MacA. *J. Biol. Chem.* **2009**, *284*, 1145–1154. [CrossRef]
37. Tikhonova, E.B.; Devroy, V.K.; Lau, S.Y.; Zgurskaya, H.I. Reconstitution of the Escherichia coli macrolide transporter: The periplasmic membrane fusion protein MacA stimulates the ATPase activity of MacB. *Mol. Microbiol.* **2007**, *63*, 895–910. [CrossRef]
38. Barrera, N.P.; Isaacson, S.C.; Zhou, M.; Bavro, V.N.; Welch, A.; Schaedler, T.A.; Seeger, M.A.; Miguel, R.N.; Korkhov, V.M.; Van Veen, H.W.; et al. Mass spectrometry of membrane transporters reveals subunit stoichiometry and interactions. *Nat. Methods* **2009**, *6*, 585–587. [CrossRef]
39. Xu, Y.; Sim, S.H.; Nam, K.H.; Jin, X.L.; Kim, H.M.; Hwang, K.Y.; Lee, K.; Ha, N.C. Crystal structure of the periplasmic region of MacB, a noncanonic ABC transporter. *Biochemistry* **2009**, *48*, 5218–5225. [CrossRef]
40. Yum, S.; Xu, Y.; Piao, S.; Sim, S.H.; Kim, H.M.; Jo, W.S.; Kim, K.J.; Kweon, H.S.; Jeong, M.H.; Jeon, H.; et al. Crystal structure of the periplasmic component of a tripartite macrolide-specific efflux pump. *J. Mol. Biol.* **2009**, *387*, 1286–1297. [CrossRef]
41. Xu, Y.; Sim, S.H.; Song, S.; Piao, S.; Kim, H.M.; Jin, X.L.; Lee, K.; Ha, N.C. The tip region of the MacA alpha-hairpin is important for the binding to TolC to the Escherichia coli MacAB-TolC pump. *Biochem. Biophys Res. Commun.* **2010**, *394*, 962–965. [CrossRef] [PubMed]
42. Xu, Y.; Song, S.; Moeller, A.; Kim, N.; Piao, S.; Sim, S.H.; Kang, M.; Yu, W.; Cho, H.S.; Chang, I.; et al. Functional implications of an intermeshing cogwheel-like interaction between TolC and MacA in the action of macrolide-specific efflux pump MacAB-TolC. *J. Biol. Chem.* **2011**, *286*, 13541–13549. [CrossRef] [PubMed]
43. Lee, M.; Kim, H.L.; Song, S.; Joo, M.; Lee, S.; Kim, D.; Hahn, Y.; Ha, N.C.; Lee, K. The alpha-barrel tip region of Escherichia coli TolC homologs of Vibrio vulnificus interacts with the MacA protein to form the functional macrolide-specific efflux pump MacAB-TolC. *J. Microbiol.* **2013**, *51*, 154–159. [CrossRef] [PubMed]
44. Fitzpatrick, A.W.; Llabrés, S.; Neuberger, A.; Blaza, J.N.; Bai, X.C.; Okada, U.; Murakami, S.; Van Veen, H.W.; Zachariae, U.; Scheres, S.H.; et al. Structure of the MacAB-TolC ABC-type tripartite multidrug efflux pump. *Nat. Microbiol.* **2017**, *2*, 17070. [CrossRef]
45. Okada, U.; Yamashita, E.; Neuberger, A.; Morimoto, M.; van Veen, H.W.; Murakami, S. Crystal structure of tripartite-type ABC transporter MacB from Acinetobacter baumannii. *Nat. Commun.* **2017**, *8*, 1336. [CrossRef] [PubMed]
46. Yang, H.B.; Hou, W.T.; Cheng, M.T.; Jiang, Y.L.; Chen, Y.; Zhou, C.Z. Structure of a MacAB-like efflux pump from Streptococcus pneumoniae. *Nat. Commun.* **2018**, *9*, 196. [CrossRef] [PubMed]
47. Modali, S.D.; Zgurskaya, H.I. The periplasmic membrane proximal domain of MacA acts as a switch in stimulation of ATP hydrolysis by MacB transporter. *Mol. Microbiol.* **2011**, *81*, 937–951. [CrossRef]
48. Lu, S.; Zgurskaya, H.I. Role of ATP binding and hydrolysis in assembly of MacAB-TolC macrolide transporter. *Mol. Microbiol.* **2012**, *86*, 1132–1143. [CrossRef]
49. Batista Dos Santos, W.; Souabni, H.; Picard, M. Corseting a tripartite ABC transporter to make it fit for transport. *Biochimie* **2022**, *205*, 117–123. [CrossRef]
50. Mühlradt, P.F.; Golecki, J.R. Asymmetrical distribution and artifactual reorientation of lipopolysaccharide in the outer membrane bilayer of Salmonella typhimurium. *Eur. J. Biochem.* **1975**, *51*, 343–352. [CrossRef]
51. Beveridge, T.J. Structures of gram-negative cell walls and their derived membrane vesicles. *J. Bacteriol.* **1999**, *181*, 4725–4733. [CrossRef]
52. Raetz, C.R.; Whitfield, C. Lipopolysaccharide endotoxins. *Annu. Rev. Biochem.* **2002**, *71*, 635. [CrossRef] [PubMed]
53. Whitfield, C.; Trent, M.S. Biosynthesis and export of bacterial lipopolysaccharides. *Annu. Rev. Biochem.* **2014**, *83*, 99–128. [CrossRef] [PubMed]
54. Bertani, B.; Ruiz, N. Function and biogenesis of lipopolysaccharides. *EcoSal Plus* **2018**, *8*. [CrossRef] [PubMed]
55. Trent, M.S.; Ribeiro, A.A.; Lin, S.; Cotter, R.J.; Raetz, C.R. An Inner Membrane Enzyme in Salmonella and Escherichia coli That Transfers 4-Amino-4-deoxy-L-arabinose to Lipid A: Induction in Polymyxin-Resistant Mutants and Role of a Novel Lipid-Linked Donor. *J. Biol. Chem.* **2001**, *276*, 43122–43131. [CrossRef] [PubMed]
56. Nummila, K.; Kilpeläinen, I.; Zähringer, U.; Vaara, M.; Helander, I.M. Lipopolysaccharides of polymyxin B-resistant mutants of Escherichia coii are extensively substituted by 2-aminoethyl pyrophosphate and contain aminoarabinose in lipid A. *Mol. Microbiol.* **1995**, *16*, 271–278. [CrossRef] [PubMed]
57. Kawasaki, S.; Moriguchi, R.; Sekiya, K.; Nakai, T.; Ono, E.; Kume, K.; Kawahara, K. The cell envelope structure of the lipopolysaccharide-lacking gram-negative bacterium Sphingomonas paucimobilis. *J. Bacteriol.* **1994**, *176*, 284–290. [CrossRef]
58. Salazar, J.C.; Hazlett, K.R.; Radolf, J.D. The immune response to infection with Treponema pallidum, the stealth pathogen. *Microbes Infect.* **2002**, *4*, 1133–1140. [CrossRef]
59. Zhang, G.; Meredith, T.C.; Kahne, D. On the essentiality of lipopolysaccharide to Gram-negative bacteria. *Curr. Opin. Microbiol.* **2013**, *16*, 779–785. [CrossRef]

60. Narita S-i Tokuda, H. Biochemical characterization of an ABC transporter LptBFGC complex required for the outer membrane sorting of lipopolysaccharides. *FEBS Lett.* **2009**, *583*, 2160–2164. [CrossRef]
61. Freinkman, E.; Chng, S.-S.; Kahne, D. The complex that inserts lipopolysaccharide into the bacterial outer membrane forms a two-protein plug-and-barrel. *Proc. Natl. Acad. Sci. USA* **2011**, *108*, 2486–2491. [CrossRef] [PubMed]
62. Freinkman, E.; Okuda, S.; Ruiz, N.; Kahne, D. Regulated Assembly of the Transenvelope Protein Complex Required for Lipopolysaccharide Export. *Biochemistry* **2012**, *51*, 4800–4806. [CrossRef] [PubMed]
63. Thomas, C.; Tampé, R. Multifaceted structures and mechanisms of ABC transport systems in health and disease. *Curr. Opin. Struct. Biol.* **2018**, *51*, 116–128. [CrossRef] [PubMed]
64. Ruiz, N.; Gronenberg, L.S.; Kahne, D.; Silhavy, T.J. Identification of two inner-membrane proteins required for the transport of lipopolysaccharide to the outer membrane of Escherichia coli. *Proc. Natl. Acad. Sci. USA* **2008**, *105*, 5537–5542. [CrossRef]
65. Luo, Q.; Yang, X.; Yu, S.; Shi, H.; Wang, K.; Xiao, L.; Zhu, G.; Sun, C.; Li, T.; Li, D.; et al. Structural basis for lipopolysaccharide extraction by ABC transporter LptB2FG. *Nat. Struct. Mol. Biol.* **2017**, *24*, 469–474. [CrossRef]
66. Sherman, D.J.; Lazarus, M.B.; Murphy, L.; Liu, C.; Walker, S.; Ruiz, N.; Kahne, D. Decoupling catalytic activity from biological function of the ATPase that powers lipopolysaccharide transport. *Proc. Natl. Acad. Sci. USA* **2014**, *111*, 4982–4987. [CrossRef]
67. Wang, Z.; Xiang, Q.; Zhu, X.; Dong, H.; He, C.; Wang, H.; Zhang, Y.; Wang, W.; Dong, C. Structural and functional studies of conserved nucleotide-binding protein LptB in lipopolysaccharide transport. *Biochem. Biophys. Res. Commun.* **2014**, *452*, 443–449. [CrossRef]
68. Tran, A.X.; Dong, C.; Whitfield, C. Structure and functional analysis of LptC, a conserved membrane protein involved in the lipopolysaccharide export pathway in Escherichia coli. *J. Biol. Chem.* **2010**, *285*, 33529–33539. [CrossRef]
69. Sperandeo, P.; Lau, F.K.; Carpentieri, A.; De Castro, C.; Molinaro, A.; Deho, G.; Silhavy, T.J.; Polissi, A. Functional analysis of the protein machinery required for transport of lipopolysaccharide to the outer membrane of Escherichia coli. *J. Bacteriol.* **2008**, *190*, 4460–4469. [CrossRef]
70. Bos, M.P.; Tefsen, B.; Geurtsen, J.; Tommassen, J. Identification of an outer membrane protein required for the transport of lipopolysaccharide to the bacterial cell surface. *Proc. Natl. Acad. Sci. USA* **2004**, *101*, 9417–9422. [CrossRef]
71. Wu, T.; McCandlish, A.C.; Gronenberg, L.S.; Chng, S.S.; Silhavy, T.J.; Kahne, D. Identification of a protein complex that assembles lipopolysaccharide in the outer membrane of Escherichia coli. *Proc. Natl. Acad. Sci. USA* **2006**, *103*, 11754–11759. [CrossRef]
72. Dong, H.; Xiang, Q.; Gu, Y.; Wang, Z.; Paterson, N.G.; Stansfeld, P.J.; He, C.; Zhang, Y.; Wang, W.; Dong, C. Structural basis for outer membrane lipopolysaccharide insertion. *Nature* **2014**, *511*, 52–56. [CrossRef] [PubMed]
73. Qiao, S.; Luo, Q.; Zhao, Y.; Zhang, X.C.; Huang, Y. Structural basis for lipopolysaccharide insertion in the bacterial outer membrane. *Nature* **2014**, *511*, 108–111. [CrossRef]
74. Suits, M.D.; Sperandeo, P.; Dehò, G.; Polissi, A.; Jia, Z. Novel structure of the conserved gram-negative lipopolysaccharide transport protein A and mutagenesis analysis. *J. Mol. Biol.* **2008**, *380*, 476–488. [CrossRef]
75. Bowyer, A.; Baardsnes, J.; Ajamian, E.; Zhang, L.; Cygler, M. Characterization of interactions between LPS transport proteins of the Lpt system. *Biochem. Biophys. Res. Commun.* **2011**, *404*, 1093–1098. [CrossRef] [PubMed]
76. Sperandeo, P.; Villa, R.; Martorana, A.M.; Šamalikova, M.; Grandori, R.; Deho, G.; Polissi, A. New insights into the Lpt machinery for lipopolysaccharide transport to the cell surface: LptA-LptC interaction and LptA stability as sensors of a properly assembled transenvelope complex. *J. Bacteriol.* **2011**, *193*, 1042–1053. [CrossRef] [PubMed]
77. Dong, H.; Zhang, Z.; Tang, X.; Paterson, N.G.; Dong, C. Structural and functional insights into the lipopolysaccharide ABC transporter LptB2FG. *Nat. Commun.* **2017**, *8*, 1–11. [CrossRef] [PubMed]
78. Tang, X.; Chang, S.; Luo, Q.; Zhang, Z.; Qiao, W.; Xu, C.; Zhang, C.; Niu, Y.; Yang, W.; Wang, T.; et al. Cryo-EM structures of lipopolysaccharide transporter LptB(2)FGC in lipopolysaccharide or AMP-PNP-bound states reveal its transport mechanism. *Nat. Commun.* **2019**, *10*, 4175. [CrossRef]
79. Li, Y.; Orlando, B.J.; Liao, M. Structural basis of lipopolysaccharide extraction by the LptB2FGC complex. *Nature* **2019**, *567*, 486–490. [CrossRef]
80. Luo, Q.; Shi, H.; Xu, X. Cryo-EM structures of LptB2FG and LptB2FGC from Klebsiella pneumoniae in complex with lipopolysaccharide. *Biochem. Biophys. Res. Commun.* **2021**, *571*, 20–25. [CrossRef]
81. Owens, T.W.; Taylor, R.J.; Pahil, K.S.; Bertani, B.R.; Ruiz, N.; Kruse, A.C.; Kahne, D. Structural basis of unidirectional export of lipopolysaccharide to the cell surface. *Nature* **2019**, *567*, 550–553. [CrossRef] [PubMed]
82. Wilson, A.; Ruiz, N. The transmembrane alpha-helix of LptC participates in LPS extraction by the LptB2 FGC transporter. *Mol. Microbiol.* **2022**, *118*, 61–76. [CrossRef] [PubMed]
83. Bertani, B.R.; Taylor, R.J.; Nagy, E.; Kahne, D.; Ruiz, N. A cluster of residues in the lipopolysaccharide exporter that selects substrate variants for transport to the outer membrane. *Mol. Microbiol.* **2018**, *109*, 541–554. [CrossRef] [PubMed]
84. Hamad, M.A.; Di Lorenzo, F.; Molinaro, A.; Valvano, M.A. Aminoarabinose is essential for lipopolysaccharide export and intrinsic antimicrobial peptide resistance in Burkholderia cenocepacia. *Mol. Microbiol.* **2012**, *85*, 962–974. [CrossRef] [PubMed]
85. Gronow, S.; Brade, H. Invited review: Lipopolysaccharide biosynthesis: Which steps do bacteria need to survive? *J. Endotoxin Res.* **2001**, *7*, 3–23. [CrossRef]
86. Khare, D.; Oldham, M.L.; Orelle, C.; Davidson, A.L.; Chen, J. Alternating access in maltose transporter mediated by rigid-body rotations. *Mol. Cell* **2009**, *33*, 528–536. [CrossRef]

87. Lundstedt, E.A.; Simpson, B.W.; Ruiz, N. LptB-LptF coupling mediates the closure of the substrate-binding cavity in the LptB2FGC transporter through a rigid-body mechanism to extract LPS. *Mol. Microbiol.* **2020**, *114*, 200–213. [CrossRef]
88. Simpson, B.W.; Owens, T.W.; Orabella, M.J.; Davis, R.M.; May, J.M.; Trauger, S.A.; Kahne, D.; Ruiz, N. Identification of residues in the lipopolysaccharide ABC transporter that coordinate ATPase activity with extractor function. *MBio* **2016**, *7*, e01729-16. [CrossRef]
89. Simpson, B.W.; Pahil, K.S.; Owens, T.W.; Lundstedt, E.A.; Davis, R.M.; Kahne, D.; Ruiz, N. Combining mutations that inhibit two distinct steps of the ATP hydrolysis cycle restores wild-type function in the lipopolysaccharide transporter and shows that ATP binding triggers transport. *MBio* **2019**, *10*, e01931-19. [CrossRef]
90. Okuda, S.; Sherman, D.J.; Silhavy, T.J.; Ruiz, N.; Kahne, D. Lipopolysaccharide transport and assembly at the outer membrane: The PEZ model. *Nat. Rev. Microbiol.* **2016**, *14*, 337–345. [CrossRef]
91. Sherman, D.J.; Xie, R.; Taylor, R.J.; George, A.H.; Okuda, S.; Foster, P.J.; Needleman, D.J.; Kahne, D. Lipopolysaccharide is transported to the cell surface by a membrane-to-membrane protein bridge. *Science* **2018**, *359*, 798–801. [CrossRef]
92. Botte, M.; Ni, D.; Schenck, S.; Zimmermann, I.; Chami, M.; Bocquet, N.; Egloff, P.; Bucher, D.; Trabuco, M.; Cheng, R.K.; et al. Cryo-EM structures of a LptDE transporter in complex with Pro-macrobodies offer insight into lipopolysaccharide translocation. *Nat. Commun.* **2022**, *13*, 1–10. [CrossRef] [PubMed]
93. Gu, Y.; Stansfeld, P.J.; Zeng, Y.; Dong, H.; Wang, W.; Dong, C. Lipopolysaccharide is inserted into the outer membrane through an intramembrane hole, a lumen gate, and the lateral opening of LptD. *Structure* **2015**, *23*, 496–504. [CrossRef] [PubMed]
94. Malojčić, G.; Andres, D.; Grabowicz, M.; George, A.H.; Ruiz, N.; Silhavy, T.J.; Kahne, D. LptE binds to and alters the physical state of LPS to catalyze its assembly at the cell surface. *Proc. Natl. Acad. Sci. USA* **2014**, *111*, 9467–9472. [CrossRef] [PubMed]
95. Chng, S.S.; Ruiz, N.; Chimalakonda, G.; Silhavy, T.J.; Kahne, D. Characterization of the two-protein complex in Escherichia coli responsible for lipopolysaccharide assembly at the outer membrane. *Proc. Natl. Acad. Sci. USA* **2010**, *107*, 5363–5368. [CrossRef] [PubMed]
96. Ruiz, N.; Chng, S.S.; Hiniker, A.; Kahne, D.; Silhavy, T.J. Nonconsecutive disulfide bond formation in an essential integral outer membrane protein. *Proc. Natl. Acad. Sci. USA* **2010**, *107*, 12245–12250. [CrossRef] [PubMed]
97. Chimalakonda, G.; Ruiz, N.; Chng, S.S.; Garner, R.A.; Kahne, D.; Silhavy, T.J. Lipoprotein LptE is required for the assembly of LptD by the β-barrel assembly machine in the outer membrane of Escherichia coli. *Proc. Natl. Acad. Sci. USA* **2011**, *108*, 2492–2497. [CrossRef]
98. Xie, R.; Taylor, R.J.; Kahne, D. Outer Membrane Translocon Communicates with Inner Membrane ATPase To Stop Lipopolysaccharide Transport. *J. Am. Chem. Soc.* **2018**, *140*, 12691–12694. [CrossRef]
99. Baeta, T.; Giandoreggio-Barranco, K.; Ayala, I.; Moura, E.C.; Sperandeo, P.; Polissi, A.; Simorre, J.P.; Laguri, C. The lipopolysaccharide-transporter complex LptB2FG also displays adenylate kinase activity in vitro dependent on the binding partners LptC/LptA. *J. Biol. Chem.* **2021**, *297*, 101313. [CrossRef]
100. Randak, C.; Welsh, M.J. An intrinsic adenylate kinase activity regulates gating of the ABC transporter CFTR. *Cell* **2003**, *115*, 837–850. [CrossRef]
101. Kaur, H.; Lakatos-Karoly, A.; Vogel, R.; Nöll, A.; Tampé, R.; Glaubitz, C. Coupled ATPase-adenylate kinase activity in ABC transporters. *Nat. Commun.* **2016**, *7*, 13864. [CrossRef] [PubMed]
102. Villa, R.; Martorana, A.M.; Okuda, S.; Gourlay, L.J.; Nardini, M.; Sperandeo, P.; Dehò, G.; Bolognesi, M.; Kahne, D.; Polissi, A. The Escherichia coli Lpt transenvelope protein complex for lipopolysaccharide export is assembled via conserved structurally homologous domains. *J. Bacteriol.* **2013**, *195*, 1100–1108. [CrossRef] [PubMed]
103. Falchi, F.A.; Taylor, R.J.; Rowe, S.J.; Moura, E.C.; Baeta, T.; Laguri, C.; Simorre, J.P.; Kahne, D.E.; Polissi, A.; Sperandeo, P. Suppressor Mutations in LptF Bypass Essentiality of LptC by Forming a Six-Protein Transenvelope Bridge That Efficiently Transports Lipopolysaccharide. *mBio* **2022**, *0*, e02202-22. [CrossRef] [PubMed]
104. Benedet, M.; Falchi, F.A.; Puccio, S.; Di Benedetto, C.; Peano, C.; Polissi, A.; Deho, G. The lack of the essential LptC protein in the trans-envelope lipopolysaccharide transport machine is circumvented by suppressor mutations in LptF, an inner membrane component of the Escherichia coli transporter. *PLoS ONE* **2016**, *11*, e0161354. [CrossRef]
105. Silhavy, T.J.; Kahne, D.; Walker, S. The bacterial cell envelope. *Cold Spring Harb Perspect. Biol.* **2010**, *2*, a000414. [CrossRef]
106. Malinverni, J.C.; Silhavy, T.J. An ABC transport system that maintains lipid asymmetry in the gram-negative outer membrane. *Proc. Natl. Acad. Sci. USA* **2009**, *106*, 8009–8014. [CrossRef]
107. Powers, M.J.; Trent, M.S. Phospholipid retention in the absence of asymmetry strengthens the outer membrane permeability barrier to last-resort antibiotics. *Proc. Natl. Acad. Sci. USA* **2018**, *115*, E8518–E8527. [CrossRef]
108. Sutterlin, H.A.; Shi, H.; May, K.L.; Miguel, A.; Khare, S.; Huang, K.C.; Silhavy, T.J. Disruption of lipid homeostasis in the Gram-negative cell envelope activates a novel cell death pathway. *Proc. Natl. Acad. Sci. USA* **2016**, *113*, E1565–E1574. [CrossRef]
109. Thong, S.; Ercan, B.; Torta, F.; Fong, Z.Y.; Wong, H.Y.A.; Wenk, M.R.; Chng, S.S. Defining key roles for auxiliary proteins in an ABC transporter that maintains bacterial outer membrane lipid asymmetry. *Elife* **2016**, *5*, e19042. [CrossRef]
110. Benning, C. A role for lipid trafficking in chloroplast biogenesis. *Prog. Lipid Res.* **2008**, *47*, 381–389. [CrossRef]
111. Mohn, W.W.; Van Der Geize, R.; Stewart, G.R.; Okamoto, S.; Liu, J.; Dijkhuizen, L.; Eltis, L.D. The actinobacterial mce4 locus encodes a steroid transporter. *J. Biol. Chem.* **2008**, *283*, 35368–35374. [CrossRef]
112. Pandey, A.K.; Sassetti, C.M. Mycobacterial persistence requires the utilization of host cholesterol. *Proc. Natl. Acad. Sci. USA* **2008**, *105*, 4376–4380. [CrossRef] [PubMed]

113. Low, W.-Y.; Thong, S.; Chng, S.-S. ATP disrupts lipid-binding equilibrium to drive retrograde transport critical for bacterial outer membrane asymmetry. *Proc. Natl. Acad. Sci. USA* **2021**, *118*, e2110055118. [CrossRef] [PubMed]
114. Tang, X.; Chang, S.; Qiao, W.; Luo, Q.; Chen, Y.; Jia, Z.; Coleman, J.; Zhang, K.; Wang, T.; Zhang, Z.; et al. Structural insights into outer membrane asymmetry maintenance in Gram-negative bacteria by MlaFEDB. *Nat. Struct. Mol. Biol.* **2021**, *28*, 81–91. [CrossRef] [PubMed]
115. Abellón-Ruiz, J.; Kaptan, S.S.; Baslé, A.; Claudi, B.; Bumann, D.; Kleinekathöfer, U.; van den Berg, B. Structural basis for maintenance of bacterial outer membrane lipid asymmetry. *Nat. Microbiol.* **2017**, *2*, 1616–1623. [CrossRef] [PubMed]
116. Chong, Z.S.; Woo, W.F.; Chng, S.S. Osmoporin OmpC forms a complex with MlaA to maintain outer membrane lipid asymmetry in E scherichia coli. *Mol. Microbiol.* **2015**, *98*, 1133–1146. [CrossRef]
117. Ekiert, D.C.; Bhabha, G.; Isom, G.L.; Greenan, G.; Ovchinnikov, S.; Henderson, I.R.; Cox, J.S.; Vale, R.D. Architectures of lipid transport systems for the bacterial outer membrane. *Cell* **2017**, *169*, 273–285.e17. [CrossRef]
118. Ercan, B.; Low, W.Y.; Liu, X.; Chng, S.S. Characterization of interactions and phospholipid transfer between substrate binding proteins of the OmpC-Mla system. *Biochemistry* **2018**, *58*, 114–119. [CrossRef]
119. Hughes, G.W.; Hall, S.C.; Laxton, C.S.; Sridhar, P.; Mahadi, A.H.; Hatton, C.; Piggot, T.J.; Wotherspoon, P.J.; Leney, A.C.; Ward, D.G.; et al. Evidence for phospholipid export from the bacterial inner membrane by the Mla ABC transport system. *Nat. Microbiol.* **2019**, *4*, 1692–1705. [CrossRef]
120. Isom, G.L.; Davies, N.J.; Chong, Z.S.; Bryant, J.A.; Jamshad, M.; Sharif, M.; Cunningham, A.F.; Knowles, T.J.; Chng, S.S.; Cole, J.A.; et al. MCE domain proteins: Conserved inner membrane lipid-binding proteins required for outer membrane homeostasis. *Sci. Rep.* **2017**, *7*, 8608. [CrossRef]
121. Chi, X.; Fan, Q.; Zhang, Y.; Liang, K.; Wan, L.; Zhou, Q.; Li, Y. Structural mechanism of phospholipids translocation by MlaFEDB complex. *Cell Res.* **2020**, *30*, 1127–1135. [CrossRef] [PubMed]
122. Oldham, M.L.; Chen, J. Crystal structure of the maltose transporter in a pretranslocation intermediate state. *Science* **2011**, *332*, 1202–1205. [CrossRef] [PubMed]
123. Shibagaki, N.; Grossman, A.R. The role of the STAS domain in the function and biogenesis of a sulfate transporter as probed by random mutagenesis. *J. Biol. Chem.* **2006**, *281*, 22964–22973. [CrossRef] [PubMed]
124. Kolich, L.R.; Chang, Y.T.; Coudray, N.; Giacometti, S.I.; MacRae, M.R.; Isom, G.L.; Teran, E.M.; Bhabha, G.; Ekiert, D.C. Structure of MlaFB uncovers novel mechanisms of ABC transporter regulation. *Elife* **2020**, *9*, e60030. [CrossRef] [PubMed]
125. Kamischke, C.; Fan, J.; Bergeron, J.; Kulasekara, H.D.; Dalebroux, Z.D.; Burrell, A.; Kollman, J.M.; Miller, S.I. The Acinetobacter baumannii Mla system and glycerophospholipid transport to the outer membrane. *Elife* **2019**, *8*, e40171. [CrossRef]
126. Coudray, N.; Isom, G.L.; MacRae, M.R.; Saiduddin, M.N.; Bhabha, G.; Ekiert, D.C. Structure of bacterial phospholipid transporter MlaFEDB with substrate bound. *Elife* **2020**, *9*, e62518. [CrossRef]
127. Zhou, C.; Shi, H.; Zhang, M.; Zhou, L.; Xiao, L.; Feng, S.; Im, W.; Zhou, M.; Zhang, X.; Huang, Y. Structural insight into phospholipid transport by the MlaFEBD complex from P. aeruginosa. *J. Mol. Biol.* **2021**, *433*, 166986. [CrossRef]
128. Mann, D.; Fan, J.; Somboon, K.; Farrell, D.P.; Muenks, A.; Tzokov, S.B.; DiMaio, F.; Khalid, S.; Miller, S.I.; Bergeron, J.R. Structure and lipid dynamics in the maintenance of lipid asymmetry inner membrane complex of A. baumannii. *Commun. Biol.* **2021**, *4*, 1–9. [CrossRef]
129. Zhang, Y.; Fan, Q.; Chi, X.; Zhou, Q.; Li, Y. Cryo-EM structures of Acinetobacter baumannii glycerophospholipid transporter. *Cell Discov.* **2020**, *6*, 86. [CrossRef]
130. Yeow, J.; Tan, K.W.; Holdbrook, D.A.; Chong, Z.S.; Marzinek, J.K.; Bond, P.J.; Chng, S.S. The architecture of the OmpC–MlaA complex sheds light on the maintenance of outer membrane lipid asymmetry in Escherichia coli. *J. Biol. Chem.* **2018**, *293*, 11325–11340. [CrossRef]
131. Hughes, G.W.; Sridhar, P.; Nestorow, S.A.; Wotherspoon, P.J.; Cooper, B.F.; Knowles, T.J. MlaFEDB displays flippase activity to promote phospholipid transport towards the outer membrane of Gram-negative bacteria. *bioRxiv* **2020**. [CrossRef]
132. Narita, S.I.; Tokuda, H. Bacterial lipoproteins; biogenesis, sorting and quality control. *Biochim. Biophys. Acta. Mol. Cell Biol. Lipids.* **2017**, *1862*, 1414–1423. [CrossRef]
133. Grabowicz, M. Lipoproteins and Their Trafficking to the Outer Membrane. *EcoSal Plus* **2019**, *8*. [CrossRef] [PubMed]
134. Hayashi, S.; Wu, H.C. Lipoproteins in bacteria. *J. Bioenerg. Biomembr.* **1990**, *22*, 451–471. [CrossRef] [PubMed]
135. Babu, M.M.; Priya, M.L.; Selvan, A.T.; Madera, M.; Gough, J.; Aravind, L.; Sankaran, K. A database of bacterial lipoproteins (DOLOP) with functional assignments to predicted lipoproteins. *J. Bacteriol.* **2006**, *188*, 2761–2773. [CrossRef] [PubMed]
136. Pugsley, A.P. The complete general secretory pathway in gram-negative bacteria. *Microbiol. Rev.* **1993**, *57*, 50–108. [CrossRef]
137. Giménez, M.I.; Dilks, K.; Pohlschröder, M. Haloferax volcanii twin-arginine translocation substates include secreted soluble, C-terminally anchored and lipoproteins. *Mol. Microbiol.* **2007**, *66*, 1597–1606. [CrossRef]
138. Sankaran, K.; Wu, H.C. Lipid modification of bacterial prolipoprotein. Transfer of diacylglyceryl moiety from phosphatidylglycerol. *J. Biol. Chem.* **1994**, *269*, 19701–19706. [CrossRef]
139. Inouye, S.; Franceschini, T.; Sato, M.; Itakura, K.; Inouye, M. Prolipoprotein signal peptidase of Escherichia coli requires a cysteine residue at the cleavage site. *EMBO J.* **1983**, *2*, 87–91. [CrossRef]
140. Vogeley, L.; El Arnaout, T.; Bailey, J.; Stansfeld, P.J.; Boland, C.; Caffrey, M. Structural basis of lipoprotein signal peptidase II action and inhibition by the antibiotic globomycin. *Science* **2016**, *351*, 876–880. [CrossRef]

141. Jackowski, S.; Rock, C.O. Transfer of fatty acids from the 1-position of phosphatidylethanolamine to the major outer membrane lipoprotein of Escherichia coli. *J. Biol. Chem.* **1986**, *261*, 11328–11333. [CrossRef] [PubMed]
142. Gupta, S.D.; Wu, H.C. Identification and subcellular localization of apolipoprotein N-acyltransferase in Escherichia coli. *FEMS Microbiol. Lett.* **1991**, *62*, 37–41. [CrossRef] [PubMed]
143. Yamaguchi, K.; Yu, F.; Inouye, M. A single amino acid determinant of the membrane localization of lipoproteins in E. coli. *Cell* **1988**, *53*, 423–432. [CrossRef] [PubMed]
144. Gennity, J.M.; Inouye, M. The protein sequence responsible for lipoprotein membrane localization in Escherichia coli exhibits remarkable specificity. *J. Biol. Chem.* **1991**, *266*, 16458–16464. [CrossRef] [PubMed]
145. Matsuyama, S.; Tajima, T.; Tokuda, H. A novel periplasmic carrier protein involved in the sorting and transport of Escherichia coli lipoproteins destined for the outer membrane. *EMBO J.* **1995**, *14*, 3365–3372. [CrossRef]
146. Matsuyama, S.; Yokota, N.; Tokuda, H. A novel outer membrane lipoprotein, LolB (HemM), involved in the LolA (p20)-dependent localization of lipoproteins to the outer membrane of Escherichia coli. *EMBO J.* **1997**, *16*, 6947–6955. [CrossRef]
147. Takeda, K.; Miyatake, H.; Yokota, N.; Matsuyama, S.I.; Tokuda, H.; Miki, K. Crystal structures of bacterial lipoprotein localization factors, LolA and LolB. *EMBO J.* **2003**, *22*, 3199–3209. [CrossRef]
148. Yakushi, T.; Masuda, K.; Narita, S.I.; Matsuyama, S.I.; Tokuda, H. A new ABC transporter mediating the detachment of lipid-modified proteins from membranes. *Nat. Cell Biol.* **2000**, *2*, 212–218. [CrossRef]
149. Kaplan, E.; Greene, N.P.; Crow, A.; Koronakis, V. Insights into bacterial lipoprotein trafficking from a structure of LolA bound to the LolC periplasmic domain. *Proc. Natl. Acad. Sci. USA* **2018**, *115*, E7389–E7397. [CrossRef]
150. Kaplan, E.; Greene, N.P.; Jepson, A.E.; Koronakis, V. Structural basis of lipoprotein recognition by the bacterial Lol trafficking chaperone LolA. *Proc. Natl. Acad. Sci. USA* **2022**, *119*, e2208662119. [CrossRef]
151. Tang, X.; Chang, S.; Zhang, K.; Luo, Q.; Zhang, Z.; Wang, T.; Qiao, W.; Wang, C.; Shen, C.; Zhang, Z.; et al. Structural basis for bacterial lipoprotein relocation by the transporter LolCDE. *Nat. Struct. Mol. Biol.* **2021**, *28*, 347–355. [CrossRef] [PubMed]
152. Sharma, S.; Zhou, R.; Wan, L.; Feng, S.; Song, K.; Xu, C.; Li, Y.; Liao, M. Mechanism of LolCDE as a molecular extruder of bacterial triacylated lipoproteins. *Nat. Commun.* **2021**, *12*, 4687. [CrossRef] [PubMed]
153. Bei, W.; Luo, Q.; Shi, H.; Zhou, H.; Zhou, M.; Zhang, X.; Huang, Y. Cryo-EM structures of LolCDE reveal the molecular mechanism of bacterial lipoprotein sorting in Escherichia coli. *PLoS Biol.* **2022**, *20*, e3001823. [CrossRef] [PubMed]

3.2. Chapter 2: Optimisation of the purification of the ABC transporter HlyB from *Escherichia coli*

Title:	Optimisation of the purification of the ABC transporter HlyB from *Escherichia coli*
Authors:	**Florestan L. Bilsing**, Sander Smits, Lutz Schmitt
Published in:	to be submitted
Own contribution:	Designing the experiments Performing the experiments Data evaluation Preparation of the figures Writing of the manuscript

Optimisation of the purification of the ABC transporter HlyB from *Escherichia coli*

Florestan L. Bilsing[1], Sander Smits[1,2], Lutz Schmitt[1]*

[1]Heinrich Heine University Düsseldorf, Faculty of Mathematics and Natural Sciences, Institute of Biochemistry, Universitätsstraße 1, 40225 Düsseldorf
[2]Heinrich Heine University Düsseldorf, Faculty of Mathematics and Natural Sciences, Center for Structural Studies, Universitätsstraße 1, 40225 Düsseldorf

*Corresponding author: Lutz Schmitt, Heinrich Heine University Düsseldorf, Faculty of Mathematics and Natural Sciences, Institute of Biochemistry, Universitätsstraße 1, 40225 Düsseldorf, Germany, Tel.: +49 211 81 10773, E-Mail: lutz.schmitt@hhu.de

Abstract

The ATP-binding cassette (ABC) transporter hemolysin B (HlyB) is a central part of the hemolysin A (HlyA) type 1 secretion system (T1SS) from *Escherichia coli* (*E. coli*). It is not only responsible for ATP hydrolysis to provide the energy for the secretion process, but also plays an important role in substrate recognition via two different substrate binding sites. This high level of complexity makes the HlyA T1SS and its ABC transporter HlyB a highly interesting target for membrane protein research. To enable structural and functional research on membrane proteins, a reliable expression and purification protocol for production of high-quality protein is necessary. Therefore multiple parameters need to be taken into account and several conditions need to be tested and optimised. Here we report the optimisation of a purification protocol for the ABC transporter HlyB. We could improve sample purity by changing the affinity tag from a His-tag to a TwinStrep-tag. In addition, we observed a change in growth behaviour of the cells due to the change of the affinity tag. Furthermore we compared the detergents DDM and GDN for the purification of HlyB. We conclude that a combination of Fos-Cholin-14 for solubilisation and the novel detergent GDN for the purification in combination with a TwinStrep-tag on the N-terminus of HlyB result in high-quality protein samples that are suitable for functional and structural studies.

Introduction

The ATP-binding cassette (ABC) transporter hemolysin B (HlyB) is part of the hemolysin A (HlyA) type 1 secretion system (T1SS) in *Escherichia coli* (*E. coli*) and provides the energy necessary for substrate translocation [1, 2]. The substrate HlyA is a 110 kDa toxin and secreted unfolded via its T1SS without periplasmic intermediates across the inner and outer membrane of *E. coli* [3-5]. The secretion process requires a complex interplay between all components of the T1SS [6-11]. One central part of the T1SS is the ABC transporter HlyB. HlyB consists of three domains: the so-called C39 peptidase-like domain (CLD) at the N-terminus, the transmembrane domain (TMD) and the nucleotide binding domain (NBD) at the C-terminus. The CLD shares about 40% homology with C39 peptidases but lacks peptidase activity. Within the secretion process the CLD fulfils a dual role. It harbours a substrate recognition site and serves as contact site for stabilisation of the IMC [6, 12]. The TMD of HlyB is build up by six transmembrane helices (TMH) which add up to 12 TMH in the homodimer. So far no classical substrate binding site within the TMD was detected but cross-linking studies tracked a translocation channel through the centre of the TMD dimer interface [7, 12]. The NBD of HlyB exhibits the classical highly conserved motifs such as Walker A, Walker B, C-loop and D-loop [13]. Furthermore, it is well characterized in terms of structure and biochemical function [13-15]. A histidine residue crucial for ATP hydrolysis was determined in the H-loop of the NDB [16]. Besides the nucleotide binding the NBD of HlyB shows additional interaction with the substrate HlyA [9, 17]. Recently the structure of the so-called inner membrane complex (IMC) composed of the ABC transporter HlyB and the membrane fusion protein hemolysin D (HlyD) was published. Within the IMC, HlyB adopts an unexpected stoichiometry by forming a trimer of dimers [12].

For structural and functional studies sufficient amounts of protein is crucial. Standard membrane protein expression and purification protocols are available and provide a good starting point [18, 19]. However large quantities of membrane proteins are very demanding and require adaptations of standard protocols combined with various screenings for the right condition [20-22]. First of all the choice of the right expression host is important [23]. Furthermore genetic modifications of the expression host or the membrane protein are possible strategies for successful membrane protein production and stabilisation [24, 25]. Next the choice of the detergent needs to be addressed and probably involves a lot of screening and a suitable read out [26-28]. Depending on the

purification strategy the affinity tag and its position might be another important factor [29].

Here we present an optimisation of the expression and purification of the ABC transporter HlyB from *E. coli* for structural studies. We used the already published protocol for functional studies [30] as a starting point and adapted different parameters such as choice of affinity tag, expression conditions and detergent. We could show that the TwinStrep-tag strongly improved protein purity but decreased protein yield during expression. In addition we could observe loss of ATPase activity in Fos-Choline-14 and stabilisation of possible higher oligomers of HlyB in GDN.

Material and Methods

Cloning of pBAD-TSHlyB

E. coli DH5α was used for cloning. pBAD-TSHlyB was generated via Gibson Assembly using a double-stranded DNA oligomer for the TwinStrep-tag (TS) and the primers (Table S1) TSHlyB_fwd and TSHlyB_rev to amplify the vector from pBAD-HisHlyB. The 10xHis-tag (His) on the N-terminus of HlyB was replaced by a TwinStrep-tag on the N-terminus.

Expression and purification of HisHlyB

Expression of HisHlyB was performed in *E. coli* C41Δ*acrAB*Δ*ompF*(DE3) using a pBAD based plasmid with an 10xHis-tag following published protocol [7].

The purification of HisHlyB was adapted from a published protocol [30]. Cell pellet after harvest was resuspended in buffer A (50 mM NaH_2PO_4 pH 8, 300 mM NaCl) and one cOmplete EDTA-free inhibitor cocktail tablet and a spatulas tip of DNAse I were added. Cell disruption was performed by three passes through Microfluidizer M-110P (Microfluidics) at 1.5 kbar. Centrifugation was performed at 18,000 xg for 30 minutes at 4 °C to get rid of cell debris. Supernatant was centrifuged for 90 minutes at 38,000 rpm (Type 45 Ti, Beckman Coulter) at 4 °C to pellet membranes. Membranes were resuspended in buffer A, adjusted to 10 mg/ml and solubilised for 1 hours at 4 °C using 0.5 % Fos-Choline-14 (FC14). Non-solubilized material was removed by filtration through a 0.45 µm filter. The solubilized membrane was diluted 1:4 with buffer A to get a final concentration of FC14 of 0.1%. The supernatant was loaded on a 5 ml HiTrap Chelating HP (Cytiva) column (Zn^{2+}-loaded) equilibrated with 5 column volumes (CV)

buffer A1 (50 mM NaH_2PO_4 pH 8, 300 mM NaCl, 0.015 % DDM, 2 mM imidazole). Column was washed with 2 CV buffer A1 and 4 CV buffer A2 (50 mM NaH_2PO_4 pH 8, 300 mM NaCl, 0.015 % DDM, 40 mM imidazole). HisHlyB was eluted with buffer A3 (50 mM NaH_2PO_4 pH 8, 300 mM NaCl, 0.015 % DDM, 25 mM EDTA). Fractions containing HisHlyB were combined and concentrated using an Amicon Ultra-15 centrifugal filter unit (Millipore) with a MWCO of 100 kDa. The concentrated sample was centrifuged for 30 minutes at 17,000 xg and 4 °C and supernatant was applied on Superose 6 Increase 10/300 GL equilibrated with buffer B (100 mM Hepes pH 8, 250 mM NaCl, 0.015% DDM). Fractions containing HlyB were combined and concentrated using an Amicon Ultra-4 centrifugal filter unit (Millipore) with a MWCO of 100 kDa.
For the purification of HisHlyB in lysophosphatidylglycerol (LPG), 1% LPG was used for solubilisation instead of FC14 and 1.2 mM LPG was used in buffers instead of DDM.

Solubilizationtest for HisHlyB

For the solubilization test of HisHlyB the membrane was diluted to 10 mg/ml in buffer C (50 mM NaP_i, pH 8, 150 mM NaCl). The detergents were used at a concentration of 1% and the final volume of the sample was 1 ml. The sample was incubated at 4 °C for 1 hour under constant agitation. After centrifugation for 20 min at 100,000 xg the supernatant was applied on a 10% SDS-PAGE gel.

Expression and purification of TSHlyB

HlyB was expressed in *E. coli* C41ΔacrABΔompF(DE3) using a pBAD based plasmid containing an N-terminal TwinStrep-tag. Cells were grown in 50 ml 2YT medium in a 300 ml baffled flask supplemented with 100 µg/ml ampicillin at 37 °C and 180 rpm overnight. Expression cultures of 1 L 2YT supplemented with 100 µg/ml ampicillin in 5 L baffled flasks were inoculated from the precultures to an OD_{600} of 0.1 and incubated at 37 °C and 120 rpm. Expression was induced at OD_{600} of 0.7 by addition of 10 mM arabinose and expression was performed for 3 h. Cells were harvested via centrifugation at 5,000 xg for 20 minutes at 4 °C. Pellet was resuspended in buffer A1 and 1 cOmplete EDTA-free inhibitor cocktail tablet and a spatulas tip of DNAse I were added. Cell disruption was performed by three passes through Microfluidizer M-110P (Microfluidics) at 1.5 kbar. Centrifugation was performed at 18,000 xg for 30 minutes at 4 °C to get rid of cell debris. Supernatant was centrifuged for 90 minutes at 38,000 rpm (Type 45 Ti, Beckman Coulter) at 4 °C to pellet membranes. Membranes were

resuspended in buffer A (50 mM NaH_2PO_4 pH 8, 300 mM NaCl) and adjusted to 10 mg/ml and solubilised for 1 hours at 4 °C using 0.5 % Fos-Choline-14. Non-solubilized material was removed by centrifugation for 30 minutes at 38,000 rpm (Type 45 Ti, Beckman Coulter) at 4 °C and diluted once with buffer A. Supernatant was loaded on a 5 ml StrepTrap HP (Cytiva) column equilibrated with buffer A4 (50 mM NaH_2PO_4 pH 8, 300 mM NaCl, 0.015 % DDM). Column was washed 10 CV with buffer A4 and HlyB was eluted with 6 CV buffer A5 (50 mM NaH_2PO_4 pH 8, 300 mM NaCl, 0.015 % DDM, 2.5 mM desthiobiotin). Fractions containing HlyB were combined and concentrated using an Amicon Ultra-15 centrifugal filter unit (Millipore) with a MWCO of 100 kDa. The concentrated sample was centrifuged for 30 minutes at 17,000 xg and 4 °C and supernatant was applied on Superose 6 Increase 10/300 GL equilibrated with buffer D (20 mM Hepes pH 8, 100 mM NaCl, 0.015% DDM). Fractions containing HlyB were combined and concentrated using an Amicon Ultra-4 centrifugal filter unit (Millipore) with a MWCO of 100 kDa. For the purification in FC14 only, the buffers contained 0.01% FC14. For the purification with exchange of detergent from FC14 to GDN, the buffers contained 0.0063 % GDN. For the purification in GDN only, the membrane was solubilized at 20 mg/ml with 1.5% GDN and all buffers contained 0.0042% GDN.

Blue Native-PAGE

For the Blue Native-PAGE the NativePAGE Novex Bis-Tris Gel System (Invitrogen) was used. Samples were prepared with 4x Sample Buffer (50 mM BisTris, 6 N HCl, 50 mM NaCl, 10% glycerol (w/v), 0.001% ponceau S, pH 7.2) and NativePAGE 5% G-250 Sample Additive (5% Coomassie G-250). The run was performed at 4 °C using NativePAGE Anode Buffer (50 mM BisTris, 50 mM Tricine, pH 6.8) and NativePAGE Cathode Buffer Dark Blue (50 mM BisTris, 50 mM Tricine, pH 6.8, 0.02 % Coomassie G-250) for 15 min at 100 V. Next the NativePAGE Cathode Buffer Dark Blue was exchanged to NativePAGE Cathode Buffer Light Blue (50 mM BisTris, 50 mM Tricine, pH 6.8, 0.002 % Coomassie G-250) and electrophoresis was performed 45 min at 150 V and one additional hour at 250 V.

Malachite Green ATPase activity assay

For measuring ATPase activity the Malachite Green assay [31] was used with the following adaptations. ATP was used in final concentrations of 4 mM and $MgCl_2$ was used in a final concentration of 10 mM. Negative controls contained no $MgCl_2$.

Reactions were started by addition of ATP and incubated for 40 minutes at 25 °C. The reaction was stopped by adding the reaction set up (25 µl) to 175 µl 10 mM H_2SO_4. The assay was stained by adding 50 µl freshly prepared staining solution (0.096% (w/v) malachite green, 1.48% (w/v) ammonium molybdate, 0,17% (v/v) Tween-20 in 15 % H_2SO_4) and absorption at 595 nm was measured after 8 min of incubation at RT.

Results

Purifications using HisHlyB

In the published protocol for purification of HlyB [30] Fos-Cholin-14 (FC14) was used for solubilisation and detergent exchange to DDM was performed during affinity purification. HlyB contained a 10xHis-Tag and was used for functional studies immediately after IMAC.

We sticked to the published protocol and tried to improve purity by subsequent size exclusion chromatography (SEC) (Figure 1A). SDS-PAGE and Western blot analysis were used to monitor the success (Figure 1B). Samples from the main elution peak were used for initial cryo-EM analysis and 2D classification (Figure 1C).

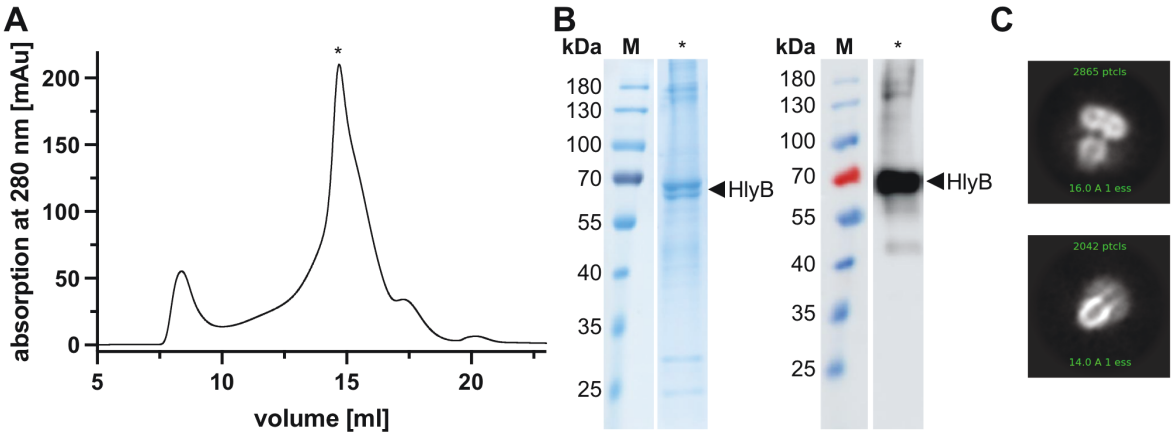

Figure 1: Purification of HisHlyB in DDM. A: *SEC analysis of HisHlyB on Superose 6 Inc. 10/300 GL.* ***B:*** *SDS-PAGE (left) and Western blot (right) analysis of purified HisHlyB. M: marker proteins with their approximated molecular weight. *: sample from HisHlyB main elution peak. The band for HlyB is marked with a black triangle. Protein-specific anti-HlyB antibody was used for detection.* ***C:*** *Two out of 60 2D classes from single particle cryo-EM analysis of the main elution peak. Number of particles and average resolution are indicated in green letters.*

Although only one peak was visible in the SEC profile the SDS-PAGE showed multiple protein bands. HisHlyB migrated as a prominent double band at around 70 kDa, as confirmed by Western blot analysis (Figure 1B). Furthermore, we could show ATPase activity for HisHlyB in DDM (data not shown). In line with the non-homogenous SDS-PAGE only a few 2D classes could be assigned to HisHlyB (Figure 1C). As additional

purification polishing steps did not yield a sample of higher purity we tried to improve the purification process at different stages.

We tested whether a different detergent than Fos-Choline-14 can be used for solubilisation of HisHlyB. We tried DDM, LMNG and GDN and compared the solubilisation efficiency to FC14 (Figure 2).

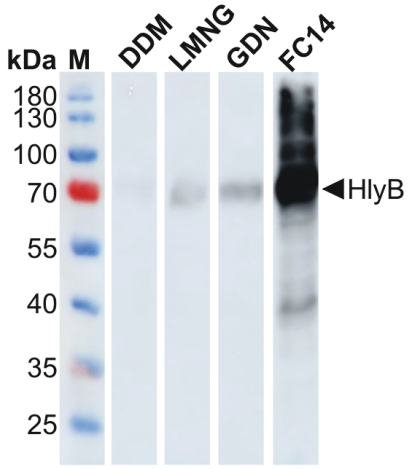

Figure 2: Western blot for comparison of solubilization efficiency for HisHlyB using DDM, LMNG, GDN and Fos-Choline-14. *Supernatant samples after solubilization with the indicated detergent. M: marker proteins with their approximated molecular weight. The signal for HlyB is marked with a black triangle. Protein-specific anti-HlyB antibody was used for detection.*

The Western blot analysis revealed almost no solubilization of HisHlyB with DDM and only low amounts with LMNG or GDN. FC14 was the best detergent for solubilization of HisHlyB. We found that the lyso-lipid lysophosphatiylglyerol (LPG) is capable of solubilizing and stabilizing membrane proteins just like a detergent [32, 33].

Therefore, HisHlyB was solubilized with LPG and purified via IMAC and SEC in the presence of LPG (Figure 3).

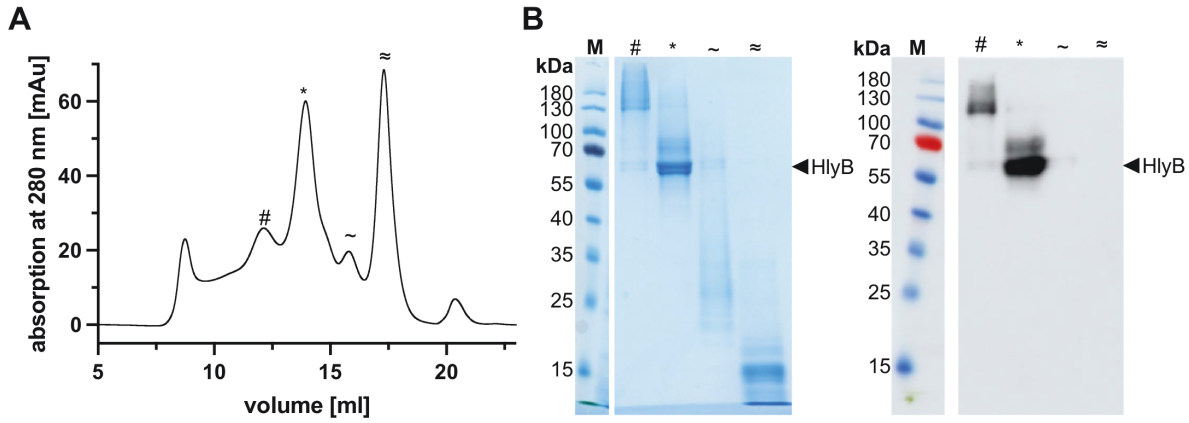

Figure 3: Purification of HisHlyB in LPG. A: *SEC of HisHlyB on Superose 6 Inc. 10/300 GL.* ***B:*** *SDS-PAGE (left) and Western blot (right) analysis of purified HisHlyB. M: marker proteins with their approximated molecular weight. #/*/~/≈: sample from main elution peaks. The signal for HlyB is marked with a black triangle. Protein-specific anti-HlyB antibody was used for detection.*

The SEC profile showed multiple peaks (Figure 3A) and SDS-PAGE analysis revealed a good separation of HisHlyB from other impurities (Figure 3B). Western blot analysis confirmed the second peak at an elution volume of around 14 ml to be the HisHlyB elution peak (* peak, Figure 3A). However, none of the peaks showed ATPase activity (data not shown). As HisHlyB in LPG (Figure 3) showed better purity than previous purifications (Figure 1) but was lacking ATPase activity we tested a different strategy to purify HlyB in an active state and tried a more specific affinity tag than a 10xHis-tag.

Purifications using TSHlyB

To achieve better purification results we cloned a TwinStrep-tag on the N-teminus of HlyB (TSHlyB) instead of the 10xHis-tag. First we investigated whether or not the tag influences expression and tried two different expression protocols (Figure 4)

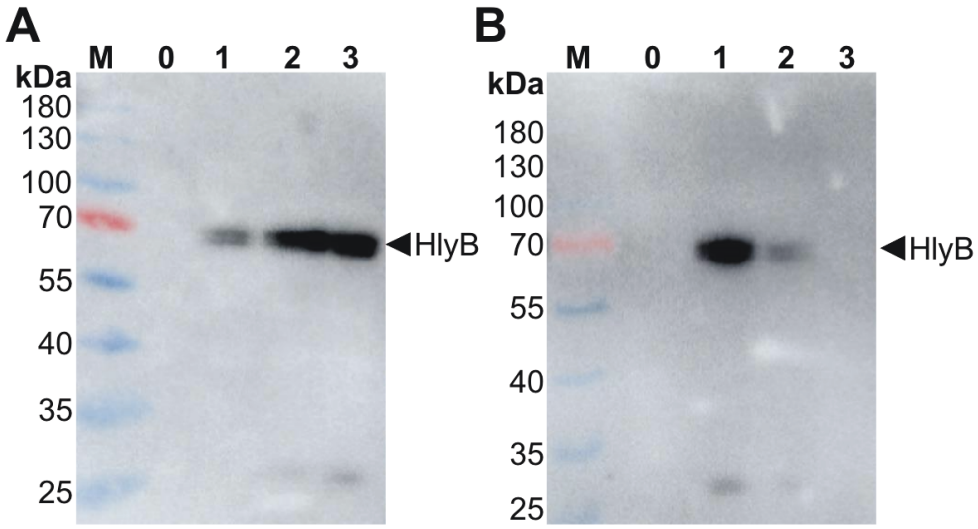

Figure 4:Western blot of the test expression of TSHlyB. A: *Expression induced at OD_{600} = 0.6.* ***B:*** *Expression induced at OD_{600} = 2.0. M: marker proteins with their approximated molecular weight. 0 - 3: sample after 0 – 3 hours of expression. The signal for HlyB is marked with a black triangle. Protein-specific anti-HlyB antibody was used for detection.*

The expression analysis of TSHlyB showed best results for induction at OD_{600} = 0.6 and expression for 3 hours (Figure 4A). Interestingly the expression protocol with a later induction of expression at an OD_{600} = 4.0 and expression for 2 hours (Figure 4B), which was best for HisHlyB, did not result in good expression of TSHlyB. Amounts of TSHlyB even decreased again after 1 hour of expression. The expression of TSHlyB in general was much weaker than the expression of HisHlyB.

To increase expression a codon optimised construct of TSHlyB was generated. This approach did not result in improvement of expression and led to ambiguous results (data not shown). Therefore the initial construct was used for further experiments.

TSHlyB was solubilized and purified in FC14 via StrepTrap-affinity purification and SEC (Figure 5).

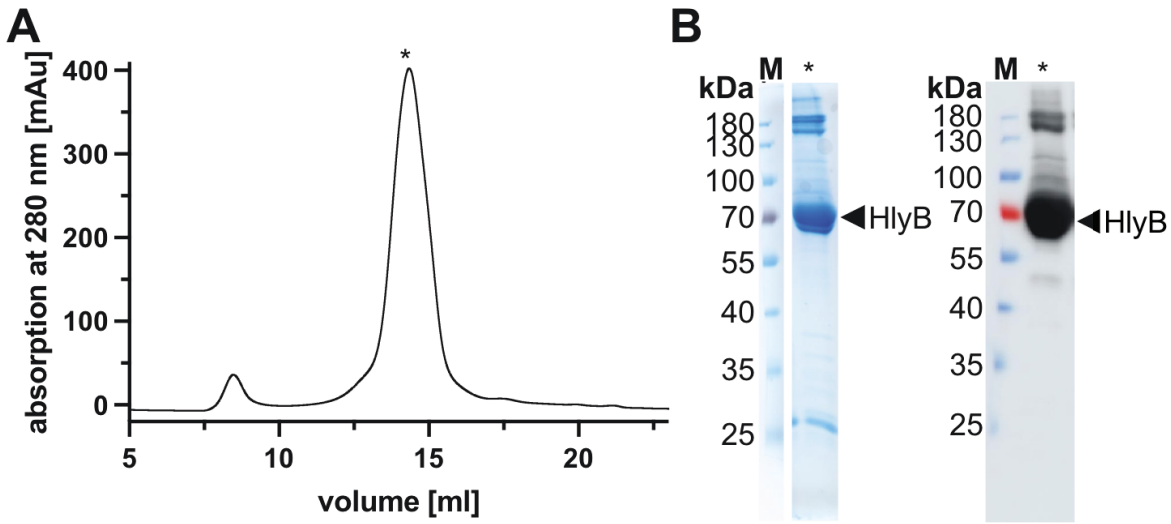

Figure 5: Purification of TSHlyB in FC14. A: *SEC analysis of TSHlyB on Superose 6 Inc. 10/300 GL.* ***B:*** *SDS-PAGE (left) and Western blot (right) analysis of purified TSHlyB. M: marker proteins with their approximated molecular weight. *: sample from HlyB main elution peak. The signal for HlyB is marked with a black triangle. Protein-specific anti-HlyB antibody was used for detection.*

The SEC profile of TSHlyB in FC14 showed only one single peak at 14.5 ml. The peak contained mainly TSHlyB but also other impurities as revealed from SDS-PAGE and Western blot analysis (Figure 5B). Furthermore, no ATPase activity was detected for TSHlyB in FC14 (data not shown).

To investigate whether restoring of ATPase activity by changing the detergent is possible, we adapted the purification protocol to the HisHlyB protocol. FC14 was used for solubilization of TSHlyB and DDM in all subsequent buffers for purification. The SEC profile of TSHlyB in DDM after FC14 solubilization showed a main peak at 16 ml with a shoulder at 14.5 ml (Figure 6A).

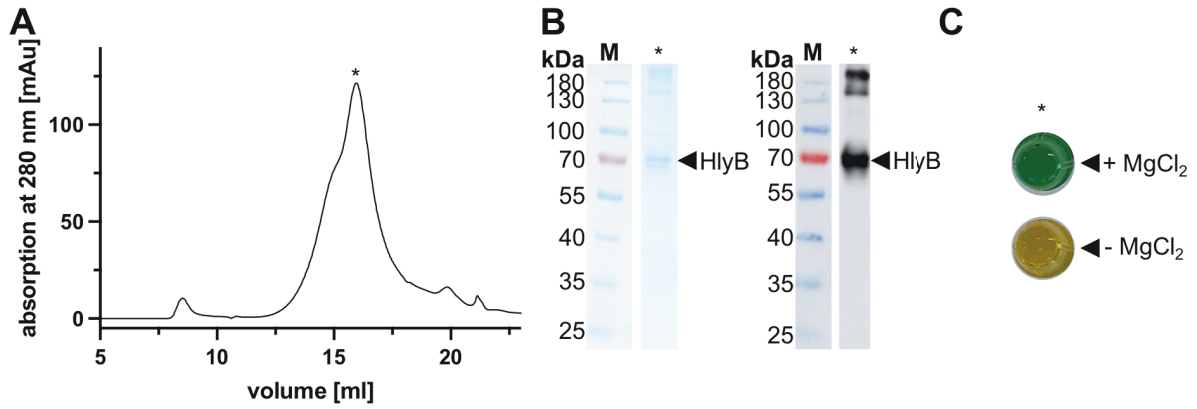

Figure 6: Purification of TSHlyB in DDM after solubilization in FC14. A: *SEC analysis of TSHlyB on Superose 6 Inc. 10/300 GL.* ***B:*** *SDS-PAGE (left) and Western blot (right) analysis of purified TSHlyB. M: marker proteins with their approximated molecular weight. *: sample from HlyB main elution peak. The signal for HlyB is marked with a black triangle. Protein-specific anti-HlyB antibody was used for detection.* ***C:*** *Wells from ATPase activity assay from TSHlyB in DDM after SEC. *: sample from HlyB main elution peak. Positive sample (+ $MgCl_2$) and negative background control (- $MgCl_2$) are indicated.*

The main elution peak contained TSHlyB as seen from SDS-PAGE and Western blot analysis (Figure 6B) and showed ATPase activity (Figure 6C). The shoulder did not show any additional bands on SDS-PAGE therefore we investigated in how far the change of detergent influences the SEC profile and protein purity. We performed a purification of TSHlyB starting with FC14 for solubilization and changing to GDN during the affinity purification. The SEC profile (Figure 7A) was similar to the profile in DDM (Figure 6A) with a peak at 16 ml and a shoulder at 14.5 ml. The shoulder was even more prominent in GDN.

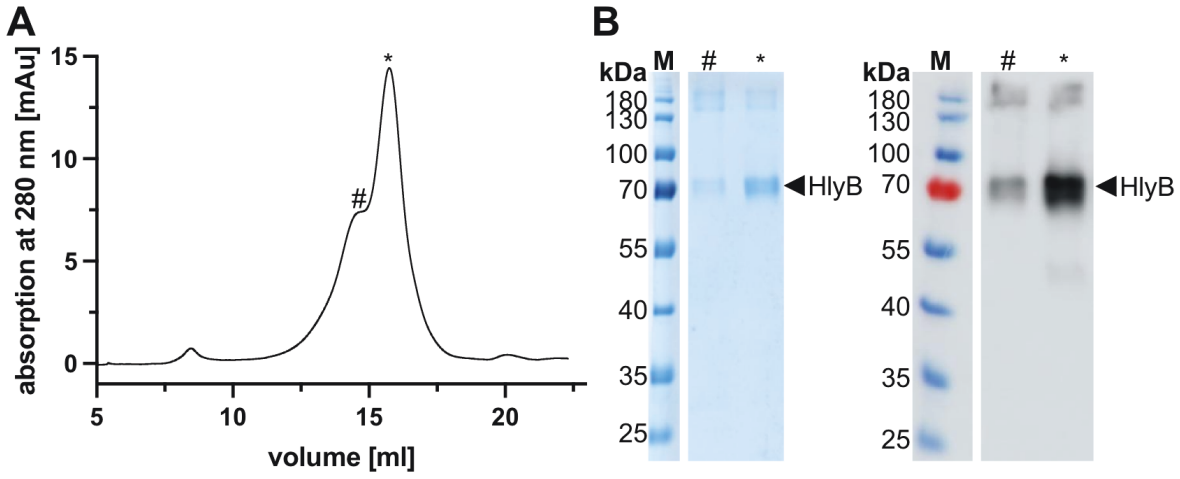

Figure 7: Purification of TSHlyB in GDN after solubilization in FC14. A: *SEC analysis of TSHlyB on Superose 6 Inc. 10/300 GL.* ***B:*** *SDS-PAGE (left) and Western blot (right) analysis of purified TSHlyB. M: marker proteins with their approximated molecular weight. *: sample from HlyB main elution peak. The signal for HlyB is marked with a black triangle. Protein-specific anti-HlyB antibody was used for detection.*

SDS-PAGE and Western blot analysis (Figure 6B) revealed no difference between shoulder (peak #) and main elution peak (peak *). Even prolonging of the washing step during affinity purification did not change the SEC profile.

After the publication on the structure of the inner membrane complex (IMC) [12] was published, we performed solubilization and purification of TSHlyB in GDN. The SEC profile of this purification attempt showed multiple overlapping peaks (Figure 8A). To evaluate them SDS-PAGE, Western blot, Blue Native-PAGE analysis and ATPase activity were performed (Figure 8B - D).

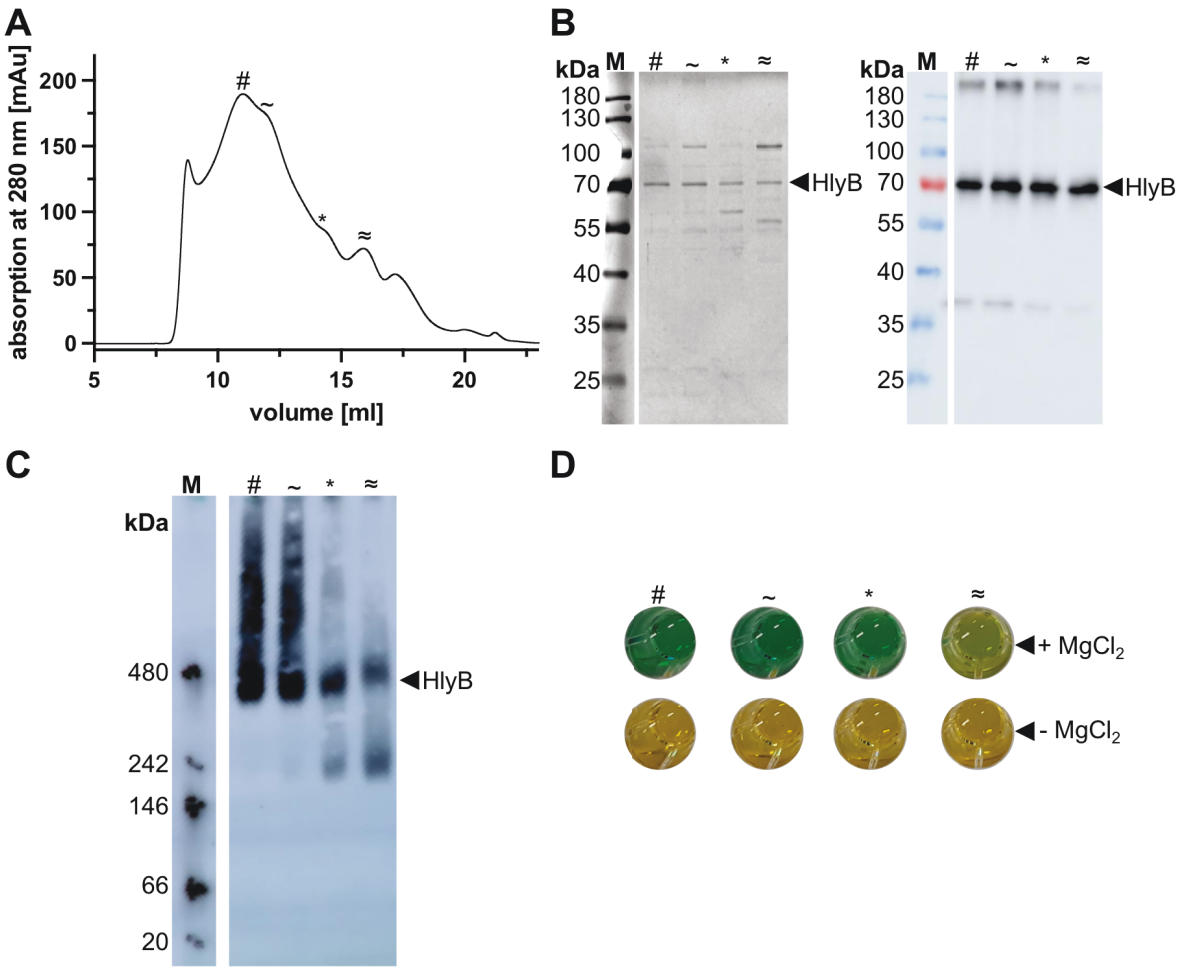

Figure 8: Purification of TSHlyB in GDN. A: *SEC analysis of TSHlyB on Superose 6 Inc. 10/300 GL.* ***B:*** *SDS-PAGE (left) and Western blot (right) analysis of purified TSHlyB. M: marker proteins with their approximated molecular weight. #/~/*/≈: sample from indicated elution peak. The signal for HlyB is marked with a black triangle. Protein-specific anti-HlyB antibody was used for detection.* ***C:*** *Western blot analysis of Blue Native-PAGE analysis of TSHlyB in GDN. #/~/*/≈: sample from indicated elution peak.* ***D:*** *Wells from ATPase activity assay from TSHlyB in GDN after SEC. #/~/*/≈: sample from indicated elution peak. Positive sample (+ $MgCl_2$) and negative background control (- $MgCl_2$) are indicated.*

All elution peaks contained HlyB as seen from Western blot analysis. Different impurities were visible via Coomassie stained SDS-PAGE for each peak (Figure 8B). Western blot of Blue Native-PAGE analysis showed a prominent band for TSHlyB at

approximately 480 kDa. In addition, the first two peaks (peak # & peak ~, Figure 8) showed signals at higher molecular masses, while the later ones (peak * & peak , Figure 8) showed signals at a lower molecular mass as seen from the band at approximately 240 kDa. All peaks showed ATPase activity (Figure 8D) with peak * showing the highest specific ATPase activity with an ATP turnover rate of 10 nmol per mg protein and minute. Purification in GDN did not improve purity, but enabled stabilisation of different possible oligomeric species.

Discussion

As part of the HlyA T1SS the ABC transporter HlyB fulfils multiple roles. On the one hand it provides the energy for the secretion process by hydrolysing ATP, on the other hand it recognizes the substrate via two different recognition sites. To investigate structure and function of HlyB a solid protocol for expression and purification of high-quality protein is necessary. In this study, we were able to rely on an already established protocol for functional studies [30] and extended it.

For HisHlyB in DDM we could observe only one peak in the SEC profile, but multiple bands on the SDS-PAGE (Figure 1). In contrast the use of the lyso-lipid LPG enabled us to precisely separate HisHlyB from all other contaminations during SEC (Figure 3). DDM is known to build large micelles and a rather mobile detergent belt [34] which in our case might interfere with separation during SEC. Although HisHlyB exhibits high purity in LPG after SEC, it does not show any ATPase activity. This underlines the importance of a sufficient read out for every screening experiment. In terms of purity, LPG works excellent, but in terms of activity it does not provide a useful alternative to DDM. Partial unfolding or stabilising an ATP hydrolysis-incompetent conformation might be an explanation for the loss of activity in LPG. This is also in line with the slight change of elution volume towards bigger particles, when comparing HisHlyB in LPG to DDM. Further analysis on protein folding such as Native-PAGE or DSF in combination with light scattering might provide an answer here and showed similar results for other integral membrane proteins [35]. Buffer exchange via dialysis might be an option to investigate whether the loss of activity in LPG is reversible, when changing to a different detergent like DDM, after SEC purification. Our findings regarding ATPase activity in FC14 indicate that loss of ATPase activity due to the detergent is indeed reversible. For TSHlyB we couldn’t see ATPase activity in FC14 (Figure 5) but when

changing to DDM or GDN (Figure 6 and 7) after solubilisation in FC14 we could detect ATPase activity.

We observed that the identity of the affinity tag can have a major impact on protein production (Figure 4). When changing form His-tag to TwinStrep-tag we observed a decrease in expression levels and change in growth behaviour. This is in line with published data showing that an N-terminal His-tag can increase recombinant expression in *E. coli* [36]. It remains elusive whether the TwinStrep-tag has a negative effect on protein production or the effect seen here in this study is simply the lack of increase of expression caused by the removal of the His-tag. Furthermore we could demonstrate that in terms of purity, the TwinStrep-tag (Figure 6) is superior to the 10xHis-tag (Figure 1).

Use of the detergent GDN for solubilisation and purification did not improve purity of our sample (Figure 8). Although GDN is known to stabilize challenging proteins and proteins complexes, it is often applied after the solubilisation step [37]. This also fits in with our results, as change to GDN during purification (Figure 7) leads to a better sample in terms of purity than starting already at the solubilisation step with GDN (Figure 8). As all peaks observed for GDN purification (Figure 8) show ATPase activity and contain TSHlyB, some of the early elution peaks might represent higher oligomeric species of TSHlyB.

In conclusion, we could optimize the purification of HlyB by changing the affinity tag from a His-tag to a more specific TwinStrep-tag and by changing to the detergent GDN during affinity purification.

Author contribution

FLB, SS and LS conceived the experiments and evaluated the data. FLB performed the experiments. FLB wrote the initial draft. FLB, SS and LS wrote the final version of the manuscript.

Funding

This work was supported by the Deutsche Forschungsgemeinschaft (DFG, CRC 1208 project A01 to LS).

Acknowledgement

We thank all former and current members of the Institute of Biochemistry for their support and productive discussions.

References

1. Koronakis, V., E. Koronakis, and C. Hughes, *Comparison of the haemolysin secretion protein HlyB from Proteus vulgaris and Escherichia coli; site-directed mutagenesis causing impairment of export function.* Mol Gen Genet, 1988. **213**(2-3): p. 551-5.
2. Cross, M.A., et al., *HlyB-dependent secretion of hemolysin by uropathogenic Escherichia coli requires conserved sequences flanking the chromosomal hly determinant.* J Bacteriol, 1990. **172**(3): p. 1217-24.
3. Spitz, O., et al., *Type I Secretion Systems-One Mechanism for All?* Microbiol Spectr, 2019. **7**(2).
4. Kanonenberg, K., C.K. Schwarz, and L. Schmitt, *Type I secretion systems - a story of appendices.* Res Microbiol, 2013. **164**(6): p. 596-604.
5. Kanonenberg, K., et al., *Type I secretion system-it takes three and a substrate.* FEMS Microbiol Lett, 2018. **365**(11).
6. Lecher, J., et al., *An RTX transporter tethers its unfolded substrate during secretion via a unique N-terminal domain.* Structure, 2012. **20**(10): p. 1778-87.
7. Reimann, S., et al., *Interdomain regulation of the ATPase activity of the ABC transporter haemolysin B from Escherichia coli.* Biochem J, 2016. **473**(16): p. 2471-83.
8. Spitz, O., et al., *Identity Determinants of the Translocation Signal for a Type 1 Secretion System.* Front Physiol, 2021. **12**: p. 804646.
9. Pourhassan, N.Z., et al., *Investigations on the substrate binding sites of hemolysin B, an ABC transporter, of a type 1 secretion system.* Front Microbiol, 2022. **13**: p. 1055032.
10. Schlor, S., et al., *In vivo and in vitro studies on interactions between the components of the hemolysin (HlyA) secretion machinery of Escherichia coli.* Mol Gen Genet, 1997. **256**(3): p. 306-19.
11. Balakrishnan, L., C. Hughes, and V. Koronakis, *Substrate-triggered recruitment of the TolC channel-tunnel during type I export of hemolysin by Escherichia coli.* J Mol Biol, 2001. **313**(3): p. 501-10.
12. Zhao, H., J. Lee, and J. Chen, *The hemolysin A secretion system is a multi-engine pump containing three ABC transporters.* Cell, 2022. **185**(18): p. 3329-3340 e13.
13. Schmitt, L., et al., *Crystal structure of the nucleotide-binding domain of the ABC-transporter haemolysin B: identification of a variable region within ABC helical domains.* J Mol Biol, 2003. **330**(2): p. 333-42.
14. Zaitseva, J., et al., *A structural analysis of asymmetry required for catalytic activity of an ABC-ATPase domain dimer.* EMBO J, 2006. **25**(14): p. 3432-43.
15. Zaitseva, J., et al., *Functional characterization and ATP-induced dimerization of the isolated ABC-domain of the haemolysin B transporter.* Biochemistry, 2005. **44**(28): p. 9680-90.
16. Zaitseva, J., et al., *H662 is the linchpin of ATP hydrolysis in the nucleotide-binding domain of the ABC transporter HlyB.* EMBO J, 2005. **24**(11): p. 1901-10.

17. Benabdelhak, H., et al., *A specific interaction between the NBD of the ABC-transporter HlyB and a C-terminal fragment of its transport substrate haemolysin A.* J Mol Biol, 2003. **327**(5): p. 1169-79.
18. Jeffery, C.J., *Expression, Solubilization, and Purification of Bacterial Membrane Proteins.* Curr Protoc Protein Sci, 2016. **83**: p. 29 15 1-29 15 15.
19. Kubicek, J., et al., *Expression and purification of membrane proteins.* Methods Enzymol, 2014. **541**: p. 117-40.
20. Mathieu, K., et al., *Functionality of membrane proteins overexpressed and purified from E. coli is highly dependent upon the strain.* Sci Rep, 2019. **9**(1): p. 2654.
21. Errasti-Murugarren, E., P. Bartoccioni, and M. Palacin, *Membrane Protein Stabilization Strategies for Structural and Functional Studies.* Membranes (Basel), 2021. **11**(2).
22. Mégret-Cavalier, M., et al., *Starting with an Integral Membrane Protein Project for Structural Biology: Production, Purification, Detergent Quantification, and Buffer Optimization—Case Study of the Exporter CntI from Pseudomonas aeruginosa*, in *Bacterial Secretion Systems : Methods and Protocols*, L. Journet and E. Cascales, Editors. 2024, Springer US: New York, NY. p. 415-430.
23. Miroux, B. and J.E. Walker, *Over-production of proteins in Escherichia coli: mutant hosts that allow synthesis of some membrane proteins and globular proteins at high levels.* J Mol Biol, 1996. **260**(3): p. 289-98.
24. Kanonenberg, K., et al., *Shaping the lipid composition of bacterial membranes for membrane protein production.* Microb Cell Fact, 2019. **18**(1): p. 131.
25. Magnani, F., et al., *A mutagenesis and screening strategy to generate optimally thermostabilized membrane proteins for structural studies.* Nat Protoc, 2016. **11**(8): p. 1554-71.
26. Stock, C. and I. Hanelt, *Membrane Protein Solubilization and Quality Control: An Example of a Primary Active Transporter.* Methods Mol Biol, 2020. **2127**: p. 93-103.
27. Geertsma, E.R., et al., *Quality control of overexpressed membrane proteins.* Proc Natl Acad Sci U S A, 2008. **105**(15): p. 5722-7.
28. Wycisk, V., M.C. Wagner, and L.H. Urner, *Trends in the Diversification of the Detergentome.* Chempluschem, 2023: p. e202300386.
29. Graeber, E. and V.M. Korkhov, *Affinity Purification of Membrane Proteins.* Methods Mol Biol, 2020. **2127**: p. 129-137.
30. Kanonenberg, K., S.H.J. Smits, and L. Schmitt, *Functional Reconstitution of HlyB, a Type I Secretion ABC Transporter, in Saposin-A Nanoparticles.* Sci Rep, 2019. **9**(1): p. 8436.
31. Baykov, A.A., O.A. Evtushenko, and S.M. Avaeva, *A malachite green procedure for orthophosphate determination and its use in alkaline phosphatase-based enzyme immunoassay.* Anal Biochem, 1988. **171**(2): p. 266-70.
32. Majeed, S., et al., *Lipid Membrane Mimetics in Functional and Structural Studies of Integral Membrane Proteins.* Membranes (Basel), 2021. **11**(9).
33. Koehler, J., et al., *Lysophospholipid micelles sustain the stability and catalytic activity of diacylglycerol kinase in the absence of lipids.* Biochemistry, 2010. **49**(33): p. 7089-99.
34. Stetsenko, A. and A. Guskov, *An Overview of the Top Ten Detergents Used for Membrane Protein Crystallization.* Crystals, 2017. **7**(7): p. 197.
35. Kotov, V., et al., *High-throughput stability screening for detergent-solubilized membrane proteins.* Scientific Reports, 2019. **9**(1): p. 10379.

36. Park, W.J., et al., *Over-expression of recombinant proteins with N-terminal His-tag via subcellular uneven distribution in Escherichia coli.* Acta Biochim Biophys Sin (Shanghai), 2015. **47**(7): p. 488-95.
37. Lee, H.J., et al., *Impact of novel detergents on membrane protein studies.* Chem, 2022. **8**(4): p. 980-1013.

Supplementary Information

Table S1: Primers used for cloning. *Small letters indicate bases that introduce overhangs for Gibson Assembly and do not match the template sequence.*

Name	Sequence (5' – 3')	Purpose
TSHlyB_fwd	agggtggtggtattgaaggtaga AATTCTGATTCTTGTCA TAAAATTGATTATGGGT TATACG	Amplification of pBAD-HisHlyB to prepare the vector for Gibson Assemly to change His-tag toTwinStrep-tag
TSHlyB_rev	tcgaattgtgggtgagacca CATGGTTAATTCCT CCTGTTAGCCC	Amplification of pBAD-HisHlyB to prepare the vector for Gibson Assemly to change His-tag to TwinStrep-tag

Table S2: DNA oligomers for Gibson Assembly.

Name	Sequence (5' – 3')	Purpose
TwinStrep-tag	TGGTCTCACCCACAATTCGA GAAGGGCGGTGGTTCTGGC GGTGGTTCTGGAGGTTCCTC TGCCTGGAGCCACCCGCAG TTCGAAAAGGGTGGTGGTAT TGAAGGTAGA	Double-stranded DNA oligomer for Gibson Assembly coding for the TwinStrep-tag

3.3. Chapter 3: Reconstitution of the ABC transporter HlyB from *Escherichia coli*

Title: Reconstitution of the ABC transporter HlyB from *Escherichia coli*

Authors: **Florestan L. Bilsing**, Sander Smits, Lutz Schmitt

Published in: to be submitted

Own contribution:
Designing the experiments
Performing the experiments
Data evaluation
Preparation of the figures
Writing of the manuscript

Reconstitution of the ABC transporter HlyB from *Escherichia coli*

Florestan L. Bilsing[1], Sander Smits[1,2], Lutz Schmitt[1]*

[1]Heinrich Heine University Düsseldorf, Faculty of Mathematics and Natural Sciences, Institute of Biochemistry, Universitätsstraße 1, 40225 Düsseldorf
[2]Heinrich Heine University Düsseldorf, Faculty of Mathematics and Natural Sciences, Center for Structural Studies, , Universitätsstraße 1, 40225 Düsseldorf

*Corresponding author: Lutz Schmitt, Heinrich Heine University Düsseldorf, Faculty of Mathematics and Natural Sciences, Institute of Biochemistry, Universitätsstraße 1, 40225 Düsseldorf, Germany, Tel.: +49 211 81 10773, E-Mail: lutz.schmitt@hhu.de

Abstract

Type 1 secretion systems (T1SSs) are present among pathogenic Gram-negative bacteria and used to secrete transporter specific substrates like virulence factors and toxins. Hydrolysis of ATP by ATP-binding cassette (ABC) transporters provides the energy for this secretion process. The ABC transporter HlyB is a well-studied example and part of the hemolysin A (HlyA) T1SS from *Escherichia coli* (*E. coli*). Although studied for decades, structural information for the ABC transporter HlyB was still limited, until recently the structure of the so-called inner membrane complex build by HlyB and HlyD was determined via single-particle cryo-EM in the detergent digitonin. To stabilize membrane proteins in a detergent free environment several membrane mimetics and detergent alternatives were developed over the past years.

To rule out detergent effects and to investigate the influence of lipids on the structure of HlyB we aimed to reconstitute HlyB in a detergent free environment. Therefore we used the MSP-based nanodisc system, the saposin A (SapA) lipid protein (salipro) system and the peptidisc system. We could successfully reconstitute HlyB in SapA and lysophosphatidylglycerol (LPG), but we encountered several pitfalls in the use of native lipids for reconstitution of HlyB in SapA. For peptidisc reconstitution we could observe a stabilisation of the inactive HlyB monomer for our given experimental set up. In addition we were successful in reconstitution of HlyB into MSP-based nanodisc using the lipid POPC.

Introduction

Type 1 secretion systems (T1SSs) are present in many Gram-negative pathogens and facilitate the secretion of virulence factors and toxins [1-3]. One of the best studied T1SS is the hemolysin A (HlyA) T1SS from pathogenic *Escherichia coli* (*E. coli*) [4-15]. It enables the transport of the pore forming toxin HlyA [16, 17]. This process is powered by ATP hydrolysis via the ATP-binding cassette (ABC) transporter hemolysin B (HlyB) [5, 18, 19]. HlyB is active as a dimer and each monomer is build up by a C39 peptidase-like domain (CLD), a transmembrane domain (TMD) and a nucleotide binding domain (NBD) [10, 18, 20]. Within the HlyA T1SS, HlyB adopts an oligomeric assembly of a trimer of dimers stabilized by the membrane fusion protein (MFP) hemolysin D (HlyD) [15]. Structural and functional studies of the HlyA T1SS and the isolated ABC transporter HlyB have so far mainly been performed in a detergent environment [10, 15]. But on the one hand, detergents can influence protein structures and conformations or cause problems in structure determination methods [21-23] and on the other hand the presence of lipids can play a crucial role in membrane protein structure and function [24-26]. This is why detergent alternatives and reconstitution of membrane proteins into lipid environment becomes more and more important.

Over the past decades many detergent alternatives were developed and successfully applied for membrane protein research [27]. Probably the best known and widely used tool is the membrane scaffold protein (MSP)-based nanodisc [28-33]. The alpha-helical MSP forms a ring-like structure and encapsulates as a dimeric self-assembly a lipid bilayer (Figure 1A). Within this lipid bilayer a previously purified membrane protein can be stabilized. The choice of the MSP determines the diameter of the formed disc and the number of incorporated lipid molecules [34-36]. The lipid composition is freely selectable and allows for precise control of the membrane protein surrounding [28]. The number of applications for MSP-based nanodiscs constantly increases by further method developments, like “dark” nanodiscs that allow the noise-free use of nanodiscs in differential scanning fluorimetry (DSF) [37]. A crucial factor in self-assembly of the MSP-based nanodisc is the ratio of membrane protein to MSP to lipid, that needs to be carefully investigated for each membrane protein [28, 38].

Another lipoprotein disc-like assembly is the sapsoin A (SapA) lipoprotein nanoparticle system often referred to as salipro [39, 40]. It is a highly versatile system that encapsulates previously purified membrane proteins within a lipid bilayer and allows the use of different lipids [41]. Unlike the MSP-based nanodiscs, salipro does not

exhibit a precise number of SapA molecules per lipoprotein nanoparticle (Figure 1B). The number of SapA molecules that build a lipoprotein particle can vary and therefore adapt to membrane proteins of different sizes [12, 42-44]. Recent advances in salipro method development even allow for reconstitution of target membrane proteins with native lipids at an early stage of the purification process. This method called DirectMX reduces the detergent exposure to a minimum and uses the lipids from the target membrane for salipro formation during the solubilisation step [45].

An alternative to lipid containing reconstitution systems is the peptidisc system [46]. The peptidisc uses the nanodisc scaffold peptide (NSP) in reversed order of the amino acids (NSP_r). NSP_r is a short bi-helical peptide that wraps around the hydrophobic transmembrane part of the membrane protein without any need for additional lipids (Figure 1C). The number of NSP_r per membrane protein is not fixed and can vary from protein to protein. There are multiple ways and options to apply the peptide during the membrane protein purification process, making it a versatile tool in membrane protein research [46-50]. Application of the NSP_r is possible “in-gel”, “on-column”, “on-bead” or “on-gradient” [46, 49]. On top of that, the PeptiQuick workflow allows, similar to the DirectMX method for salipro, a stabilisation of the membrane protein of interest already during a very early step of the purification process, reducing the detergent exposure time to a minimum [48].

Here we report the use of different detergent alternatives to stabilize the ABC transporter HlyB in a detergent free environment. We improved the already published protocol for functional reconstitution of HlyB in SapA nanoparticles [12] to enable first structural investigations. Furthermore we tested different applications for the NSP_r peptide to stabilize functional HlyB. Finally we managed to reconstitute HlyB into MSP-based nanodisc using the lipid POPC.

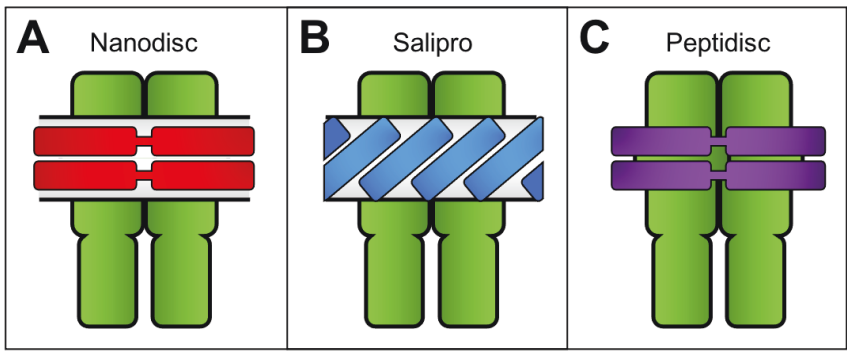

Figure 1: Schematic of different membrane reconstitution systems. A: *MSP-based nanodisc assembly with two copies of MSP (red) encapsulating a dimeric membrane protein (green) in a lipid bilayer (grey).* ***B:*** *Sap A lipoprotein nanoparticle assembly with multiple copies of SapA (blue) encapsulating a dimeric membrane protein (green) in a lipid bilayer (grey).* ***C:*** *Peptidisc assembly with two copies of NSP_r (purple) encapsulating a dimeric membrane protein (green). For simplicity only two copies of NSP_r are shown.*

Material and Methods

Expression and purification of HlyB

Expression and purification of HlyB was performed as previously described (Chapter 2 – Optimisation of the purification of the ABC transporter HlyB from *Escherichia coli*).

Expression and purification of SapA

SapA was expressed and purified according to the published protocol [39]. Purified SapA was stored in buffer A (100 mM Hepes pH 7.5, 150 mM NaCl) at -20 °C at a concentration of 1.2 – 3 mg/ml.

Reconstitution into SapA nanoparticles

Reconstitution of HlyB into SapA nanoparticles was performed according to the published protocol with slight modifications [12]. HlyB was purified via IMAC and SEC and the lysophospholipid lysophosphatidylglycerol (LPG) was used instead of lyso-phosphatidylcholin (LPC). LPG (16:0) was purchased as powder (Avanti Polar Lipids) and dissolved in buffer B (100 mM Hepes pH 8, 250 mM NaCl, 0.02% DDM) at a concentration of 5 mg/ml. DOPE, DOPG, DOPC and *E. coli* total lipid extract were purchased as chloroform solutions (Avanti Polar Lipids). DOPE/G/C were mixed in a molar ratio of DOPE : DOPG : DOPC of 50 : 38 : 12. After evaporation of chloroform the lipids were dissolved in buffer C (100 mM Hepes pH 8, 250 mM NaCl, 1% DDM). HlyB, Sap A and lipids were mixed in small batches in a ratio of 1 : 6 : 646 for LPG and 1 : 5 : 400 for DOPE/G/C. For each batch 40 µl lipids were incubated at 30 °C for 5 minutes and 60 µl HlyB (1.6 - 2 mg/ml) were added. After additional 5 minutes of incubation at 30 °C, 60 µl SapA (1.2 mg/ml) were added and incubated for 5 minutes at 30 °C. 500 µl Buffer D (100 mM Hepes pH 8, 250 mM NaCl) were added and incubated at room temperature. 10 to 30 batches were pooled and concentrated. The concentrated sample was centrifuged for 30 min at 17,000 xg and 4 °C and the supernatant was applied on Superose 6 Increase 10/300 GL equilibrated in Buffer D. Peak fractions containing reconstituted HlyB were used for thin layer chromatography (TLC) and negative stain TEM or single particle cryo-EM analysis.

DirectMX of HlyB using SapA and LPG

DirectMX of HlyB was performed similar to DirectMX of the IMC as previously described (Chapter 4 – Purification of the inner membrane complex of HlyA T1SS from

E. coli). Membranes of *E. coli* C41Δ*acrAB*Δ*ompF*(DE3) expressing pBAD-HisHlyB were diluted to 12 mg/ml and solubilized with 1% LPG. After affinity purification, buffer was exchanged using a gravity flow column to buffer D (20 mM Hepes pH 8, 100 mM NaCl). Elution fractions were used for SDS PAGE analysis and ATPase activity assay.

Malachite Green ATPase activity assay

ATPase activity was measured via Malachite Green assay [51] as described earlier (Chapter 2 – Optimisation of the purification of the ABC transporter HlyB from *Escherichia coli*).

Reconstitution into peptidisc

Peptidisc was purchased as powder (Peptidisc Lab) and dissolved in buffer E (10 mM Tris pH 6.8). HlyB was reconstituted into peptidisc following the published protocols [46, 48]. In brief, HlyB was purified via SEC and mixed with peptidisc (3 mg/ml) in a molar ratio of 1:80, 1:40 or 1:2 yielding a final volume of 500 µl. This mixture was injected onto a Superose 6 Increase 10/300 GL column equilibrated with buffer F (50 mM NaP_i pH 8, 300 mM NaCl). For reconstitution via the PeptiQuick method, HlyB was solubilised in 0.5 % Fos-Cholin-14 (FC14) and bound to Ni-NTA resin. The resin was washed two times with 10 column volumes (CV) buffer G1 (50 mM NaP_i pH 8, 300 mM NaCl, 10 mM imidazole, 0.005 % FC14). Next the resin was incubated with 1/5 CV buffer H1 (50 mM NaP_i pH 8, 300 mM NaCl, 10 mg/ml peptidisc) and 6 CV buffer H2 (50 mM NaP_i pH 8, 300 mM NaCl, 1 mg/ml peptidisc). The resin was washed with two times 10 CV buffer G2 (50 mM NaP_i pH 8, 300 mM NaCl, 10 mM imidazole) and HlyB in peptidisc was eluted with buffer J (50 mM NaP_i pH 8, 300 mM NaCl, 400 mM imidazole). Elution fractions were concentrated and centrifuged for 10 minutes at 4 °C and 100,000 xg. The supernatant was applied on Superdex 200 Increase 10/300 GL equilibrated in buffer F.

Reconstitution of HlyB using MSP2N2

HlyB was used at a concentration of 1 mg/ml after SEC. POPC was purchased as chloroform solution (Avanti Polar Lipids). After evaporation of chloroform, DOPC was solved in buffer K (20 mM Hepes pH 8, 100 mM NaCl) at 5 mg/ml and 0.5 % Triton X-100 were added. The lipid was incubated for 20 minutes at 40 °C and kept on ice afterwards. HlyB and MSP2N2 were added to the lipid simultaneously at a molar ratio

of HlyB : MSP2N2 : POPC of 1 : 10 : 2165. The mixture was incubated on ice for 30 minutes and 0.8 g/ml BioBeads were added. Incubation with BioBeads was performed over night at 4 °C under constant agitation. The supernatant was centrifuged the next day for 30 minutes at 4 °C and 17,000 xg. The supernatant was applied on Superose 6 Increase 10/300 GL column equilibrated in buffer K.

Results

Reconstitution of HlyB using Saposin A

SapA LPG nanoparticles

To reconstitute HlyB for structural studies into SapA nanoparticles, we applied the already published protocol for functional reconstitution of HlyB into SapA nanoparticles with some modifications [12]. HlyB was used for reconstitution after purification via IMAC and SEC and we used the lysolipid LPG instead of LPC. The optimal ratio of HlyB : SapA : lipid was 1 : 6 : 646. Reconstituted HlyB was separated from empty SapA LPG nanoparticles via SEC (Figure 2A). Fractions from the elution peaks were analysed via SDS PAGE and Western blot (Figure 2B). Samples from reconstituted HlyB in SapA LPG were used for negative stain TEM (Figure 2C) and single particle cryo-EM analysis (Figure 2D).

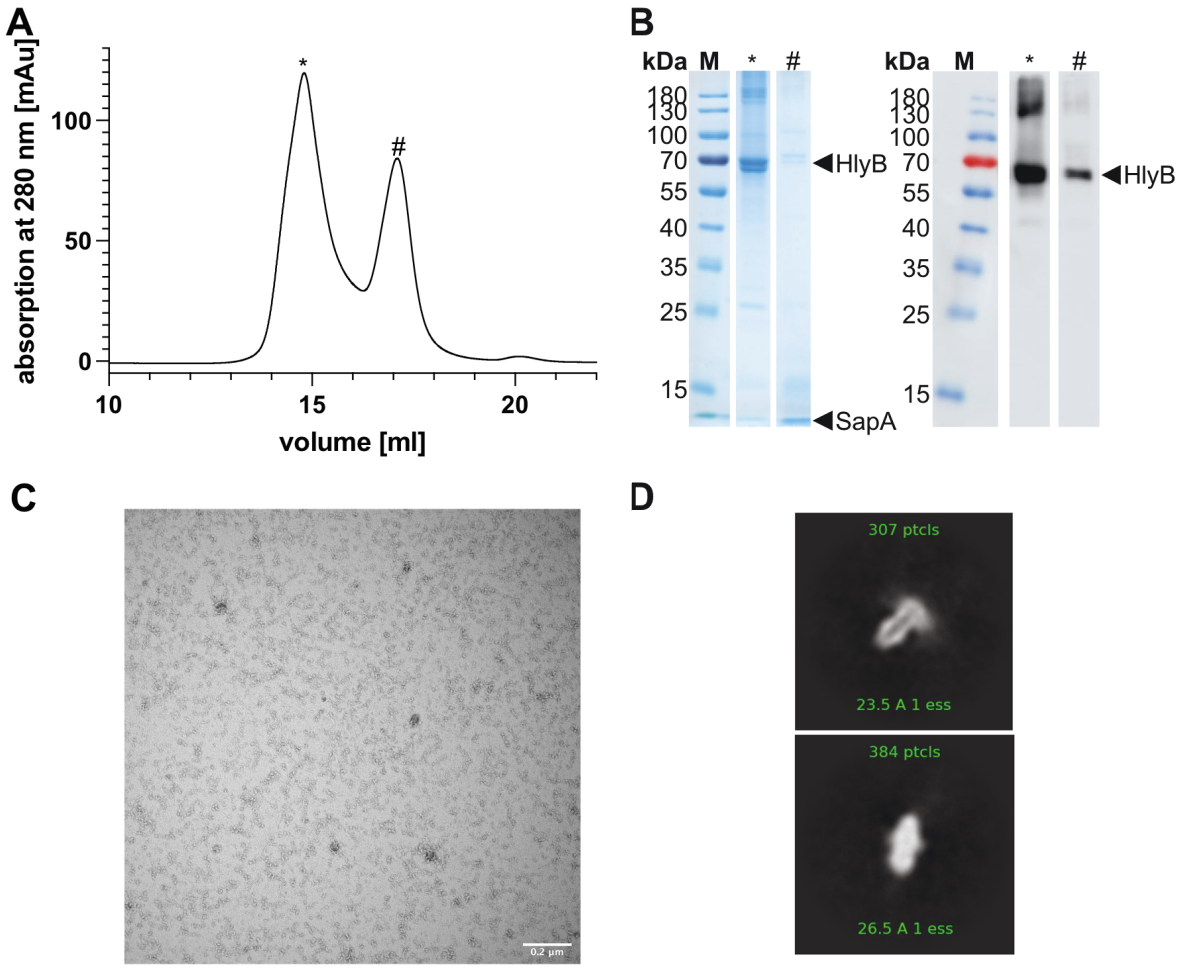

Figure 2: Reconstitution of HlyB in SapA LPG. A: *SEC analysis of HlyB in SapA LPG on Superose 6 Inc. 10/300 GL.* ***B:*** *SDS-PAGE (left) and Western blot (right) analysis of reconstituted HlyB. M: marker proteins with their approximated molecular weight. *: sample from main elution peak of reconstituted HlyB. #: sample from main elution peak of empty SapA LPG nanoparticles. The signals for HlyB and SapA are marked with black triangles. Protein-specific anti-HlyB antibody was used for detection.* ***C:*** *Grid from negative stain TEM analysis of the main elution peak of reconstituted HlyB in SapA LPG.* ***D:*** *Two out of 46 2D classes from single particle cryo-EM analysis of the main elution peak of reconstituted HlyB in SapA LPG. Number of particles and average resolution are indicated in green letters.*

The SEC profile of reconstitution of HlyB in SapA LPG nanoparticles showed two distinct peaks at approx. 15 and 17 ml (Figure 2A). The first peak contained reconstituted HlyB in SapA LPG and the second peak contained empty SapA LPG nanoparticles as seen from SDS PAGE and Western blot analysis (Figure 2B). HlyB migrates as a prominent double band at around 70 kDa (peak *, Figure 2B). HlyB and SapA were confirmed via MS analysis (Table S1 and S2) in addition to Western blot analysis for HlyB (right panel, Figure 2B). Although, number and size of particles was promising from negative stain TEM analysis (Figure 2C), the single particle cryo-EM analysis revealed a non-homogenous sample. Only 2 out of 46 2D classes were assigned to HlyB.

SapA DOPE/G/C nanoparticles

Next we tried whether the use of natural lipids can improve sample quality. The use of *E. coli* total lipid extract was not successful as HlyB aggregated during reconstitution and no peaks were visible during SEC. Therefore we prepared a self-made lipid mixture of DOPE, DOPG and DOPC in a molar ratio of 50:38:12. We adjusted the molar ratio of HlyB : SapA : lipids to 1 : 5 : 400 and could observe one non-homogenous peak in the SEC profile. Analysis of this peak via SDS PAGE and thin layer chromatography (TLC) were performed (Figure 3).

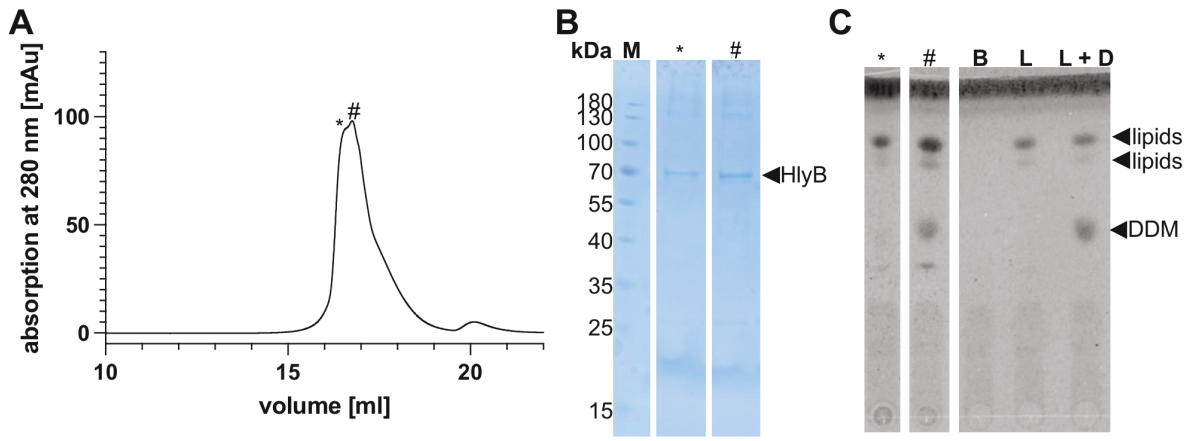

Figure 3: Reconstitution of HlyB in SapA DOPE/G/C. A: *SEC analysis of HlyB in SapA DOPE/G/C on Superose 6 Inc. 10/300 GL.* ***B:*** *SDS-PAGE analysis of reconstituted HlyB. M: marker proteins with their approximated molecular weight. */#: samples from main elution peak. The signal for HlyB is marked with a black triangle.* ***C:*** *thin layer chromatography analysis of reconstituted HlyB. */#: samples from main elution peaks. B: buffer control. L: lipid control (DOPE/G/C). L+D: lipid plus detergent (DDM) control. The signals for lipids and DDM are marked with black triangles.*

The SEC profile from reconstitution of HlyB in SapA DOPE/G/C showed a peak with at least two different species (Figure 3A). SDS PAGE analysis did not show any difference between the samples of those two species (Figure 3B). TLC analysis revealed that the second part of the peak (sample #) still contained DDM (Figure 3C). It was not possible to completely remove DDM from the sample and judging by the elution volume, the success of correct assembly of reconstituted dimeric HlyB remained questionable.

To minimize the amount of detergent and enabling use of native lipids, we tried a different strategy for reconstitution. We applied the published DirectMX method [45] to remove detergents from the purification process as soon as possible and circumvent detergent specific impurities as observed for BmrA [52].

DirectMX using SapA and LPG

E. coli membranes were solubilized with LPG and SapA to reconstitute HlyB into SapA particles with native lipids. Reconstituted HlyB was purified via IMAC and PD10 buffer exchange column. Elution fractions were analysed via SDS PAGE, Western blot, silver stained 20% tris-tricine gel and ATPase activity measurement (Figure 4).

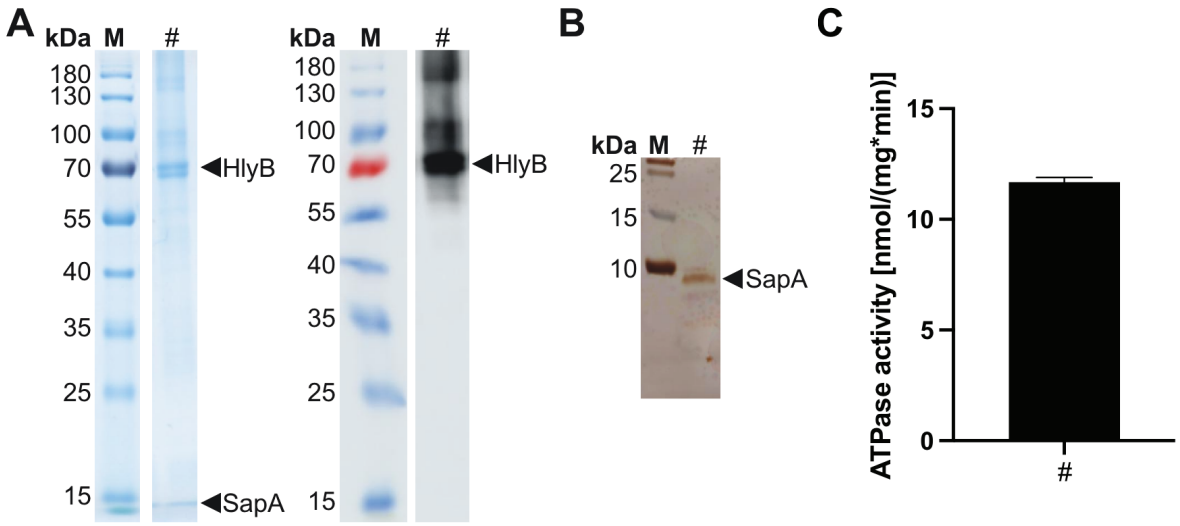

Figure 4: Analysis of DirectMX reconstitution of HlyB. A: *SDS-PAGE (left) and Western blot (right) analysis of SapA reconstituted HlyB via DirectMX. M: marker proteins with their approximated molecular weight. #: sample from main elution peak of reconstituted HlyB. The signals for HlyB and SapA are marked with black triangles. Protein-specific anti-HlyB antibody was used for detection.* ***B:*** *Silver stained 20% tris-tricine gel analysis of SapA reconstituted HlyB via DirectMX. M: marker proteins with their approximated molecular weight. #: sample from main elution peak of reconstituted HlyB. The signal for SapA is marked with a black triangle.* ***C:*** *ATPase activity measurement of SapA reconstituted HlyB via DirectMX. #: sample from main elution peak of reconstituted HlyB. ATP was used at a final concentration of 4 mM. Activity was measured as a single point measurement after 40 min reaction time. Standard deviation from 2 individual measurements.*

HlyB was successfully reconstituted and purified in SapA via the DirectMX method as seen from SDS PAGE and Western blot analysis (Figure 4A). The silver stained 20% tris-tricine gel confirms presence of SapA after IMAC and buffer exchange (Figure 4B). Furthermore, an ATPase activity of HlyB reconstituted in SapA and native lipids was determined to 11.7 nmol/(mg*min) (Figure 4C).

Peptidisc

Another alternative to stabilize membrane proteins in a detergent free environment is the use of peptidisc. HlyB was purified via SEC, mixed with petidisc peptides in a molar ratio of 1 : 80 and applied on a SEC column equilibrated in detergent free buffer. Samples were used for an additional affinity purification and elution fractions were analysed via SDS PAGE and Western blot (Figure 5).

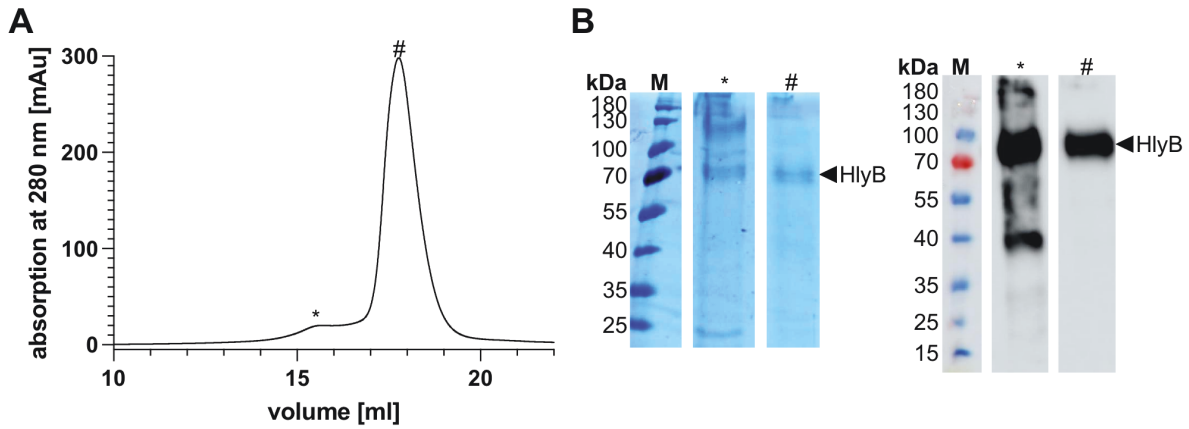

Figure 5: Reconstitution of HlyB in peptidisc. A: *SEC analysis of HlyB in peptidisc on Superose 6 Inc. 10/300 GL.* ***B:*** *SDS-PAGE (left) and Western blot (right) analysis of reconstituted HlyB in peptidisc. M: marker proteins with their approximated molecular weight. */#: samples from main elution peaks. The signal for HlyB is marked with a black triangle. Protein-specific anti-HlyB antibody was used for detection.*

The SEC profile of reconstituted HlyB in peptidisc showed a small peak at 15.5 ml and a large peak at 18 ml (Figure 5A). Interestingly both peaks contained HlyB as seen from SDS PAGE and Western blot after subsequent affinity purification (Figure 5B). From the elution volume we concluded that probably the first peak is dimeric HlyB in peptidisc and the second peak corresponds to monomeric HlyB in peptidisc. Next we tried to increase the amount of reconstituted dimeric HlyB by limiting the number of peptidisc molecules. We tried ratios of HlyB to Peptidisc of 1:40 and 1:2 (data not shown). Both ratios resulted in a similar SEC profile as from the 1:80 ratio (Figure 5A) and did not improve the amount of dimeric HlyB in peptidisc.

Besides mixing the peptidisc with already purified protein prior to SEC it is possible to incorporate the membrane protein into peptidisc already during affinity purification [48]. HlyB was solubilized in Fos-Choline-14 and incubated with peptidisc during affinity purification. Elution and SEC were performed in detergent free buffers. Elution fractions were analysed via SDS PAGE and Western blot (Figure 6).

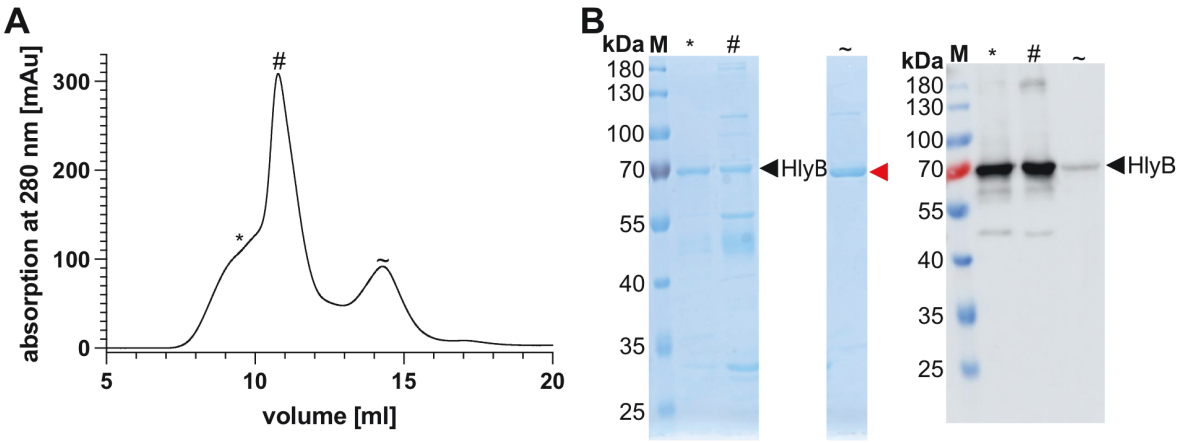

Figure 6: Reconstitution of HlyB in peptidisc via PeptiQuick method. *SEC analysis of HlyB in Peptidisc on Superdex 200 Inc. 10/300 GL.* ***B:*** *SDS-PAGE (left) and Western blot (right) analysis of reconstituted HlyB in peptidisc. M: marker proteins with their approximated molecular weight. */#/~: samples from main elution peaks. The signal for HlyB is marked with a black triangle. A prominent impurity in sample ~ is marked by a red triangle. Protein-specific anti-HlyB antibody was used for detection.*

The SEC profile after PeptiQuick method shows three peaks, where only the third peak at around 14 ml is clearly separated from the first two peaks at 9 and 11 ml (Figure 6A). Only the first two peaks showed presence of reconstituted HlyB. While the first peak looked pure on Coomassie stained SDS PAGE (sample *, Figure 6B), multiple additional bands were visible for the second peak (peak #, Figure 6B). SDS PAGE and Western blot analysis revealed that peak number three (peak ~, Figure 6) shows a band at 70 kDa, similar to the band of HlyB, but does not contain HlyB, but an unknown impurity. As reproducibility with this setup was not given, and peptidisc seemed to mainly stabilize monomeric HlyB (Figure 5), we continued with the nanodisc system as an alternative for detergent free membrane protein stabilisation.

Reconstitution of HlyB using MSP2N2

MSP2N2 POPC nanodiscs

For reconstitution into MSP-based nanodiscs, we first purified HlyB via IMAC and SEC and used POPC and MSP2N2 in a molar ratio of HlyB : MSPN2 : POPC of 1 : 10 : 2165. Reconstitution was analysed via SEC, SDS PAGE and Western blot (Figure 7).

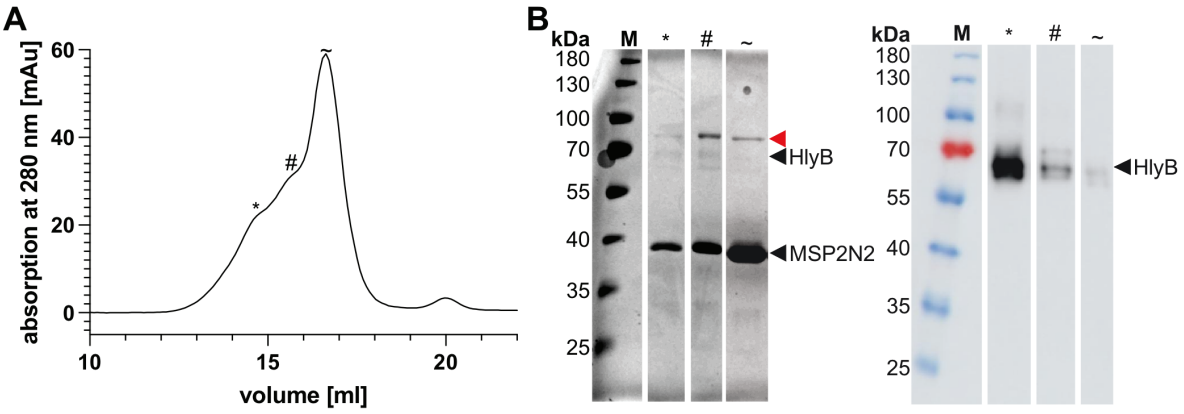

Figure 7: Reconstitution of HlyB in MSP2N2 POPC. A: *SEC analysis of HlyB in MSP-based nanodisc on Superose 6 Inc. 10/300 GL.* ***B:*** *SDS-PAGE (left) and Western blot (right) analysis of reconstituted HlyB in MSP-based nanodisc. M: marker proteins with their approximated molecular weight. */#/~: samples from main elution peaks. The signals for HlyB and MSP2N2 are marked with a black triangles. A prominent impurity in sample ~ is marked by a red triangle. Protein-specific anti-HlyB antibody was used for detection.*

The SEC profile from reconstitution of HlyB into MSP-based nanodiscs showed three peaks with poor separation (Figure 7A). The first peak (peak *, Figure 7) contained HlyB reconstituted into MSP2N2 POPC nanodiscs, while the second peak contained a different protein of about 85 kDa (peak #, Figure 7), as seen from SDS PAGE and Western blot. The third peak contained lipid-only MSP2N2 POPC nanodiscs (peak ~, Figure 7). Reconstitution of HlyB into MSP-based nanodiscs was successfully performed and enabled stabilization in a detergent free environment.

Discussion

Detergent alternatives that mimic the membrane or at least stabilize the membrane protein in a detergent free environment have become more and more important over the past decades for membrane protein research. On the one hand they allow to circumvent downsides from detergent exposure and on the other hand they enable investigation in more native like environments. As there is no one-method-fits-all solution, the different available methods have to be tested and optimized for each individual membrane protein. Here we tried different reconstitution methods for stabilisation of HlyB in a detergent free environment for structural studies.

Although a protocol for functional reconstitution of HlyB in SapA nanoparticles was published already [12], optimisation of this protocol was necessary to enable structural analysis. The reconstitution set up using LPG and SapA seem to stabilize a lot of different proteins besides HlyB, which stay within the sample during the purification

process and make structure determination difficult (Figure 2). LPG is structure wise more a detergent than a lipid and it therefore might, in addition to its contribution to the nanoparticles, act as a detergent-like stabiliser for other proteins.

Our finding that reconstitution of HlyB via salipro in *E. coli* total lipids was not successful is in line with previously published investigations that show that formation of SapA lipidnanoparticles is difficult when using *E. coli* polar lipid extract [41]. The additional lipids in the *E. coli* total extract, compared to the *E. coli* polar extract seem to have no influence on the success. Furthermore, we could show that remaining detergent after the reconstitution process is disturbing lipid nanoparticle formation and successful reconstitution (Figure 3). The effect of too much detergent in the salipro set up is probably similar to the effect of adding too less lipids, as investigated for MSP and POPC by Skar-Gislinge *et al.* [38]. The formation of mixed micelles of lipid and detergent molecules is therefore limiting the number of available lipids for nanoparticle formation and leads to the formation of misshaped nanoparticles. Another explanation might be a limiting amount of SapA molecules in our set up. As seen for DtpA a 20-fold excess of SapA molecules compared to target reconstituted protein can be necessary for successful reconstitution into salipro nanoparticles [41].

The DirectMX approach to reconstitute HlyB into salipro nanoparticles with lipids from native membranes is promising but limited by the yield. Although functional assays were performed (Figure 4C) the amount was not sufficient for structural investigations. Upscaling of the process is possible but would be very time consuming and require a lot of material.

Reconstitution into peptidisc by mixing purified HlyB with NSP_r was possible for HlyB but as judged from the elution profile after SEC (Figure 5), peptidisc mainly stabilized the HlyB monomer. As the NSP_r directly interacts with the hydrophobic part of the protein, the interaction between peptidisc and TMD of HlyB appears to be so strong that it disrupts the HlyB dimer interface. Monomeric HlyB was only observed for this reconstitution process, where no lipids were present. This might be a hint that the HlyB dimer is stabilized by the presence of lipids, as shown for UapA [53]. In addition some densities in the recently published structure of the inner membrane complex build by HlyB and HlyD were assigned to ordered lipids [15]. The monomeric non-functional state of HlyB is biologically non-relevant and was therefore not further investigated.

Furthermore, HlyB was successfully reconstituted into MSP-based nanodiscs with the lipid POPC (Figure 7). Although a prominent impurity is still visible after reconstitution,

a separation of HlyB in MSP POPC and the impurity is possible via SEC. Further improvement of the reconstitution set up would be necessary but was initially stopped due to the already mentioned and recently published single particle cryo-EM structure of the inner membrane complex formed by HlyB and HlyD [15].
We could successfully reconstitute HlyB using salipro or MSP-based nanodisc system. We conclude that structure determination of those samples is possible, when optimized for the right set up of lipid, lipid amount and detergent concentration, as seen for HlyB in SapA LPG (Figure 2).

Author contribution

FLB, SS and LS conceived the experiments and evaluated the data. FLB performed the experiments. FLB wrote the initial draft. FLB, SS and LS wrote the final version of the manuscript.

Funding

This work was supported by the Deutsche Forschungsgemeinschaft (DFG, CRC 1208 project A01 to LS).

Acknowledgement

We thank all former and current members of the Institute of Biochemistry for their support and productive discussions. We thank Dr. Kerstin Kanonenberg for preliminary work on HlyB reconstitution. In addition we thank Eymen Hachani for kindly providing MSP2N2.

References

1. Holland, I.B., L. Schmitt, and J. Young, *Type 1 protein secretion in bacteria, the ABC-transporter dependent pathway (review).* Mol Membr Biol, 2005. **22**(1-2): p. 29-39.
2. Holland, I.B., et al., *Type I Protein Secretion-Deceptively Simple yet with a Wide Range of Mechanistic Variability across the Family.* EcoSal Plus, 2016. **7**(1).
3. Kanonenberg, K., et al., *Type I secretion system-it takes three and a substrate.* FEMS Microbiol Lett, 2018. **365**(11).
4. Koronakis, V., et al., *The HlyB/HlyD-dependent secretion of toxins by gram-negative bacteria.* FEMS Microbiol Immunol, 1992. **5**(1-3): p. 45-53.
5. Cross, M.A., et al., *HlyB-dependent secretion of hemolysin by uropathogenic Escherichia coli requires conserved sequences flanking the chromosomal hly determinant.* J Bacteriol, 1990. **172**(3): p. 1217-24.
6. Schlor, S., et al., *In vivo and in vitro studies on interactions between the components of the hemolysin (HlyA) secretion machinery of Escherichia coli.* Mol Gen Genet, 1997. **256**(3): p. 306-19.
7. Leeds, J.A. and R.A. Welch, *RfaH enhances elongation of Escherichia coli hlyCABD mRNA.* J Bacteriol, 1996. **178**(7): p. 1850-7.
8. Balakrishnan, L., C. Hughes, and V. Koronakis, *Substrate-triggered recruitment of the TolC channel-tunnel during type I export of hemolysin by Escherichia coli.* J Mol Biol, 2001. **313**(3): p. 501-10.
9. Schmitt, L., et al., *Crystal structure of the nucleotide-binding domain of the ABC-transporter haemolysin B: identification of a variable region within ABC helical domains.* J Mol Biol, 2003. **330**(2): p. 333-42.
10. Reimann, S., et al., *Interdomain regulation of the ATPase activity of the ABC transporter haemolysin B from Escherichia coli.* Biochem J, 2016. **473**(16): p. 2471-83.
11. Lenders, M.H., et al., *In vivo quantification of the secretion rates of the hemolysin A Type I secretion system.* Sci Rep, 2016. **6**: p. 33275.
12. Kanonenberg, K., S.H.J. Smits, and L. Schmitt, *Functional Reconstitution of HlyB, a Type I Secretion ABC Transporter, in Saposin-A Nanoparticles.* Sci Rep, 2019. **9**(1): p. 8436.
13. Spitz, O., et al., *Identity Determinants of the Translocation Signal for a Type 1 Secretion System.* Front Physiol, 2021. **12**: p. 804646.
14. Pourhassan, N.Z., et al., *Investigations on the substrate binding sites of hemolysin B, an ABC transporter, of a type 1 secretion system.* Front Microbiol, 2022. **13**: p. 1055032.
15. Zhao, H., J. Lee, and J. Chen, *The hemolysin A secretion system is a multi-engine pump containing three ABC transporters.* Cell, 2022. **185**(18): p. 3329-3340 e13.
16. Valeva, A., et al., *Putative identification of an amphipathic alpha-helical sequence in hemolysin of Escherichia coli (HlyA) involved in transmembrane pore formation.* Biol Chem, 2008. **389**(9): p. 1201-7.
17. Jumpertz, T., et al., *Mutations affecting the extreme C terminus of Escherichia coli haemolysin A reduce haemolytic activity by altering the folding of the toxin.* Microbiology (Reading), 2010. **156**(Pt 8): p. 2495-2505.
18. Zaitseva, J., et al., *Functional characterization and ATP-induced dimerization of the isolated ABC-domain of the haemolysin B transporter.* Biochemistry, 2005. **44**(28): p. 9680-90.
19. Zaitseva, J., et al., *H662 is the linchpin of ATP hydrolysis in the nucleotide-binding domain of the ABC transporter HlyB.* EMBO J, 2005. **24**(11): p. 1901-10.

20. Gentschev, I. and W. Goebel, *Topological and functional studies on HlyB of Escherichia coli.* Mol Gen Genet, 1992. **232**(1): p. 40-8.
21. Guo, Y., *Be Cautious with Crystal Structures of Membrane Proteins or Complexes Prepared in Detergents.* Crystals, 2020. **10**(2): p. 86.
22. Gewering, T., et al., *Know your detergents: A case study on detergent background in negative stain electron microscopy.* J Struct Biol, 2018. **203**(3): p. 242-246.
23. Chipot, C., et al., *Perturbations of Native Membrane Protein Structure in Alkyl Phosphocholine Detergents: A Critical Assessment of NMR and Biophysical Studies.* Chem Rev, 2018. **118**(7): p. 3559-3607.
24. Bogdanov, M., E. Mileykovskaya, and W. Dowhan, *Lipids in the assembly of membrane proteins and organization of protein supercomplexes: implications for lipid-linked disorders.* Subcell Biochem, 2008. **49**: p. 197-239.
25. Renard, K. and B. Byrne, *Insights into the Role of Membrane Lipids in the Structure, Function and Regulation of Integral Membrane Proteins.* Int J Mol Sci, 2021. **22**(16).
26. Jodaitis, L., T. van Oene, and C. Martens, *Assessing the Role of Lipids in the Molecular Mechanism of Membrane Proteins.* Int J Mol Sci, 2021. **22**(14).
27. Young, J.W., *Recent advances in membrane mimetics for membrane protein research.* Biochem Soc Trans, 2023. **51**(3): p. 1405-1416.
28. Ritchie, T.K., et al., *Chapter 11 - Reconstitution of membrane proteins in phospholipid bilayer nanodiscs.* Methods Enzymol, 2009. **464**: p. 211-31.
29. Prabudiansyah, I., R. van der Valk, and M.E. Aubin-Tam, *Reconstitution and functional characterization of the FtsH protease in lipid nanodiscs.* Biochim Biophys Acta Biomembr, 2021. **1863**(2): p. 183526.
30. Arana, M.R., M.C. Fiori, and G.A. Altenberg, *Functional and structural comparison of the ABC exporter MsbA studied in detergent and reconstituted in nanodiscs.* Biochem Biophys Res Commun, 2019. **512**(3): p. 448-452.
31. Bayburt, T.H. and S.G. Sligar, *Single-molecule height measurements on microsomal cytochrome P450 in nanometer-scale phospholipid bilayer disks.* Proc Natl Acad Sci U S A, 2002. **99**(10): p. 6725-30.
32. Marin, V.L., et al., *Functional assays of membrane-bound proteins with SAMDI-TOF mass spectrometry.* Angew Chem Int Ed Engl, 2007. **46**(46): p. 8796-8.
33. Olsen, J.A., et al., *Structure of the human lipid exporter ABCB4 in a lipid environment.* Nat Struct Mol Biol, 2019.
34. Denisov, I.G., et al., *Directed self-assembly of monodisperse phospholipid bilayer Nanodiscs with controlled size.* J Am Chem Soc, 2004. **126**(11): p. 3477-87.
35. Hagn, F., et al., *Optimized phospholipid bilayer nanodiscs facilitate high-resolution structure determination of membrane proteins.* J Am Chem Soc, 2013. **135**(5): p. 1919-25.
36. Schachter, I., et al., *Confinement in Nanodiscs Anisotropically Modifies Lipid Bilayer Elastic Properties.* J Phys Chem B, 2020. **124**(33): p. 7166-7175.
37. Selvasingh, J.A., et al., *Dark nanodiscs as a model membrane for evaluating membrane protein thermostability by differential scanning fluorimetry.* bioRxiv, 2023.
38. Skar-Gislinge, N., et al., *Comprehensive Study of the Self-Assembly of Phospholipid Nanodiscs: What Determines Their Shape and Stoichiometry?* Langmuir, 2018. **34**(42): p. 12569-12582.
39. Frauenfeld, J., et al., *A saposin-lipoprotein nanoparticle system for membrane proteins.* Nat Methods, 2016. **13**(4): p. 345-51.

40. Popovic, K., et al., *Structure of saposin A lipoprotein discs.* Proc Natl Acad Sci U S A, 2012. **109**(8): p. 2908-12.
41. Flayhan, A., et al., *Saposin Lipid Nanoparticles: A Highly Versatile and Modular Tool for Membrane Protein Research.* Structure, 2018. **26**(2): p. 345-355 e5.
42. Zhang, Y., et al., *Asymmetric opening of the homopentameric 5-HT3A serotonin receptor in lipid bilayers.* Nat Commun, 2021. **12**(1): p. 1074.
43. Nagamura, R., et al., *Structural basis for oligomerization of the prokaryotic peptide transporter PepTSo2.* Acta Crystallogr F Struct Biol Commun, 2019. **75**(Pt 5): p. 348-358.
44. Nguyen, N.X., et al., *Cryo-EM structure of a fungal mitochondrial calcium uniporter.* Nature, 2018. **559**(7715): p. 570-574.
45. Lloris-Garcera, P., et al., *DirectMX - One-Step Reconstitution of Membrane Proteins From Crude Cell Membranes Into Salipro Nanoparticles.* Front Bioeng Biotechnol, 2020. **8**: p. 215.
46. Carlson, M.L., et al., *The Peptidisc, a simple method for stabilizing membrane proteins in detergent-free solution.* Elife, 2018. **7**.
47. Carlson, M.L., et al., *Profiling the Escherichia coli membrane protein interactome captured in Peptidisc libraries.* Elife, 2019. **8**.
48. Saville, J.W., L. Troman, and F. Duong Van Hoa, *PeptiQuick, a One-Step Incorporation of Membrane Proteins into Biotinylated Peptidiscs for Streamlined Protein Binding Assays.* J Vis Exp, 2019(153).
49. Angiulli, G., et al., *New approach for membrane protein reconstitution into peptidiscs and basis for their adaptability to different proteins.* Elife, 2020. **9**.
50. Harris, A., et al., *Structure and efflux mechanism of the yeast pleiotropic drug resistance transporter Pdr5.* Nat Commun, 2021. **12**(1): p. 5254.
51. Baykov, A.A., O.A. Evtushenko, and S.M. Avaeva, *A malachite green procedure for orthophosphate determination and its use in alkaline phosphatase-based enzyme immunoassay.* Anal Biochem, 1988. **171**(2): p. 266-70.
52. Wiseman, B., et al., *Stubborn contaminants: influence of detergents on the purity of the multidrug ABC transporter BmrA.* PLoS One, 2014. **9**(12): p. e114864.
53. Pyle, E., et al., *Structural Lipids Enable the Formation of Functional Oligomers of the Eukaryotic Purine Symporter UapA.* Cell Chem Biol, 2018. **25**(7): p. 840-848 e4.

Supplementary Information

Table S1: Top three hits from MS results from HlyB gel slice at approx. 70 kDa after reconstitution of HlyB using SapA and LPG.

Description	Coverage [%]	# Peptides	# PSMs	# Unique Peptides	MW [kDa]	Score
HlyB	51	47	3336	47	83.5	1000316
BamA	47	37	196	37	90.5	55232
SapA	70	5	152	5	11.6	44000

Table S2: Top three hits from MS results from SapA gel slice at approx. 10 kDa after reconstitution of HlyB using SapA and LPG.

Description	Coverage [%]	# Peptides	# PSMs	# Unique Peptides	MW [kDa]	Score
SapA	70	5	879	5	11.6	273656
HlyB	29	17	35	17	83.5	8766
BSA	31	16	31	14	69.2	7317

3.4. Chapter 4: Purification of the inner membrane complex of the HlyA T1SS from Escherichia coli

Title: Purification of the inner membrane complex of the HlyA T1SS from *Escherichia coli*

Authors: **Florestan L. Bilsing**, Eymen Hachani, Cigdem Günes, Sander Smits, Lutz Schmitt

Published in: to be submitted

Own contribution:
Designing the experiments
Expression and purification of IMC from 2 plasmids
Expression and purification of IMC from pBAD and pK184
Spheroplast preparation
Purification via SMA and DirectMX
Expression and purification of HlyB and SapA
ATPase activity assays
Coreconstitution of HlyB and HlyD (with Eymen Hachani)
Purification of IMC from pQLink
Data evaluation
Preparation of the figures
Writing of the manuscript

Purification of the inner membrane complex of HlyA T1SS from *E. coli*

Florestan L. Bilsing[1], Eymen Hachani[1], Cigdem Günes[1], Sander Smits[1,2], Lutz Schmitt[1]*

[1]Heinrich Heine University Düsseldorf, Faculty of Mathematics and Natural Sciences, Institute of Biochemistry, Universitätsstraße 1, 40225 Düsseldorf
[2]Heinrich Heine University Düsseldorf, Faculty of Mathematics and Natural Sciences, Center for Structural Studies, , Universitätsstraße 1, 40225 Düsseldorf

*Corresponding author: Lutz Schmitt, Heinrich Heine University Düsseldorf, Faculty of Mathematics and Natural Sciences, Institute of Biochemistry, Universitätsstraße 1, 40225 Düsseldorf, Germany, Tel.: +49 211 81 10773, E-Mail: lutz.schmitt@hhu.de

Abstract

Gram-negative bacteria use Type 1 secretion systems (T1SS) to secrete proteins important for pathogenicity. One of the best studied T1SS is the hemolysin A (HlyA) T1SS from uropathogenic *E. coli* strains. It requires the interplay of the three proteins TolC, HlyB and HlyD. While TolC is located in the outer membrane, HlyB and HlyD form a so called inner membrane complex (IMC) in the inner membrane. To study the IMC's structure and function, the purification of the IMC in its native state is inevitable. Since the state of a purified membrane protein is highly dependent on its surrounding it is important to carefully chose and screen for the detergent or membrane mimetic that suits the needs of the protein and the experiment best. Here we report a process of testing different conditions to purify the IMC of HlyA T1SS from *E. coli* in its native state. We focused on different purification strategies using one or two plasmids, different affinity tags and different detergents. We also tried purification protocols with only a single step of detergent usage like DirectMX or no detergent usage such as solubilisation and purification with styrene maleic acid copolymers (SMA). Furthermore, we were partially successful with an *in vitro* co-reconstitution of the IMC from separately purified components. Finally, the use of digitonin as the detergent of choice turned out to be the most effective way to isolate and purify the native IMC from *E. coli* membranes.

Introduction

Gram-negative bacteria have derived a number of different secretion systems [1]. The simplest one in terms of complexity and number of proteins involved is probably the Type 1 secretion system (T1SS) [2]. One of the best studied T1SSs is the hemolysin A (HlyA) T1SS from uropathogenic *E. coli* [3-7]. The HlyA T1SS is build up by the outer membrane protein, TolC and the so-called inner membrane complex (IMC). This IMC is formed by the ATP binding cassette (ABC) transporter HlyB and the membrane fusion protein (MFP) HlyD [8]. Although, the HlyA T1SS may be simple in terms of complexity, the structure of the IMC was not known until recently [9]. Single particle cryo-EM analysis of the IMC purified in the detergent digitonin revealed valuable insights into the structure and stoichiometry of the IMC.

Detergents are usually the first choice when it comes to membrane protein purification. They are easy to apply and available in a huge variety, which is also one of the pitfalls of detergent usage, as one has to screen for the right detergent suitable for the experiment [10-13]. Each detergent has its specific benefits and downsides and just because a detergent works for the purification of one membrane protein it doesn't mean it also works for the purification of another membrane protein. In addition, a detergent suitable for solubilization doesn't have to be a suitable detergent for purification and structure determination [14]. Besides maltosides, the detergent digitonin and its synthetic analogue glyco-diosgenin (GDN) have been one of the most frequently used detergents for unique membrane protein structure determination during the past 10 years [14-18]. But as digitonin is a natural product, it is very expensive and shows batch-to-batch variation. Furthermore, detergents in general can cause artifacts or interfere with specific methods especially in structure determination [11, 19, 20].

This is why besides detergents a variety of membrane mimetic systems are used in membrane protein research. Those membrane mimetic systems allow protein solubilization, purification or stabilization with only low amounts of detergents or even no detergent at all. MSP based nanodiscs or Salipro provide a detergent free environment at a late stage of the purification process and detergent is still required for solubilization and purification [21-23]. Other methods like DirectMX or Peptidisc rely on an initial detergent solubilization step before purification can proceed in a detergent free environment [24, 25]. The use of amphipols, styrene maleic acid copolymers

(SMA) or diisobutylene maleic acid copolymers (DIBMA) allows direct extraction of a membrane protein without the need of any detergent [26-30].

Another important point to consider for protein purification is the choice of affinity tag and its position. It was shown for several protein structures derived via X-ray crystallography of proteins with a histidine-tag that the tag generally does not have a significant influence on the structure [31]. Other studies showed that tags reduce flexibility and favor specific conformations [32]. In addition, an influence of the affinity-tag on protein activity and stability was observed [33, 34] and also predicted via computational protein structure modeling [35]. Therefore especially for protein complexes the position of the tag is crucial as it might not only influence activity or structure of single proteins, but interfere with interaction sites between different proteins of a complex and therefore prevent complex formation.

Here we present different strategies for the functional isolation and purification of the IMC of the HlyA T1SS from *E. coli.* We tested different expression strategies with focus on different plasmids and affinity tags for purification. Furthermore we tried to decipher the role of detergents for successful isolation of the IMC. We also tested mild purification strategies like sucrose gradient purification without any affinity tag. We could report initial success for an in vitro co-reconstitution of the proteins of the IMC, although further analysis needs to verify the final result. By minor adaptions of a recently published protocol [9] we could successfully isolate transport competent and ATPase active IMC in the detergent digitonin.

Material and Methods

Expression of IMC from 2 plasmids

For expression of the IMC from two separate plasmids *E. coli* C43ΔacrAB(DE3) was used with the plasmids pBAD-HisHlyB and pET28-HisHlyD and grown in a fermenter. Both constructs contained an N-terminal 10xHis-tag and a specific protease cleavage side between protein and tag. Cells were grown overnight in 25 ml 2YT medium in a 100 ml non-baffled flask supplemented with 100 µg/ml ampicillin and 30 µg/ml kanamycin at 37 °C and 180 rpm. Precultures of 250 ml 2YT medium supplemented with 100 µg/ml ampicillin and 30 µg/ml kanamycin in a 1 L non-baffled flask were inoculated from the overnight grown cultures to an OD_{600} of 0.1 and incubated at 37 °C and 180 rpm for four hours. Precultures were centrifuged for 20 minutes at 20 °C

and 4,000 xg, cells were resuspended in 50 ml 2YT medium and added to 7 L minimal medium (15 g/L KH_2PO_4, 20 g/L glycerol, 5 g/L $(NH_4)_2SO_4$, 3 g/L $MgSO_4$ x 7 H_2O, 0.015 g/L $CaCl_2$, 0.15 g/L $FeSO_4$ x 7 H_2O, 0.1 g/L $ZnCl_2$, 1 g/L $C_6H_5Na_3O_7$ x 2 H_2O, 1.5 ml/L thiamine solution (5 g/L), 1.5 ml/L trace elements solution (2 g/L Al_2SO_4 x 18 H_2O, 0.75 g/L $CoSO_4$ x 7 H_2O, 2.5 g/L $CuSO_4$ x 5 H_2O, 0.5 g/L H_3BO_3, 24 g/L $MnSO_4$ x H_2O, 3 g/L Na_2MoO_4 x 2 H_2O, 25 g/L $NiSO_4$ x 6 H_2O, 15 g/L $ZnSO_4$ x 7 H_2O, 2 ml/L H_2SO_4 (30%))) supplemented with 100 µg/ml carbenicillin and 30 µg/ml kanamycin in a 10 L fermenter. $FeSO_4$ x 7 H_2O, thiamine solution and trace elements solution were added after autoclaving the media. Cells from two precultures were used for one fermentation. Cells were grown in a fed batch process at a pH of 6.8 and 36 °C to an OD_{600} of about 30 using a stepwise increase of feeding to obtain linear growth. Feeding solution contained 50% glycerol, 2 ml/L thiamine solution, 2 ml/L trace elements solution, 100 µg/ml carbenicillin and 30 µg/ml kanamycin. Expression of HlyB was induced by addition of 10 mM arabinose and one hour later expression of HlyD was induced by the addition of 1 mM IPTG. Cells were harvested after 1 hour of expression via centrifugation at 6,000 rpm (SLC-6000, Sorvall) for 30 min at 4 °C. Cells were resuspended in buffer A (50 mM NaP_i, pH 8, 500 mM NaCl), flash frozen in liquid nitrogen and stored at – 80 °C.

Expression of IMC from 1 plasmid

pK184

For expression of the IMC from one plasmid pK184-HlyBHlyD was used with no affinity-tag or an N-terminal 6xHis-tag on HlyD in *E. coli* C41ΔacrABΔompF(DE3). Cells were grown in 50 ml 2YT medium supplemented with 100 µg/ml ampicillin in a 300 ml baffled flask at 37 °C and 180 rpm overnight. Expression cultures of 1 L 2YT medium supplemented with 100 µg/ml ampicillin in 5 L baffled flasks were inoculated from the overnight grown cultures to an OD_{600} of 0.1 and incubated at 37 °C at 120 rpm. Expression was induced at OD_{600} of 0.6 – 0.8 by addition of 1 mM IPTG and performed for three hours. Cells were harvested via centrifugation at 7,000 rpm (SLC-6000, Sorvall) for 20 min at 4 °C. Cells were resuspended in buffer B (50 mM Tris pH 8, 500 mM NaCl), flash frozen in liquid nitrogen and stored at – 80 °C.

Expression of IMC from 1 plasmid

pBAD

For expression of the IMC from one plasmid pBAD-TSHlyB-HisHlyD was used with an N-terminal TwinStrep-tag (TS) on HlyB and an N-terminal 6xHis-tag (His) on HlyD in *E. coli* C43 (DE3). Cells were grown in 50 ml 2YT medium supplemented with 100 µg/ml ampicillin in a 300 ml baffled flask at 37 °C and 180 rpm overnight. Expression cultures of 1 L 2YT medium supplemented with 100 µg/ml ampicillin in 5 L baffled flasks were inoculated from the overnight grown cultures to an OD_{600} of 0.1 and incubated at 37 °C at 120 rpm. Expression was induced at OD_{600} of 0.6 – 0.8 by addition of 10 mM arabinose and performed for three hours. Cells were harvested via centrifugation at 5,000 xg for 20 min at 4 °C. Cells were resuspended in buffer X (30 mM Tris pH 8, 150 mM NaCl, 15% glycerol), flash frozen in liquid nitrogen and stored at – 80 °C.

Expression of IMC from 1 plasmid

pQLink

For expression of the IMC from one plasmid pQLink-StrepHlyB-HisHlyD was used with an N-terminal Strep-tag (Strep) on HlyB and an N-terminal 6xHis-tag (His) on HlyD in *E. coli* C43 (DE3). Cells were grown in 50 ml 2YT medium supplemented with 100 µg/ml ampicillin in a 300 ml baffled flask at 37 °C and 180 rpm overnight. Expression cultures of 2 L 2YT medium supplemented with 100 µg/ml ampicillin in 5 L baffled flasks were inoculated from the overnight grown cultures to an OD_{600} of 0.1 and incubated at 37 °C and 180 rpm. When OD_{600} was between 0.6 – 0.8 flasks were chilled on ice for 20 minutes and expression was induced by addition of 0.2 mM IPTG and performed for 16 hours overnight at 18 °C. Cells were harvested via centrifugation at 5,000 xg for 20 minutes at 4 °C. Cells were resuspended in buffer X and centrifuged again for 20 minutes at 5,000 xg and 4 °C. Pellets were flash frozen in liquid nitrogen and stored at – 20 °C.

Spheroplast preparation

8 g cells were resuspended in 50 ml 1 M glucose and 3 ml solution A (1 M Tris pH 8), 2.4 ml lysozyme (5 mg/ml in 20 mM Tris pH 8), 0.6 ml EDTA (125 mM EDTA-NaOH pH 8) and a spatulas tip DNAse I were added and incubated at room temperature for 15 minutes. After addition of 10 ml stop solution (10 mM Tris pH 8, 20 mM $MgCl_2$, 0.7 M sucrose) cells were incubated for 20 min at 8 °C with gentile agitation. Spheroplasts

were harvested by centrifugation for 10 min at 17,000 xg and 4 °C. Pellet was resuspended in buffer C (100 mM Hepes pH 8, 250 mM NaCl).

Membrane preparation

Cells / spheroplasts were mixed with one cOmplete EDTA-free inhibitor cocktail tablet and a spatulas tip of DNAse I and disrupted by three passes through Microfluidizer M-110P (Microfluidics) at 1.5 kbar. Centrifugation was performed at 18,000 xg for 30 minutes at 4 °C to remove cell debris. Supernatant was centrifuged for 90 minutes at 38,000 rpm (Type 45 Ti, Beckman Coulter) at 4 °C to pellet membranes. Membranes were resuspended in appropriate buffer and stored at – 80 °C.

IMC Purification

***E. coli* C43ΔacrAB(DE3) with pBAD-HisHlyB and pET28-HisHlyD**

Membranes were diluted in buffer A1 (50 mM NaP_i, pH 8, 300 mM NaCl) to 10 mg/ml. Solubilisation was performed with 0.3 % Fos-Choline-16 for 1 hour at 4 °C. Non-solubilised material was removed by centrifugation for 30 minutes at 42,000 rpm (Type 45 Ti, Beckman Coulter) at 4 °C. Supernatant was diluted three times, 2 mM imidazole was added and loaded on a 5 ml HiTrap IMAC HP (Cytiva) column (Ni^{2+}) equilibrated in buffer A2 (50 mM NaP_i, pH 8, 300 mM NaCl, 0.015% DDM / 0.003 % LMNG, 2 mM imidazole). The column was washed with two column volumes (CV) of buffer A2 and stepwise 3 CV each with 5%, 10%, 15% and 20% of buffer A3 (50 mM NaP_i, pH 8, 300 mM NaCl, 0.015% DDM / 0.003 % LMNG, 250 mM imidazole). Next the column was washed with 6 CV of 25% of buffer A3 and the IMC was eluted with 4 CV of 100 % of buffer A3. Fractions containing IMC were combined and concentrated using an Amicon Ultra-15 centrifugal filter unit (Millipore) with a MWCO of 100 kDa. The concentrated sample was centrifuged for 30 minutes at 17,000 xg and 4 °C and supernatant was applied on Superose 6 Increase 10/300 GL equilibrated with buffer C1 (100 mM Hepes pH 8, 250 mM NaCl, 0.015% DDM / 0.003 % LMNG). Fractions containing IMC were combined, concentrated, if required (Amicon Ultra-4 centrifugal filter unit (Millipore) with a MWCO of 100 kDa), and used for analysis.

Sucrose gradient of SMA solubilised IMC

For solubilisation via SMA the membrane was diluted to 20 mg/ml in buffer B. SMA (2:1) was used in a final concentration of 2.5 % and incubated at room temperature for

2 hours. Non-solubilised material was removed by centrifugation for 45 minutes at 100,000 xg at 4 °C. 800 µl of supernatant were placed on top of a 10 – 25 % sucrose gradient in buffer B and centrifuged for 16 hours at 30,000 rpm (SW 40 Ti, Beckman Coulter) at 4 °C. Fractions were collected from top to bottom and analysed via SDS-PAGE or Blue Native-PAGE and Western Blot. Fractions that were used for IMAC were diluted five times to reduce viscosity. For each fraction 50 µl Ni-NTA beads were used and equilibrated with buffer B1 (50 mM Tris pH 8, 500 mM NaCl, 2 mM imidazole). Samples was incubated with beads for 2 hours at 4 °C and washed with 10 CV buffer B1 and 3 CV buffer B2 (50 mM Tris pH 8, 500 mM NaCl, 50 mM imidazole). Elution was performd with buffer B3 (50 mM Tris pH 8, 500 mM NaCl, 250 mM imidazole). Elution fractions were analysed via SDS-PAGE and Western Blot.

DirectMX

Membranes from *E. coli* C41ΔacrABΔompF(DE3) pK184-HlyB-HisHlyD was diluted with buffer A1 to 5 ml to a concentration of 10 mg/ml and solubilized with 1 % LPG for 1 hour at 4 °C with constant agitation. Non-solubilised material was removed by centrifugation for 10 minutes at 100,000 xg at 4 °C. The supernatant was incubated with 9 ml saposin A (2.5 mg/ml) for 30 minutes at 4 °C under constant agitation. After addition of 6 mM imidazole the sample was applied on a 5 ml HiTrap Chelating HP (Cytiva) column (Zn^{2+}) equilibrated with buffer A4 (50 mM NaP_i, pH 8, 300 mM NaCl, 2 mM imidazole). The column was washed with 5 CV buffer A4 and 5 CV buffer A5 (50 mM NaP_i, pH 8, 300 mM NaCl, 40 mM imidazole). Target protein was eluted with 5 CV buffer A6 (50 mM NaP_i, pH 8, 300 mM NaCl, 25 mM EDTA). Elution fractions were analysed via SDS-PAGE and Western Blot.

IMC without an affinity-tag

Membranes from *E. coli* C41ΔacrABΔompF(DE3) pK184-HlyBHlyD were diluted in buffer B to 10 mg/ml. Solubilisation was performed with 1 % LMNG for 1 hour at 4 °C. Non-solubilised material was removed by centrifugation for 45 minutes at 100,000 xg at 4 °C. 800 µl supernatant were placed on top of a 10 – 25 % sucrose gradient in buffer D (10 mM Tris pH 8, 0.003 % LMNG) and centrifuged or 16 hours at 30,000 rpm (SW 40 Ti, Beckman Coulter) at 4 °C. Fractions were collected from top to bottom and analysed via SDS-PAGE or Blue Native-PAGE and Western Blot.

***E. coli* C43 (DE3) with pBAD-TSHlyB-HisHlyD**

Membranes were diluted in buffer X1 (30 mM Tris pH 8, 150 mM NaCl) to 20 mg/ml and solubilised for 1.5 hours under constant agitation at 4 °C with 1% digitonin. Non-solubilised material was removed by centrifugation for 45 minutes at 100,000 xg and 4 °C. Supernatant was loaded on a 1 ml StrepTrap HP (Cytiva) column multiple times overnight. The column was washed with 15 CV buffer X2 (30 mM Tris pH 8, 150 mM NaCl, 0.1% digitonin) and target protein was eluted with 5 CV of buffer X3 (30 mM Tris pH 8, 150 mM NaCl, 0.1% digitonin, 5 mM desthiobiotin). Elution fractions were combined and applied on a 1 ml HisTrap FF (Cytiva) column (Ni^{2+}). The column was washed with 15% of buffer X4 (30 mM Tris pH 8, 150 mM NaCl, 0.1% digitonin, 200 mM imidazole) prior to elution of IMC with 5 CV buffer X4. Elution fractions were combined and concentrated using an Amicon Ultra-4 centrifugal filter unit (Millipore) with a MWCO of 100 kDa. The concentrated sample was centrifuged for 30 minutes at 17,000 xg and 4 °C and supernatant was applied on Superose 6 Increase 3.2/300 GL equilibrated with buffer X2. Elution fractions were analysed via SDS-PAGE, Western Blot and ATPase activity assay.

***E. coli* C43 (DE3) with pQLink-StrepHlyB-HisHlyD**

Membranes were diluted in buffer X1 to 20 mg/ml. Solubilization was performed for 1 hour at 4 °C using 1 % digitonin. Non-solubilized material was removed by centrifugation for 30 minutes at 42,000 rpm (Type 70 Ti, Beckman Coulter) and 4 °C. Supernatant was incubated in a ratio of 50 ml membrane with 1 ml Strep-Tactin MacroPrep resin (IBA Lifesciences) overnight under agitation at 4 °C. Each 1 ml resin was transferred into a gravity flow column and washed with 15 CV buffer X2. The resin was incubated for 5 minutes with 2 CV buffer X3 and IMC was eluted with 3 additional CV buffer X3. Elution fractions were concentrated using Amicon Ultra-15 centrifugal filter unit (Millipore) with a MWCO of 100 kDa. Sample was centrifuged for 30 minutes at 17,000 xg and 4 °C and applied on Superose 6 Increase 3.2/300 GL equilibrated with buffer X2. Elution fractions were analysed via SDS-PAGE, Western Blot and ATPase activity assay.

Expression and purification of HlyB

HlyB was expressed in *E. coli* C41ΔacrABΔompF(DE3) using a pBAD based plasmid containing an N-terminal TwinStrep-tag. Cells were grown in 50 ml 2YT medium in a

300 ml baffled flask supplemented with 100 µg/ml ampicillin at 37 °C and 180 rpm overnight. Expression cultures of 1 L 2YT supplemented with 100 µg/ml ampicillin in 5 L baffled flasks were inoculated from the precultures to an OD_{600} of 0.1 and incubated at 37 °C and 120 rpm. Expression was induced at OD_{600} of 0.7 by addition of 10 mM arabinose and expression was performed for 3 h. Cells were harvested via centrifugation at 5,000 xg for 20 minutes at 4 °C. Pellet was resuspended in buffer A1 and 1 cOmplete EDTA-free inhibitor cocktail tablet and a spatulas tip of DNAse I were added. Cell disruption was performed by three passes through Microfluidizer M-110P (Microfluidics) at 1.5 kbar. Centrifugation was performed at 18,000 xg for 30 minutes at 4 °C to get rid of cell debris. Supernatant was centrifuged for 90 minutes at 38,000 rpm (Type 45 Ti, Beckman Coulter) at 4 °C to pellet membranes. Membranes were resuspended in buffer E (50 mM NaH_2PO_4 pH 8, 300 mM NaCl) and adjusted to 10 mg/ml and solubilised for 1 hours at 4 °C using 0.5 % Fos-Choline-14. Non-solubilized material was removed by centrifugation for 30 minutes at 38,000 rpm (Type 45 Ti, Beckman Coulter) at 4 °C and diluted once with buffer E. Supernatant was loaded on a 5 ml StrepTrap HP (Cytiva) column equilibrated with buffer E1 (50 mM NaH_2PO_4 pH 8, 300 mM NaCl, 0.015 % DDM). Column was washed 10 CV with buffer E1 and HlyB was eluted with 6 CV buffer E2 (50 mM NaH_2PO_4 pH 8, 300 mM NaCl, 0.015 % DDM, 2.5 mM desthiobiotin). Fractions containing HlyB were combined and concentrated using an Amicon Ultra-15 centrifugal filter unit (Millipore) with a MWCO of 100 kDa. The concentrated sample was centrifuged for 30 minutes at 17,000 xg and 4 °C and supernatant was applied on Superose 6 Increase 10/300 GL equilibrated with buffer F (20 mM Hepes pH 8, 100 mM NaCl, 0.015% DDM). Fractions containing HlyB were combined and concentrated using an Amicon Ultra-4 centrifugal filter unit (Millipore) with a MWCO of 100 kDa and used for co-reconstitution.

Expression and purification of HlyD

Performed by Eymen Hachani (unpublished data).

Expression and purification of MSP2N2 and SapA

MSP2N2 and SapA were expressed and purified according to published protocols [22, 23].

Co-reconstitution of HlyB and HlyD

SapA

For co-reconstitution of the IMC by mixing purified HlyB and HlyD a ratio of HlyB to HlyD of 1:3 was used. The molar ratio for IMC to SapA to lipid was 1:6:600. As a lipid for co-reconstitution LPG or POPC was used. For one co-reconstitution 8 to 10 batches with a final volume of 100 µl were used. HlyB, HlyD and lipids were mixed and incubated for 5 minutes at 30 °C. SapA was added to the mixture and incubated for 5 min at 30 °C. Each batch was diluted 10 times and all batches were combined and concentrated using an Amicon Ultra-15 centrifugal filter unit (Millipore) with a MWCO of 100 kDa. The concentrated sample was centrifuged for 30 minutes at 17,000 xg and 4 °C and supernatant was applied on Superose 6 Increase 10/300 GL equilibrated with buffer G (20 mM Hepes pH 8, 100 mM NaCl). Fractions containing IMC were combined and applied on a 1 ml StrepTrap HP (Cytiva) affinity column and washed with 5 CV buffer G. Reconstituted IMC was eluted with buffer G1 (20 mM Hepes pH 8, 100 mM NaCl, 5 mM desthiobiotin). Elution fractions were analysed via SDS-PAGE and Western Blot.

MSP2N2

For co-reconstitution of the IMC by mixing purified HlyB and HlyD a ratio of HlyB to HlyD of 1:3 was used. The molar ratio for IMC to MSP2N2 to lipid was 1:2:400. As a lipid for co-reconstitution POPC was used. POPC was ordered as chloroform solution (Avanti Polar Lipids) and chloroform was evaporated using a rotary evaporator. POPC was resuspended in buffer G. Lipids were incubated with 1 % Triton X-100 for 10 min at 40 °C. Lipids were chilled on ice and HlyB and HlyD and MSP2N2 were added simultaneously and incubated on ice for 30 min. 0.8 g/ml BioBeads SM-2 (Biorad) were added and sample was incubated at 4 °C overnight under constant agitation. The next day BioBeads SM-2 (Biorad) were removed, the sample was concentrated and centrifuged for 30 min at 17,000 xg and 4 °C. The supernatant was applied on a Superose 6 Increase 10/300 GL equilibrated with buffer G. Fractions containing IMC were combined and applied on a 1 ml StrepTrap HP (Cytiva) affinity column and washed with 5 CV buffer G. Reconstituted IMC was eluted with buffer G1 (20 mM Hepes pH 8, 100 mM NaCl, 5 mM desthiobiotin). Elution fractions were analysed via SDS-PAGE, Western Blot and ATPase activity assay.

Malachite Green ATPase activity assay

For measuring ATPase activity the Malachite Green assay [36] was used as described earlier (Chapter 2 – Optimisation of the purification of the ABC transporter HlyB from *Escherichia coli*).

Results

Purification of IMC

His-affinity

The IMC was purified from *E. coli* C43Δ*acrAB*(DE3) cells containing two plasmids: one plasmid for production of HlyB and one plasmid for production of HlyD. HlyB and HlyD, both contained an N-terminal 10xHis-tag. After solubilisation with Fos-Cholin-16 purification via IMAC and SEC was performed in buffers containing DDM (Figure 1).

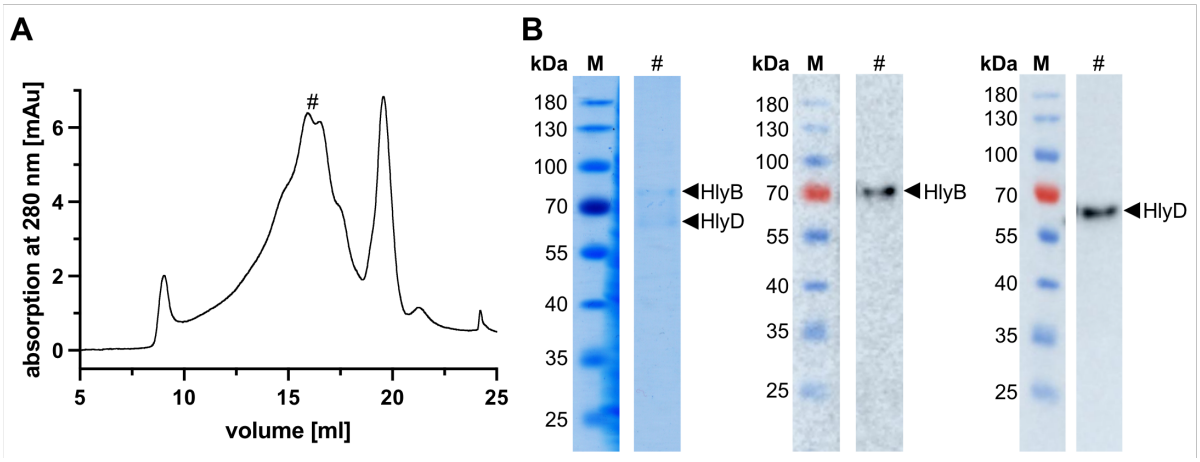

Figure 1: Purification of IMC in DDM. A: *SEC analysis of IMC on a Superose 6 Inc. 10/300 GL.* ***B:*** *SDS-PAGE (left) and Western blot analysis targeting HlyB (middle) or HlyD (right). M: marker proteins with their approximated molecular weight. #: Sample from IMC main elution peak of the SEC. The bands for HlyB and HlyD are marked with black triangles. Protein-specific, polyclonal anti-HlyB and anti-HlyD antibodies were used for detection.*

The IMC was successfully purified in DDM but the yield was very low. Main elution fractions showed a maximum of 0.06 µg IMC per mg starting protein content (corresponding to 0.18 mg/ml). We investigated whether a different detergent could improve protein yield and used LMNG instead of DDM. Solubilisation was performed with Fos-Cholin-16 and IMAC and SEC were performed in buffers containing LMNG (Figure 2).

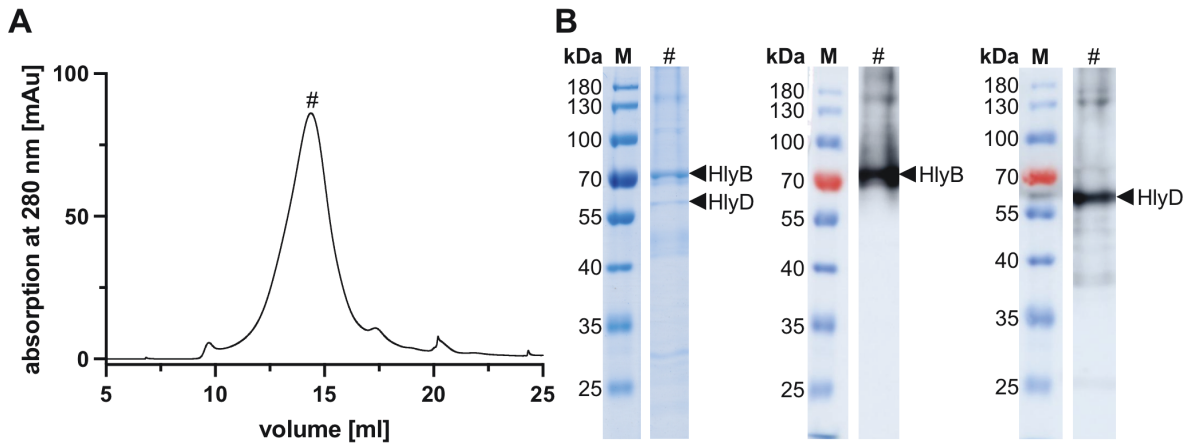

Figure 2: Purification of IMC in LMNG. A: *SEC analysis of IMC on a Superose 6 Inc. 10/300 GL.* ***B:*** *SDS-PAGE (left) and Western blot analysis targeting HlyB (middle) or HlyD (right). M: marker proteins with their approximated molecular weight. #: Sample from IMC main elution peak of the SEC. The bands for HlyB and HlyD are marked with black triangles. Protein-specific anti-HlyB and anti-HlyD antibodies were used for detection.*

Purification in LMNG compared to DDM showed a more homogeneous peak in the SEC profile and a higher IMC yield. Main elution fractions showed a maximum of 0.21 µg IMC per mg total starting protein content (0.47 mg/ml). But besides a higher yield also more impurities were visible in the SDS-PAGE analysis (Figure 2B).

To further improve purity we tested to remove the outer membrane first and prepared so called spheroplasts. Those spheroplasts were used for membrane isolation and subsequent purification of IMC via IMAC and SEC (Figure 3).

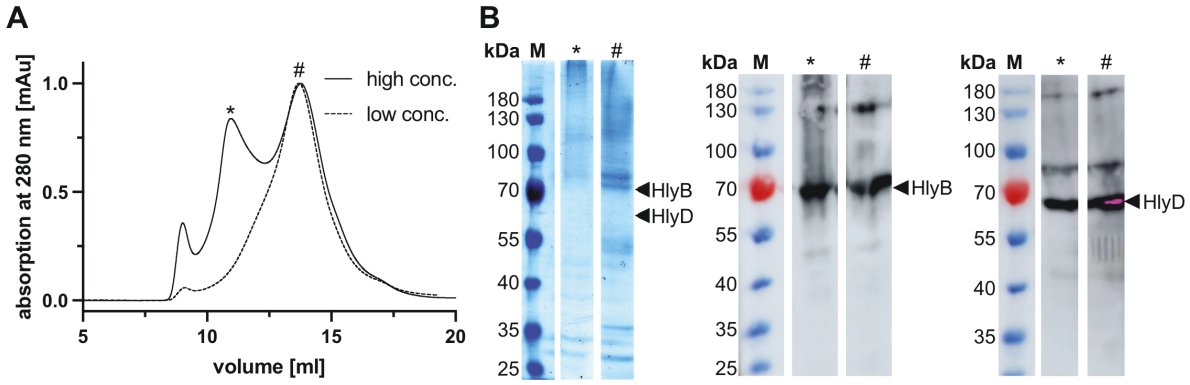

Figure 3: Purification of IMC from spheroplasts in LMNG. A: *SEC analysis of IMC on a Superose 6 Inc. 10/300 GL.* ***B:*** *SDS-PAGE (left) and Western blot analysis targeting HlyB (middle) or HlyD (right). M: marker proteins with their approximated molecular weight. #: Sample from IMC main elution peak of the SEC. *: Sample from additional peak appearing at high concentrations. The bands for HlyB and HlyD are marked with black triangles. Protein-specific anti-HlyB and anti-HlyD antibodies were used for detection.*

Solubilisation was performed in Fos-Cholin-16 and purification was performed in LMNG. Compared to the purification from whole *E. coli* cells (Figure 2), the purification from spheroplasts did not result in a higher purity after SEC as seen in SDS-PAGE

analysis (Figure 3B, left). When increasing the concentration before SEC to roughly 10 mg/ml we could observe an additional peak in the SEC profile (peak *, Figure 3A). Western blot analysis confirmed the presence of HlyB and HlyD in this additional peak (Figure 3B).

Styrene Maleic Anhydride (SMA)

As we observed multiple peaks in the SEC profile containing HlyB and HlyD depending on the concentration, we tried to isolate the IMC in a more native like environment without generating potential purification artifacts. Therefore we tried to stabilize the IMC during solubilization and purification in its native membrane environment by using polymers instead of detergents. Here we applied SMA in combination with different purification procedures. As a very mild purification process we used sucrose density gradients for purification of SMA solubilized IMC (Figure 4).

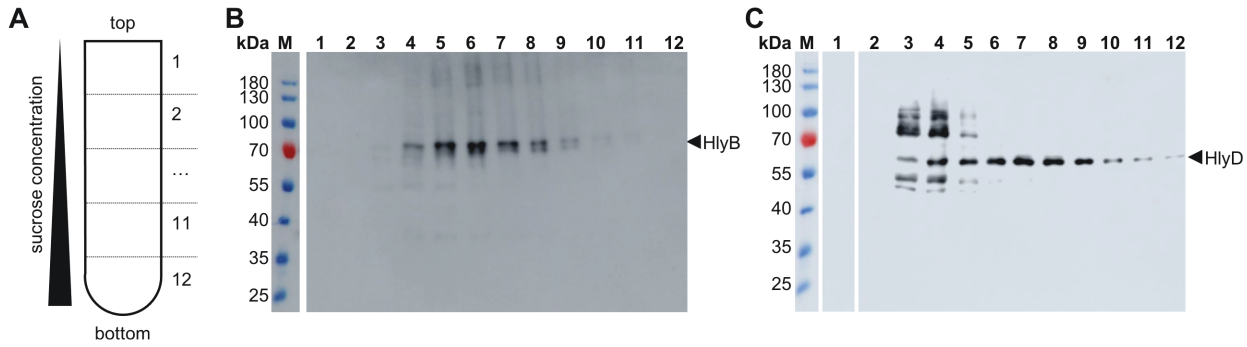

Figure 4: Sucrose gradient purification of SMA solubilized IMC. A: *SMA solubilized IMC is placed on a 10 – 25% sucrose gradient for purification. The gradient is fractionated for analysis from top to bottom.* ***B:*** *Western blot from a SDS-PAGE analysis of a 10 – 25% sucrose gradient for purification of IMC. 1 – 12: fractions from top to bottom of the sucrose gradient. M: marker proteins with their approximated molecular weight. The bands for HlyB and HlyD are marked with black triangles. Protein-specific anti-HlyB and anti-HlyD antibodies were used for detection.*

After sucrose density gradient purification of SMA solubilised IMC the gradient was fractionated and analysed via SDS-PAGE and Western blot. HlyB was detected in fraction 4 to 10 with the strongest signals in fraction 5 and 6. In contrast HlyD was detected in almost each fraction of the gradient (fraction 3 to 12) with the most intense signals in fractions 7 and 8. Fractions containing HlyB and HlyD were combined and applied on a Ni^{2+}-NTA resin for further purification. Surprisingly nothing bound to the beads and prevented further purification.

DirectMX

We tested a similar approach termed DirectMX [24] that combines solubilisation and reconstitution into saposin-lipoprotein nanoparticles (Salipro) with native lipids. For this approach we used a construct with HlyB and HlyD on the same plasmid and only one N-terminal 6xHis-tag on HlyD. For solubilisation we used lysophosphatidylglycerol (LPG) and performed an IMAC afterwards. As seen from Western blot analysis only weak signals for HlyB and HlyD were detectable in the elution from the IMAC (Figure 5, lane E). Most of the HlyB and HlyD was removed from the column already during washing with only low amounts of imidazole (Figure 5, lane W). These fractions contained many unspecific bound proteins and had a low purity, judged from Coomassie stained SDS-PAGE analysis (not shown).

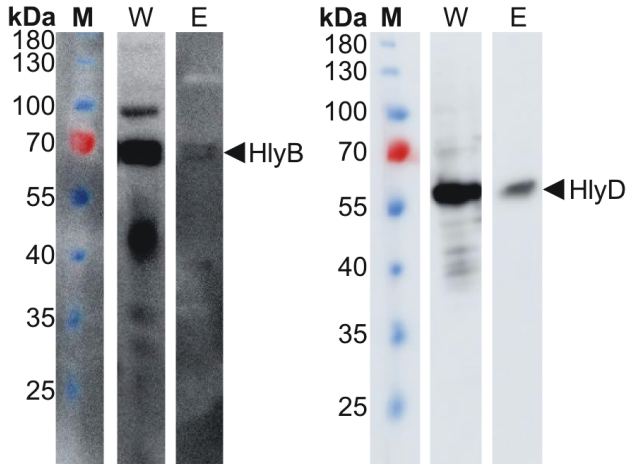

Figure 5: Western blot from Western blot analysis of IMC purified via DirectMX. *M: marker proteins with their approximated molecular weight. W: Wash fraction from IMAC. E: Elution fraction from IMAC. The bands for HlyB and HlyD are marked with black triangles. Protein-specific anti-HlyB and anti-HlyD antibodies were used for detection.*

As we could see multiple species in detergent showing signal for HlyB and HlyD in SEC analysis (Figure 3), an inconclusive result for the HlyB and HlyD signals in the fractions from the sucrose gradient after SMA solubilisation (Figure 4) and no success in DirectMX approach (Figure 5) to purify the IMC, we decided to investigate the system in a more native-like state. We created a construct without any affinity tag to make sure that the tags do not prevent IMC formation and to exclude false positive results due to the same affinity tag on both proteins. Furthermore this construct contained *hlyB* and *hlyD* one after the other on one plasmid, as in the genome of uropathogenic *E. coli*.

Purification of IMC without affinity-tags

For this purification approach we used *E. coli* C41Δ*acrAB*Δ*ompF*(DE3) cells containing only a single plasmid for production of HlyB and HlyD without any affinity tag. We prepared spheroplasts first and used those for membrane isolation. Membranes were solubilised with LMNG and purification was performed using a sucrose gradient containing LMNG. The fractions from the sucrose gradient were analysed via Blue Native-PAGE and Western blot (Figure 6).

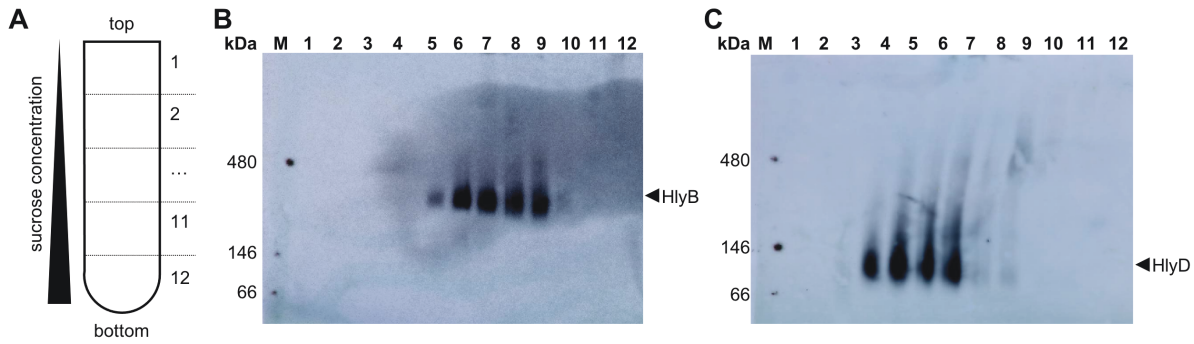

Figure 6: Sucrose gradient purification of IMC in LMNG. A: *LMNG solubilized IMC is placed on a 10 – 25% sucrose gradient for purification. The gradient is fractionated for analysis from top to bottom.* ***B:*** *Western blot from a Blue Native-PAGE analysis of a 10 – 25% sucrose gradient for purification of IMC. 1 – 12: fractions from top to bottom of the sucrose gradient. M: marker proteins with their approximated molecular weight. The bands for HlyB and HlyD are marked with black triangles. Protein-specific anti-HlyB and anti-HlyD antibodies were used for detection.*

HlyB was detected in fractions 5 to 9, while HlyD was detected in fraction 4 – 7. Besides the mismatch of the fractions, HlyB and HlyD migrated at different molecular weights lacking a signal for the IMC of HlyB and HlyD. HlyB migrated at a molecular weight of approximately 300 kDa while HlyD migrated at a molecular weight of approximately 120 kDa. Approaches in stabilising the complex before the purification by use of DSP, an bifunctional crosslinker, were not successful and did not improve purification results (not shown).

From the previous results we concluded that stability of the IMC is one of the main issues during our purification approaches, this is why we decided to purify the proteins of the IMC separately and try to form the IMC during reconstitution, as shown for MexAB from *P. aeruginosa* [37].

Co-reconstitution of HlyB and HlyD

Salipro

HlyB with an N-terminal TwinStrep-tag and HlyD with an N-terminal 10xHis-tag were purified separately in Fos-Choline-14 and combined for co-reconstitution of HlyB and HlyD into SapA LPG. The molar ratio of HlyB to HlyD was 1:3 and the molar ratio of IMC to SapA to LPG was 1:6:600. The sample was applied on a Superose 6 Inc. 10/300 GL column and fractions containing co-reconstituted HlyB and HlyD were applied on a StrepTrap affinity column and eluted with d-Desthiobiotin (Figure 7).

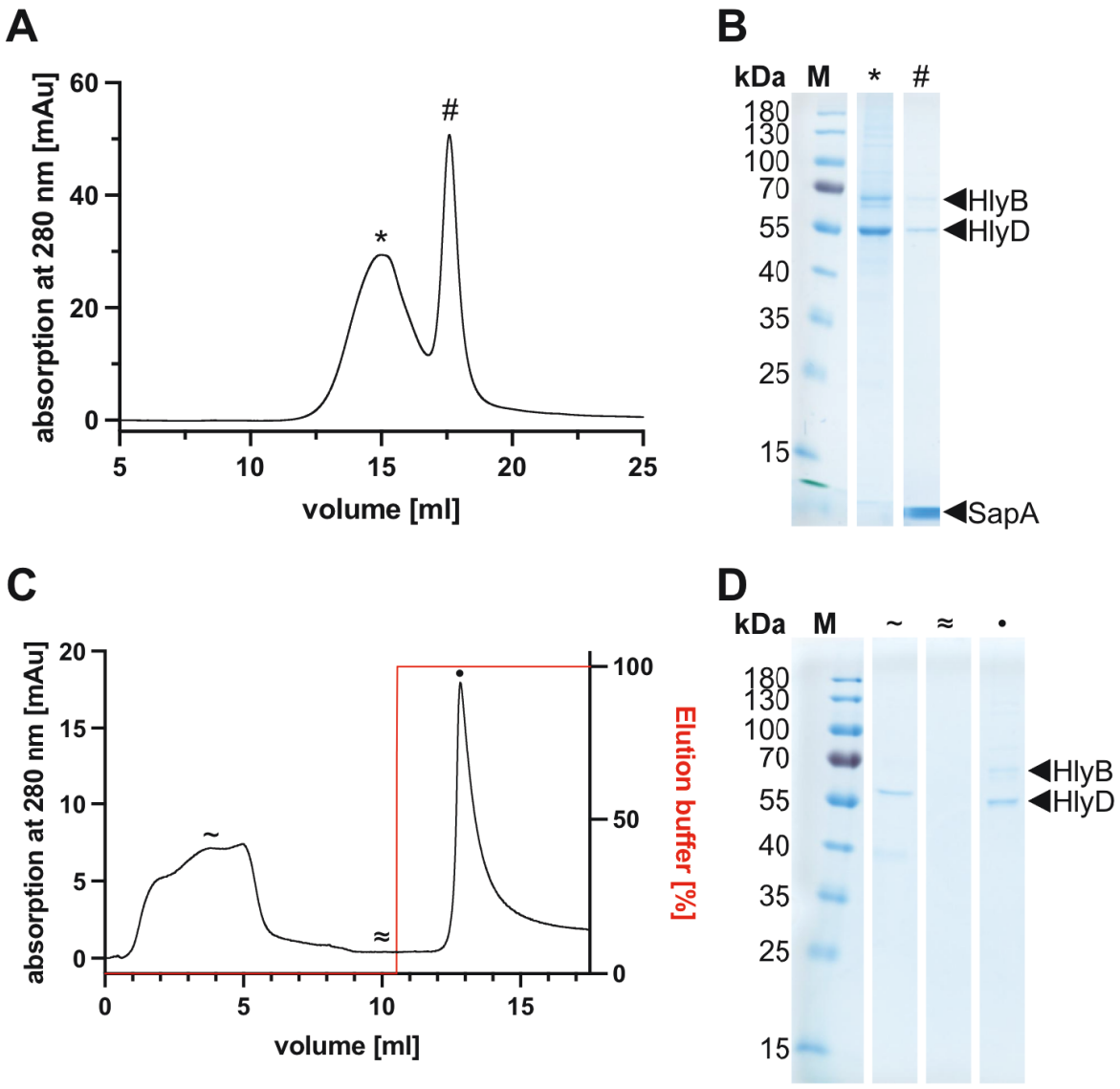

Figure 7: Co-reconstitution of HlyB and HlyD in SapA and LPG. A: *SEC analysis of HlyB and HlyD co-reconstituted in SapA and LPG on Superose 6 Inc. 10/300 GL.* ***B:*** *SDS-PAGE analysis of co-reconstituted HlyB and HlyD after SEC. M: marker proteins with their approximated molecular weight. *: sample from main elution peak of co-reconstituted HlyB and HlyD after SEC. #: sample from main elution peak of empty salipro particles after SEC. The bands for HlyB, HlyD and SapA are marked with a black triangle.* ***C:*** *Strep-tag affinity chromatogram of co-reconstituted HlyB and HlyD in SapA and LPG.* ***D:*** *SDS-PAGE analysis of co-reconstituted HlyB and HlyD after Strep-tag affinity purification. M: marker proteins with their approximated molecular weight. ~: sample from flow-through peak of the Strep-tag affinity purification. ≈: sample from wash fraction of the Strep-tag affinity purification. •: sample from main elution peak of the Strep-tag affinity purification. The bands for HlyB and HlyD are marked with a black triangle.*

The SEC of salipro reconstituted IMC showed a peak for reconstituted IMC (peak *, Figure 7A and B) and a peak for empty salipro particles (peak #, Figure 7A and B). As seen from subsequent affinity purification (Figure 7C and D) a stable complex between HlyB and HlyD had formed. But the amount of successfully reconstituted protein was less than 1 % and the complex started to aggregate upon concentration attempts. To minimize the loss of protein we tried to perform co-reconstitution without the SEC and immediate affinity purification (not shown). This approach was not successful and led to loss of HlyD. As co-reconstitution of HlyB and HlyD was possible using the salipro system we tried to improve sample quality and stabilize the system by using POPC lipids instead of lyso-lipids. The results (Figure 8) were comparable to LPG and did not further improve sample quality or quantity.

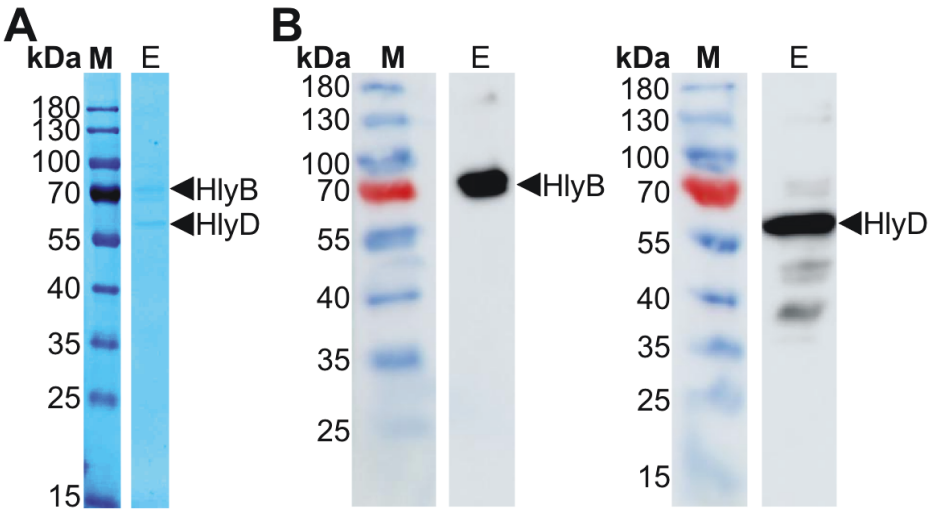

Figure 8: SDS-PAGE and Western blot analysis of co-reconstitution of HlyB and HlyD in SapA and POPC. ***A:*** *SDS-PAGE analysis of co-reconstituted HlyB and HlyD after SEC and Strep-tag affinity purification.* ***B:*** *Western blot of co-reconstituted HlyB and HlyD after SEC and Strep-tag affinity purification. M: marker proteins with their approximated molecular weight. E: Elution fraction from Strep-tag affinity purification. The bands for HlyB and HlyD are marked with black triangles. Protein-specific anti-HlyB and anti-HlyD antibodies were used for detection.*

Besides the principle proof of concept, the co-reconstitution of HlyB and HlyD in salipro particles did not result in sufficient sample quality or amount for further biochemical or structural studies. This is why we tried the MSP based nanodisc system for co-reconstitution of HlyB and HlyD next.

MSP Nanodisc

For co-reconstitution of HlyB and HlyD in MSP based nanodiscs we used HlyB with an N-terminal TwinStrep-tag purified in DDM and HlyD with an N-terminal 10xHis-tag purified in Fos-Choline-14. The lipid used for reconstitution was POPC and the MSP

was MSP2N2. The molar ratio of HlyB to HlyD was 1:3 and the molar ratio of IMC to MSP to lipid was 1:2:400. The sample was applied on a Superose 6 Inc. 10/300 GL SEC column and fractions containing reconstituted IMC were combined and applied on a StrepTrap affinity column. Fractions from SEC and affinity purification were used for ATPase activity determination (Figure 9).

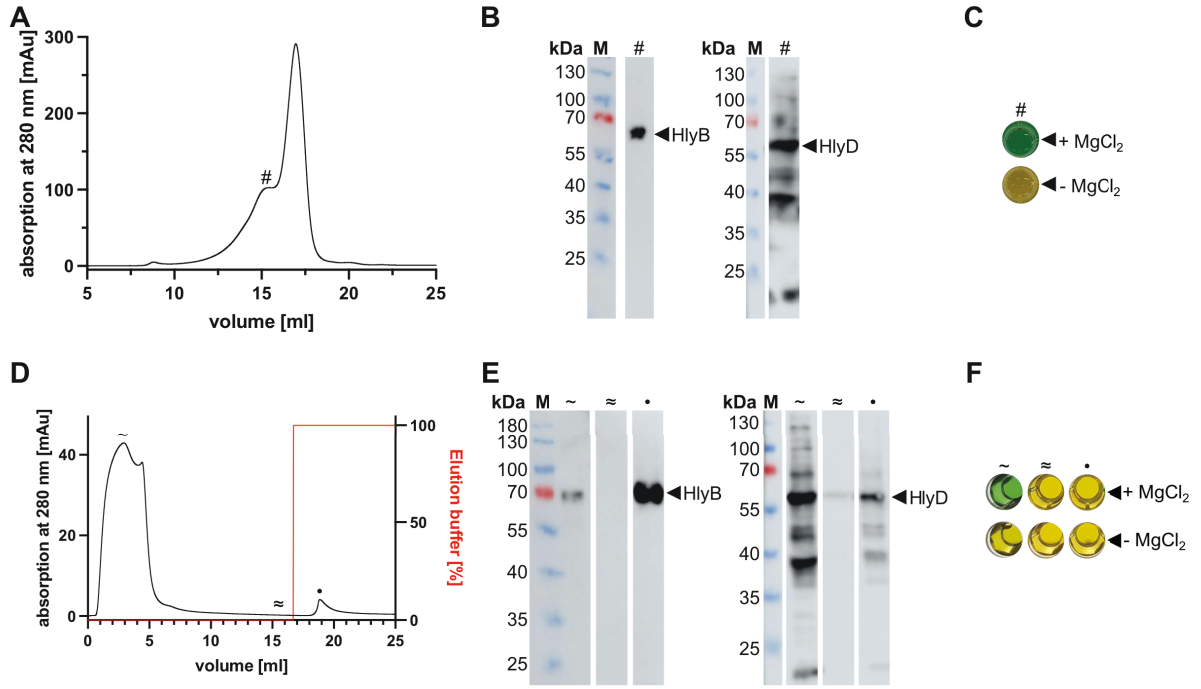

Figure 9: Co-reconstitution of HlyB and HlyD in MSP2N2 and POPC. A: *SEC analysis of HlyB and HlyD co-reconstituted in MSP2N2 and POPC on Superose 6 Inc. 10/300 GL.* ***B:*** *Western blot analysis of co-reconstituted HlyB and HlyD after SEC. M: marker proteins with their approximated molecular weight. #: sample from main elution peak of co-reconstituted HlyB and HlyD after SEC. The bands for HlyB, HlyD are marked with a black triangle.* ***C:*** *Wells from ATPase activity assay from co-reconstituted HlyB and HlyD after SEC. #: sample from main elution peak of co-reconstituted HlyB and HlyD after SEC. Positive sample (+ $MgCl_2$) and negative background control (- $MgCl_2$) are indicated.* ***D:*** *Strep-tag affinity chromatogram of co-reconstituted HlyB and HlyD in MSP2N2 and POPC.* ***E:*** *Western blot analysis of co-reconstituted HlyB and HlyD after SEC and Strep-tag affinity purification. M: marker proteins with their approximated molecular weight. ~: sample from flow-through peak of the Strep-tag affinity purification. ≈: sample from the wash fraction of the Strep-tag affinity purification. •: sample from main elution peak of the Strep-tag affinity purification. The bands for HlyB and HlyD are marked with a black triangle. Protein-specific anti-HlyB and anti-HlyD antibodies were used for detection.* ***F:*** *Wells from ATPase activity assay from co-reconstituted HlyB and HlyD after SEC and Strep-tag affinity purification. ~: sample from flow-through peak of the Strep-tag affinity purification. ≈: sample from the wash fraction of the Strep-tag affinity purification. •: sample from main elution peak of the Strep-tag affinity purification. Positive sample (+ $MgCl_2$) and negative background control (- $MgCl_2$) are indicated.*

The SEC profile of co-reconstituted HlyB and HlyD in MSP2N2 and POPC showed two peaks (Figure 9A). The first one contained successfully co-reconstituted HlyB and HlyD in MSP2N2 POPC (peak #, Figure 9A) and the second one contained empty MSP2N2 POPC nanodiscs. Presence of HlyB and HlyD were confirmed via Western blot analysis (Figure 9B). In addition the first peak showed ATPase activity as seen from malachite green ATPase activity assay (Figure 9C). After Strep-tag affinity purification of the fractions containing co-reconstituted HlyB and HlyD in MSP2N2 and POPC

(Figure 9D), the flow-through fractions showed little amounts of HlyB but high amounts of HlyD. The wash fractions did not contain any target protein. The elution fractions contained high amounts of HlyB but only little amounts of HlyD. In contrast to HlyB concentration, ATPase activity was only detected in the flow-through fractions. Although higher amounts of HlyB were present in the elution fractions than the flow-through fractions, the elution fractions did not show ATPase activity (Figure 9F). As the structure of the IMC was published in the meantime in the detergent digitonin [9], we next tested digitonin for solubilisation and purification of the IMC in our systems.

Purification of IMC in digitonin

pBAD-TSHlyB-HisHlyD

Another attempt to purify the IMC was the use of two orthogonal tags and the detergent digitonin. For the purification of IMC with two orthogonal affinity-tags a pBAD based plasmid was used. HlyB contained an N-terminal TwinStrep-tag and HlyD contained an N-terminal 6xHis-tag. Expression was performed in *E. coli* BL21(DE3) and solubilisation and purification were performed in digitonin. The IMC was purified first via Strep-tag affinity purification targeting HlyB and subsequent IMAC targeting HlyD. SEC was performed on a Superose 6 Inc. 3.2/300 GL column. Elution fractions were analysed via SDS-PAGE, Western blot and ATPase activity assay (Figure 10).

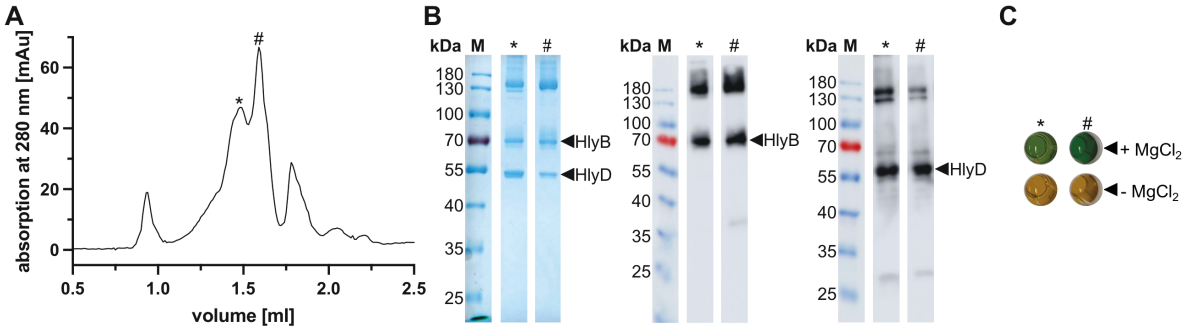

Figure 10: Purification of IMC from pBAD expression in digitonin. A: *SEC analysis of IMC on a Superose 6 Inc. 3.2/300 GL.* ***B:*** *SDS-PAGE (left) and Western blot analysis targeting HlyB (middle) or HlyD (right) of purified IMC after SEC. M: marker proteins with their approximated molecular weight. *: sample from first IMC main elution peak of the SEC #: Sample from second IMC main elution peak of the SEC. The bands for HlyB and HlyD are marked with black triangles. Protein-specific anti-HlyB and anti-HlyD antibodies were used for detection.* ***C:*** *Wells from ATPase activity assay from IMC in digitonin after SEC. *: sample from first IMC main elution peak of the SEC #: Sample from second IMC main elution peak of the SEC. Positive sample (+ $MgCl_2$) and negative background control (- $MgCl_2$) are indicated.*

The SEC profile of IMC in digitonin showed two peaks at elution volume of 1.4 and 1.6 ml (Figure 10A). Both peaks contained HlyB and HlyD in equal amounts and showed ATPase activity in malachite green ATPase activity assay (Figure 10B and C). A

difference between the two IMC species was only detectable from the shift in the elution volume in the SEC profile. Purification of IMC using digitonin improved protein purity a lot, but the amount of IMC after the purification procedure was still the limiting factor for further analysis. Furthermore the elution volume indicated a size of the particles that would be too small to fit the published structure of the IMC by Zhao et. al [9]. To circumvent this problem we tried the pQLink system used for expression of the IMC in the referred publication.

pQLink-StrepHlyB-HisHlyD

To get sufficient amount of IMC for structural and functional studies we tried the published expression and purification protocol for the IMC [9]. To ensure functionality of the system we used a construct with an N-terminal Strep-tag on HlyB and an N-terminal 6xHis-Tag on HlyD. Expression was performed in *E. coli* C43(DE3) and solubilisation and purification were performed in digitonin. The IMC was purified via Strep-tag affinity purification targeting HlyB and subsequent SEC on a Superose 6 Inc. 3.2/300 column (Figure 11).

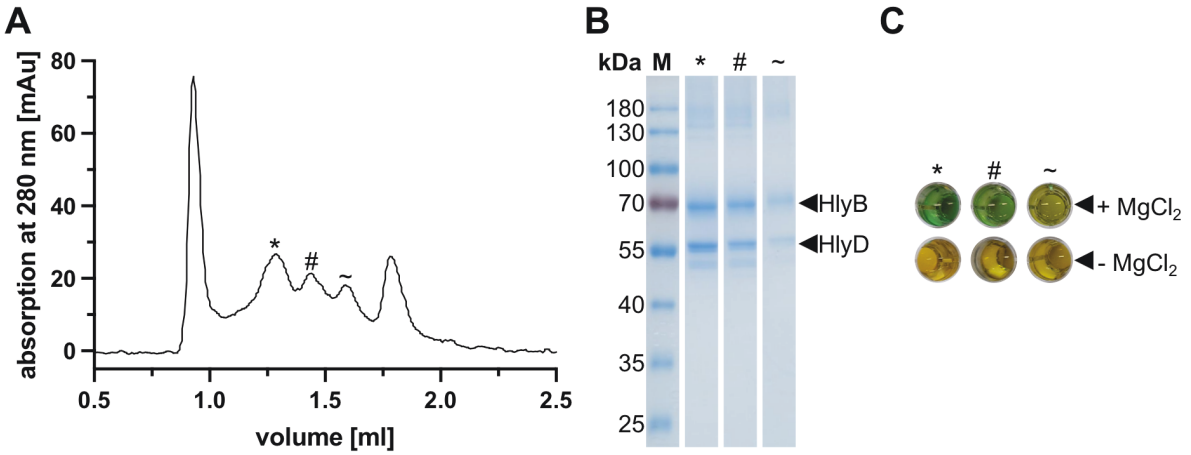

Figure 11: Purification of IMC from pQLink expression in digitonin. A: *SEC analysis of IMC on a Superose 6 Inc. 3.2/300 GL.* ***B:*** *SDS-PAGE analysis of purified IMC after SEC. M: marker proteins with their approximated molecular weight. *: sample from the first IMC main elution peak of the SEC #: sample from the second IMC main elution peak of the SEC. ~: sample from the third IMC main elution peak of the SEC. The bands for HlyB and HlyD are marked with black triangles. Protein-specific anti-HlyB and anti-HlyD antibodies were used for detection.* ***C:*** *Wells from ATPase activity assay from IMC in digitonin after SEC. *: sample from the first IMC main elution peak of the SEC. #: sample from the second IMC main elution peak of the SEC. ~: sample from the third IMC main elution peak of the SEC. Positive sample (+ $MgCl_2$) and negative background control (- $MgCl_2$) are indicated.*

In the SEC profile three peaks were detected at elution volumes of 1.3, 1.45 and 1.6 ml and all of them showed presence of HlyB and HlyD as seen by Coomassie stained SDS-PAGE (Figure 11B). In addition all three peaks showed ATPase activity in malachite green ATPase activity assay (Figure 11C). The amount of IMC and ATPase

activity declined from first to second to third peak. The pQlink system for expression in combination with digitonin for solubilisation and purification enabled purification of IMC in sufficient amounts and purity for further experiments like an *in vitro* transport assay.

Discussion

The purification of membrane proteins is a challenging task as one has to find the right conditions suitable for solubilisation and stabilisation of the target protein. In addition it is necessary to ensure that the chosen conditions do not interfere with later applications. As the field of membrane proteins research offers a wide variety of detergents but also detergent alternatives such as nanodiscs, Salipro, amphipols, SMA, peptidisc and others, the journey towards the *in vitro* studies of a specific membrane protein, be it structure or biochemical assay, usually involves a detailed screen for the right conditions. Here we present such a journey for the IMC of the HlyA T1SS from uropathogenic *E. coli*.

The choice of the detergent is a very crucial step in membrane protein purification. Fos-cholines in general are known to solubilize proteins very well, but are also known to interfere with the structure and / or activity of a solubilized protein [38, 39]. Therefore, starting with Fos-choline-16 to solubilize the IMC might already destroy the native conformation of the IMC during the solubilisation step and explain the small amounts of purified IMC (Figure 1 and 2). Nevertheless, it seems to be possible to counteract this effect in parts by changing the detergent after the solubilisation step. But as seen from DDM (Figure 1) and LMNG (Figure 2) the choice of the detergent can have a huge influence on the amount of purified protein. In the end digitonin showed best results in solubilisation and complex integrity as recently published for the IMC [9] and seen for other proteins and complexes as well [14, 16].

Also for the published DirectMX approach using the Salipro system digitonin was used in the first initial solubilisation step [24]. Here we tried lysophosphatidylglycerol (LPG) for the initial solubilisation step and were not successful (Figure 5). A repetition with digitonin might lead to better results. For the other tested detergent-free alternative using SMA we struggled with purification of initially solubilized IMC (Figure 4). While the sucrose gradient purification did not lead to a clear result, further affinity purification of SMA encapsulated IMC did not work at all. Inefficient binding of SMA encapsulated proteins was previously reported [40] and batch binding overnight was recommended

to overcome this limitation. A major issue for poor binding is an excess of free SMA. Although sucrose gradient purification should be able to remove free SMA polymers from the SMA encapsulated IMC this needs to be taken into account as a problem in affinity purification of SMA encapsulated proteins. In addition, the low binding efficiency also results in lower concentrations of imidazole needed for elution and has to be considered when washing the column [40].

Problems with disassembly of the IMC even without any affinity tag can be caused either by the detergent LMNG or be an artifact of the Blue Native (BN)-PAGE used as read out for complex formation (Figure 6). During BN-PAGE of membrane proteins the detergent needs to be substituted by the dye Coomassie. This exchange from detergent to Coomassie can also cause complexes to disassemble [41]. To finally state whether LMNG is suitable for IMC solubilisation and purification, a different read out than BN-PAGE is needed. In addition this experiment shows that HlyB and HlyD do not exclusively occur in a complex but also as individual proteins and protein oligomers. This might be due to overexpression of the system or can be caused by the detergent used for solubilisation and purification.

Our approach to co-reconstitute the IMC from separately purified proteins into Salipro based lipid discs (Figure 7 and 8) or MSP based nanodiscs (Figure 9) was partly successful. A major limitation to the applicability for the IMC in comparison to the published protocol for MexAB-TolC [37] is the additional transmembrane part of HlyD that is not present in MexA. For the IMC the transmembrane parts of HlyB and HlyD have to arrange correctly before detergent removal and incorporation into a lipid bilayer happen. This step is crucial and might need more time than given in our experimental set up. Nevertheless, we could show that a complex of HlyB and HlyD did form, although its size, when comparing our SEC elution profile to the SEC elution profile of the published IMC structure [9] is smaller. The IMC is a trimer of dimers in terms of the ABC transporter HlyB and a hexamer of HlyD with two HlyD monomers flanking one HlyB dimer. In our co-reconstitution set-up we might have isolated a dimer of HlyB flanked by a dimeric HlyD as we used the molar ratio that was assumed for the IMC (1:3 of HlyB:HlyD) prior to the published structure of the IMC.

Finally, digitonin was the “golden bullet” for purification of the IMC. The purity of our isolated IMC in digitonin (Figure 11) can be further improved by subsequent IMAC after Strep-tag affinity purification. This way HlyB-only particles can be excluded from the purification. However, one has to judge whether the additional purification step is

necessary as it might cause further loss of protein and SEC already allows separation of different species.

Author contribution

FLB, SS and LS conceived the experiments and evaluated the data. FLB performed expression and purification of IMC from 2 plasmids, expression and purification of IMC from pK184 plasmid and pBAD plasmid, spheroplast preparation, sucrose gradient purification, SMA purification, DirectMX purification, expression and purification of HlyB and SapA and performed the ATPase activity assays. FLB and EH performed co-reconstitution experiments of HlyB and HlyD. EH did cloning of IMC into pQLink expression vector and performed expression and purification of HlyD and MSP2N2. CG performed expression of IMC from pQLink plasmid. FLB performed purification from pQLink plasmid. FLB wrote the initial draft. FLB, SS and LS wrote the final version of the manuscript.

Funding

This work was supported by the Deutsche Forschungsgemeinschaft (DFG, CRC 1208 project A01 to LS).

Acknowledgement

We thank all former and current members of the Institute of Biochemistry for their support and productive discussions.

References

1. Costa, T.R., et al., *Secretion systems in Gram-negative bacteria: structural and mechanistic insights.* Nat Rev Microbiol, 2015. **13**(6): p. 343-59.
2. Kanonenberg, K., et al., *Type I secretion system-it takes three and a substrate.* FEMS Microbiol Lett, 2018. **365**(11).
3. Cross, M.A., et al., *HlyB-dependent secretion of hemolysin by uropathogenic Escherichia coli requires conserved sequences flanking the chromosomal hly determinant.* J Bacteriol, 1990. **172**(3): p. 1217-24.
4. Koronakis, V., et al., *The HlyB/HlyD-dependent secretion of toxins by gram-negative bacteria.* FEMS Microbiol Immunol, 1992. **5**(1-3): p. 45-53.
5. Lenders, M.H., et al., *In vivo quantification of the secretion rates of the hemolysin A Type I secretion system.* Sci Rep, 2016. **6**: p. 33275.
6. Reimann, S., et al., *Interdomain regulation of the ATPase activity of the ABC transporter haemolysin B from Escherichia coli.* Biochem J, 2016. **473**(16): p. 2471-83.
7. Beer, T., et al., *Quantification and surface localization of the hemolysin A type 1 secretion system at the endogenous level and under conditions of overexpression.* Appl Environ Microbiol, 2021: p. AEM0189621.
8. Thanabalu, T., et al., *Substrate-induced assembly of a contiguous channel for protein export from E.coli: reversible bridging of an inner-membrane translocase to an outer membrane exit pore.* EMBO J, 1998. **17**(22): p. 6487-96.
9. Zhao, H., J. Lee, and J. Chen, *The hemolysin A secretion system is a multi-engine pump containing three ABC transporters.* Cell, 2022. **185**(18): p. 3329-3340 e13.
10. Wycisk, V., M.C. Wagner, and L.H. Urner, *Trends in the Diversification of the Detergentome.* Chempluschem, 2023: p. e202300386.
11. Li, S., *Detergents and alternatives in cryo-EM studies of membrane proteins.* Acta Biochim Biophys Sin (Shanghai), 2022. **54**(8): p. 1049-1056.
12. Ghani, L., et al., *Foldable Detergents for Membrane Protein Study: Importance of Detergent Core Flexibility in Protein Stabilization.* Chemistry, 2022. **28**(21): p. e202200116.
13. Stetsenko, A. and A. Guskov, *An Overview of the Top Ten Detergents Used for Membrane Protein Crystallization.* Crystals, 2017. **7**(7): p. 197.
14. Choy, B.C., et al., *A 10-year meta-analysis of membrane protein structural biology: Detergents, membrane mimetics, and structure determination techniques.* Biochim Biophys Acta Biomembr, 2021. **1863**(3): p. 183533.
15. Alvadia, C., et al., *Cryo-EM structures and functional characterization of the murine lipid scramblase TMEM16F.* Elife, 2019. **8**.
16. Gu, J., et al., *The architecture of the mammalian respirasome.* Nature, 2016. **537**(7622): p. 639-43.
17. Butan, C., et al., *Single particle cryo-EM structure of the outer hair cell motor protein prestin.* Nat Commun, 2022. **13**(1): p. 290.
18. Le, L.T.M., et al., *Cryo-EM structures of human ABCA7 provide insights into its phospholipid translocation mechanisms.* EMBO J, 2023. **42**(3): p. e111065.
19. Guo, Y., *Be Cautious with Crystal Structures of Membrane Proteins or Complexes Prepared in Detergents.* Crystals, 2020. **10**(2): p. 86.
20. Gewering, T., et al., *Know your detergents: A case study on detergent background in negative stain electron microscopy.* J Struct Biol, 2018. **203**(3): p. 242-246.
21. Pettersen, J.M., Y. Yang, and A.S. Robinson, *Advances in nanodisc platforms for membrane protein purification.* Trends Biotechnol, 2023. **41**(8): p. 1041-1054.

22. Ritchie, T.K., et al., *Chapter 11 - Reconstitution of membrane proteins in phospholipid bilayer nanodiscs.* Methods Enzymol, 2009. **464**: p. 211-31.
23. Frauenfeld, J., et al., *A saposin-lipoprotein nanoparticle system for membrane proteins.* Nat Methods, 2016. **13**(4): p. 345-51.
24. Lloris-Garcera, P., et al., *DirectMX - One-Step Reconstitution of Membrane Proteins From Crude Cell Membranes Into Salipro Nanoparticles.* Front Bioeng Biotechnol, 2020. **8**: p. 215.
25. Carlson, M.L., et al., *The Peptidisc, a simple method for stabilizing membrane proteins in detergent-free solution.* Elife, 2018. **7**.
26. Tribet, C., R. Audebert, and J.L. Popot, *Amphipols: polymers that keep membrane proteins soluble in aqueous solutions.* Proc Natl Acad Sci U S A, 1996. **93**(26): p. 15047-50.
27. Knowles, T.J., et al., *Membrane proteins solubilized intact in lipid containing nanoparticles bounded by styrene maleic acid copolymer.* J Am Chem Soc, 2009. **131**(22): p. 7484-5.
28. Oluwole, A.O., et al., *Solubilization of Membrane Proteins into Functional Lipid-Bilayer Nanodiscs Using a Diisobutylene/Maleic Acid Copolymer.* Angew Chem Int Ed Engl, 2017. **56**(7): p. 1919-1924.
29. Popot, J.L., et al., *Amphipols from A to Z.* Annu Rev Biophys, 2011. **40**: p. 379-408.
30. Marconnet, A., et al., *Solubilization and Stabilization of Membrane Proteins by Cycloalkane-Modified Amphiphilic Polymers.* Biomacromolecules, 2020. **21**(8): p. 3459-3467.
31. Carson, M., et al., *His-tag impact on structure.* Acta Crystallogr D Biol Crystallogr, 2007. **63**(Pt 3): p. 295-301.
32. Bräuer, M., et al., *The influence of commonly used tags on structural propensities and internal dynamics of peptides.* Monatshefte für Chemie - Chemical Monthly, 2019. **150**(5): p. 913-925.
33. Khan, F., et al., *Histidine affinity tags affect MSP1(42) structural stability and immunodominance in mice.* Biotechnol J, 2012. **7**(1): p. 133-47.
34. Araujo, A.P., et al., *Influence of the histidine tail on the structure and activity of recombinant chlorocatechol 1,2-dioxygenase.* Biochem Biophys Res Commun, 2000. **272**(2): p. 480-4.
35. Freydank, A.C., W. Brandt, and B. Drager, *Protein structure modeling indicates hexahistidine-tag interference with enzyme activity.* Proteins, 2008. **72**(1): p. 173-83.
36. Baykov, A.A., O.A. Evtushenko, and S.M. Avaeva, *A malachite green procedure for orthophosphate determination and its use in alkaline phosphatase-based enzyme immunoassay.* Anal Biochem, 1988. **171**(2): p. 266-70.
37. Tsutsumi, K., et al., *Structures of the wild-type MexAB-OprM tripartite pump reveal its complex formation and drug efflux mechanism.* Nat Commun, 2019. **10**(1): p. 1520.
38. Chipot, C., et al., *Perturbations of Native Membrane Protein Structure in Alkyl Phosphocholine Detergents: A Critical Assessment of NMR and Biophysical Studies.* Chem Rev, 2018. **118**(7): p. 3559-3607.
39. Geertsma, E.R., et al., *Quality control of overexpressed membrane proteins.* Proc Natl Acad Sci U S A, 2008. **105**(15): p. 5722-7.
40. Broadbent, L., et al., *Detergent-Free Membrane Protein Purification Using SMA Polymer.* Methods Mol Biol, 2022. **2507**: p. 389-404.
41. Eubel, H., H.P. Braun, and A.H. Millar, *Blue-native PAGE in plants: a tool in analysis of protein-protein interactions.* Plant Methods, 2005. **1**(1): p. 11.

Supplementary Information
Plasmids:

Table S1: Plasmids used in this study.

Name			HlyB		HlyD	
	Backbone	**Antibiotic resistance**	**Tag**	**Position**	**Tag**	**Position**
pBAD-HisHlyB	pBAD	Ampicillin	10xHis-tag	N-terminus		
pET28-HisHlyD	pET	Kanamycin			10xHis-tag	N-terminus
pK184-HlyB-HisHlyD	pK184	Kanamycin	-	-	6xHis-tag	N-terminus
pK184-HlyB-HlyD	pK184	Kanamycin	-	-	-	-
pBAD-TSHlyB-HisHlyD	pBAD	Ampicillin	TwinStrep-tag	N-terminus	6xHis-tag	N-terminus
pQLink-StrepHlyB-HisHlyD	pQLink	Ampicillin	6xHis-tag	N-terminus	-	N-terminus

3.5. Chapter 5: *In vitro* transport assay for the HlyA T1SS from *Escherichia coli*

Title: *In vitro* transport assay for the HlyA T1SS from *Escherichia coli*

Authors: **Florestan L. Bilsing**, Sakshi Khosa, Eymen Hachani, Cigdem Günes, Sander Smits, Lutz Schmitt

Published in: to be submitted

Own contribution:
Designing the experiments
Expression and purification of TolC
Reconstitution of TolC into liposomes and flotation assay
Purification of IMC
Reconstitution of IMC into MSP2N2 nanodiscs
ATPase activity assays
In vitro transport assay
Data evaluation
Preparation of the figures
Writing of the manuscript

In vitro transport assay for the HlyA T1SS from *Escherichia coli*

Florestan L. Bilsing[1], Sakshi Khosa[1], Eymen Hachani[1], Cigdem Günes[1], Sander Smits[1,2], Lutz Schmitt[1]*

[1]Heinrich Heine University Düsseldorf, Faculty of Mathematics and Natural Sciences, Institute of Biochemistry, Universitätsstraße 1, 40225 Düsseldorf
[2]Heinrich Heine University Düsseldorf, Faculty of Mathematics and Natural Sciences, Center for Structural Studies, Universitätsstraße 1, 40225 Düsseldorf

*Corresponding author: Lutz Schmitt, Heinrich Heine University Düsseldorf, Faculty of Mathematics and Natural Sciences, Institute of Biochemistry, Universitätsstraße 1, 40225 Düsseldorf, Germany, Tel.: +49 211 81 10773, E-Mail: lutz.schmitt@hhu.de

Abstract

The hemolysin A type 1 secretion system (HlyA T1SS) from *Escherichia coli* (*E. coli*) is one of the best studied T1SSs. It secretes the toxin HlyA in a single step without periplasmic intermediates from the cytosol to the extracellular space. Secretion occurs in an unfolded state and is driven by ATP hydrolysis. Although structural information for the single components of the HlyA T1SS is partially available, the details of their interplay in secretion remains unknown. In this study we present an *in vitro* transport assay for the HlyA T1SS. By reconstitution of the outer membrane protein TolC into liposomes and reconstitution of the inner membrane complex (IMC) into MSP based nanodiscs we can assemble the T1SS *in vitro* in a detergent free environment. In addition, this set up allows to trace transport between two different compartments. We present the single steps necessary for assembling the HlyA T1SS *in vitro* and performing the transport assay. Furthermore we could show as a proof of concept transport of a shortened version of the substrate, termed HlyA1 with our *in vitro* transport assay.

Introduction

Secretion in Gram-negative bacteria is a challenge as a substrate has to cross two membranes without disturbing the overall integrity of the cell [1]. For small substrates and one membrane this might be an easy task by providing a transporter with alternating access to each side of the membrane [2]. This process gets more complex for secretion of small molecules in Gram-negative bacteria across two membranes in one step via tripartite efflux systems like MacAB and AcrAB [3-6]. For large protein substrates of several 100 amino acids, like members of the repeats in toxin (RTX) protein family [7], that are transported via type 1 secretion systems (T1SSs) this task becomes even more challenging. It is hard to imagine that there is something like a classical binding pocket for such large substrates as known for many ABC transporters transporting small molecules [8]. Therefore, a more complex interplay between several components of the T1SS, that are located on different sides of the membrane, is necessary. One of the best studied T1SS is the hemolysin A (HlyA) T1SS from *E. coli* [9-11]. It is build up by an ATP-binding cassette (ABC) transporter termed hemolysin B (HlyB), a membrane fusion protein (MFP) termed hemolysin D (HlyD) and the outer membrane Protein TolC. Together those three proteins transport the substrate called HlyA with a length of 1024 amino acids in an unfolded state. Secretion occurs in a single step without periplasmic intermediates. It is known that HlyB and HlyD form a so called inner membrane complex (IMC) in the inner membrane even in the absence of the substrate HlyA [12]. The ABC transporter HlyB contains a specific N-terminal domain termed C39 peptidase-like domain (CLD) which is important for substrate recognition [13]. Recently, the structure of the IMC has been solved providing valuable insights into its detailed organization and revealing an additional role of the HlyB CLD in stabilising the IMC through charged interactions with the MFP HlyD [14]. In addition to the CLD also the nucleotide binding domain (NBD) of HlyB is involved in substrate recognition [15, 16]. In the presence of HlyA, TolC is recruited to the IMC and a continuous channel for secretion is formed [17]. The substrate HlyA is a pore forming toxin that is transported in an unfolded state and only folds outside the cell upon Ca^{2+} binding [18]. Although structures of the different components of the HlyA T1SS are known, the mechanistic details and biochemical characteristics of the secretion process remain unknown [14, 19, 20]. As investigations *in-situ* allow for native environment and less preparation artifacts the major drawback is the traceability of the process of interest among all other metabolic processes of the cell especially for

functional assays. Therefore *in vitro* set ups allow investigations with very low level of interfering side effects and a precise reaction set up if the protein of interest can be purified and stabilized in adequate amounts [21]. Advanced tools facilitate *in vitro* work with membrane proteins providing a wide range of membrane mimetics nowadays, like SMA and DIBMA polymers [22-24], MSP based nanodiscs [25, 26], Salipro [27] or proteoliposomes [28]. Those accomplishments even allow assemblies with multiple membrane mimetics as seen for the *in vitro* transport assay of MacAB-TolC [29].

Here we report an *in vitro* transport assay for the HlyA T1SS from *E. coli*. We successfully purified the components of the T1SS and reconstituted them in membrane mimetic systems. By using a MSP based nanodisc system for the IMC and liposomes for the outer membrane protein TolC, we build a two compartment system allowing transport from solution into the lumen of the liposomes. The substrate HlyA1, a truncated secretion competent version of HlyA, was added in an unfolded state and preincubated prior to addition of ATP to start the assay. Successful transport was monitored by limited accessibility of the translocated substrate inside the proteoliposomes for externally added proteinase K [30] with subsequent Western blot analysis (Figure 1).

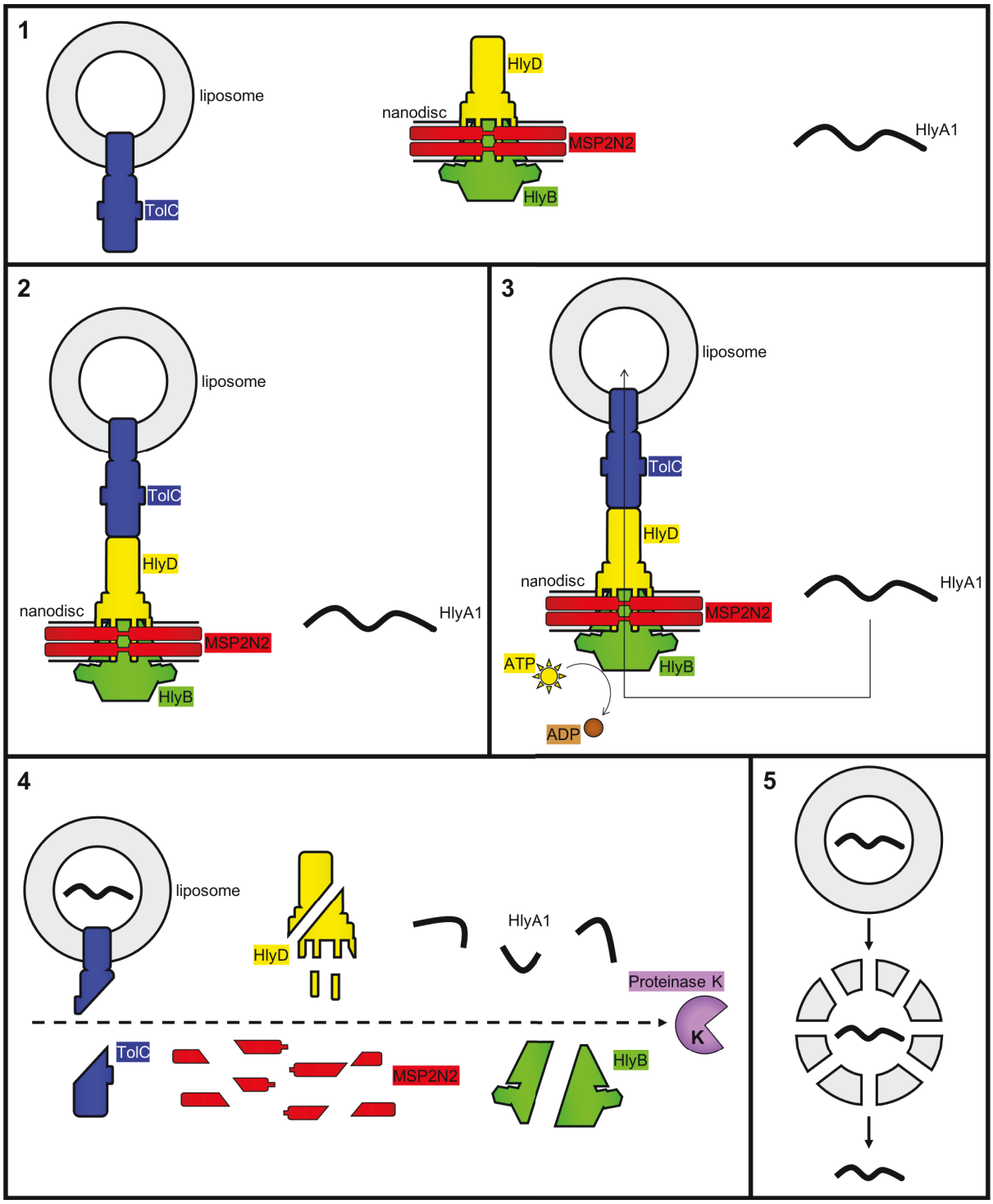

Figure 1: Schematic of the in vitro transport assay for the HlyA T1SS from E. coli. ***1:*** *TolC (blue) was reconstituted in liposomes, IMC (yellow and green) was reconstituted in MSP (red) based nanodiscs and HlyA (black) was provided in an unfolded state.* ***2:*** *Mixing of all components and incubation allows assembly of the tripartite T1SS.* ***3:*** *Upon addition of ATP (yellow) substrate translocation into the lumen of the liposome occurs powered by ATP hydrolysis.* ***4:*** *Proteinase K (purple) is added and digests every protein outside the liposomes.* ***5:*** *After proteinase K inactivation liposomes (grey) are destroyed and transport of substrate is analyzed via Western blot.*

Material and methods

Expression and purification of TolC

TolC was expressed in *E. coli* BL21(DE3) from a pET based plasmid containing a C-terminal 6x His-tag with a thrombin cleavage side. Cells were grown in 50 ml 2YT medium in a 300 ml baffled flask supplemented with 100 µg/ml ampicillin at 37 °C and 180 rpm overnight. Expression cultures of 2 L 2YT supplemented with 100 µg/ml ampicillin in 5 L baffled flasks were inoculated from the precultures to an OD_{600} of 0.1 and incubated at 37 °C and 180 rpm. Expression was induced at OD_{600} of 0.6 to 0.8 by addition of 1 mM IPTG and expression was performed for 2 h. Cells were harvested via centrifugation at 5,000 xg for 20 minutes at 4 °C. Pellet was resuspended in buffer A (20 mM Hepes pH 8, 100 mM NaCl) and 1 cOmplete EDTA-free inhibitor cocktail tablet and a spatulas tip of DNAse I were added. Cell disruption was performed by three passes through Microfluidizer M-110P (Microfluidics) at 1.5 kbar. Centrifugation was performed at 18,000 xg for 30 minutes at 4 °C to get rid of cell debris. Supernatant was centrifuged for 90 minutes at 38,000 rpm (Type 45 Ti, Beckman Coulter) at 4 °C to pellet membranes. Membranes were resuspended in buffer A and diluted to a total protein concentration of 20 mg/ml.

Solubilization was performed for 2 hours at 4 °C using 2 % Triton X-100. Non-solubilized material was removed by centrifugation for 30 minutes at 38,000 rpm (Type 45 Ti, Beckman Coulter) at 4 °C. Supernatant was loaded on a 5 ml HiTrap Chelating HP (Cytiva) column (Zn^{2+}) equilibrated with buffer B (20 mM Hepes pH 8, 300 mM NaCl, 10 mM imidazole, 0.01 % DDM). Column was washed 30 column volumes (CV) with buffer B and 15 CV of Buffer C (20 mM Hepes pH 8, 300 mM NaCl, 100 mM imidazole, 0.01 % DDM). TolC was eluted with 5 CV buffer D (20 mM Hepes pH 8, 300 mM NaCl, 250 mM imidazole, 0.01 % DDM). Fractions containing TolC were combined, 10 U/mg protein of thrombin containing a His-Tag were added and dialyzed over night against 5 L of buffer E (20 mM Hepes pH 8, 100 mM NaCl, 0.01 % DDM) at 4 °C. Dialysed sample was concentrated using an Amicon Ultra-15 centrifugal filter unit (Millipore) with a MWCO of 100 kDa. Concentrated sample was centrifuged for 30 minutes at 17,000 xg and 4 °C and supernatant was applied on Superose 6 Increase 10/300 GL equilibrated with buffer E. Fractions containing TolC were combined and concentrated using Amicon Ultra-4 centrifugal filter unit (Millipore) with a MWCO of 100 kDa. For storage TolC was flash frozen in liquid nitrogen and stored at – 80 °C.

Reconstitution of TolC into liposomes

For reconstitution of TolC into DOPC liposomes DOPC stock solution in chloroform (Avanti Polar Lipids) was evaporated using rotary evaporator (300, mbar, 200 mbar and 0 mbar, 10 minutes each) and resuspended in buffer F (30 mM Tris pH 8, 150 mM NaCl). Liposomes were frozen in liquid nitrogen and thawed at room temperature 2 times. Next liposomes were extruded 11 times using a 400 nm membrane. The amount of Triton X-100 necessary for swelling the liposomes for reconstitution was determined for each set of prepared liposome by stepwise addition of Triton X-100 and monitoring absorption at 540 nm [28]. After addition of Triton X-100, TolC was added at a protein-to-lipid ratio of 1 :33 and incubated at room temperature for 15 minutes. 10 mg BioBeads SM-2 (Biorad) were added and sample was incubated under agitation at 4 °C for 10 min. A second time 10 mg BioBeads SM-2 (Biorad) were added and sample was incubated under agitation at 4 °C for 10 min. A third time 10 mg BioBeads SM-2 (Biorad) were added and sample was incubated under agitation at 4 °C overnight. The next day a fourth time 10 mg BioBeads SM-2 (Biorad) were added and sample was incubated under agitation at 4 °C for 2 hours. BioBeads SM-2 (Biorad) were removed and the supernatant was centrifugedat 100,000 xg for 30 minutes at 4 °C. The supernatant was discarded and the proteoliposome pellet was resuspended in 1/10 of buffer F and used for *in vitro* transport assay or flotation assay.

Flotation Assay

100 µl Proteoliposomes were mixed with 100 µl 60% sucrose solution (60% sucrose in 30 mM Tris pH 8, 150 mM NaCl) and placed on the bottom of a S120-AT3 (Thermo Scientific) rotor tube. 250 µl 20% sucrose solution (20% sucrose in 30 mM Tris pH 8, 150 mM NaCl) followed by 50 µl 5% sucrose solution (5% sucrose in 30 mM Tris pH 8, 150 mM NaCl) were carefully put on top. Gradient was centrifuged for 1 hour at 4 °C and 80,000 rpm (S120-AT3, Thermo Scientific) and fractions were collected with a gel loading tip from bottom to top. Samples were used for TCA precipitation and analysed via SDS-PAGE.

Expression and purification of inner membrane complex (IMC)

E. coli C43(DE3) and a pQLink based plasmid were used to produce IMC. HlyB was produced with an N-terminal Strep-tag and HlyD with an N-terminal 6x His-Tag. Cells were grown in 50 ml 2YT medium in a 300 ml baffled flask supplemented with 100

µg/ml ampicillin at 37 °C and 180 rpm overnight. Expression cultures of 2 L 2YT supplemented with 100 µg/ml ampicillin in 5 L baffled flasks were inoculated from the precultures to an OD_{600} of 0.1 and incubated at 37 °C and 180 rpm. Expression was induced at OD_{600} of 0.6 to 0.8 by addition of 0.2 mM IPTG and expression was performed at 18 °C overnight. Cells were harvested via centrifugation at 5,000 xg for 20 minutes at 4 °C. Pellet was resuspended in buffer G (30 mM Tris pH 8, 150 mM NaCl, 15 % glycerol) and 1 cOmplete EDTA-free inhibitor cocktail tablet and a spatulas tip of DNAse I were added. Cell disruption was performed by three passes through Microfluidizer M-110P (Microfluidics) at 1.5 kbar. Centrifugation was performed at 18,000 xg for 30 minutes at 4 °C to get rid of cell debris. Supernatant was centrifuged for 90 minutes at 45,000 rpm (Type 45 Ti, Beckman Coulter) at 4 °C to pellet membranes. Membranes were resuspended in buffer H (30 mM Tris pH 8, 150 mM NaCl) and diluted to a total protein concentration of 20 mg/ml. Solubilization was performed for 1 hour at 4 °C using 1 % digitonin. Non-solubilized material was removed by centrifugation for 30 minutes at 42,000 rpm (Type 70 Ti, Beckman Coulter) at 4 °C. Supernatant was incubated in a ratio of 50 ml membrane with 1 ml Strep-Tactin MacroPrep resin (IBA Lifesciences) overnight under agitation at 4 °C. The resin was transferred into a gravity flow column and washed with 15 CV buffer I (30 mM Tris pH 8, 150 mM NaCl, 0.1 % digitonin). The resin was incubated for 5 minutes with 2 CV buffer J (30 mM Tris pH 8, 150 mM NaCl, 5 mM D-desthiobiotin, 0.1 % digitonin) and IMC was eluted with 3 additional CV buffer J. Elution fractions were concentrated using Amicon Ultra-15 centrifugal filter unit (Millipore) with a MWCO of 100 kDa. Sample was centrifuged for 30 minutes at 17,000 xg at 4 °C to remove aggregates and supernatant was used for reconstitution into MSP based nanodisc.

Reconstitution of IMC into MSP2N2 nanodisc

For reconstitution of IMC into MSP2N2 lipid nanodisc a lipid mixture of DOPE, DOPG and DOPC in a molar ratio of 1:1:1 was used. Lipids were ordered as individual chloroform solutions (Avanti Polar Lipids) and mixed in the desired ratio. Chloroform was evaporated using a rotary evaporator and lipids were resuspended in buffer H (20 mM Tris pH 8, 150 mM NaCl) at a final concentration of 3.8 mg/ml. Lipids were extruded 11 times using a 400 nm membrane and incubated with 1 % Triton X-100 for 10 min at 40 °C. Lipids were chilled on ice and IMC and MSP2N2 were added simultaneously in a final molar ratio of 1:4:600 (calculated for IMC = 6x HlyB + 6x

HlyD). Sample was incubated on ice for 30 minutes prior to addition of 150 mg BioBeads SM-2 (Biorad) and incubation at 4 °C overnight under constant agitation. The next day BioBeads SM-2 (Biorad) were removed and the sample was centrifuged for 30 min at 17,000 xg and 4 °C. The supernatant was concentrated and used for *in vitro* transport assay. For analytical SEC concentrated IMC in MSP2N2 nanodisc was loaded on Superose 6 Increase 3.2/300 column equilibrated in buffer H.

ATPase activity assay

For measuring ATPase activity the Malachite Green assay [31] was used as described earlier (Chapter 2 – Optimisation of the purification of the ABC transporter HlyB from *Escherichia coli*).

Expression and purification of HlyA1 and MSP2N2

HlyA1 and MSP2N2 were expressed and purified according to published protocols [26, 32].

In vitro transport assay

For the *in vitro* transport assay TolC proteoliposomes and IMC in MSP2N2 nanodiscs were mixed with 10 mM $MgCl_2$, energy regeneration mix (10 mM phosphokreatin and 50 µg/ml kreatinkinase) and 0.1 mg/ml HlyA1 in a total volume of 50 µl. The mixture was incubated overnight at 4 °C and gentil agitation and transport assay was started by addition of 5 mM ATP. The assay was performed at 25 °C for 8 hours. 5 µl reference sample was taken (sample R) and 1 µl proteinase K (10 mg/ml) was added to the remaining 45 µl, shortly vortexed and incubated for 30 minutes at room temperature. 150 µl TCA (20 %) were added, shortly vortexed and incubated overnight at 4 °C. The sample was centrifuged for 15 minutes at 17,000 xg and 4 °C and supernatant was removed. The Pellet was washed with 500 µl ice cold acetone and centrifuged at 17,000 xg and 4 °C or 5 minutes. The supernatant was removed and the pellet was incubated with an open lid at 37 °C for 1 hour. The pellet was resuspended in 2x SDS sample buffer and 1 µl 1 M Tris pH 8 was added (sample S). SDS-PAGE with subsequent Western blot analysis was performed with reference sample R and assay sample S on a 15 % tris-glycine gel. A primary Antibody targeting HlyA secretion signal was used in combination with HRP-conjugated secondary antibody.

Results

TolC purification

TolC was expressed in *E. coli* BL21(DE3) and purified from the membrane fraction after cell disruption. TolC was solubilized using 2 % Triton X-100 and purified in DDM via IMAC and size exclusion chromatography (SEC) (Figure 1A). The SEC chromatogram revealed two peaks. As seen from SDS-PAGE analysis both peaks contained trimeric TolC (Figure 1B). Trimeric TolC migrated on an SDS-PAGE at around 130 kDa. Only after boiling of the sample and adding reducing agent dithiothreitol (DTT), TolC migrated exclusively as a monomer (95, Figure 1B). Monomeric TolC was visible as a double band at around 55 kDa. The first elution peak contains a minor impurity, seen as a band slightly below 40 kDa. The second elution peak did not contain any impurities. Both peaks were combined, concentrated and used for reconstitution into liposomes.

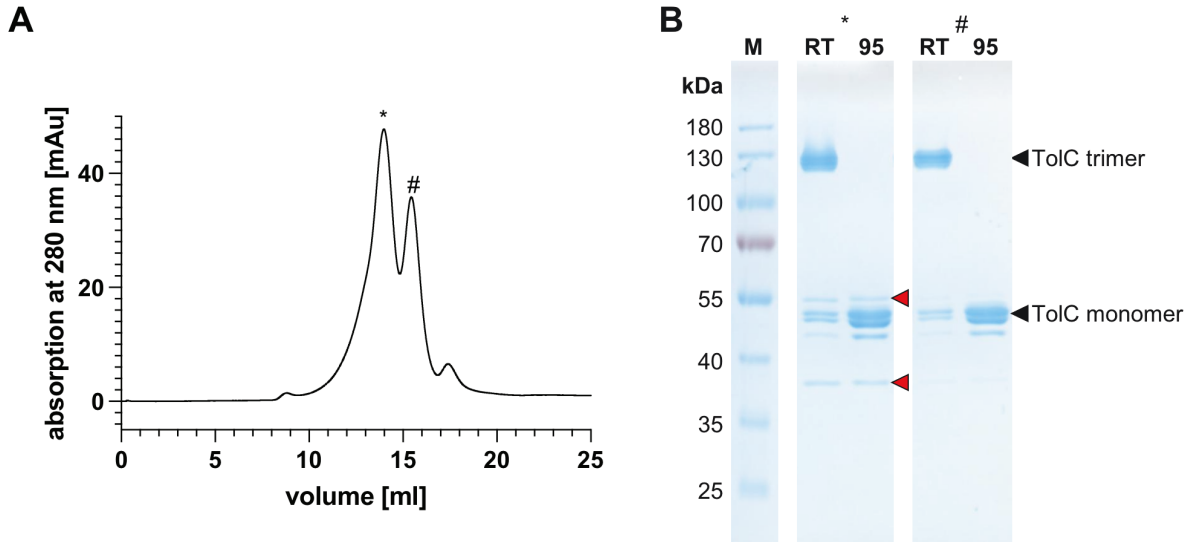

Figure 2: Purification of TolC. A: *Gel filtration analysis of TolC on Superose 6 Inc. 10/300 GL. TolC eluted in two peaks, marked * and #.* ***B:*** *SDS-PAGE analysis of purified TolC. M: marker proteins with their approximated molecular weight. *: sample from TolC first elution peak. #: sample from TolC second elution peak. RT: sample was incubated at room temperature before loading on the gel. 95: sample was incubated at 95 °C for 5 minutes and DTT was added before loading on the gel. Bands for TolC trimer and monomer are indicated and marked with a black triangle. Impurities are marked with a red triangle.*

TolC reconstitution

We reconstituted TolC into DOPC liposomes at a protein-to-lipid ratio of 1:33 (wt/wt). To confirm successful reconstitution of TolC we performed a flotation assay with TolC proteoliposomes in a sucrose gradient. Fractions from the gradient were analysed via SDS-PAGE (Figure 2). Proteoliposomes were placed on the bottom of a sucrose gradient ranging from 5 (top) to 30 % (bottom) sucrose. As proteoliposomes are filled

with buffer containing no sucrose, they float to the top of the gradient during centrifugation. In contrast, proteins in solution stay on the bottom of the gradient. After performing the flotation assay with TolC proteoliposomes the strongest band for TolC was detected in the top fraction and band intensity decreased from top fraction to bottom fractions (Figure 2B). On the other hand, no band for TolC was visible in the top fraction for the flotation assay performed with TolC in detergent. Here a strong band for TolC was visible in the bottom fraction of the gradient (Figure 2C). This data verifies effective reconstitution of TolC into DOPC liposomes.

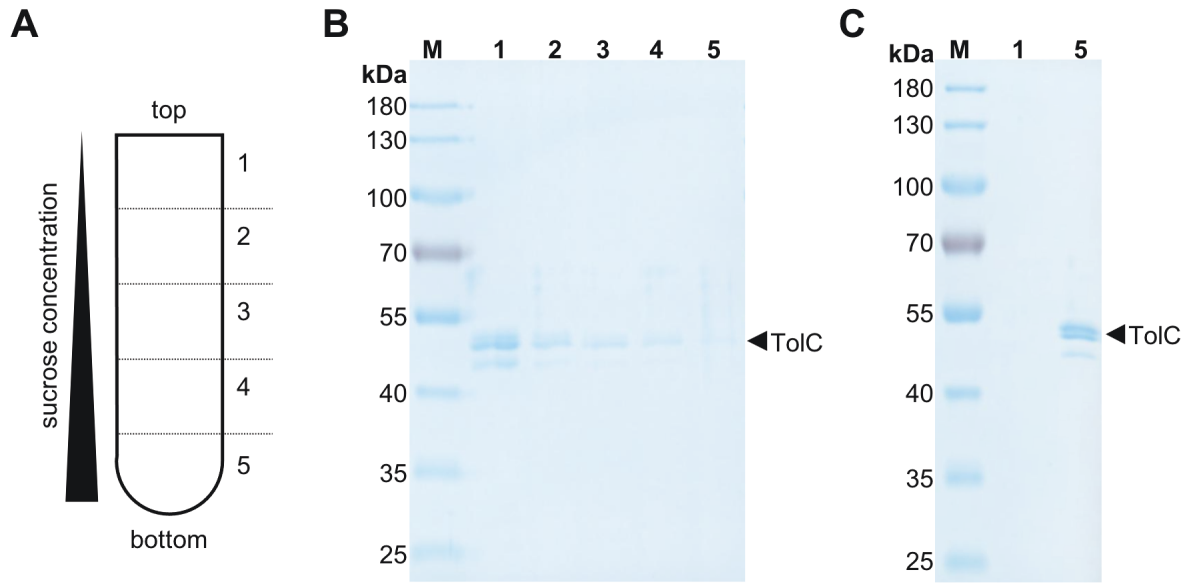

Figure 3: Flotation assay of TolC proteoliposomes. A: *A sample of protein, liposomes or proteoliposomes is placed on the bottom of a sucrose gradient and centrifuged. The gradient is fractionated for analysis.* ***B:*** *SDS-PAGE analysis of a 5 – 30 % sucrose gradient after flotation assay with TolC proteoliposomes. M: marker proteins with their approximated molecular weight. 1-5: fractions from top to bottom of the sucrose gradient. The band for monomeric TolC is marked with a black triangle.* ***C:*** *SDS-PAGE analyss of a 5 – 30 % sucrose gradient after flotation assay with TolC in DDM. M: marker proteins with their approximated molecular weight. 1-5: fractions from top to bottom of the sucrose gradient. The band for monomeric TolC is marked with a black triangle.*

IMC reconstitution

The inner membrane complex (IMC) build by HlyB and HlyD, was purified in digitonin via StrepTactin affinity resin. We chose MSP2N2 as membrane scaffold protein (MSP) as it builds nanodiscs with a diameter of approximately 16 nm, large enough to incorporate the IMC. As lipids we chose a mixture of DOPE, DOPG and DOPC in a molar ratio of 1:1:1. We reconstituted IMC into MSP based nanodiscs at a molar ratio of IMC:MSP:lipid of 1:4:600. To further evaluate reconstitution we performed an analytical gel filtration on a Superose 6 Increase 3.2/300 column with subsequent SDS-PAGE analysis and ATPase activity assay (Figure 3). SEC of IMC in nanodisc showed several merged peaks at elution volumes between 1.2 and 1.5 ml. In addition a distinct

peak for empty nanodisc was visible at around 1.7 ml (Figure 3A). The peak containing reconstituted IMC was marked with an asterisk. SDS-PAGE analysis confirmed presence of HlyB, HlyD and MSP2N2 (Figure 3B). Furthermore, the fraction showed ATPase activity as observed from the green colour in the ATPase activity assay (Figure 3C). Calculation of precise ATPase activity values was limited due to the low amount of protein used for analytical gel filtration. Considering an overall dilution factor of 10 during size exclusion and only 25 % HlyB of the total protein content assessed by SDS-PAGE, we could calculate an ATPase activity of about 200 nmol/(mg*min). Nevertheless this value has to be treated with care, as protein concentration was very low and therefore errors have a huge impact. For the transport assay we immediately used reconstituted IMC after BioBeads incubation overnight without further purification steps.

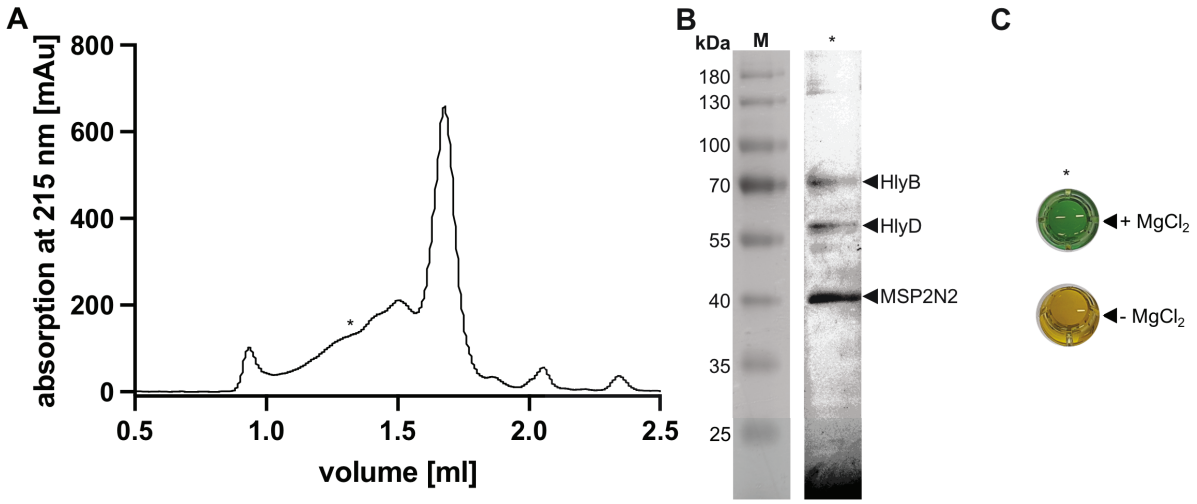

Figure 4: Reconstitution of IMC in MSP2N2 and a lipid mixture of DOPE, DOPG, DOPC. A: *Gel filtration analysis of reconstituted IMC on Superose 6 Increase 3.2/300.* ***B:*** *SDS-PAGE analysis of reconstituted IMC. M: marker proteins with their approximated molecular weight. *: sample from main elution peak of reconstituted IMC. HlyB, HlyD and MSP2N2 are marked with a black triangle.* ***C:*** *Wells from ATPase activity assay from reconstituted IMC. *: sample from main elution peak of reconstituted IMC. Positive sample (+ $MgCl_2$) and negative background control (- $MgCl_2$) are indicated.*

<u>In vitro transport assay</u>

The basic idea of this transport assay is to assemble the HlyA T1SS *in vitro* in a two-compartment system to investigate transport. Therefore we used TolC reconstituted in liposomes and IMC reconstituted in a MSP based lipid nanodisc. If substrate is transported it will translocate into the lumen of the liposome. Here it is protected from proteinase K digestion as proteinase K can't enter the liposome. Therefore detection of the substrate via Western blot analysis is taken as a read out, as substrate can only

be detected if transport into the liposome occurred. For our *in vitro* transport assay we combined TolC DOPC proteoliposomes and IMC reconstituted in MSP2N2 nanodisc using DOPE, DOPG and DOPC. We also added $MgCl_2$, an energy regeneration system and a short secretion competent version of the substrate HlyA, called HlyA1. After incubation overnight ATP was added and the *in vitro* transport assay was performed for 8 h at 25 °C. After taking a reference sample, transport was stopped by addition of proteinase K, digesting every protein outside the liposomes. By TCA precipitation and SDS-PAGE sample preparation proteinase K was inhibited and vesicles containing transported substrate were disrupted. Reference sample and assay sample were analysed via Western blot using an antibody targeting the secretion signal of HlyA (Figure 5).

We could detect transport of HlyA1 in the sample of our *in vitro* transport assay (Figure 5, lane S, black triangle). Furthermore, we could detect additional signals for a prominent impurity in our sample after proteinase K digestion (Figure 5, lane S, red triangle) and for dimeric HlyA1 in the reference sample (Figure 5, lane R, blue triangle). Compared to the reference sample the signal for HlyA1 in the sample after proteinase K treatment is less than 10%. However, this signal serves as a first proof of concept for our *in vitro* transport assay for the HlyA T1SS.

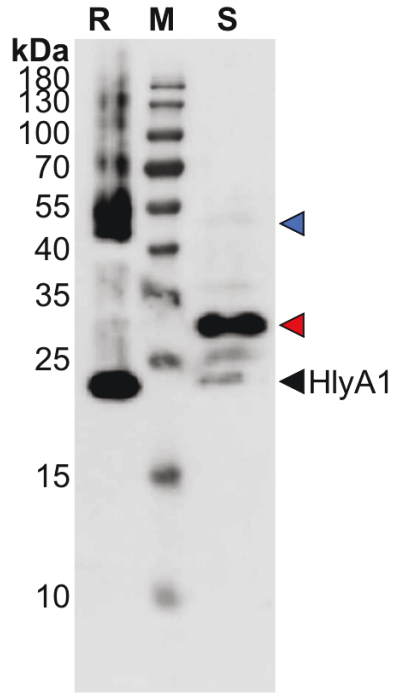

Figure 5: Western blot analysis of HlyA T1SS in vitro transport assay. *M: marker proteins with their approximated molecular weight. R: 5 µl reference sample from the assay before proteinase K digestion. S: TCA precipitated sample from the assay after proteinase K digestion. HlyA1 is marked with a black triangle. Dimeric HlyA1 in the reference sample is marked with a blue triangle and an unknown impurity after proteinase K digestion is marked with a red triangle. Antibody targeting the secretion signal of HlyA was used*

Discussion

Secretion of large substrates in Gram-negative bacteria requires a complex interplay between different proteins and is still not understood in detail. While some tripartite efflux systems for small substrates are already well characterized in structure and function [4, 5, 29, 33-36], Type 1 secretion systems (T1SS) transporting large substrates are still lacking the information of structure-function-relationship for the whole entity. One of the best studied T1SS is the hemolysin A (HlyA) T1SS from *E. coli* [16, 37-40]. Recently the structure of the inner membrane complex (IMC) of the HlyA T1SS was published and shed some light on the functionality and stoichiometry of the system [14]. But as the IMC is only one half of the T1SS and the secretion process also involves the outer membrane protein TolC further research targeting the whole system is necessary. Here we describe a set-up for an *in vitro* transport assay to investigate the biochemistry of the secretion process.

By reconstitution of TolC into liposomes a two-compartment system is created allowing transport from one compartment (solution outside the liposomes) into the other compartment (lumen of the vesicles). The reconstitution of TolC can occur in two orientations. The periplasmic part of TolC is either facing the outside of the vesicle or the inside. As we do not completely dissolve the liposomes for reconstitution we expect the majority of TolC periplasmic part to face the outside of the liposome. Else the large periplasmic part would need to cross the partly destabilized membrane which is thermodynamically unfavourable. Therefore, most of the reconstituted TolC should be accessible for our transport assay. These assumptions are in line with published data for bacteriorhodopsin in 1988 where increasing amounts of Triton X-100 favour a more equal distribution of orientation [41]. As TolC with a periplasmic part oriented into the lumen of the vesicle does not interfere with our assay, as long as it is not 100 %, we did not attempt to quantify the orientation of TolC so far. A quantitative determination would be necessary to use the assay for quantitative analysis relying on for instance the total number of active transport systems. If quantitative analysis is not possible one could completely dissolve the liposomes during reconstitution and therefore favouring an equal distribution of orientation.

To make sure that we do not face a limitation of space inside the liposome, we calculated the total number of substrates that fit into one liposome. Given the diameter of the liposomes with 400 nm and a thickness of the lipid bilayer of about 5 nm [42] we could calculate the volume inside the liposome to approximately 31,000,000 nm^3. For

the sake of simplicity we assumed our substrate to be a box and calculated the volume of HlyA1 taking SAXS data from purified full length HlyA (not published). HlyA has a three dimensional dimension of about 1000 nm^3. Taking into account that HlyA1 is roughly one fourth of HlyA, the volume of HlyA1 is about 250 nm^3. With these assumptions up to 124,000 substrate molecules can fit into one liposome.

The Western blot targeting the secretion signal of HlyA reveals a first hint of actual transport of substrate into the liposome (Figure 5). Nevertheless this result has to be treated with care as the band is less than 10 % of the reference sample and the reference sample contains only 10 % of the initially added substrate. Taking these intensities into account this would indicate that less than 1 % of HlyA1 was transported. Improvement of transport for this *in vitro* system is necessary and possible via optimization of the reconstitution process of IMC into MSP nanodiscs (Figure 4A) to have more fully assembled T1SS. In addition, investigations regarding the optimal ratio of IMC in nanodiscs, TolC in liposomes and HlyA1 has to be determined.

Once this *in vitro* transport assay is further developed it opens the possibility to study the secretion via HlyA T1SS in detail in a controlled environment. This would allow to study for instance the influence on secretion of external factors like ion strength or Ca^{2+} concentration. Also a stoichiometric calculation of number of hydrolysed ATP molecules per secreted substrate would be possible.

Author contribution

FLB, SS and LS conceived the experiments and evaluated the data. FLB performed expression and purification of TolC, reconstitution of TolC into liposomes and flotation assay, purification of IMC, reconstitution into MSP2N2 nanodiscs, ATPase activity assay and the in vitro transport assay. SK purified HlyA1. EH purified MSP2N2 and performed cloning of IMC into pQLink expression vector. CG performed expression of IMC. FLB wrote the initial draft. FLB, SS and LS wrote the final version of the manuscript.

Funding

This work was supported by the Deutsche Forschungsgemeinschaft (DFG, CRC 1208 project A01 to LS).

Acknowledgement

We thank all former and current members of the Institute of Biochemistry for their support and productive discussions. We thank Michael Kamel for support and helpful guidance in setting up the *in vitro* transport assay.

References

1. Costa, T.R., et al., *Secretion systems in Gram-negative bacteria: structural and mechanistic insights.* Nat Rev Microbiol, 2015. **13**(6): p. 343-59.
2. Jardetzky, O., *Simple allosteric model for membrane pumps.* Nature, 1966. **211**(5052): p. 969-70.
3. Jang, S., *AcrAB-TolC, a major efflux pump in Gram negative bacteria: toward understanding its operation mechanism.* BMB Rep, 2023. **56**(6): p. 326-334.
4. Chen, M., et al., *In situ structure of the AcrAB-TolC efflux pump at subnanometer resolution.* Structure, 2022. **30**(1): p. 107-113 e3.
5. Fitzpatrick, A.W.P., et al., *Structure of the MacAB-TolC ABC-type tripartite multidrug efflux pump.* Nat Microbiol, 2017. **2**: p. 17070.
6. Alav, I., et al., *Structure, Assembly, and Function of Tripartite Efflux and Type 1 Secretion Systems in Gram-Negative Bacteria.* Chem Rev, 2021. **121**(9): p. 5479-5596.
7. Ristow, L.C. and R.A. Welch, *RTX Toxins Ambush Immunity's First Cellular Responders.* Toxins (Basel), 2019. **11**(12).
8. Baril, S.A., T. Gose, and J.D. Schuetz, *How Cryo-EM Has Expanded Our Understanding of Membrane Transporters.* Drug Metabolism and Disposition, 2023. **51**(8): p. 904-922.
9. Felmlee, T., S. Pellett, and R.A. Welch, *Nucleotide sequence of an Escherichia coli chromosomal hemolysin.* J Bacteriol, 1985. **163**(1): p. 94-105.
10. Cross, M.A., et al., *HlyB-dependent secretion of hemolysin by uropathogenic Escherichia coli requires conserved sequences flanking the chromosomal hly determinant.* J Bacteriol, 1990. **172**(3): p. 1217-24.
11. Leeds, J.A. and R.A. Welch, *RfaH enhances elongation of Escherichia coli hlyCABD mRNA.* J Bacteriol, 1996. **178**(7): p. 1850-7.
12. Thanabalu, T., et al., *Substrate-induced assembly of a contiguous channel for protein export from E.coli: reversible bridging of an inner-membrane translocase to an outer membrane exit pore.* EMBO J, 1998. **17**(22): p. 6487-96.
13. Lecher, J., et al., *An RTX transporter tethers its unfolded substrate during secretion via a unique N-terminal domain.* Structure, 2012. **20**(10): p. 1778-87.
14. Zhao, H., J. Lee, and J. Chen, *The hemolysin A secretion system is a multi-engine pump containing three ABC transporters.* Cell, 2022. **185**(18): p. 3329-3340 e13.
15. Benabdelhak, H., et al., *A specific interaction between the NBD of the ABC-transporter HlyB and a C-terminal fragment of its transport substrate haemolysin A.* J Mol Biol, 2003. **327**(5): p. 1169-79.
16. Pourhassan, N.Z., et al., *Investigations on the substrate binding sites of hemolysin B, an ABC transporter, of a type 1 secretion system.* Front Microbiol, 2022. **13**: p. 1055032.

17. Balakrishnan, L., C. Hughes, and V. Koronakis, *Substrate-triggered recruitment of the TolC channel-tunnel during type I export of hemolysin by Escherichia coli.* J Mol Biol, 2001. **313**(3): p. 501-10.
18. Bumba, L., et al., *Calcium-Driven Folding of RTX Domain beta-Rolls Ratchets Translocation of RTX Proteins through Type I Secretion Ducts.* Mol Cell, 2016. **62**(1): p. 47-62.
19. Koronakis, V., et al., *Crystal structure of the bacterial membrane protein TolC central to multidrug efflux and protein export.* Nature, 2000. **405**(6789): p. 914-9.
20. Kim, J.S., et al., *Crystal Structure of a Soluble Fragment of the Membrane Fusion Protein HlyD in a Type I Secretion System of Gram-Negative Bacteria.* Structure, 2016. **24**(3): p. 477-85.
21. Tiefenauer, L. and S. Demarche, *Challenges in the Development of Functional Assays of Membrane Proteins.* Materials (Basel), 2012. **5**(11): p. 2205-42.
22. Knowles, T.J., et al., *Membrane proteins solubilized intact in lipid containing nanoparticles bounded by styrene maleic acid copolymer.* J Am Chem Soc, 2009. **131**(22): p. 7484-5.
23. Broadbent, L., et al., *Detergent-Free Membrane Protein Purification Using SMA Polymer.* Methods Mol Biol, 2022. **2507**: p. 389-404.
24. Oluwole, A.O., et al., *Solubilization of Membrane Proteins into Functional Lipid-Bilayer Nanodiscs Using a Diisobutylene/Maleic Acid Copolymer.* Angew Chem Int Ed Engl, 2017. **56**(7): p. 1919-1924.
25. Pettersen, J.M., Y. Yang, and A.S. Robinson, *Advances in nanodisc platforms for membrane protein purification.* Trends Biotechnol, 2023. **41**(8): p. 1041-1054.
26. Ritchie, T.K., et al., *Chapter 11 - Reconstitution of membrane proteins in phospholipid bilayer nanodiscs.* Methods Enzymol, 2009. **464**: p. 211-31.
27. Frauenfeld, J., et al., *A saposin-lipoprotein nanoparticle system for membrane proteins.* Nat Methods, 2016. **13**(4): p. 345-51.
28. Geertsma, E.R., et al., *Membrane reconstitution of ABC transporters and assays of translocator function.* Nat Protoc, 2008. **3**(2): p. 256-66.
29. Souabni, H., et al., *Quantitative real-time analysis of the efflux by the MacAB-TolC tripartite efflux pump clarifies the role of ATP hydrolysis within mechanotransmission mechanism.* Commun Biol, 2021. **4**(1): p. 493.
30. Cunningham, K., et al., *SecA protein, a peripheral protein of the Escherichia coli plasma membrane, is essential for the functional binding and translocation of proOmpA.* EMBO J, 1989. **8**(3): p. 955-9.
31. Baykov, A.A., O.A. Evtushenko, and S.M. Avaeva, *A malachite green procedure for orthophosphate determination and its use in alkaline phosphatase-based enzyme immunoassay.* Anal Biochem, 1988. **171**(2): p. 266-70.
32. Thomas, S., S.H. Smits, and L. Schmitt, *A simple in vitro acylation assay based on optimized HlyA and HlyC purification.* Anal Biochem, 2014. **464**: p. 17-23.
33. Du, D., et al., *Structure of the AcrAB-TolC multidrug efflux pump.* Nature, 2014. **509**(7501): p. 512-5.
34. Du, D., et al., *Purification of AcrAB-TolC Multidrug Efflux Pump for Cryo-EM Analysis.* Methods Mol Biol, 2018. **1700**: p. 71-81.
35. Du, D., et al., *Interactions of a Bacterial RND Transporter with a Transmembrane Small Protein in a Lipid Environment.* Structure, 2020. **28**(6): p. 625-634 e6.
36. Tsutsumi, K., et al., *Structures of the wild-type MexAB-OprM tripartite pump reveal its complex formation and drug efflux mechanism.* Nat Commun, 2019. **10**(1): p. 1520.

37. Schmitt, L., et al., *Crystal structure of the nucleotide-binding domain of the ABC-transporter haemolysin B: identification of a variable region within ABC helical domains.* J Mol Biol, 2003. **330**(2): p. 333-42.
38. Zaitseva, J., et al., *H662 is the linchpin of ATP hydrolysis in the nucleotide-binding domain of the ABC transporter HlyB.* EMBO J, 2005. **24**(11): p. 1901-10.
39. Reimann, S., et al., *Interdomain regulation of the ATPase activity of the ABC transporter haemolysin B from Escherichia coli.* Biochem J, 2016. **473**(16): p. 2471-83.
40. Spitz, O., et al., *Identity Determinants of the Translocation Signal for a Type 1 Secretion System.* Front Physiol, 2021. **12**: p. 804646.
41. Rigaud, J.L., M.T. Paternostre, and A. Bluzat, *Mechanisms of membrane protein insertion into liposomes during reconstitution procedures involving the use of detergents. 2. Incorporation of the light-driven proton pump bacteriorhodopsin.* Biochemistry, 1988. **27**(8): p. 2677-2688.
42. Regan, D., et al., *Lipid Bilayer Thickness Measured by Quantitative DIC Reveals Phase Transitions and Effects of Substrate Hydrophilicity.* Langmuir, 2019. **35**(43): p. 13805-13814.

3.6. Chapter 6: Functional and structural characterization of the ABC transporter RtxB from *Kingella kingae*

Title: Functional and structural characterization of the ABC transporter RtxB from *Kingella kingae*

Authors: **Florestan L. Bilsing**, Sakshi Khosa, Sander Smits, Lutz Schmitt

Published in: to be submitted

Own contribution:
Designing the experiments
Expression and purification of RtxB
Reconstitution of RtxB into Msp1D1 nanodiscs
ATPase activity assays
Data evaluation
Preparation of the figures
Writing of the manuscript

Functional and structural characterization of the ABC transporter RtxB from *Kingella kingae*

Florestan L. Bilsing[1], Sakshi Khosa[1], Sander Smits[1,2], Lutz Schmitt[1]*

[1]Heinrich Heine University Düsseldorf, Faculty of Mathematics and Natural Sciences, Institute of Biochemistry, Universitätsstraße 1, 40225 Düsseldorf
[2]Heinrich Heine University Düsseldorf, Faculty of Mathematics and Natural Sciences, Center for Structural Studies, , Universitätsstraße 1, 40225 Düsseldorf

*Corresponding author: Lutz Schmitt, Heinrich Heine University Düsseldorf, Faculty of Mathematics and Natural Sciences, Institute of Biochemistry, Universitätsstraße 1, 40225 Düsseldorf, Germany, Tel.: +49 211 81 10773, E-Mail: lutz.schmitt@hhu.de

Abstract

Over the past decades the clinical relevance of *Kingella kingae* (*K. kingae*) a Gram-negative bacterium causing invasive infections in children at the age of 6 to 48 month increased drastically. A key player in cytotoxicity of *K. kingae* is a type 1 secretion system (T1SS) exporting a haemolytic toxin with the help of the ATP-binding cassette (ABC) transporter RtxB. To treat *K. kingae* infections, it is essential to understand the mode of action in a macroscopic and microscopic scale. Therefore fundamental research on all components involved in *K. kingae* invasive infections is important. Here we present the purification and initial characterisation of the ABC transporter RtxB in an ATPase active state in detergent. Additionally, we could purify RtxB to a homogeneity suitable for single particle cryo EM analysis. We determined the kinetic parameters of RtxB ATPase activity and define its pH optimum. Furthermore, we could reconstitute RtxB in MSP based nanodiscs and observed an increased ATPase activity in a lipid bilayer as well as an increase in stability at elevated temperatures.

Introduction

Kingella kingae was identified in 1960 and was first described in 1968 as a new Gram-negative β-hemolytic bacteria species assigned to the genus *Moraxella* [1]. In 1976 the species was transferred to the genus of *Kingella gen. nov.* in the family of *Neisseriaceae* [2]. As it was rarely isolated from patients, its clinical relevance was rated low in the beginning [3, 4]. Over the past 30 years, as cultivation and diagnostic advanced, its relevance as a paediatric pathogen of children in the age between 6 and 48 months increased [5-9]. As part of the commensal flora *K. kingae* colonizes the upper respiratory tract and can lead to invasive diseases such as bone infections, bacteraemia or even endocarditis [6, 9-12]. Although *K. kingae* is recently known for causing invasive diseases it is still poorly understood what exactly triggers invasion [7]. Besides biofilm formation [13] one of the key players in *K. kingae* invasive infections is the RTX toxin RtxA [14, 15]. RtxA is secreted via a Type 1 secretion system (T1SS) build up by an ABC transporter (RtxB), a periplasmic adapter protein (RtxD) and an outer membrane protein (TolC) [15-17] (Figure 1).

Secretion of the toxin is powered by ATP hydrolysis performed by the ABC transporter RtxB [15]. As an ABC transporter of a bacterial T1SS, RtxB is a so-called half-size transporter and active as a dimer [18, 19]. The ABC transporter RtxB belongs to the group 2 of T1SS ABC transporters and is build up by three domains [20]. Besides the transmembrane domain (TMD) and the nucleotide binding domain (NBD) it possesses an additional N-terminal domain, termed C39 peptidase-like domain (CLD). This domain shares sequence and structure similarity with a C39 peptidase but lacks peptidase activity [20]. For the RtxB homolog HlyB from *Escherichia coli* (*E. coli*) it was shown that the CLD is crucial for substrate recognition and secretion [21]. Furthermore it was shown that for the isolated HlyB a deletion of the CLD increases ATPase activity, therefore postulating a regulation of its ATPase activity via the CLD [22]. Recently we could show that it is possible to create chimeric transporters of HlyB and RtxB that are still able to secrete the RTX toxin HlyA, indicating an interplay between all three domains that is at least to some extend exchangeable between homologous transporters (Anlauf et al., to be published).

Studying membrane proteins *in vitro* is a challenging tasks due to their hydrophobic membrane part. Detergents are used to shield the hydrophobic parts of the protein [23]. As the impact of a used detergents is not always clear a native like surrounding is preferred as provided by membrane mimetics [24]. One of these is the membrane

scaffold protein (MSP) based nanodisc system [25]. It enables incorporation of a membrane protein into a lipid bilayer. By the choice of MSP and lipids one can adjust the system to the needs of the membrane protein.

Here we report a purification and characterisation of the ABC transporter RtxB from the emerging paediatric pathogen *Kingella kingae*. We successfully purified the transporter in LMNG and investigated its ATPase activity at different pH levels. We could show that for RtxB the single histidine to alanine mutation within the H-loop of its NBD is ATPase deficient as it was shown for HlyB [26]. By creating a chimeric transporter we tested whether the regulatory effect of the CLD of HlyB from *E. coli* is transferable on RtxB from *K. kingae*. Furthermore we successfully reconstituted RtxB into a lipid bilayer using MSP based nanodiscs and investigated the influence of reconstitution on ATPase activity at elevated temperatures of up to 60 °C.

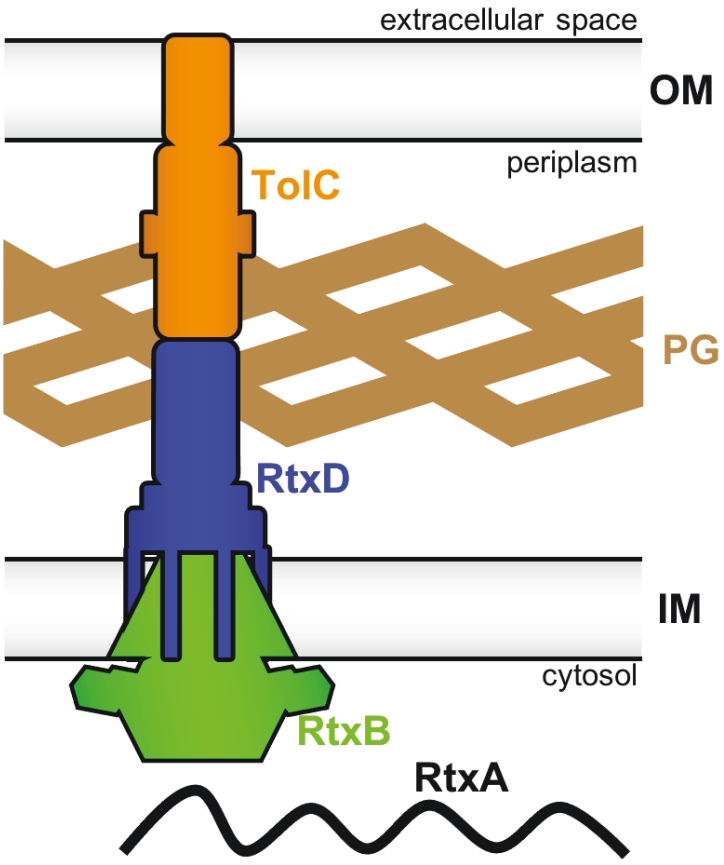

Figure 1: Schematic of the RtxA T1SS. *RtxB (green) and RtxD (blue) in the inner memebrane (IM) form a continuous channel with TolC (orange) in the outer membrane (OM) to secrete the unfolded substrate RtxA (black) from the cytosol to the extracellular space. The peptidoglycan layer (PG) in the periplasm is shown as brown grid.*

Material and Methods

Plasmid construction

E. coli DH5α was used for cloning. The gene for RtxB (UniProt-ID: F5S9L7) was amplified from genomic DNA of *Kingella kingae* ATCC 23330 (DSM 7536) ordered at German Collection of Microorganisms and Cell Cultures GmbH (DSMZ) and cloned into pBAD based expression vector with an N-terminal 10x His-tag. The ATPase deficient RtxB H662A (RtxB-HA) mutant was generated via side directed mutagenesis using primers listed in table S1. The chimeric RtxB-EKK with the CLD from HlyB from *E. coli* and TMD and NBD from RtxB from *K. kingae*, was generated via Gibson Assembly [27] using plasmid for expression of HlyB [22] and primers listed in table S1.

Protein expression and purification

E. coli BL21(DE3) was used for expression of RtxB, RtxB-HA and RtxB-EKK. Cells containing the appropriate plasmid were grown over night at 37 °C and 180 rpm in a 300 ml baffled flask containing 50 ml 2YT medium and 100 µg/ml ampicillin. Overnight grown cultures were used to inoculate 1 L 2YT medium in a 5 L baffled flask containing 100 µg/ml ampicillin to an OD_{600} of 0.1. Flasks were incubated at 37 °C and 120 rpm to an OD_{600} of 0.6 - 0.8 and expression was induced by addition of 1 mM arabinose. Cells were harvested after 3 h of expression via centrifugation at 5,000 xg for 20 minutes at 4 °C. Cells from 4 L expression were used for one purification. Cells were resuspended in buffer A (50 mM Na_2HPO_4 pH 8, 300 mM NaCl) containing one cOmplete EDTA-free inhibitor cocktail tablet and a spatulas tip of DNAseI. Cells were lysed by three passes through Microfluidizer M-110P (Microfluidics) at 1.5 kbar. Cell debris was removed by centrifugation at 18,000 xg for 30 minutes at 4 °C and the supernatant was centrifuged for 90 minutes at 38,000 rpm (Type 45 Ti, Beckman Coluter) at 4 °C. The membrane pellet was resuspended in buffer A and used for solubilization. For solubilization, the membrane was diluted to 10 mg/ml using buffer A and incubated over night with 1 % LMNG and 1 cOmplete EDTA-free inhibitor cocktail tablet. Non-solubilized material was removed via centrifugation for 30 minutes at 38,000 rpm (Type 45 Ti, Beckman Coluter) at 4 °C. Imidazole was added to the supernatant at a final concentration of 2 mM and it was loaded on a 5 ml HiTrap IMAC HP (Cytiva) column (Ni^{2+}) equilibrated with buffer B (50 mM Na_2HPO_4 pH 8, 300 mM NaCl 2 mM imidazole, 0.002 % LMNG). The column was washed with 10 column volumes (CV) of buffer B and 10 CV of buffer C (50 mM Na_2HPO_4 pH 8, 300 mM NaCl

90 mM imidazole, 0.002 % LMNG) RtxB was eluted with buffer D (50 mM Na_2HPO_4 pH 8, 300 mM NaCl 300 mM imidazole, 0.002 % LMNG). Fractions containing RtxB were combined and concentrated using an Amicon Ultra-15 centrifugal filter unit (Millipore) with a MWCO of 100 kDa. Concentrated protein sample was centrifuged for 30 minutes at 17,000 xg at 4 °C and supernatant was applied on a Superose 6 Increase 10/300 GL (Cytiva) column equilibrated in buffer E (20 mM Tris pH 8, 150 mM NaCl, 0.002 % LMNG). Peak fractions containing RtxB were either immediately used or combined and concentrated using Ultra-4 centrifugal filter unit (Millipore) with a MWCO of 100 kDa. For storage RtxB was flash frozen in liquid nitrogen and stored at – 80 °C.

ATPase activity assay

For measuring ATPase activity the Malachite Green assay [28] was used with the following adaptations. RtxB, RtxB-HA and RtxB-EKK were used at a concentration of 1 µM in buffer E. Reconstituted RtxB in MSP1D1 was used at a total protein concentration of 0.08 mg/ml in buffer F (20 mM Tris pH 8, 150 mM NaCl) resulting in 0.5 µM RtxB as estimated from Coomassie stained SDS PAGE. ATP was used in final concentrations ranging from 0 to 5 mM and $MgCl_2$ was used in a final concentration of 10 mM. Negative controls contained no $MgCl_2$. The reaction was started by addition of ATP and incubated for 40 minutes at 25 °C. ATPase assay to investigate thermostability were conducted at temperatures from 15 to 60 °C and were incubated for only 30 minutes. The reaction was stopped by adding the reaction set up (25 µl) to 175 µl 10 mM H_2SO_4. The assay was stained by adding 50 µl freshly prepared staining solution (0.096% (w/v) malachite green, 1.48% (w/v) ammonium molybdate, 0,17% (v/v) Tween-20 in 15 % H_2SO_4) and absorption at 595 nm was measured after 8 min of incubation at RT. Datapoints were visualized using GraphPad Prism (GraphPad) and analysed via allosteric sigmoidal enzyme kinetic fit (Hill equation): $y = \frac{v_{max} * x^h}{{k_{half}}^h + x^h}$ with x being ATP concentration and y enzyme velocity.

For ATPase activity measurements at different pH values, buffers listed in table S2 were used for dilution of RtxB to a final concentration of 1 µM. ATP and $MgCl_2$ were used at concentrations of 4 mM and 10 mM respectively.

Reconstitution into MSP based nanodisc

Reconstitution of RtxB into MSP based nanodisc was performed with a lipid mixture of DOPE, DOPG and DOPC in a molar ratio of 1:1:1. Lipids were ordered as individual

chloroform solutions (Avanti Polar Lipids) and mixed in the desired ratio. Chloroform was evaporated using a rotary evaporator and lipids were resuspended in buffer F at a final concentration of 3.8 mg/ml. Lipids were extruded 11 times using a 400 nm membrane and incubated with 1 % Triton X-100 for 10 min at 40 °C. Next, lipids were chilled on ice and RtxB and MSPD1 were added simultaneously in a final molar ratio of 1:1:75 (calculated for monomeric RtxB). Sample was incubated on ice for 30 minutes prior to addition of 0.8 g/ml BioBeads and incubation at 4 °C over night under constant agitation. The next day supernatant was centrifuged for 30 min at 17,000 xg and 4 °C and supernatant was applied on Superdex200 Increase 10/300 GL equilibrated in buffer F. Peak fractions containing reconstituted RtxB were either immediately used or combined and concentrated using Ultra-4 centrifugal filter unit (Millipore) with a MWCO of 100 kDa.

Cryo-EM sample preparation and data collection

An aliquot of 4 µl purified RtxB (~0.5 mg/ml) was applied to glow-discharged 200-mesh Quantifoil R1.2/1.3 200 grids. The grids were blotted for 5 sec and plunged into the liquid ethane using an EM GP 2 Plunge Freezer (Leica Microsystems) operated at 4°C and 95% humidity. The grids were screened on Talos Arctica (Thermo Fisher Scientific) electron microscope and 9753 movie stacks were collected on a Titan Krios (Thermo Fisher Scientific) electron microscope at Ernst Ruska-Centre for Microscopy and Spectroscopy with Electrons (ER-C) department for Structural Biology (ER-C-3), Forschungszentrum Jülich GmbH. The images were recorded with a K3 camera (Gatan) in super-resolution mode at a nominal magnification of 105000 × (calibrated pixel size of 0.82 Å on the specimen level) and a defocus range from −1.0 to −3.0 µm. Exposures were dose-fractionated into 60 frames, with a total dose of 58.52 electrons per $Å^2$.

Cryo-EM image processing

The RtxB dataset was processed using cryoSPARC (Punjani et al., 2017). The image stacks were subjected to beam-induced motion correction using Warp (Tegunov, D. and Cramer, P., 2018. Real-time cryo-EM data pre-processing with Warp. *BioRxiv*, p.338558.). Contrast transfer function (CTF) parameters for each micrograph were estimated using the cryoSPARC patch CTF algorithm. Particles were picked from the micrographs using a blob picker in cryoSPARC. The auto-picked 951952 particles

were extracted with a box size of 256 pixels. Multiple initial maps (K = 3) were generated from the dataset using stochastic gradient descent-based *ab-initio* reconstruction in cryoSPARC and all particles were classified to three classes by heterogeneous refinement in cryoSPARC with the initial maps for guided multi-reference 3D classification. Particles from the best class were subjected to 3D non-uniform (NU) refinement and local refinement (Punjani et al., 2020).

Results

Purification and ATPase activity of RtxB

To produce sufficient amounts of RtxB from *Kingella kingae* (*K. kingae*) for structural and biochemical analysis, we used *E. coli* BL21(DE3) as an expression host. We used a plasmid encoded construct of RtxB containing an N-terminal 10xHis-tag for affinity purification. After membrane isolation RtxB was solubilized with 1% LMNG and purified via IMAC and subsequent size exclusion chromatography (SEC) (Figure 2A). SDS PAGE (Figure 2B) was used to assess protein purity. Besides Western Blot analysis (Figure 2B) and protein mass spectrometry was used to confirm protein identity (Table S3).

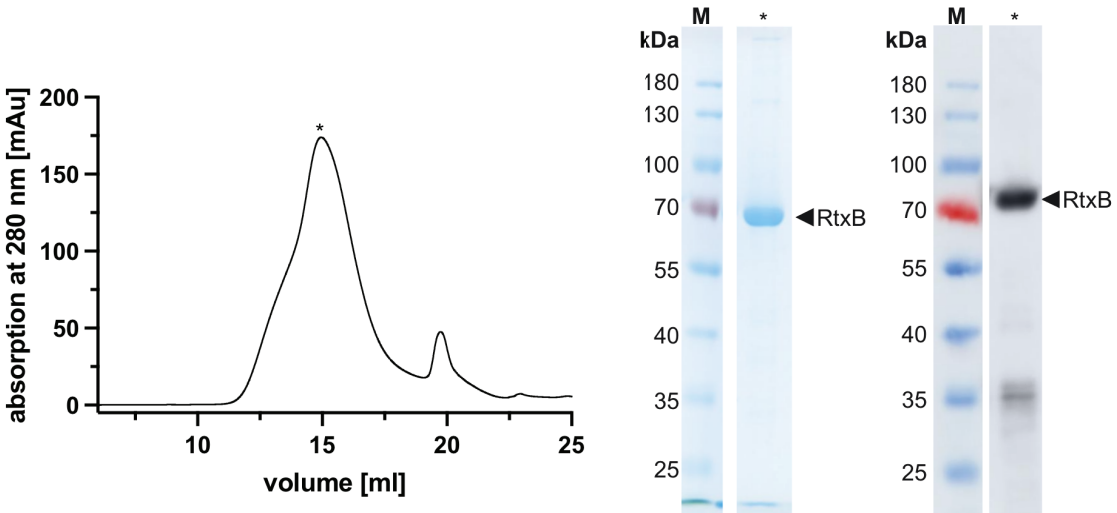

Figure 2: Purification of RtxB. A: *SEC analysis of RtxB on a Superose 6 Inc. 10/300 GL.* ***B:*** *SDS PAGE (left) and Western blot (right) analysis of purified RtxB. M: marker proteins with their approximated molecular weight. *: sample from RtxB main elution peak of the SEC. The band for RtxB is marked with a black triangle. Anti-PentaHis antibody was used for detection.*

RtxB was isolated with a high degree of purity and elutes as a single peak at 15 ml on a Superose 6 Inc 10/300 GL SEC column. For ATPase activity measurements and structure determination we used the fractions of the centre of the peak.

To investigate ATPase activity of RtxB we used the Malachite Green assay. We measured the amount of free phosphate after a reaction time of 40 min for ATP concentrations from 0 to 5 mM at 1 µM RtxB. Kinetic parameters for ATPase activity of RtxB were determined using an allosteric sigmoidal fit (Figure 3A). We calculated a maximum turnover rate (v_{max}) of ATP to ADP + P_i of 209 ± 10 nmol per mg protein and minute. Affinity of RtxB for ATP (k_{half}) was 0.46 ± 0.06 mM. The Hill slope (h) was 2.0 ± 0.5 showing positive cooperativity. To confirm that ATPase activity is derived from RtxB only, we used an ATPase deficient H662A mutant (RtxB-HA). RtxB-HA was purified and analyzed using the same protocols and showed no ATPase activity (Figure 3, red squares).

The homologous ABC transporter HlyB from *E. coli* shows tight regulation of its ATPase activity by the N-terminal C39 peptidase-like domain (CLD) [22]. To investigate whether this regulatory effect can be applied to RtxB as well, we constructed a chimeric protein taking the CLD of HlyB from *E. coli* and transmembrane domain (TMD) and nucleotide binding domain (NBD) of RtxB from *K. kingae* (RtxB-EKK). ATPase activity of RtxB-EKK was comparable to wildtype RtxB (v_{max} = 192 ± 8 nmol/(mg*min), k_{half} = 0.43 ± 0.05 mM and h = 2.0 ± 0.3). This indicates a very specific interplay in ATPase regulation between CLD and NBD in HlyB from *E. coli* which is not directly transferable to RtxB from *K. kingae*.

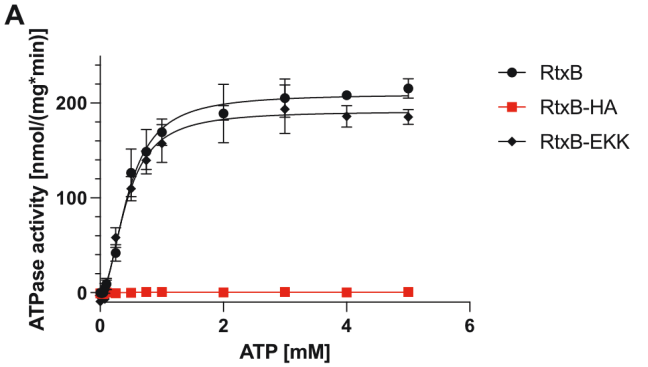

B

	k_{half} [mM]	v_{max} [nmol / (mg*min)]	h
RtxB	0.46 ± 0.06	209	2.0 ± 0.5
RtxB-HA	0.58	0.6	-
RtxB-EKK	0.43 ± 0.05	192	2.0 ± 0.3

Figure 3: ATPase activity of RtxB, RtxB-HA and RtxB-EKK for varying ATP concentrations*. RtxB, RtxB-HA and RtxB-EKK were used at a concentration of 1 µM. Activity was measured as a single point measurement after 40 minutes reaction time.* ***A:*** *Each datapoint with standard deviation is a mean value of three individual measurements.* ***B:*** *Kinetic parameters for each variant from an allosteric sigmoidal enzyme kinetics fit. Maximum enzyme velocity (v_{max}), substrate concentration necessary for half-maximal enzyme velocity (k_{half}) and hill slope (h) are displayed.*

ATPase activity of RtxB at various pH values

To further characterize RtxB and screen for optimal *in vitro* conditions we investigated the influence of the pH value on ATPase activity. ATPase activity was measured at 4 mM ATP in buffers ranging from pH 4 to pH 10. To adjust the pH RtxB was diluted to

1 µM with buffer of the desired pH. The highest ATPase activity for RtxB was observed at around pH 8 to 9. Almost no ATPase activity was detected at pH 4 and a decrease of activity compared to maximal activity was seen at pH 10.

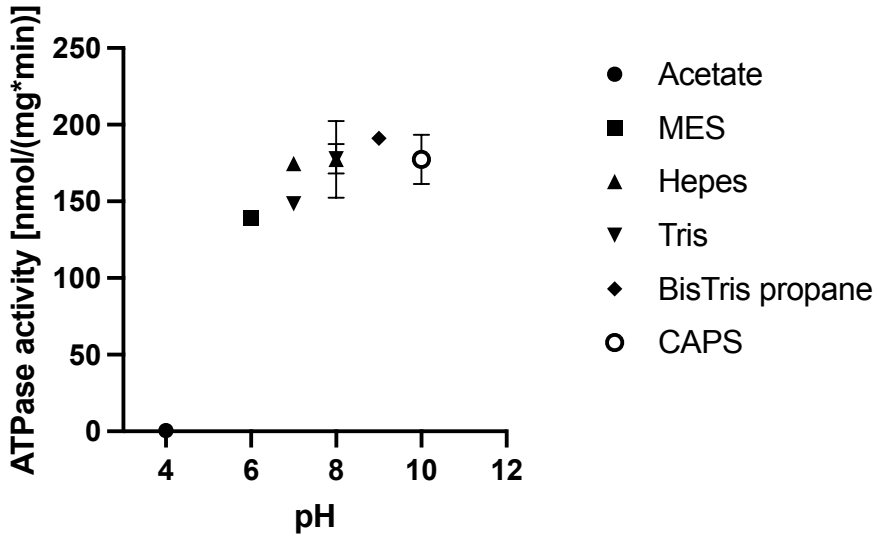

Figure 4: ATPase activity measurements of RtxB at different pH values. *Buffer components were used at a concentration of 20 mM. RtxB was used at a concentration of 1 µM and ATP at a final concentration of 4 mM. Activity was measured as a single point measurement after 40 min reaction time. Each datapoint with standard deviation is a mean value of at least 3 individual measurements.*

Reconstitution into MSP nanodisc

For reconstitution of purified RtxB into MSP based nanodisc, we used MSP1D1 and a lipid mixture of DOPE, DOPG and DOPC (molar lipid ratio 1:1:1). RtxB was mixed with MSP and lipids in a molar ratio of 1:1:75 (calculated for monomer of RtxB). For better separation of RtxB in nanodisc and lipid-only nanodisc we applied the sample on a Superdex 200 Inc. 10/300 GL column. Reconstituted RtxB elutes as a single peak at around 10.5 ml whereas lipid-only nanodiscs elute at 12 ml (Figure 5A). Bands for RtxB and MSP1D1 on the SDS PAGE confirm successful reconstitution. Furthermore the Western blot targeting the His-Tag of RtxB and MSP1D1 verifies protein identity (Figure 5B). RtxB reconstituted into a lipid bilayer shows slightly higher ATPase activity compared to RtxB in LMNG. V_{max} for RtxB in lipid nanodisc is 265 ± 14 nmol/(mg*min), k_{half} is 0.52 ± 0.06 mM and h = 2.3 ± 0.6 (Figure 5C and D).

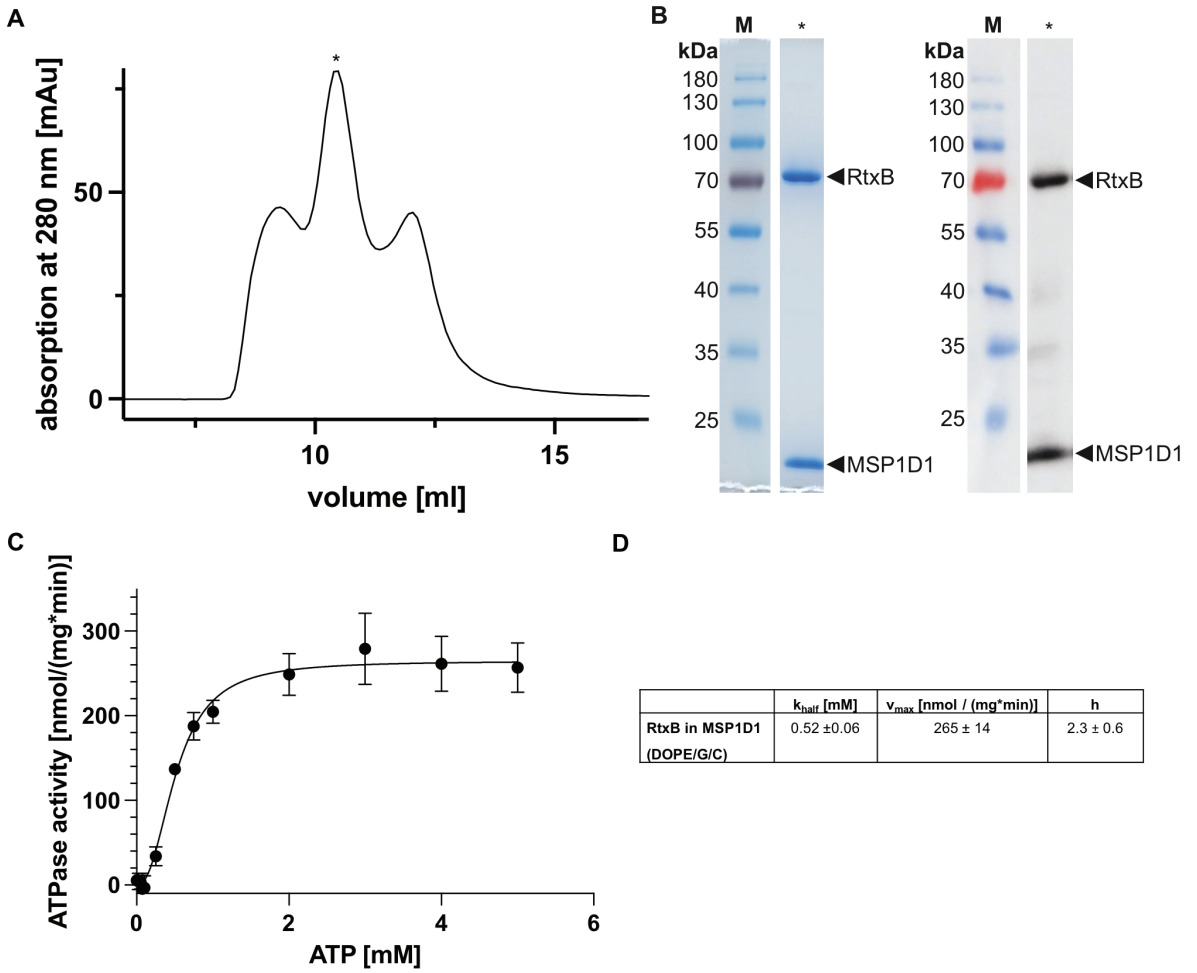

	k_{half} [mM]	v_{max} [nmol / (mg*min)]	h
RtxB in MSP1D1 (DOPE/G/C)	0.52 ±0.06	265 ± 14	2.3 ± 0.6

Figure 5: Reconstitution of RtxB using MSP1D1 and a lipid mixture of DOPE, DOPG and DOPC. A: *Gel filtration analysis of reconstituted RtxB on Superdex 200 Inc. 10/300 GL.* ***B:*** *SDS PAGE (left) and Western blot (right) analysis of reconstituted RtxB. M: marker proteins with their approximated molecular weight. *: Sample from reconstituted RtxB main elution peak. The bands for RtxB and MSP1D1 are marked with a black triangle. Anti-PentaHis antibody was used for detection.* ***C:*** *ATPase activity of reconstituted RtxB at different ATP concentrations. Activity was measured as a single point measurement after 40 minutes reaction time. Each datapoint with standard deviation is a mean value of 3 individual measurements.* ***D:*** *Kinetic parameters for each variant from an allosteric sigmoidal enzyme kinetics fit. Maximum enzyme velocity (v_{max}), Substrate concentration necessary for half-maximal enzyme velocity (k_{half}) and hill slope (h) are displayed.*

As RtxB showed slightly higher activity in a lipid bilayer compared to in a detergent micelle, we next wanted to further investigate the impact of a lipid bilayer. To test this we measured ATPase activity of reconstituted RtxB and detergent solubilized RtxB at different temperatures ranging from 15 to 60 °C (Figure 6). For all tested temperatures ATPase activity of RtxB is higher in nanodisc than in detergent micelle. RtxB in detergent shows an increase of ATPase activity from 15 to 42 °C, with highest ATPase activity of 360 nmol/(mg*min) at 42 °C and a decrease of activity at even higher temperatures. RtxB in nanodisc shows an increase in ATPase activity from 15 to 37 °C with highest ATPase activity of 465 nmol/(mg*min) at 37 °C. At higher temperatures ATPase activity remains the same. No decrease of ATPase activity is observed at

higher temperatures for RtxB reconstituted into nanodisc, as is the case for RtxB in a detergent micelle.

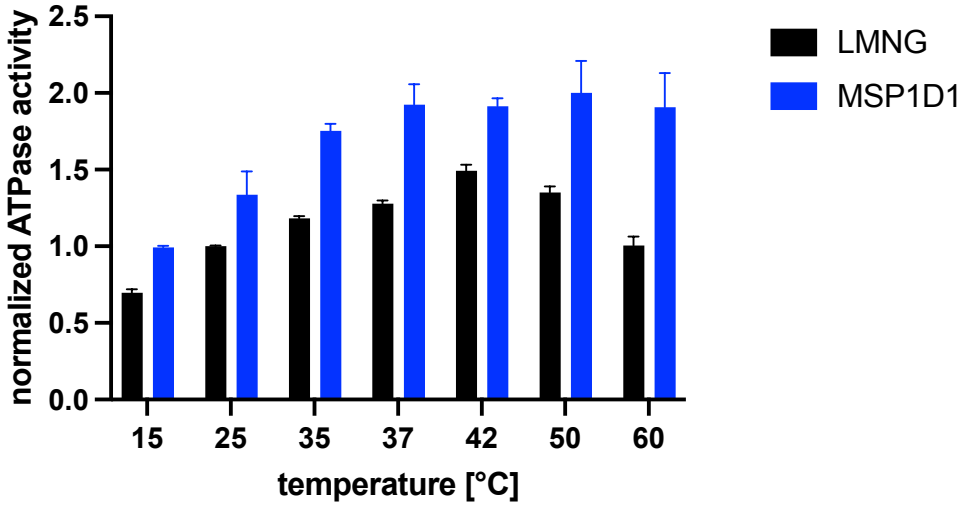

Figure 6: Normalized ATPase activity of RtxB in detergent and in nanodisc at different temperatures. *ATPase activity was normalized to RtxB activity at 25 °C in LMNG. ATP was used at a final concentration of 4 mM. Activity was measured as a single point measurement after 30 min reaction time. Each datapoint with standard deviation is a mean value of 3 individual measurements.*

Cryo-EM structure of RtxB in detergent

Structural investigation of RtxB were performed in detergent using single particle cryo-EM analysis. RtxB wildtype without additives was used for grid preparation. A first dataset resulted in a 3D class with an overall resolution of 6.3 Å according to FSC analysis (Figure 7A and B). The NBD, CLD and detergent micelle around the TMD are clearly visible. The angular distribution of the particles was promising (Figure 7C), but high intrinsic flexibility of the NBDs and CLDs limited the resolution so far. A second dataset was collected and image processing was performed with focus on the intrinsic less flexible TMD (Figure 7D – F).

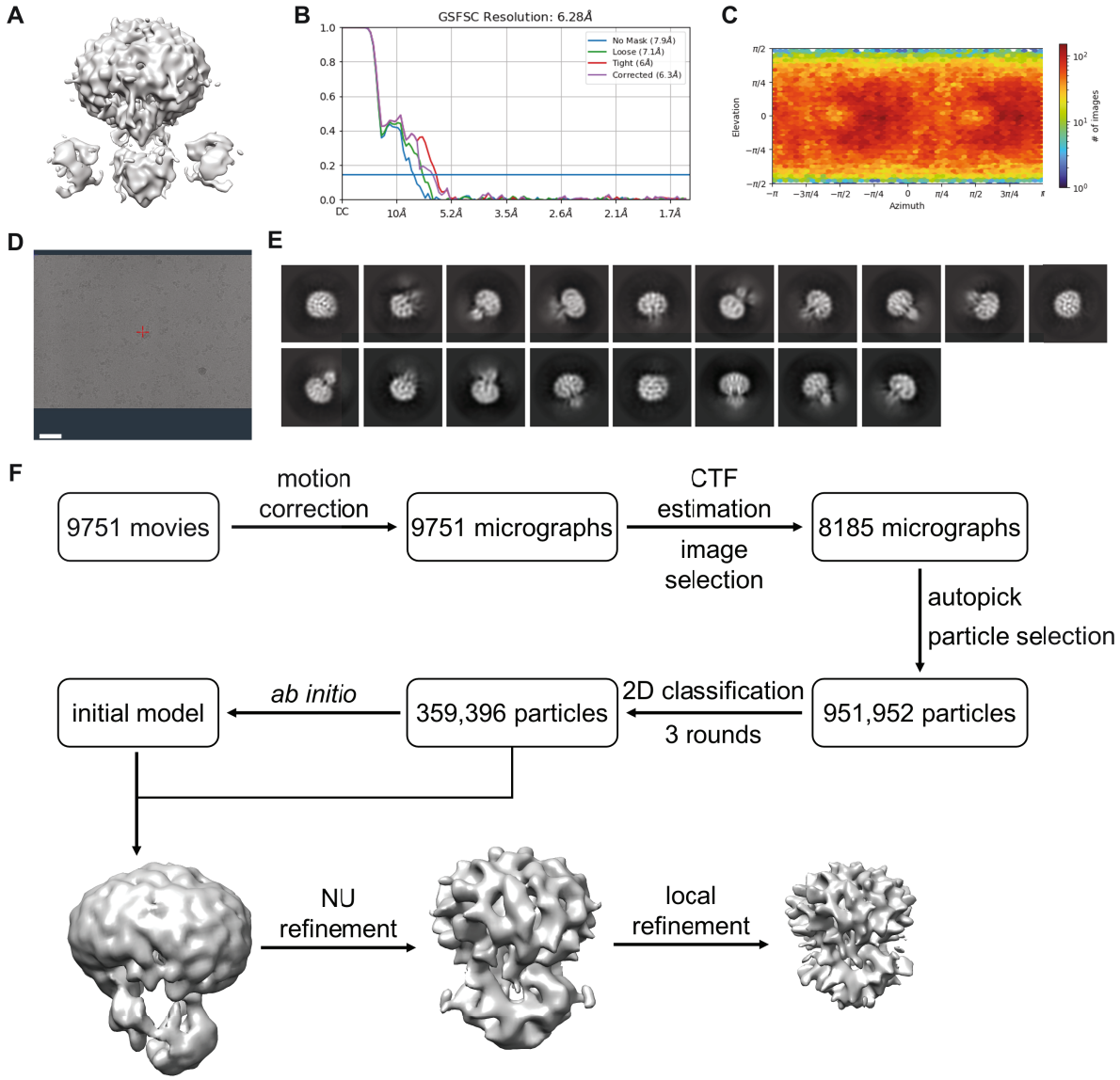

Figure 7: Single particle cryo-EM analysis of RtxB wildtype. *Please note this figure contains two different datasets (dataset 1: A – C and dataset 2: D – F). Refinement for dataset 1 focuses on the whole protein, whereas refinement of dataset 2 focuses on the TMD.* ***A:*** *3D class of RtxB wildtype dataset 1.* ***B:*** *Fourier shell correlation (FSC) curves. No mask (blue), loose (green) tight (red) and corrected (purple). Gold-standard FSC (GSFSC) with 6.3 Å resolution at 0.143.* ***C:*** *Azimuth plot of the particles included in the 3D class of RtxB wildtype dataset 1.* ***D:*** *Cryo-EM grid image of RtxB wildtype dataset 2. The white bar is 50 nm.* ***E:*** *2D classes of RtxB wildtype dataset 2.* ***F:*** *Image processing flowchart for RtxB wildtype dataset 2 with refinement focus on the TMD.*

Discussion

Over the past years it was shown that *K. kingae* is an emerging pathogen in paediatric invasive infections [6, 29]. One of the key players in *K. kingae* cytotoxicity is the toxin RtxA which is secreted via a T1SS system powered by the ABC transporter RtxB [16]. To being able to tackle the threat of invasive *K. kingae* infections it is indispensable to understand the mode of actions leading to secretion of the cytotoxin RtxA. One step

towards this goal is the functional purification and characterization of the ABC transporter RtxB described in this work.

RtxB was successfully produced in *E. coli* BL21(DE3) and purified in LMNG (Figure 2). We could determine a maximum basal ATPase activity of RtxB in LMNG of 209 ± 10 nmol/(mg*min) and could demonstrate for RtxB that histidine 662 is a crucial residue for ATPase activity (Figure 3) [26]. The closest biochemically described homolog of RtxB, HlyB from *E. coli* exhibits a 20-fold reduced maximum basal ATPase of 8 nmol/(mg*min) in LMNG [22]. Interestingly, the ATPase activity of HlyB from *E. coli* is tightly regulated by the N-terminal C39 peptidase-like domain (CLD) and increases approximately by the factor of 15 when the CLD is deleted. We investigated whether this regulating effect of the HlyB CLD can be applied on RtxB as well. Recently we could show that it is possible to swap domains of HlyB and RtxB and yet maintain at least partially native functionality (Anlauf et al., to be published). Our chimeric construct RtxB-EKK derived from the CLD of HlyB from *E. coli* and the transmembrane domain (TMD) and the nucleotide binding domain (NBD) of RtxB from *K. kingae* shows almost the same basal ATPase activity as wildtype RtxB and an identical k_{half} value (Figure 3). Therefore we conclude that the regulatory effect of the CLD on ATPase activity within HlyB is not transferable to the homologous transporter RtxB but underlies specific interactions within HlyB that are missing or different in RtxB.

RtxB shows highest ATPase activity at pH levels of 8 to 9 and no activity at pH 4 (Figure 4). With this pH optimum RtxB differs from its homolog HlyB from *E. coli* and other ABC transporters that showed a pH dependent maximum ATPase activity at close to neutral pH levels [30, 31].

We could show that reconstitution of RtxB into MSP based nanodiscs enhances ATPase activity of RtxB (Figure 5C and D) compared to detergent solubilized RtxB (Figure 3). This effect of increased activity in MSP based nanodisc compared to detergent solubilized protein was seen for the ABC transporter MsbA as well [32]. In addition, for HlyB the effect was even more striking as ATPase activity increased by the factor of 10 when reconstituted into SaposinA based lipid nanoparticles compared to LMNG [33]. A possible explanation is the proper orientation of the transporter and its domains in a lipid bilayer favouring ATP hydrolysis compared to a detergent micelle. A higher flexibility in a detergent micelle might favour certain conformations that are unable to bind or hydrolyse ATP and therefore reduce the maximum ATPase activity in detergent. Those effects are not only limited to the comparison of detergent vs lipid

bilayer but can also occur within different detergents as seen for LmrA [34]. Furthermore we could show that besides overall increased ATPase activity of reconstituted RtxB, ATPase activity of RtxB is preserved at elevated temperatures of up to 60 °C, when reconstituted in MSP based nanodiscs. This effect of thermal stabilization in nanodisc was also shown for DsbB increasing its unfolding midpoint melting temperature from about 50 °C in detergent to 70 °C in MSP based nanodisc [35]. Those results are in line with the stabilisation of membrane proteins in a lipid bilayer. This stabilizing effect might be even more increased by the constraining MSP wrapping around the lipid bilayer.

The structure of RtxB wildtype in LMNG is limited in resolution due to the high intrinsic flexibility of the NBD and CLD (Figure 7). A similar issue was recently reported for the peptide secreting ABC transporter ComA [36]. Here the use of the ATPase deficient mutant, different divalent cations or ATPγS and ATP helped to stabilize certain conformations and improve the resolution of the refined models to up to 2.8 Å. However, the cytosolic domain was not resolved anymore. It might also be possible to improve the resolution for RtxB, by using the ATPase deficient mutant RtxB H662A, ATPγS or different divalent cations.

Author contribution

FLB, SS and LS conceived the experiments and evaluated the data. FLB performed the experiments. SK performed the cryo-EM data collection. FLB wrote the initial draft. FLB, SK, SS and LS wrote the final version of the manuscript.

Funding

This work was supported by the Deutsche Forschungsgemeinschaft (DFG, CRC 1208 project A01 to LS).

Acknowledgement

We thank all former and current members of the Institute of Biochemistry for their support and productive discussions. We thank Prof. Dr. Carsten Sachse (Ernst-Ruska-Centre for Microscopy and Spectroscopy with Electrons, ER-C-3/Structural Biology,

Forschungszentrum Jülich) for access to the Electron Cryo-Microscopes. We thank the Center for Advanced Imaging (Faculty of Mathematics and Natural Sciences, Heinrich Heine University Düsseldorf) for access to the TEM for Negative Stain EM. We are grateful to Dr. Isabelle Erenburg for identification of the T1SS of *K. kingae*. We also thank Dr. Olivia Spitz for preliminary work on RtxB. In addition we thank Eymen Hachani for kindly providing MSP1D1.

References

1. Henriksen, S.D. and K. Bovre, *Moraxella kingii sp.nov., a haemolytic, saccharolytic species of the genus Moraxella.* J Gen Microbiol, 1968. **51**(3): p. 377-85.
2. Henriksen, S.D. and K. Bovre, *Transfer of Moraxella kingae Henriksen and Bøvre to the Genus Kingella gen. nov. in the Family Neisseriaceae.* International Journal of Systematic and Evolutionary Microbiology, 1976. **26**(4): p. 447-450.
3. Odum, L. and W. Frederiksen, *Identification and characterization of Kingella kingae.* Acta Pathol Microbiol Scand B, 1981. **89**(5): p. 311-5.
4. Henriksen, S.D., *Moraxella, Acinetobacter, and the Mimeae.* Bacteriol Rev, 1973. **37**(4): p. 522-61.
5. Yagupsky, P., *Diagnosing Kingella kingae infections in infants and young children.* Expert Rev Anti Infect Ther, 2017. **15**(10): p. 925-934.
6. Yagupsky, P., E. Porsch, and J.W. St Geme, 3rd, *Kingella kingae: an emerging pathogen in young children.* Pediatrics, 2011. **127**(3): p. 557-65.
7. Yagupsky, P., N. Peled, and O. Katz, *Epidemiological features of invasive Kingella kingae infections and respiratory carriage of the organism.* J Clin Microbiol, 2002. **40**(11): p. 4180-4.
8. Yagupsky, P., et al., *High prevalence of Kingella kingae in joint fluid from children with septic arthritis revealed by the BACTEC blood culture system.* J Clin Microbiol, 1992. **30**(5): p. 1278-81.
9. Yagupsky, P., *Kingella kingae: from medical rarity to an emerging paediatric pathogen.* Lancet Infect Dis, 2004. **4**(6): p. 358-67.
10. Yagupsky, P., et al., *Respiratory carriage of Kingella kingae among healthy children.* Pediatr Infect Dis J, 1995. **14**(8): p. 673-8.
11. Kiang, K.M., et al., *Outbreak of osteomyelitis/septic arthritis caused by Kingella kingae among child care center attendees.* Pediatrics, 2005. **116**(2): p. e206-13.
12. El Houmami, N., et al., *Patterns of Kingella kingae Disease Outbreaks.* Pediatr Infect Dis J, 2016. **35**(3): p. 340-6.
13. Kaplan, J.B., et al., *In vitro characterization of biofilms formed by Kingella kingae.* Mol Oral Microbiol, 2017. **32**(4): p. 341-353.
14. Chang, D.W., et al., *RTX toxin plays a key role in Kingella kingae virulence in an infant rat model.* Infect Immun, 2014. **82**(6): p. 2318-28.
15. Kehl-Fie, T.E. and J.W. St Geme, 3rd, *Identification and characterization of an RTX toxin in the emerging pathogen Kingella kingae.* J Bacteriol, 2007. **189**(2): p. 430-6.
16. Filipi, K., et al., *Kingella kingae RtxA Cytotoxin in the Context of Other RTX Toxins.* Microorganisms, 2022. **10**(3).

17. Spitz, O., et al., *Type I Secretion Systems-One Mechanism for All?* Microbiol Spectr, 2019. **7**(2).
18. Hollenstein, K., R.J. Dawson, and K.P. Locher, *Structure and mechanism of ABC transporter proteins.* Curr Opin Struct Biol, 2007. **17**(4): p. 412-8.
19. Biemans-Oldehinkel, E., M.K. Doeven, and B. Poolman, *ABC transporter architecture and regulatory roles of accessory domains.* FEBS Lett, 2006. **580**(4): p. 1023-35.
20. Kanonenberg, K., C.K. Schwarz, and L. Schmitt, *Type I secretion systems - a story of appendices.* Res Microbiol, 2013. **164**(6): p. 596-604.
21. Lecher, J., et al., *An RTX transporter tethers its unfolded substrate during secretion via a unique N-terminal domain.* Structure, 2012. **20**(10): p. 1778-87.
22. Reimann, S., et al., *Interdomain regulation of the ATPase activity of the ABC transporter haemolysin B from Escherichia coli.* Biochem J, 2016. **473**(16): p. 2471-83.
23. Ratkeviciute, G., B.F. Cooper, and T.J. Knowles, *Methods for the solubilisation of membrane proteins: the micelle-aneous world of membrane protein solubilisation.* Biochem Soc Trans, 2021. **49**(4): p. 1763-1777.
24. Young, J.W., *Recent advances in membrane mimetics for membrane protein research.* Biochem Soc Trans, 2023. **51**(3): p. 1405-1416.
25. Ritchie, T.K., et al., *Chapter 11 - Reconstitution of membrane proteins in phospholipid bilayer nanodiscs.* Methods Enzymol, 2009. **464**: p. 211-31.
26. Zaitseva, J., et al., *H662 is the linchpin of ATP hydrolysis in the nucleotide-binding domain of the ABC transporter HlyB.* EMBO J, 2005. **24**(11): p. 1901-10.
27. Gibson, D.G., *Enzymatic assembly of overlapping DNA fragments.* Methods Enzymol, 2011. **498**: p. 349-61.
28. Baykov, A.A., O.A. Evtushenko, and S.M. Avaeva, *A malachite green procedure for orthophosphate determination and its use in alkaline phosphatase-based enzyme immunoassay.* Anal Biochem, 1988. **171**(2): p. 266-70.
29. Gouveia, C., et al., *Kingella kingae Displaced S. aureus as the Most Common Cause of Acute Septic Arthritis in Children of All Ages.* Pediatr Infect Dis J, 2021. **40**(7): p. 623-627.
30. Liu, C.E., P.Q. Liu, and G.F. Ames, *Characterization of the adenosine triphosphatase activity of the periplasmic histidine permease, a traffic ATPase (ABC transporter).* J Biol Chem, 1997. **272**(35): p. 21883-91.
31. Zaitseva, J., et al., *Functional characterization and ATP-induced dimerization of the isolated ABC-domain of the haemolysin B transporter.* Biochemistry, 2005. **44**(28): p. 9680-90.
32. Arana, M.R., M.C. Fiori, and G.A. Altenberg, *Functional and structural comparison of the ABC exporter MsbA studied in detergent and reconstituted in nanodiscs.* Biochem Biophys Res Commun, 2019. **512**(3): p. 448-452.
33. Kanonenberg, K., S.H.J. Smits, and L. Schmitt, *Functional Reconstitution of HlyB, a Type I Secretion ABC Transporter, in Saposin-A Nanoparticles.* Sci Rep, 2019. **9**(1): p. 8436.
34. Infed, N., et al., *Influence of detergents on the activity of the ABC transporter LmrA.* Biochim Biophys Acta, 2011. **1808**(9): p. 2313-21.
35. Selvasingh, J.A., et al., *Dark nanodiscs as a model membrane for evaluating membrane protein thermostability by differential scanning fluorimetry.* bioRxiv, 2023.
36. Yu, L., et al., *Structural basis of peptide secretion for Quorum sensing by ComA.* Nat Commun, 2023. **14**(1): p. 7178.

Supplemental Information

Table S1: Primers used for cloning. *Small letters indicate bases that introduce mutation or are overhangs for Gibson Assembly and do not match the template sequence.*

Name	Sequence (5' – 3')	Purpose
RtxB_HA_fw	GATTATCGCGgcgCGATTATCTACGGTTCGCCAC	Introduction of H662A mutant into pBEX_RtxB
RtxB_HA_rev	AGTACCGTCCGTCCCTGA	Introduction of H662A mutant into pBEX_RtxB
RtxB_ΔCLD_fw	tattcttatcGCATCTCGCGCATCCGTG	Amplification of RtxB without the CLD and introduction of overhangs matching sequence of HlyB_CLD
RtxB_ΔCLD_rev	aagaatcagaTGGACCTTGAAACAAAACTTCTAAATGATG	Amplification of RtxB without the CLD and introduction of overhangs matching sequence of HlyB-CLD
HlyB_CLD_fw	tcaaggtccaTCTGATTCTTGTCATAAAATTG	Amplification of HlyB-CLD and introduction of overhangs matching RtxB sequence
HlyB_CLD_rev	cgcgagatgcGATAAGAATAATATGCCCCTG	Amplification of HlyB_CLD and introduction of overhangs matching RtxB sequence

Table S2: Buffers used for pH dependent ATPase activity measurements.

pH	Buffer substance	Additives
4	20 mM Na-acetate	150 mM NaCl, 0.002 % LMNG
6	20 mM MES	150 mM NaCl, 0.002 % LMNG
7	20 mM Hepes	150 mM NaCl, 0.002 % LMNG
7	20 mM Tris	150 mM NaCl, 0.002 % LMNG
8	20 mM Hepes	150 mM NaCl, 0.002 % LMNG
8	20 mM Tris	150 mM NaCl, 0.002 % LMNG
9	20 mM BisTris propane	150 mM NaCl, 0.002 % LMNG
10	20 mM CAPS	150 mM NaCl, 0.002 % LMNG

Table S3: Top three hits from MS results from RtxB gel slice at approx. 70 kDa after SEC.

Protein	Peptides	Unique peptides	Sequence coverage [%]	Mol. weight [kDa]	Q-value	Score	Intensity	MS/MS count
RtxB	39	39	60	81	0	323	5.71E+10	3045
DnaK	23	23	43	69	0	221	2.3E+08	88
FtsH	14	14	28	71	0	118	78962000	33

4. Discussion

The research object of this thesis was the hemolysin A type 1 secretion system (HlyA T1SS) from uropathogenic *E. coli*. T1SSs in general are present in Gram-negative bacteria and enable transport from inside the cell to the extracellular space in one single step without periplasmic intermediate(s). Besides the substrate, which usually determines the name of the T1SS, they contain an ATP-binding cassette (ABC) transporter, a membrane fusion protein (MFP) and an outer membrane protein (OMP). The ABC transporter and the MFP are located in the inner membrane (IM) and form the so-called inner membrane complex (IMC). As the name suggests, the OMP is located in the outer membrane (OM). In case of the HlyA T1SS the substrate is the repeats in toxin (RTX) protein HlyA, the ABC transporter is HlyB, the MFP is HlyD and the OMP is TolC. Although known for more than 70 years, the precise architecture of the system as well as its functional details are not fully understood [143]. We still do not know for instance how a substrate of 1024 amino acids can be secreted by the ABC transporter HlyB or in which way lipids can influence the secretion efficiency. Neither do we know how many ATP molecules are needed per transported substrate molecule or what the molecular details are that confer substrate specificity on the transporter side.

To tackle these question we need an appropriate experimental set-up. Therefore the main aim of this thesis was to establish the *in vitro* reconstitution of the HlyA T1SS. This requires solid purification and reconstitution protocols for the individual components of the secretion channel. The protocols for the purification of a truncated substrate variant, so-called HlyA1, as well as for the purification and reconstitution of the OMP TolC were already established [205]. For the ABC transporter HlyB as well as the IMC, the expression, purification and reconstitution protocols had to be adjusted or newly established for the needs of this thesis [151]. Therefore, additional aims of this thesis were the expression, purification and reconstitution of the ABC transporter HlyB as well as the IMC with the goal to obtain functional and structural data. Furthermore an aim was the biochemical and structural characterisation of RtxB from *Kingella kingae*, an ABC transporter homologous to HlyB from *E. coli*. The corresponding T1SS might serve as an alternative system in future studies.

4.1. The *in vitro* reconstitution of the HlyA T1SS

The main aim of this thesis was to establish an *in vitro* reconstitution of the HlyA T1SS. For this, the OMP TolC was reconstituted in the membrane of a vesicle and the IMC was reconstituted in lipid nanoparticles such as a MSP-based nanodisc. As a substrate for the *in vitro* assay the truncated secretion competent construct HlyA1 was used. It was possible to show as a proof of principle that the in vitro reconstitution of the HlyA T1SS was successful and *in vitro* secretion was observed (Chapter 5).

To study the secretion process of the HlyA T1SS *in vitro* allows for a precise control of the system's environment and results in a low level of interfering reactions and events. This way it will be possible to determine for instance the number of hydrolysed ATP molecules per transported substrate molecule or influences of external stimuli such as different pH or antibiotics. Furthermore an *in vitro* set up allows to study the hierarchy of assembly and transport mechanism, as seen for the tripartite efflux system MacAB-TolC [207]. Here the *in vitro* set up was used to clarify the role of ATP hydrolysis within the mechano-transmission mechanism [207]. Furthermore, it is possible to use a giant unilamellar vesicle (GUV) instead of a small liposome for TolC reconstitution (unpublished data). This would allow to directly monitor the transport of a fluorescently labelled substrate via confocal or super-resolution fluorescence microscopy as seen for Ca^{2+} efflux via SERCA [208, 209]. Highly advanced systems already allow for 3D imaging of GUVs with single molecule sensitivity [210].

A downside of this established *in vitro* set up so far is that the read out via Western blot analysis only reports successful transport (Chapter 5, Figure 5). Especially for the study of the assembly of the T1SS it would be interesting to have a read out for the assembly itself. Here the flotation assay, used for the validation of the TolC reconstitution (Chapter 5, Figure 3), can be used as a read out for assembly of the whole T1SS as well. It was shown previously for SecA that during such a liposome flotation assay proteins externally bound to the liposomes stay with the liposome [211]. Such a readout for the assembly of the HlyA T1SS would also allow to determine the bottleneck of the yet low transport efficiency (less than 1%) for the *in vitro* transport assay (Chapter 5, Figure 5). So far it remains elusive whether the transport itself is hampered in the *in vitro* set up or the number of assembled T1SSs is just not sufficient. This raises the question what stabilizes the tripartite assembly. It was shown for MacA-TolC, EmrA-TolC and AcrA-TolC that the interaction of MFP and TolC scales with the

oligomerisation kinetics of the MFP [195]. MacA forms a hexameric assembly in crystals, while AcrA and HlyD only show dimeric assemblies [186, 212, 213]. This might already indicate a rather weak interaction between HlyD and TolC and reveal a possible bottleneck of the *in vitro* assembly. A detailed investigation of the requirements for assembly and incubation time needed for the IMC and TolC would be helpful in the future. Surface plasmon resonance (SPR) studies as performed for the MacAB-TolC-like DevBCA-TolC system from the cyanobacterium *Anabaena sp*. PCC 7120, could shed light on the assembly mechanism of the HlyA T1SS [214]. For DevBCA-TolC the hexameric assembly of the MFP DevB was crucial for TolC interaction and export activity of the system [214]. Whether HlyD needs to form a hexameric assembly with its alpha-helical domains prior to TolC recruitment or whether the assembly occurs in a stepwise manner, needs to be answered in the future. The periplasmic part of HlyD alone does not form a stable hexameric assembly as seen from its crystal structure and even within the IMC the periplasmic part of HlyD exhibits a high flexibility [154, 186]. Thus, the question remains what else stabilizes the T1SS assembly. As the recruitment of TolC requires substrate recognition via HlyD, it is likely that binding of the substrate to HlyD induces a change in the conformation or an increase in oligomer stability [172]. Substrate bound structures are therefore of great importance.

It should also be taken into account, that there might be other factors or proteins involved in HlyA T1SS assembly besides the actual proteins building the translocation channel like HlyB, HlyD and TolC, or the substrate HlyA. Small proteins with less than 100 amino acids for instance can play important roles in membrane protein complex stability or even function as seen for AcrAB-TolC and the small protein AcrZ [215, 216]. AcrZ is supposed to directly influence the ability of AcrAB-TolC to export certain classes of antibiotics [217]. In *E. coli* numerous of those small proteins have been discovered and about 30% of them are localised at or to the membrane [218]. Taken this information into account and the fact that TolC for instance is also not part of the *hly* operon, it might be possible that more than just four proteins are involved in the assembly and secretion of HlyA.

A possible influence of the peptidoglycan layer on HlyA T1SS stability was left unconsidered so far. However it is known for other tripartite export systems, that some parts of their assembly interact with the peptidoglycan layer. *In situ* and crosslinking studies for example showed an interaction of AcrA with the peptidoglycan [194]. In

addition, an interaction between MexA and the peptidoglycan layer was observed and a potential stabilizing role for its quaternary structure was suggested [219]. The requirement of such a peptidoglycan stabilisation for the HlyA T1SS would add another level of complexity to the *in vitro* set-up. On the other hand the *in vitro* assembly of the tripartite MacAB-TolC system did not require additional peptidoglycan stabilisation [207]. But as discussed earlier, MacA most likely exhibits a much more stable oligomeric assembly than HlyD.

To increase stability *in vitro*, it might be beneficial to force the IMC in the nanodisc and TolC in the liposome into spatial proximity to promote assembly. *In vivo* the membrane architecture allows only lateral diffusion of the components of the T1SS as they are embedded in the inner and outer membrane. When reconstituted, the membrane proteins behave like soluble particles in solution which can diffuse in three dimensions. By using anchor lipids such as NTA lipids in one compartment and a histidine-tag in the other compartment one could force the components into spatial proximity (Figure 1) [220, 221]. Additional options are the use of biotinylated lipids or an exposed strep-tag on one of the proteins. Other membrane anchors besides lipids or proteins might be applicable as well as shown for a synthetic vesicle-to-vesicle communication system [222]. However, a detailed analysis of possible linker length and characteristic is necessary, to have and keep the right distance between both components.

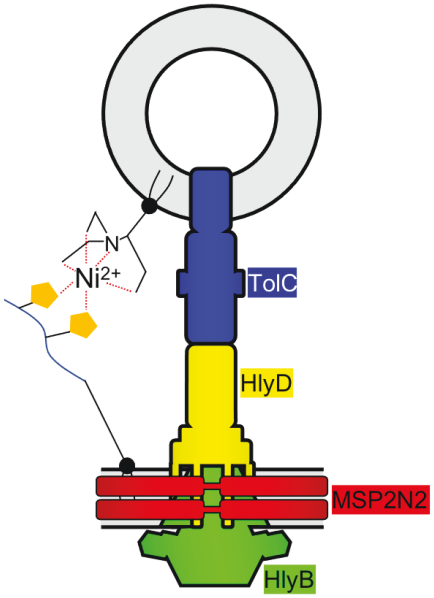

Figure 11: Schematic of the HlyA T1SS assembled in vitro with the help of NiNTA lipids and a histidine-tag. *TolC (blue) is reconstituted in a liposome and HlyB (green) and HlyD (yellow) are reconstituted into MSP (red) based nanodisc. The liposome contains lipids with a NiNTA headgroup modification (black lines, Ni^{2+}). The nanodisc contains lipids with a poly-histidine tag headgroup modification (black lines, blue line, yellow pentagons). Interaction with the Ni^{2+} ion are indicated by red dotted lines. This figure makes no claim to the accuracy of the stoichiometry or scale.*

On the way to the development of the *in vitro* reconstitution of the HlyA T1SS, a co-reconstitution of separately purified HlyB and HlyD was tested (Chapter 4). Self-assembly of a tripartite system was successfully shown previously for MexAB-OprM by mixing separately purified components [223]. However, the co-reconstitution of the IMC formed by HlyB and HlyD was only partly successful. We could observe a co-elution of both components after affinity purification, but faced issues in the stability of this assembly (Chapter 4, Figure 7, 8 and 9). Before the recently published structure of the IMC revealed its stoichiometric ratio, the molar ratio of HlyB to HlyD in the IMC was expected to be 2 : 3 or 1 : 3, as crosslinking studies detected a trimeric assembly of HlyD [172]. As our investigations regarding co-reconstitution of the IMC were performed before the cryo-EM structure was published, we used a molar ratio of HlyB to HlyD of 1 : 3. The recently published structure of the IMC revealed a ratio of HlyB to HlyD of 1: 1 with six copies of each forming a trimer of dimers of HlyB and a hexamer of HlyD [154]. This implicates that the amount of HlyB used for our co-reconstitution was too little to fully assemble stable complexes and might explain our stability issues (Chapter 4). Now that the structure of the IMC of the HlyA T1SS is known, the idea of an artificial co-reconstitution is even more tempting. An assembly by simply mixing all components would allow to incorporate specific defects such as an IMC with one ATPase deficient dimer or incorporation of modified HlyD molecules. Of course such an incorporation would be stochastically driven and requires further validation.

4.2. Membrane protein purification for structural or functional analysis

As this thesis dealt with membrane protein purification and reconstitution, it is important to consider the requirements for the sample for the different subsequent analyses. While a low purity might be sufficient for an activity assay, it will be problematic for structural analysis. It is possible, for instance, to measure ATPase activity of the H^+-ATPase from yeast from crude membranes when having the right controls for a specific readout [224, 225]. In contrast, when preparing samples for structural analysis, the aim is usually to achieve the highest purity possible. However, a highly purified protein might not be active because it might lack its interaction partners or activation factors. In the case of a membrane protein even the detergent that enables a high purity can

be the sub-optimal environment for activity. Closely connected to the choice of the detergent, the significance of lipids for membrane protein structure, oligomerisation and function is becoming ever clearer [226]. The purification of HlyB for instance (Chapter 2) showed that although purification of HlyB in LPG (Chapter 2, Figure 3) allowed for a high purity protein preparation, no ATPase activity was detected. Reasons for this can be diverse, such as altering of the functional structure due to the detergent or missing lipids for activity. On the other hand, the already existing protocol for HlyB purification enabled functional studies, but did not result in a sample appropriate for structural analysis and therefore required adjustments (Chapter 2) [151].

Another issue for sample preparation lies within the flexibility of a protein. While a certain degree of flexibility is usually required for activity it is problematic for high-resolution structure determination. Mutants can be used to reduce flexibility or additives can be used to trap certain conformations, but it is always important to verify how far these interventions influence the protein activity. An ABC transporter adopts several different conformations under turnover conditions which requires flexibility and movement of certain parts of the protein [179, 227, 228]. But flexible parts usually do not resolve to high resolution in cryo-EM structures. This issue is especially important for HlyB (Chapter 2) and RtxB (Chapter 6) as they both have an additional N-terminal domain, the so-called CLD, that shows high flexibility. This was also observed in the structure of the IMC, where only one of the two CLDs was resolved [154]. In the 3D class for RtxB a density for the CLDs is visible but the resolution is limited due to the high flexibility of the CLDs (Chapter 6, Figure 7). An idea to reduce flexibility of the CLD of RtxB would be to add potential binding partners, such as the substrate or the MFP. For the RtxB homolog HlyB it was shown that substrate and MFP interact with the CLD [154, 177]. Therefore binding of the CLD to the interaction partners will most likely stabilize a certain conformation. Another option to lower flexibility and improve the resolution is to use the ATPase deficient mutant in combination with ATP or to add non hydrolysable ATP (ATPγS) as it was done for ComA, an ABC transporter that also contains a highly flexible N-terminal domain [229]. For ComA this approach trapped different conformations of the ABC transporter and enabled caption of high resolution structures.

Besides intrinsic flexibility of the protein, the detergents and additives used for membrane protein purification can prevent the acquisition of high-resolution structures

[230]. Therefore methods to remove excess detergent prior to cryo-EM grid preparation, such as GraDeR [231], or the use of membrane mimetics to avoid detergent at the step of grid preparation [230] are more and more important. Also the 2D classes in this thesis for HlyB (Chapter 2, Figure 1) and RtxB (Chapter 6, Figure 7) were derived from samples in detergent. Especially for the detergent LMNG, which was used for RtxB it is known that removing free excess LMNG is rather difficult, but simplifies high-resolution data acquisition [231]. A recently published systematic analysis of high-resolution membrane protein structures listed the detergents and additives used at the different steps of purification and structure determination [232]. This would be a good starting point for improvement of the structural data of RtxB and HlyB in the future. LMNG, as used for RtxB, is among the very often used detergents for membrane protein purification for high-resolution structure determination, however, in the subsequent steps of structure determination it is often mixed with the detergent GDN or additives like cholesteryl hemisuccinate [232]. Furthermore many of the high-resolution structures were derived from membrane proteins in nanodisc [232]. As reconstitution of HlyB (Chapter 3, Figure 7) as well as RtxB (Chapter 6, Figure 5) into nanodiscs was successful, it is coherent to use those samples for structural analysis in the future.

4.3. The RtxA T1SS from *Kingella kingae* and other homologous systems

K. kingae is an emerging pathogen in children at the age between 6 and 48 month. The RtxA T1SS from *K. kingae* is a homologous system to the already well studied HlyA T1SS from uropathogenic *E. coli* [206]. To study homologous systems, besides well-established systems can be beneficial for structure determination, as homologous systems might exhibit a higher stability. Furthermore, to have structures of multiple homologous systems can provide valuable insights into conserved structural motifs. On the other hand it is important to study homologous systems, as it allows to determine structural as well as biochemical differences that might be derived from adaption to the biological niche of the individual organism or from other specific adaptions.

For the ABC transporter RtxB a 20-fold higher basal ATPase activity compared to HlyB was detected in the detergent LMNG (Chapter 6, Figure 3). The ATPase activity of HlyB is rather low and is regulated via the N-terminal domain, the so-called CLD [150]. A 10-fold increase in ATPase activity of HlyB was observed when deleting the CLD [150]. This regulating effect of the CLD from HlyB is not transferable to RtxB as seen from the ATPase activity of RtxB and the chimeric RtxB containing the CLD of HlyB in this thesis (Chapter 6, Figure 3). Furthermore, sequence and structure alignments revealed a striking difference between the CLD of RtxB and HlyB (Figure 2). Residue 82 is an arginine residue in the CLD of HlyB that was shown to interact with the substrate HlyA [154, 177]. In the CLD of RtxB the equivalent residue is an aspartate residue, that alters the surface charge at this position drastically, from positive/neutral to negative (Figure 2 C and D).

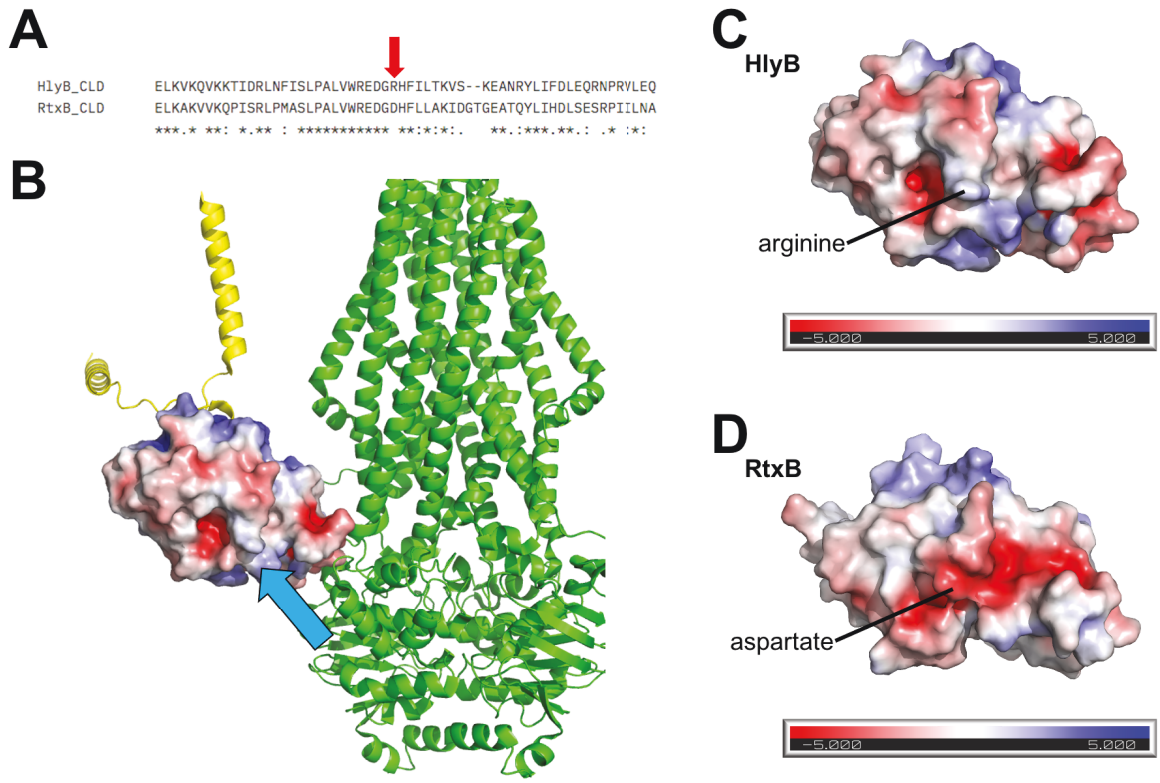

Figure 12: Comparison of the CLD from HlyB and RtxB. A: *Sequence comparison of CLD of HlyB and RtxB. The sequence of HlyB is shown from residue 54 to 111. The sequence of RtxB is shown from residue 53 to 112. An * indicates identical residues, a : indicates residues with strongly similar properties and a . indicates residues with weakly similar properties. A red arrow highlights residue 82 in HlyB CLD and residue 81 in RtxB CLD.* ***B:*** *Cryo-EM structure of the IMC with a focus on the CLD of HlyB. The HlyB dimer is shown as a cartoon representation in green and the interacting HlyD is shown in a cartoon representation in yellow (PDB: 7SGR). The CLD of HlyB is shown as surface representation with indicated electrostatics from the APBS Electrostatics Plugin from PyMOL with values ranging from -5 (red) to 5 (blue). The viewing angle for part C and D is indicated by a light blue arrow* ***C:*** *The CLD of HlyB shown as surface representation with indicated electrostatics from the APBS Electrostatics Plugin from PyMOL with values ranging from -5 (red) to 5 (blue) and viewed from the cytosolic side. Arginine 82 is indicated. (PDB: 7SGR)* ***D:*** *The CLD of RtxB shown as surface representation with indicated electrostatics from the APBS Electrostatics Plugin from PyMOL with values ranging from -5 (red) to 5 (blue) and viewed from the cytosolic side. Aspartate 81 is indicated. (PDB: AF-A0A1X7QMJ5-F1).*

As this residue is involved in substrate binding it might be a key residue for substrate specificity. This finding is in line with the recently proposed substrate recognition mechanism conferred by a dual recognition of the substrate via the CLD and the NBD of the ABC transporter [153]. While the NBD is binding the amphipathic helix of the secretion signal, the CLD is binding within the RTX domain [153, 177, 205]. It was shown that the distance between the amphipathic helix and the RTX domain has a severe influence on the secretion efficiency. In addition to the distance a specific interaction of the CLD and residues close to or inside the RTX domain might be important for substrate specificity as well (Figure 2). This brings up the question where the specificity is derived from within the RTX domain, as the RTX motif is conserved among the substrates [155]. Structures and biochemical analysis of RtxB and RtxA as well as of other homologs and their substrates might provide an answer to this question in the future. A high resolution structure of RtxB with the substrate bound would allow first conclusions. Substrate interaction studies between RtxB and RtxA and other substrates of the T1SS RTX protein family could elucidate further on this assumption. Beyond this, it is important to study homologous systems as it broadens our knowledge and allows to define systems or redefine them with the help of novel findings. The more information we have the more precise the differentiation between two systems or the organisation within a system can be. Which in turn helps us to better understand them. The T1SS for instance is characterized by a single secretion step from the cytosol to the extracellular space without periplasmic intermediates [131]. However recent findings challenge this single step mechanism, and systems that possess periplasmic intermediates were described [8]. By continuous investigation of systems and its homologs it is possible to decipher whether complete new findings are just an exception to the rule or a newly discovered feature.

To conclude, within the framework of this thesis the *in vitro* reconstitution of the HlyA T1SS from *E. coli* was established. In addition, as a proof of principle a substrate secretion assay was successfully performed for this *in vitro* reconstituted system. This enables *in vitro* investigations of the system in the future to answer questions such as how many ATP molecules are needed for the secretion of one substrate molecule. Furthermore, the ABC transporter RtxB from the homologous RtxA T1SS from *Kingella kingae* was successfully purified and biochemically characterised. First structural investigations enabled a rough overview on the structure. Improvements in sample

quality and data acquisition will hopefully allow for a high-resolution structure of RtxB in the near future.

5. References

1. Rajagopal, M. and S. Walker, *Envelope Structures of Gram-Positive Bacteria.* Curr Top Microbiol Immunol, 2017. **404**: p. 1-44.
2. Maher, C. and K.A. Hassan, *The Gram-negative permeability barrier: tipping the balance of the in and the out.* mBio, 2023: p. e0120523.
3. Joyce, L.R. and K.S. Doran, *Gram-positive bacterial membrane lipids at the host-pathogen interface.* PLoS Pathog, 2023. **19**(1): p. e1011026.
4. Morein, S., et al., *Wild-type Escherichia coli cells regulate the membrane lipid composition in a "window" between gel and non-lamellar structures.* J Biol Chem, 1996. **271**(12): p. 6801-9.
5. Silhavy, T.J., D. Kahne, and S. Walker, *The bacterial cell envelope.* Cold Spring Harb Perspect Biol, 2010. **2**(5): p. a000414.
6. Christie, P.J., *The Rich Tapestry of Bacterial Protein Translocation Systems.* Protein J, 2019. **38**(4): p. 389-408.
7. Spitz, O., et al., *Type I Secretion Systems-One Mechanism for All?* Microbiol Spectr, 2019. **7**(2).
8. Hodges, F.J., et al., *Redefining the bacterial Type I protein secretion system.* Adv Microb Physiol, 2023. **82**: p. 155-204.
9. Costa, T.R., et al., *Secretion systems in Gram-negative bacteria: structural and mechanistic insights.* Nat Rev Microbiol, 2015. **13**(6): p. 343-59.
10. Tsirigotaki, A., et al., *Protein export through the bacterial Sec pathway.* Nat Rev Microbiol, 2017. **15**(1): p. 21-36.
11. Tanaka, Y., et al., *Crystal Structures of SecYEG in Lipidic Cubic Phase Elucidate a Precise Resting and a Peptide-Bound State.* Cell Rep, 2015. **13**(8): p. 1561-8.
12. Van den Berg, B., et al., *X-ray structure of a protein-conducting channel.* Nature, 2004. **427**(6969): p. 36-44.
13. Tam, P.C., et al., *Investigating the SecY plug movement at the SecYEG translocation channel.* EMBO J, 2005. **24**(19): p. 3380-8.
14. Li, W., et al., *The plug domain of the SecY protein stabilizes the closed state of the translocation channel and maintains a membrane seal.* Mol Cell, 2007. **26**(4): p. 511-21.
15. Papanikou, E., S. Karamanou, and A. Economou, *Bacterial protein secretion through the translocase nanomachine.* Nat Rev Microbiol, 2007. **5**(11): p. 839-51.
16. Crane, J.M. and L.L. Randall, *The Sec System: Protein Export in Escherichia coli.* EcoSal Plus, 2017. **7**(2).
17. Randall, L.L., *Peptide binding by chaperone SecB: implications for recognition of nonnative structure.* Science, 1992. **257**(5067): p. 241-5.
18. Driessen, A.J., P. Fekkes, and J.P. van der Wolk, *The Sec system.* Curr Opin Microbiol, 1998. **1**(2): p. 216-22.
19. Green, E.R. and J. Mecsas, *Bacterial Secretion Systems: An Overview.* Microbiol Spectr, 2016. **4**(1).
20. Lee, H.C. and H.D. Bernstein, *The targeting pathway of Escherichia coli presecretory and integral membrane proteins is specified by the hydrophobicity of the targeting signal.* Proc Natl Acad Sci U S A, 2001. **98**(6): p. 3471-6.
21. Froderberg, L., et al., *Targeting and translocation of two lipoproteins in Escherichia coli via the SRP/Sec/YidC pathway.* J Biol Chem, 2004. **279**(30): p. 31026-32.

22. du Plessis, D.J., et al., *The lateral gate of SecYEG opens during protein translocation.* J Biol Chem, 2009. **284**(23): p. 15805-14.
23. Egea, P.F. and R.M. Stroud, *Lateral opening of a translocon upon entry of protein suggests the mechanism of insertion into membranes.* Proc Natl Acad Sci U S A, 2010. **107**(40): p. 17182-7.
24. Lill, R., et al., *SecA protein hydrolyzes ATP and is an essential component of the protein translocation ATPase of Escherichia coli.* EMBO J, 1989. **8**(3): p. 961-6.
25. Schiebel, E., et al., *Delta mu H+ and ATP function at different steps of the catalytic cycle of preprotein translocase.* Cell, 1991. **64**(5): p. 927-39.
26. Paetzel, M., et al., *Signal peptidases.* Chem Rev, 2002. **102**(12): p. 4549-80.
27. Palmer, T. and B.C. Berks, *The twin-arginine translocation (Tat) protein export pathway.* Nat Rev Microbiol, 2012. **10**(7): p. 483-96.
28. Simone, D., et al., *Diversity and evolution of bacterial twin arginine translocase protein, TatC, reveals a protein secretion system that is evolving to fit its environmental niche.* PLoS One, 2013. **8**(11): p. e78742.
29. Berks, B.C., *The twin-arginine protein translocation pathway.* Annu Rev Biochem, 2015. **84**: p. 843-64.
30. Jack, R.L., et al., *Constitutive expression of Escherichia coli tat genes indicates an important role for the twin-arginine translocase during aerobic and anaerobic growth.* J Bacteriol, 2001. **183**(5): p. 1801-4.
31. Rodriguez, F., et al., *Structural model for the protein-translocating element of the twin-arginine transport system.* Proc Natl Acad Sci U S A, 2013. **110**(12): p. E1092-101.
32. Zhang, Y., et al., *Solution structure of the TatB component of the twin-arginine translocation system.* Biochim Biophys Acta, 2014. **1838**(7): p. 1881-8.
33. Porcelli, I., et al., *Characterization and membrane assembly of the TatA component of the Escherichia coli twin-arginine protein transport system.* Biochemistry, 2002. **41**(46): p. 13690-7.
34. Ramasamy, S., et al., *The glove-like structure of the conserved membrane protein TatC provides insight into signal sequence recognition in twin-arginine translocation.* Structure, 2013. **21**(5): p. 777-88.
35. Bolhuis, A., et al., *TatB and TatC form a functional and structural unit of the twin-arginine translocase from Escherichia coli.* J Biol Chem, 2001. **276**(23): p. 20213-9.
36. Rose, P., et al., *Substrate-dependent assembly of the Tat translocase as observed in live Escherichia coli cells.* PLoS One, 2013. **8**(8): p. e69488.
37. Leake, M.C., et al., *Variable stoichiometry of the TatA component of the twin-arginine protein transport system observed by in vivo single-molecule imaging.* Proc Natl Acad Sci U S A, 2008. **105**(40): p. 15376-81.
38. Stanley, N.R., T. Palmer, and B.C. Berks, *The twin arginine consensus motif of Tat signal peptides is involved in Sec-independent protein targeting in Escherichia coli.* J Biol Chem, 2000. **275**(16): p. 11591-6.
39. Mori, H. and K. Cline, *A twin arginine signal peptide and the pH gradient trigger reversible assembly of the thylakoid [Delta]pH/Tat translocase.* J Cell Biol, 2002. **157**(2): p. 205-10.
40. Luke, I., et al., *Proteolytic processing of Escherichia coli twin-arginine signal peptides by LepB.* Arch Microbiol, 2009. **191**(12): p. 919-25.
41. Mould, R.M. and C. Robinson, *A proton gradient is required for the transport of two lumenal oxygen-evolving proteins across the thylakoid membrane.* J Biol Chem, 1991. **266**(19): p. 12189-93.

42. Hospenthal, M.K. and G. Waksman, *The Remarkable Biomechanical Properties of the Type 1 Chaperone-Usher Pilus: A Structural and Molecular Perspective.* Microbiol Spectr, 2019. **7**(1).
43. Fan, E., et al., *Type V Secretion Systems in Bacteria.* Microbiol Spectr, 2016. **4**(1).
44. Famelis, N., S. Geibel, and D. van Tol, *Mycobacterial type VII secretion systems.* Biol Chem, 2023. **404**(7): p. 691-702.
45. Dautin, N., *Folding Control in the Path of Type 5 Secretion.* Toxins (Basel), 2021. **13**(5).
46. Henderson, I.R. and J.P. Nataro, *Virulence functions of autotransporter proteins.* Infect Immun, 2001. **69**(3): p. 1231-43.
47. Albenne, C. and R. Ieva, *Job contenders: roles of the beta-barrel assembly machinery and the translocation and assembly module in autotransporter secretion.* Mol Microbiol, 2017. **106**(4): p. 505-517.
48. Ruiz-Perez, F., et al., *Roles of periplasmic chaperone proteins in the biogenesis of serine protease autotransporters of Enterobacteriaceae.* J Bacteriol, 2009. **191**(21): p. 6571-83.
49. Pavlova, O., et al., *Mechanistic link between beta barrel assembly and the initiation of autotransporter secretion.* Proc Natl Acad Sci U S A, 2013. **110**(10): p. E938-47.
50. Chapman, M.R., et al., *Role of Escherichia coli curli operons in directing amyloid fiber formation.* Science, 2002. **295**(5556): p. 851-5.
51. Olsen, A., A. Jonsson, and S. Normark, *Fibronectin binding mediated by a novel class of surface organelles on Escherichia coli.* Nature, 1989. **338**(6217): p. 652-5.
52. Olsen, A., et al., *The RpoS sigma factor relieves H-NS-mediated transcriptional repression of csgA, the subunit gene of fibronectin-binding curli in Escherichia coli.* Mol Microbiol, 1993. **7**(4): p. 523-36.
53. Collinson, S.K., et al., *Thin, aggregative fimbriae mediate binding of Salmonella enteritidis to fibronectin.* J Bacteriol, 1993. **175**(1): p. 12-8.
54. Kikuchi, T., et al., *Curli fibers are required for development of biofilm architecture in Escherichia coli K-12 and enhance bacterial adherence to human uroepithelial cells.* Microbiol Immunol, 2005. **49**(9): p. 875-84.
55. Collinson, S.K., et al., *Purification and characterization of thin, aggregative fimbriae from Salmonella enteritidis.* J Bacteriol, 1991. **173**(15): p. 4773-81.
56. Barnhart, M.M. and M.R. Chapman, *Curli biogenesis and function.* Annu Rev Microbiol, 2006. **60**: p. 131-47.
57. Zogaj, X., et al., *Production of cellulose and curli fimbriae by members of the family Enterobacteriaceae isolated from the human gastrointestinal tract.* Infect Immun, 2003. **71**(7): p. 4151-8.
58. Hammar, M., et al., *Expression of two csg operons is required for production of fibronectin- and congo red-binding curli polymers in Escherichia coli K-12.* Mol Microbiol, 1995. **18**(4): p. 661-70.
59. Evans, M.L., et al., *The bacterial curli system possesses a potent and selective inhibitor of amyloid formation.* Mol Cell, 2015. **57**(3): p. 445-55.
60. Prigent-Combaret, C., et al., *Complex regulatory network controls initial adhesion and biofilm formation in Escherichia coli via regulation of the csgD gene.* J Bacteriol, 2001. **183**(24): p. 7213-23.
61. Thanassi, D.G., E.T. Saulino, and S.J. Hultgren, *The chaperone/usher pathway: a major terminal branch of the general secretory pathway.* Curr Opin Microbiol, 1998. **1**(2): p. 223-31.

62. Lukaszczyk, M., B. Pradhan, and H. Remaut, *The Biosynthesis and Structures of Bacterial Pili.* Subcell Biochem, 2019. **92**: p. 369-413.
63. Jones, C.H., et al., *Adhesin presentation in bacteria requires molecular chaperones and ushers.* Infect Immun, 1992. **60**(11): p. 4445-51.
64. Zavialov, A., et al., *FGL chaperone-assembled fimbrial polyadhesins: anti-immune armament of Gram-negative bacterial pathogens.* FEMS Microbiol Rev, 2007. **31**(4): p. 478-514.
65. Wurpel, D.J., et al., *Chaperone-usher fimbriae of Escherichia coli.* PLoS One, 2013. **8**(1): p. e52835.
66. Behzadi, P., *Classical chaperone-usher (CU) adhesive fimbriome: uropathogenic Escherichia coli (UPEC) and urinary tract infections (UTIs).* Folia Microbiol (Praha), 2020. **65**(1): p. 45-65.
67. Jones, C.H., et al., *FimC is a periplasmic PapD-like chaperone that directs assembly of type 1 pili in bacteria.* Proc Natl Acad Sci U S A, 1993. **90**(18): p. 8397-401.
68. Klemm, P. and G. Christiansen, *The fimD gene required for cell surface localization of Escherichia coli type 1 fimbriae.* Mol Gen Genet, 1990. **220**(2): p. 334-8.
69. Junker, M., R.N. Besingi, and P.L. Clark, *Vectorial transport and folding of an autotransporter virulence protein during outer membrane secretion.* Mol Microbiol, 2009. **71**(5): p. 1323-32.
70. Thanassi, D.G., et al., *Protein secretion in the absence of ATP: the autotransporter, two-partner secretion and chaperone/usher pathways of gram-negative bacteria (review).* Mol Membr Biol, 2005. **22**(1-2): p. 63-72.
71. Peterson, J.H., et al., *Secretion of a bacterial virulence factor is driven by the folding of a C-terminal segment.* Proc Natl Acad Sci U S A, 2010. **107**(41): p. 17739-44.
72. Bhoite, S., et al., *Curli Biogenesis: Bacterial Amyloid Assembly by the Type VIII Secretion Pathway.* EcoSal Plus, 2019. **8**(2).
73. Louros, N.N., et al., *Intrinsic aggregation propensity of the CsgB nucleator protein is crucial for curli fiber formation.* J Struct Biol, 2016. **195**(2): p. 179-189.
74. Bunduc, C.M., W. Bitter, and E.N.G. Houben, *Structure and Function of the Mycobacterial Type VII Secretion Systems.* Annu Rev Microbiol, 2020. **74**: p. 315-335.
75. Bunduc, C.M., et al., *Reconstitution of a minimal ESX-5 type VII secretion system suggests a role for PPE proteins in the outer membrane transport of proteins.* mSphere, 2023. **8**(5): p. e0040223.
76. Beckham, K.S., et al., *Structure of the mycobacterial ESX-5 type VII secretion system membrane complex by single-particle analysis.* Nat Microbiol, 2017. **2**: p. 17047.
77. Rosenberg, O.S., et al., *Substrates Control Multimerization and Activation of the Multi-Domain ATPase Motor of Type VII Secretion.* Cell, 2015. **161**(3): p. 501-512.
78. Voulhoux, R., et al., *Involvement of the twin-arginine translocation system in protein secretion via the type II pathway.* EMBO J, 2001. **20**(23): p. 6735-41.
79. Vincent, M.S., et al., *Dynamic proton-dependent motors power type IX secretion and gliding motility in Flavobacterium.* PLoS Biol, 2022. **20**(3): p. e3001443.
80. Shiue, S.J., et al., *Mutation of a key residue in the type II secretion system ATPase uncouples ATP hydrolysis from protein translocation.* Mol Microbiol, 2007. **65**(2): p. 401-12.
81. Ellison, C.K., et al., *A bifunctional ATPase drives tad pilus extension and retraction.* Sci Adv, 2019. **5**(12): p. eaay2591.
82. Cianciotto, N.P. and R.C. White, *Expanding Role of Type II Secretion in Bacterial Pathogenesis and Beyond.* Infect Immun, 2017. **85**(5).

83. Chernyatina, A.A. and H.H. Low, *Core architecture of a bacterial type II secretion system.* Nat Commun, 2019. **10**(1): p. 5437.
84. Korotkov, K.V., et al., *Structural and functional studies on the interaction of GspC and GspD in the type II secretion system.* PLoS Pathog, 2011. **7**(9): p. e1002228.
85. Zhang, Y., et al., *Structure-guided disruption of the pseudopilus tip complex inhibits the Type II secretion in Pseudomonas aeruginosa.* PLoS Pathog, 2018. **14**(10): p. e1007343.
86. Reichow, S.L., et al., *Structure of the cholera toxin secretion channel in its closed state.* Nat Struct Mol Biol, 2010. **17**(10): p. 1226-32.
87. Korotkov, K.V. and M. Sandkvist, *Architecture, Function, and Substrates of the Type II Secretion System.* EcoSal Plus, 2019. **8**(2).
88. Camberg, J.L. and M. Sandkvist, *Molecular analysis of the Vibrio cholerae type II secretion ATPase EpsE.* J Bacteriol, 2005. **187**(1): p. 249-56.
89. Singh, P.K., J. Little, and M.S. Donnenberg, *Landmark Discoveries and Recent Advances in Type IV Pilus Research.* Microbiol Mol Biol Rev, 2022. **86**(3): p. e0007622.
90. Berry, J.L. and V. Pelicic, *Exceptionally widespread nanomachines composed of type IV pilins: the prokaryotic Swiss Army knives.* FEMS Microbiol Rev, 2015. **39**(1): p. 134-54.
91. Wolfgang, M., et al., *PilT mutations lead to simultaneous defects in competence for natural transformation and twitching motility in piliated Neisseria gonorrhoeae.* Mol Microbiol, 1998. **29**(1): p. 321-30.
92. Sato, K., et al., *Identification of a new membrane-associated protein that influences transport/maturation of gingipains and adhesins of Porphyromonas gingivalis.* J Biol Chem, 2005. **280**(10): p. 8668-77.
93. Braun, T.F., et al., *Flavobacterium johnsoniae gliding motility genes identified by mariner mutagenesis.* J Bacteriol, 2005. **187**(20): p. 6943-52.
94. Johnston, J.J., A. Shrivastava, and M.J. McBride, *Untangling Flavobacterium johnsoniae Gliding Motility and Protein Secretion.* J Bacteriol, 2018. **200**(2).
95. McBride, M.J. and Y. Zhu, *Gliding motility and Por secretion system genes are widespread among members of the phylum bacteroidetes.* J Bacteriol, 2013. **195**(2): p. 270-8.
96. Seers, C.A., et al., *The RgpB C-terminal domain has a role in attachment of RgpB to the outer membrane and belongs to a novel C-terminal-domain family found in Porphyromonas gingivalis.* J Bacteriol, 2006. **188**(17): p. 6376-86.
97. Hennell James, R., et al., *Structure and mechanism of the proton-driven motor that powers type 9 secretion and gliding motility.* Nat Microbiol, 2021. **6**(2): p. 221-233.
98. Lauber, F., et al., *Type 9 secretion system structures reveal a new protein transport mechanism.* Nature, 2018. **564**(7734): p. 77-82.
99. Hennell James, R., et al., *Structures of the Type IX Secretion/Gliding Motility Motor from across the Phylum Bacteroidetes.* mBio, 2022. **13**(3): p. e0026722.
100. Lara-Tejero, M. and J.E. Galan, *The Injectisome, a Complex Nanomachine for Protein Injection into Mammalian Cells.* EcoSal Plus, 2019. **8**(2).
101. Rappl, C., J. Deiwick, and M. Hensel, *Acidic pH is required for the functional assembly of the type III secretion system encoded by Salmonella pathogenicity island 2.* FEMS Microbiol Lett, 2003. **226**(2): p. 363-72.
102. Gartner, J.F. and M.A. Schmidt, *Comparative analysis of locus of enterocyte effacement pathogenicity islands of atypical enteropathogenic Escherichia coli.* Infect Immun, 2004. **72**(11): p. 6722-8.

103. Dacheux, D., et al., *Cell death of human polymorphonuclear neutrophils induced by a Pseudomonas aeruginosa cystic fibrosis isolate requires a functional type III secretion system.* Infect Immun, 1999. **67**(11): p. 6164-7.
104. Hueck, C.J., *Type III protein secretion systems in bacterial pathogens of animals and plants.* Microbiol Mol Biol Rev, 1998. **62**(2): p. 379-433.
105. Bergeron, J.R.C. and T.C. Marlovits, *Cryo-EM of the injectisome and type III secretion systems.* Curr Opin Struct Biol, 2022. **75**: p. 102403.
106. Meir, A., et al., *Substrate recruitment mechanism by gram-negative type III, IV, and VI bacterial injectisomes.* Trends Microbiol, 2023. **31**(9): p. 916-932.
107. Buttner, D., *Protein export according to schedule: architecture, assembly, and regulation of type III secretion systems from plant- and animal-pathogenic bacteria.* Microbiol Mol Biol Rev, 2012. **76**(2): p. 262-310.
108. Radics, J., L. Konigsmaier, and T.C. Marlovits, *Structure of a pathogenic type 3 secretion system in action.* Nat Struct Mol Biol, 2014. **21**(1): p. 82-7.
109. Cabezon, E., F. Valenzuela-Gomez, and I. Arechaga, *Primary architecture and energy requirements of Type III and Type IV secretion systems.* Front Cell Infect Microbiol, 2023. **13**: p. 1255852.
110. Worrall, L.J., D.D. Majewski, and N.C.J. Strynadka, *Structural Insights into Type III Secretion Systems of the Bacterial Flagellum and Injectisome.* Annu Rev Microbiol, 2023. **77**: p. 669-698.
111. Grohmann, E., et al., *Type IV secretion in Gram-negative and Gram-positive bacteria.* Mol Microbiol, 2018. **107**(4): p. 455-471.
112. Kohler, P.L., et al., *Mating pair formation homologue TraG is a variable membrane protein essential for contact-independent type IV secretion of chromosomal DNA by Neisseria gonorrhoeae.* J Bacteriol, 2013. **195**(8): p. 1666-79.
113. Hofreuter, D., S. Odenbreit, and R. Haas, *Natural transformation competence in Helicobacter pylori is mediated by the basic components of a type IV secretion system.* Mol Microbiol, 2001. **41**(2): p. 379-91.
114. Li, Y.G., B. Hu, and P.J. Christie, *Biological and Structural Diversity of Type IV Secretion Systems.* Microbiol Spectr, 2019. **7**(2).
115. Zehra, M., et al., *Comparative Analysis of T4SS Molecular Architectures.* J Microbiol Biotechnol, 2023. **33**(12): p. 1-11.
116. Hu, B., P. Khara, and P.J. Christie, *Structural bases for F plasmid conjugation and F pilus biogenesis in Escherichia coli.* Proc Natl Acad Sci U S A, 2019. **116**(28): p. 14222-14227.
117. Atmakuri, K., E. Cascales, and P.J. Christie, *Energetic components VirD4, VirB11 and VirB4 mediate early DNA transfer reactions required for bacterial type IV secretion.* Mol Microbiol, 2004. **54**(5): p. 1199-211.
118. Pukatzki, S., et al., *Identification of a conserved bacterial protein secretion system in Vibrio cholerae using the Dictyostelium host model system.* Proc Natl Acad Sci U S A, 2006. **103**(5): p. 1528-33.
119. Singh, R.P. and K. Kumari, *Bacterial type VI secretion system (T6SS): an evolved molecular weapon with diverse functionality.* Biotechnol Lett, 2023. **45**(3): p. 309-331.
120. Monjaras Feria, J. and M.A. Valvano, *An Overview of Anti-Eukaryotic T6SS Effectors.* Front Cell Infect Microbiol, 2020. **10**: p. 584751.
121. Jurenas, D. and E. Cascales, *T6SS: killing two bugs with one stone.* Trends Microbiol, 2022. **30**(1): p. 1-2.
122. Xiong, X., et al., *Type VI secretion system drives bacterial diversity and functions in multispecies biofilms.* Microbiol Res, 2024. **279**: p. 127570.

123. Rapisarda, C., et al., *In situ and high-resolution cryo-EM structure of a bacterial type VI secretion system membrane complex.* EMBO J, 2019. **38**(10).
124. Zoued, A., et al., *Architecture and assembly of the Type VI secretion system.* Biochim Biophys Acta, 2014. **1843**(8): p. 1664-73.
125. Brackmann, M., et al., *Using Force to Punch Holes: Mechanics of Contractile Nanomachines.* Trends Cell Biol, 2017. **27**(9): p. 623-632.
126. Basler, M., et al., *Type VI secretion requires a dynamic contractile phage tail-like structure.* Nature, 2012. **483**(7388): p. 182-6.
127. Allsopp, L.P. and P. Bernal, *Killing in the name of: T6SS structure and effector diversity.* Microbiology (Reading), 2023. **169**(7).
128. Basler, M. and J.J. Mekalanos, *Type 6 secretion dynamics within and between bacterial cells.* Science, 2012. **337**(6096): p. 815.
129. Holland, I.B., et al., *Type I Protein Secretion-Deceptively Simple yet with a Wide Range of Mechanistic Variability across the Family.* EcoSal Plus, 2016. **7**(1).
130. Kanonenberg, K., et al., *Type I secretion system-it takes three and a substrate.* FEMS Microbiol Lett, 2018. **365**(11).
131. Alav, I., et al., *Structure, Assembly, and Function of Tripartite Efflux and Type 1 Secretion Systems in Gram-Negative Bacteria.* Chem Rev, 2021. **121**(9): p. 5479-5596.
132. Holland, I.B., L. Schmitt, and J. Young, *Type 1 protein secretion in bacteria, the ABC-transporter dependent pathway (review).* Mol Membr Biol, 2005. **22**(1-2): p. 29-39.
133. Koronakis, V., E. Koronakis, and C. Hughes, *Isolation and analysis of the C-terminal signal directing export of Escherichia coli hemolysin protein across both bacterial membranes.* EMBO J, 1989. **8**(2): p. 595-605.
134. Smith, T.J., et al., *An N-Terminal Retention Module Anchors the Giant Adhesin LapA of Pseudomonas fluorescens at the Cell Surface: a Novel Subfamily of Type I Secretion Systems.* J Bacteriol, 2018. **200**(8).
135. Icke, C., et al., *Glycine acylation and trafficking of a new class of bacterial lipoprotein by a composite secretion system.* Elife, 2021. **10**.
136. Yousefian, N., et al., *Structural characterization of the EmrAB-TolC efflux complex from E. coli.* Biochim Biophys Acta Biomembr, 2021. **1863**(1): p. 183488.
137. Jang, S., *AcrAB-TolC, a major efflux pump in Gram negative bacteria: toward understanding its operation mechanism.* BMB Rep, 2023. **56**(6): p. 326-334.
138. Fitzpatrick, A.W.P., et al., *Structure of the MacAB-TolC ABC-type tripartite multidrug efflux pump.* Nat Microbiol, 2017. **2**: p. 17070.
139. Greene, N.P., et al., *Antibiotic Resistance Mediated by the MacB ABC Transporter Family: A Structural and Functional Perspective.* Front Microbiol, 2018. **9**: p. 950.
140. Quistgaard, E.M., et al., *Understanding transport by the major facilitator superfamily (MFS): structures pave the way.* Nat Rev Mol Cell Biol, 2016. **17**(2): p. 123-32.
141. Venter, H., et al., *RND-type drug e ffl ux pumps from Gram-negative bacteria: molecular mechanism and inhibition.* Front Microbiol, 2015. **6**: p. 377.
142. Felmlee, T., S. Pellett, and R.A. Welch, *Nucleotide sequence of an Escherichia coli chromosomal hemolysin.* J Bacteriol, 1985. **163**(1): p. 94-105.
143. Robinson, G.L., *The haemolysin of Bacterium coli.* J Gen Microbiol, 1951. **5**(4): p. 788-92.
144. Guzzo, J., et al., *The secretion genes of Pseudomonas aeruginosa alkaline protease are functionally related to those of Erwinia chrysanthemi proteases and Escherichia coli alpha-haemolysin.* Mol Microbiol, 1991. **5**(2): p. 447-53.

145. Letoffe, S., J.M. Ghigo, and C. Wandersman, *Secretion of the Serratia marcescens HasA protein by an ABC transporter.* J Bacteriol, 1994. **176**(17): p. 5372-7.
146. Glaser, P., et al., *Secretion of cyclolysin, the calmodulin-sensitive adenylate cyclase-haemolysin bifunctional protein of Bordetella pertussis.* EMBO J, 1988. **7**(12): p. 3997-4004.
147. Awram, P. and J. Smit, *The Caulobacter crescentus paracrystalline S-layer protein is secreted by an ABC transporter (type I) secretion apparatus.* J Bacteriol, 1998. **180**(12): p. 3062-9.
148. Kanonenberg, K., C.K. Schwarz, and L. Schmitt, *Type I secretion systems - a story of appendices.* Res Microbiol, 2013. **164**(6): p. 596-604.
149. Lenders, M.H., et al., *In vivo quantification of the secretion rates of the hemolysin A Type I secretion system.* Sci Rep, 2016. **6**: p. 33275.
150. Reimann, S., et al., *Interdomain regulation of the ATPase activity of the ABC transporter haemolysin B from Escherichia coli.* Biochem J, 2016. **473**(16): p. 2471-83.
151. Kanonenberg, K., S.H.J. Smits, and L. Schmitt, *Functional Reconstitution of HlyB, a Type I Secretion ABC Transporter, in Saposin-A Nanoparticles.* Sci Rep, 2019. **9**(1): p. 8436.
152. Spitz, O., et al., *Identity Determinants of the Translocation Signal for a Type 1 Secretion System.* Front Physiol, 2021. **12**: p. 804646.
153. Pourhassan, N.Z., et al., *Investigations on the substrate binding sites of hemolysin B, an ABC transporter, of a type 1 secretion system.* Front Microbiol, 2022. **13**: p. 1055032.
154. Zhao, H., J. Lee, and J. Chen, *The hemolysin A secretion system is a multi-engine pump containing three ABC transporters.* Cell, 2022. **185**(18): p. 3329-3340 e13.
155. Ostolaza, H., A. Soloaga, and F.M. Goni, *The binding of divalent cations to Escherichia coli alpha-haemolysin.* Eur J Biochem, 1995. **228**(1): p. 39-44.
156. Thomas, S., et al., *Equilibrium folding of pro-HlyA from Escherichia coli reveals a stable calcium ion dependent folding intermediate.* Biochim Biophys Acta, 2014. **1844**(9): p. 1500-10.
157. Sanchez-Magraner, L., et al., *The calcium-binding C-terminal domain of Escherichia coli alpha-hemolysin is a major determinant in the surface-active properties of the protein.* J Biol Chem, 2007. **282**(16): p. 11827-35.
158. Thomas, S., I.B. Holland, and L. Schmitt, *The Type 1 secretion pathway - the hemolysin system and beyond.* Biochim Biophys Acta, 2014. **1843**(8): p. 1629-41.
159. Jones, H.E., et al., *Slow changes in cytosolic free Ca2+ in Escherichia coli highlight two putative influx mechanisms in response to changes in extracellular calcium.* Cell Calcium, 1999. **25**(3): p. 265-74.
160. Hess, J., et al., *Nucleotide sequence of a plasmid-encoded hemolysin determinant and its comparison with a corresponding chromosomal hemolysin sequence.* FEMS Microbiology Letters, 1986. **34**(1): p. 1-11.
161. Schindel, C., et al., *Interaction of Escherichia coli hemolysin with biological membranes. A study using cysteine scanning mutagenesis.* Eur J Biochem, 2001. **268**(3): p. 800-8.
162. Ludwig, A., et al., *Analysis of the in vivo activation of hemolysin (HlyA) from Escherichia coli.* J Bacteriol, 1996. **178**(18): p. 5422-30.
163. Sanchez-Magraner, L., et al., *Membrane insertion of Escherichia coli alpha-hemolysin is independent from membrane lysis.* J Biol Chem, 2006. **281**(9): p. 5461-7.
164. Vazquez, R.F., et al., *Interaction of acylated and unacylated forms of E. coli alpha-hemolysin with lipid monolayers: a PM-IRRAS study.* Colloids Surf B Biointerfaces, 2017. **158**: p. 76-83.

165. Hughes, C., et al., *Activation of Escherichia coli prohemolysin to the membrane-targetted toxin by HlyC-directed ACP-dependent fatty acylation.* FEMS Microbiol Immunol, 1992. **5**(1-3): p. 37-43.
166. Hardie, K.R., et al., *In vitro activation of Escherichia coli prohaemolysin to the mature membrane-targeted toxin requires HlyC and a low molecular-weight cytosolic polypeptide.* Mol Microbiol, 1991. **5**(7): p. 1669-79.
167. Kenny, B., R. Haigh, and I.B. Holland, *Analysis of the haemolysin transport process through the secretion from Escherichia coli of PCM, CAT or beta-galactosidase fused to the Hly C-terminal signal domain.* Mol Microbiol, 1991. **5**(10): p. 2557-68.
168. Hess, J., et al., *Analysis of the haemolysin secretion system by PhoA-HlyA fusion proteins.* Mol Gen Genet, 1990. **224**(2): p. 201-8.
169. Nicaud, J.M., et al., *The C-terminal, 23 kDa peptide of E. coli haemolysin 2001 contains all the information necessary for its secretion by the haemolysin (Hly) export machinery.* FEBS Lett, 1986. **204**(2): p. 331-5.
170. Benabdelhak, H., et al., *A Specific Interaction Between the NBD of the ABC-transporter HlyB and a C-Terminal Fragment of its Transport Substrate Haemolysin A.* Journal of Molecular Biology, 2003. **327**(5): p. 1169-1179.
171. Lenders, M.H., et al., *Directionality of substrate translocation of the hemolysin A Type I secretion system.* Sci Rep, 2015. **5**: p. 12470.
172. Thanabalu, T., et al., *Substrate-induced assembly of a contiguous channel for protein export from E.coli: reversible bridging of an inner-membrane translocase to an outer membrane exit pore.* EMBO J, 1998. **17**(22): p. 6487-96.
173. Locher, K.P., *Mechanistic diversity in ATP-binding cassette (ABC) transporters.* Nat Struct Mol Biol, 2016. **23**(6): p. 487-93.
174. Wang, R.C., et al., *Analysis of the membrane organization of an Escherichia coli protein translocator, HlyB, a member of a large family of prokaryote and eukaryote surface transport proteins.* J Mol Biol, 1991. **217**(3): p. 441-54.
175. Gentschev, I. and W. Goebel, *Topological and functional studies on HlyB of Escherichia coli.* Mol Gen Genet, 1992. **232**(1): p. 40-8.
176. Schmitt, L., et al., *Crystal structure of the nucleotide-binding domain of the ABC-transporter haemolysin B: identification of a variable region within ABC helical domains.* J Mol Biol, 2003. **330**(2): p. 333-42.
177. Lecher, J., et al., *An RTX transporter tethers its unfolded substrate during secretion via a unique N-terminal domain.* Structure, 2012. **20**(10): p. 1778-87.
178. Thomas, C., et al., *Structural and functional diversity calls for a new classification of ABC transporters.* FEBS Lett, 2020. **594**(23): p. 3767-3775.
179. Thomas, C. and R. Tampe, *Structural and Mechanistic Principles of ABC Transporters.* Annu Rev Biochem, 2020. **89**: p. 605-636.
180. Koronakis, V., E. Koronakis, and C. Hughes, *Comparison of the haemolysin secretion protein HlyB from Proteus vulgaris and Escherichia coli; site-directed mutagenesis causing impairment of export function.* Mol Gen Genet, 1988. **213**(2-3): p. 551-5.
181. Zaitseva, J., et al., *Functional characterization and ATP-induced dimerization of the isolated ABC-domain of the haemolysin B transporter.* Biochemistry, 2005. **44**(28): p. 9680-90.
182. Zaitseva, J., et al., *A structural analysis of asymmetry required for catalytic activity of an ABC-ATPase domain dimer.* EMBO J, 2006. **25**(14): p. 3432-43.
183. Zaitseva, J., et al., *H662 is the linchpin of ATP hydrolysis in the nucleotide-binding domain of the ABC transporter HlyB.* EMBO J, 2005. **24**(11): p. 1901-10.

184. Schulein, R., et al., *A topological model for the haemolysin translocator protein HlyD.* Mol Gen Genet, 1992. **234**(1): p. 155-63.
185. Balakrishnan, L., C. Hughes, and V. Koronakis, *Substrate-triggered recruitment of the TolC channel-tunnel during type I export of hemolysin by Escherichia coli.* J Mol Biol, 2001. **313**(3): p. 501-10.
186. Kim, J.S., et al., *Crystal Structure of a Soluble Fragment of the Membrane Fusion Protein HlyD in a Type I Secretion System of Gram-Negative Bacteria.* Structure, 2016. **24**(3): p. 477-85.
187. Wandersman, C. and P. Delepelaire, *TolC, an Escherichia coli outer membrane protein required for hemolysin secretion.* Proc Natl Acad Sci U S A, 1990. **87**(12): p. 4776-80.
188. Koronakis, V., et al., *Structure of TolC, the outer membrane component of the bacterial type I efflux system, derived from two-dimensional crystals.* Mol Microbiol, 1997. **23**(3): p. 617-26.
189. Koronakis, V., et al., *Crystal structure of the bacterial membrane protein TolC central to multidrug efflux and protein export.* Nature, 2000. **405**(6789): p. 914-9.
190. Pei, X.Y., et al., *Structures of sequential open states in a symmetrical opening transition of the TolC exit duct.* Proc Natl Acad Sci U S A, 2011. **108**(5): p. 2112-7.
191. Wang, Z., et al., *An allosteric transport mechanism for the AcrAB-TolC multidrug efflux pump.* Elife, 2017. **6**.
192. Du, D., et al., *Structure of the AcrAB-TolC multidrug efflux pump.* Nature, 2014. **509**(7501): p. 512-5.
193. Beer, T., et al., *Quantification and surface localization of the hemolysin A type 1 secretion system at the endogenous level and under conditions of overexpression.* Appl Environ Microbiol, 2021: p. AEM0189621.
194. Shi, X., et al., *In situ structure and assembly of the multidrug efflux pump AcrAB-TolC.* Nat Commun, 2019. **10**(1): p. 2635.
195. Tikhonova, E.B., et al., *Kinetic control of TolC recruitment by multidrug efflux complexes.* Proc Natl Acad Sci U S A, 2009. **106**(38): p. 16416-21.
196. Welch, R.A. and S. Pellett, *Transcriptional organization of the Escherichia coli hemolysin genes.* J Bacteriol, 1988. **170**(4): p. 1622-30.
197. Leeds, J.A. and R.A. Welch, *RfaH enhances elongation of Escherichia coli hlyCABD mRNA.* J Bacteriol, 1996. **178**(7): p. 1850-7.
198. Leeds, J.A. and R.A. Welch, *Enhancing transcription through the Escherichia coli hemolysin operon, hlyCABD: RfaH and upstream JUMPStart DNA sequences function together via a postinitiation mechanism.* J Bacteriol, 1997. **179**(11): p. 3519-27.
199. Nieto, J.M., et al., *Suppression of transcription polarity in the Escherichia coli haemolysin operon by a short upstream element shared by polysaccharide and DNA transfer determinants.* Mol Microbiol, 1996. **19**(4): p. 705-13.
200. Bakkes, P.J., et al., *The rate of folding dictates substrate secretion by the Escherichia coli hemolysin type 1 secretion system.* J Biol Chem, 2010. **285**(52): p. 40573-80.
201. Pimenta, A.L., et al., *Antibody analysis of the localisation, expression and stability of HlyD, the MFP component of the E. coli haemolysin translocator.* Mol Gen Genet, 1999. **261**(1): p. 122-32.
202. Jaumouille, V., et al., *Cytoplasmic targeting of IpaC to the bacterial pole directs polar type III secretion in Shigella.* EMBO J, 2008. **27**(2): p. 447-57.
203. Jeong, K.C., et al., *Polar delivery of Legionella type IV secretion system substrates is essential for virulence.* Proc Natl Acad Sci U S A, 2017. **114**(30): p. 8077-8082.

204. Judd, P.K., R.B. Kumar, and A. Das, *Spatial location and requirements for the assembly of the Agrobacterium tumefaciens type IV secretion apparatus.* Proc Natl Acad Sci U S A, 2005. **102**(32): p. 11498-503.
205. Benabdelhak, H., et al., *A specific interaction between the NBD of the ABC-transporter HlyB and a C-terminal fragment of its transport substrate haemolysin A.* J Mol Biol, 2003. **327**(5): p. 1169-79.
206. Filipi, K., et al., *Kingella kingae RtxA Cytotoxin in the Context of Other RTX Toxins.* Microorganisms, 2022. **10**(3).
207. Souabni, H., et al., *Quantitative real-time analysis of the efflux by the MacAB-TolC tripartite efflux pump clarifies the role of ATP hydrolysis within mechanotransmission mechanism.* Commun Biol, 2021. **4**(1): p. 493.
208. Robinson, T., et al., *Microfluidic trapping of giant unilamellar vesicles to study transport through a membrane pore.* Biomicrofluidics, 2013. **7**(4): p. 44105.
209. Bian, T., et al., *Direct detection of SERCA calcium transport and small-molecule inhibition in giant unilamellar vesicles.* Biochem Biophys Res Commun, 2016. **481**(3-4): p. 206-211.
210. Jannasch, A., et al., *Fast 3D imaging of giant unilamellar vesicles using reflected light-sheet microscopy with single molecule sensitivity.* J Microsc, 2022. **285**(1): p. 40-51.
211. Kamel, M., et al., *Unsaturated fatty acids augment protein transport via the SecA:SecYEG translocon.* FEBS J, 2022. **289**(1): p. 140-162.
212. Yum, S., et al., *Crystal structure of the periplasmic component of a tripartite macrolide-specific efflux pump.* J Mol Biol, 2009. **387**(5): p. 1286-97.
213. Mikolosko, J., et al., *Conformational flexibility in the multidrug efflux system protein AcrA.* Structure, 2006. **14**(3): p. 577-87.
214. Staron, P., K. Forchhammer, and I. Maldener, *Structure-function analysis of the ATP-driven glycolipid efflux pump DevBCA reveals complex organization with TolC/HgdD.* FEBS Lett, 2014. **588**(3): p. 395-400.
215. Hobbs, E.C., et al., *Conserved small protein associates with the multidrug efflux pump AcrB and differentially affects antibiotic resistance.* Proc Natl Acad Sci U S A, 2012. **109**(41): p. 16696-701.
216. Hobbs, E.C., et al., *An expanding universe of small proteins.* Curr Opin Microbiol, 2011. **14**(2): p. 167-73.
217. Du, D., et al., *Interactions of a Bacterial RND Transporter with a Transmembrane Small Protein in a Lipid Environment.* Structure, 2020. **28**(6): p. 625-634 e6.
218. Yadavalli, S.S. and J. Yuan, *Bacterial Small Membrane Proteins: the Swiss Army Knife of Regulators at the Lipid Bilayer.* J Bacteriol, 2022. **204**(1): p. e0034421.
219. Ma, M., et al., *MexAB-OprM Efflux Pump Interaction with the Peptidoglycan of Escherichia coli and Pseudomonas aeruginosa.* Int J Mol Sci, 2021. **22**(10).
220. Pramanik, S., et al., *Binding of His-tagged fluorophores to lipid bilayers of giant vesicles.* Soft Matter, 2022. **18**(34): p. 6372-6383.
221. Schmitt, L., C. Dietrich, and R. Tampe, *Synthesis and Characterization of Chelator-Lipids for Reversible Immobilization of Engineered Proteins at Self-Assembled Lipid Interfaces.* Journal of the American Chemical Society, 1994. **116**(19): p. 8485-8491.
222. Ding, Y., N.H. Williams, and C.A. Hunter, *A Synthetic Vesicle-to-Vesicle Communication System.* J Am Chem Soc, 2019. **141**(44): p. 17847-17853.
223. Tsutsumi, K., et al., *Structures of the wild-type MexAB-OprM tripartite pump reveal its complex formation and drug efflux mechanism.* Nat Commun, 2019. **10**(1): p. 1520.

224. Goffeau, A. and J.P. Dufour, *Plasma membrane ATPase from the yeast Saccharomyces cerevisiae.* Methods Enzymol, 1988. **157**: p. 528-33.
225. Dufour, J.P., A. Amory, and A. Goffeau, *Plasma membrane ATPase from the yeast Schizosaccharomyces pombe.* Methods Enzymol, 1988. **157**: p. 513-28.
226. Renard, K. and B. Byrne, *Insights into the Role of Membrane Lipids in the Structure, Function and Regulation of Integral Membrane Proteins.* Int J Mol Sci, 2021. **22**(16).
227. Pollock, N.L., et al., *Conformational trapping of an ABC transporter in polymer lipid nanoparticles.* Biochem J, 2022. **479**(2): p. 145-159.
228. Hofmann, S., et al., *Conformation space of a heterodimeric ABC exporter under turnover conditions.* Nature, 2019. **571**(7766): p. 580-583.
229. Yu, L., et al., *Structural basis of peptide secretion for Quorum sensing by ComA.* Nat Commun, 2023. **14**(1): p. 7178.
230. Li, S., *Detergents and alternatives in cryo-EM studies of membrane proteins.* Acta Biochim Biophys Sin (Shanghai), 2022. **54**(8): p. 1049-1056.
231. Hauer, F., et al., *GraDeR: Membrane Protein Complex Preparation for Single-Particle Cryo-EM.* Structure, 2015. **23**(9): p. 1769-1775.
232. Venien-Bryan, C. and C.A.H. Fernandes, *Overview of Membrane Protein Sample Preparation for Single-Particle Cryo-Electron Microscopy Analysis.* Int J Mol Sci, 2023. **24**(19).

6. Acknowledgements

An dieser Stelle möchte ich mich bei den Personen bedanken, die mich über die letzten Jahre während meiner Promotion und meinem Studium unterstützt haben.

Zuallererst möchte ich mich bei meinem Doktorvater **Prof. Dr. Lutz Schmitt** bedanken. Vielen Dank für Dein entgegengebrachtes Vertrauen und die Unterstützung über die gesamte Zeit meiner Promotion und darüber hinaus. Es war mir eine große Freude, meine Arbeit in Deinem Institut anzufertigen. Du hast stets mit Rat und Tat zur Seite gestanden und immer auch die positiven Aspekte in den vielleicht nicht ganz so perfekten Ergebnissen gesehen und herausgestellt. Danke, dass Du während der gesamten Zeit mit ihren Höhen und Tiefen immer ein offenes Ohr und Lösungen für Probleme parat hattest.

Als nächstes möchte ich mich bei **Prof. Dr. Sander Smits** bedanken. Auch Dir danke ich sehr für Deine Unterstützung für mich und mein Projekt. Wenn es mal nicht lief, hattest Du meist eine zündende Idee und vor allem eine große Portion Motivation. Deine offene und direkte Art hat so manches Meeting sehr bereichert, wenn ich mal wieder jeden Stein am Wegrand umdrehen wollte. Danke auch für viele offene und produktive Gespräche bei einer Tasse Kaffee.

Ein weiterer Dank gilt **PD Dr. Ulrich Schulte**. Als Koordinator des Studiengangs Biochemie habe ich Dich früh im Studium kennen gelernt und auf Dein Organisationstalent war immer Verlass, ob bei WE-Sitzungen, Prüfungsausschüssen oder Planungen von Praktika. Auch als Kollege konnte ich von Deinem fundierten biochemischen Wissen und Deinem herzhaften Lachen profitieren, welches leider viel zu früh verstummte.

Prof. Dr. Johannes Hegemann danke ich für die Übernahme des Korreferats. Danke auch für viele aufschlussreiche Gespräche und Anregungen zu meinem Projekt während unserer Treffen zum Fortschritt der Promotion oder im Rahmen des SFB 1208.

Des Weiteren möchte ich mich bei **Prof. Dr. Carsten Sachse** für die Unterstützung im Bereich Cryo-EM bedanken. Bei **Dr. Gereon Poschmann** möchte ich mich für MS Analysen bedanken. Außerdem danke ich **Dr. Jens Reiners** für SAXS Analysen. Bei **Dr. Miriam Bäumers** möchte ich mich für die Unterstützung und Hilfe bei der Aufnahme von *negative stain* Bildern bedanken.

I would like to thank the whole **CRC 1208** for a very pleasant and fruitful atmosphere to discuss and present science. I would like to especially thank **Dr. Cordula Kruse** for the perfect organisation of every retreat and meeting within the CRC 1208. Additionally, I would like to thank all ECR representatives: **Dr. Athanasios Papadopoulos**, **Jennifer Loschwitz**, **Luca-Cesare Blawitzki** , **Dr. Madhumitha Narasimhan** and **Rocco Gentile**. It was a great pleasure to organise meetings, retreats and get-togethers with you.

Darüber hinaus möchte ich dem **iGRAD Team** einen großen Dank aussprechen, die mit einem sehr breitem Workshop Angebot meine persönliche Entwicklung unterstützt haben. Außerdem danke ich den **Heine Research Academies** für den gewährten Reisekostenzuschuss für die Teilnahme an meiner ersten großen internationalen Konferenz.

Darüber hinaus möchte ich mich bei **Dr. Andreas Schlundt** bedanken. Danke, dass Du mir als Mentor für den nächsten Karriereschritt in den letzten gut zwei Jahren alle meine Fragen beantwortet hast und immer auch Alternativen aufgezeigt und weitere Aspekte beleuchtet hast, die mir noch gänzlich unbekannt waren.

I would also like to thank **Prof. Dr. Alexej Kedrov**. Thank you very much for a lot of fruitful discussions and your continuous interest in my project. I very much appreciated your straight forward advices and chats in the corridor and office.

In addition I would like to thank **Dr. Marten Exterkate** for a lot of good conversations in the kitchen, the lab, the office or at home about science, football, board games and career opportunities. Furthermore I would like to thank for your valuable input for my project.
Ich möchte mich ebenfalls sehr bei **Junior Prof. Dr. Miriam Kutsch** bedanken für einen sehr hilfreichen Austausch zu meinem Projekt, meinen Vorträgen und Karriereoptionen. Ich hoffe wir können auch in Zukunft noch das ein oder andere Café oder Brettspiel gemeinsam entdecken.

Ein weiterer großer Dank geht an alle ehemaligen Mitglieder des Instituts, die ich während meiner Anfangszeit noch kennenlernen durfte. **Dr. Olivia Spitz**, **Dr. Julia Schumacher**, **Dr. Manuel Wagner**, **Dr. Tim Kroll**, **Dr. Jens Reiners**, **Dr. Tobias Beer**, **Dr. Isabelle Erenburg**, **Dr. Martin Prescher** und **Dr. Marcel Lagedroste**, vielen Dank für einen tollen Start in meine Promotionszeit. Ich habe einiges von euch gelernt und denke gerne an die gemeinsamen Gänge zur großen Mensa zurück, bei denen

über eigentlich alles philosophiert wurde, vor allem, wenn Tobi dabei war :D. Gesondert möchte ich Lab 29 danken: Tobias, Isabelle und Marcel. Es war mir stets eine Freude mit euch im Labor zu arbeiten und sich auszutauschen. **Dr. Martin Prescher**, Dir möchte ich für viele produktive Gespräche über unsere Forschungsthemen in der Küche oder auf dem Balkon im alten Gebäude danken. Es war stets aufschlussreich und hilfreich mit Dir Probleme aus verschiedenen Blickwinkeln zu betrachten.

Allen weiteren Weggefährten im Institut (**Dr. Alexandra Bork**, **Dr. Athanasios Papadopoulos**, **Christian Mammen**, **Cigdem Günes**, **Eymen Hachani**, **Feby Chacko**, **Hans Hannig**, **Julia Gottstein**, **Lars Bostelmann-Arp**, **Lea Nentwig**, **Dr. Manuel Anlauf**, **Dr. Maryna Löwe**, **Max Busch**, **Dr. Michael Kamel**, **Neele Wolff**, **Dr. Sakshi Khosa**, **Sergiy Gan**, **Stefanie Gala Marti**, **Vivien Knospe**, **Dr. Zohreh Pourhassan**) danke ich für viele aufschlussreiche Gespräche, gemeinsame lustige Aktivitäten wie Champions League-, Konsolen-, Cocktail-Abende und eine unvergessliche Zeit im Institut. Für Eure Zukunft wünsche ich Euch viel Erfolg.

Auch möchte ich mich bei den Studierenden bedanken, deren Abschlussarbeiten ich betreuen durfte. Danke an **Jutta Beckmann**, **Kevin Meinel**, **Rebecca Zanini**, **Maren van Soest**, **Lara Klimas** und **Payal Guliani** für euren Einsatz.

Danke an **Mathilde Bluhm**, **Tatjana Platz** und **Corinna Franzkowiak** dafür, dass Ihr etliche Fragen zu den organisatorischen Abläufen an der HHU, wie dem Einreichen einer Dienstreiseabrechnung oder dem Ausfüllen sonstiger Formulare beantwortet habt.

Ein weiterer Dank geht an **Silke Mavaro** für die Organisation der Gentechnik, von Plasmidlisten bis hin zu Formblättern.

Vielen Dank auch an **Dr. Jan Stindt** für die Organisation der Lehre und Deine stets fröhliche und unschlagbare Art, positive Stimmung zu verbreiten.

Ein besonderer Dank geht an **Martina Wesemann**. Vielen Dank für Deine Geduld, wenn es mal wieder hieß „Martina, wo finde ich X?“ oder „Hilfe Martina, Y ist kaputt!“. Ich glaube jeder wird mir zustimmen, wenn ich sage, dass ohne Dich das Labor nicht so gut laufen würde. Vielen Dank dafür! Danke auch für Deine Unterstützung bei Klonierungsarbeiten und im eLab.

Danke an das Büro **Stefanie Gala Marti**, **Lea Nentwig**, **Neele Wolff** und **Cigdem Günes**, dass ich immer Platz auf eurem Sitzsack nehmen durfte und es eigentlich immer etwas zu erzählen und zu naschen gab :P.

Besonders bedanke ich mich bei meinen Kollegen im Büro: **Sergiy Gan**, **Christian Mammen** und **Dr. Manuel Anlauf**. Danke, für die vielen erheiternden Gespräche über Forschung und gemeinsame oder unterschiedliche Leidenschaften.

Unserer DnD Runde: **Hans Hannig**, **Christian Mammen**, **Dr. Tim Kroll** und **Dr. Manuel Anlauf** möchte ich für viele fantastische Abenteuer danken. Sehr gerne denke ich auch an die MTG Runden zurück und danke besonders **Stefanie** und **Valentin Gala Marti** und **Dr. Manuel Anlauf**, die mich erst für dieses Spiel begeistert haben.

I would also like to thank **Dr. Michael Kamel** for thriving discussions about our projects and science in general. Thank you for sharing all your knowledge. I wish you all the best for your future.

I would like to especially thank **Dr. Sakshi Khosa** for your helpful guidance in a time when it seemed as if all the experiments were conspiring against me. Also I would like to thank you for your constant support.

Gesondert hervorheben möchte ich auch einen Wegbegleiter der ersten Stunde und sehr guten Freund: **Dr. Manuel Anlauf**. Vielen Dank, dass wir gemeinsam vom Bachelor bis zur Promotion durch dick und dünn gegangen sind. Jedes schiefgegangene Experiment war dank Dir ertragbarer und jedes erfolgreiche Experiment umso besser. Es hat mir großen Spaß gemacht, mit Dir die ÄKTAs auseinanderzunehmen und wieder zum Laufen zu bringen. Was haben wir uns gefreut, als der Fraktionskollektor wieder lief :P. Danke auch, dass ich meinen musikalischen Wahnsinn von der Grille bis zum „Lets go!!!!!“ im Labor mit dir teilen durfte. We tried so hard, and got so far und am Ende haben wir die *Siegeslinie* erreicht, aber es war nicht irgendein Tag, es war *ein denkwürdiger Tag*. Was wäre die Laborzeit nur ohne Dich gewesen. Zum Glück musste ich es nicht herausfinden, auch wenn Dr. Alexander Fejzagic Dich gern dazu verleitet hätte.

Ein großer Dank geht an meine Freunde, die mich während meiner Promotion begleitet und in schlechten Zeiten unterstützt und aufgefangen haben. Besonders danke ich **David Pietrzyk** und **Leonard Held** für einen legendären Besuch zum Mittagessen im Institut :D. Ebenfalls ein großer Dank an **Laurenz Ungerath** für Deine Unterstützung mit Rat und Tat in allen Lebenslagen. Ein sehr großer Dank geht an die Holland-

Truppe: **Dr. Alexander Fejzagic**, **Dr. Anne Pfitzer-Bilsing**, **Dr. Lea Sundermeyer**, **Dr. Leonie Windeln**, **Dr. Manuel Anlauf**, **Maurice Tust**, **Niklas Peters**, **Nora Bitzenhofer** und **Vivian Willers**. Kennen wir uns doch schon seit dem Bachelor, hat besonders die Promotionszeit uns alle nochmal mehr zusammengeschweißt und dass trotz teils erheblicher örtlicher Distanzen. Ich bin froh, auf Euren Rückhalt bauen zu können und möchte jedem einzelnen herzlich für die zurückliegenden Jahre der Freude, Unterstützung und Wertschätzung danken.

Des Weiteren möchte ich mich bei meiner Familie bedanken, die mich durchgehend und bedingungslos unterstützt hat. Meinen Eltern **Peter** und **Sabine Bilsing**, sowie meinen Schwestern **Arabella Bilsing**, **Floria Bilsing** und **Aurelia Lesch** und meiner Tante **Astrid Bilsing** danke ich dafür, dass sie immer an mich geglaubt haben und mir Rückhalt geboten haben. Auch meiner neu gewonnen Familie, insbesondere **Elke** und **Andreas Pfitzer**, sowie **Kai Pfitzer** danke ich für die bedingungslose Unterstützung und den Rückhalt, den sie mir geboten haben.

Zu guter Letzt möchte ich mich bei meiner Ehefrau **Dr. Anne Pfitzer-Bilsing** bedanken. Danke, dass Du mich stets unterstützt hast, vor allem in den schwierigen und anstrengenden Momenten und stets an mich geglaubt hast. Danke für Dein Verständnis und deine Liebe.

7. Declaration

Ich versichere an Eides Statt, dass die Dissertation von mir selbständig und ohne unzulässige fremde Hilfe unter Beachtung der „Grundsätze zur Sicherung guter wissenschaftlicher Praxis an der Heinrich-Heine-Universität Düsseldorf“ erstellt worden ist. Diese Dissertation wurde in der vorliegenden oder in ähnlicher Form noch bei keiner anderen Institution eingereicht. Ich habe bisher keine erfolglosen oder erfolgreichen Promotionsversuche unternommen.

Ort, Datum	Florestan Leander Bilsing